DECENTRALIZED SINGLE-BEACON ACOUSTIC NAVIGATION: COMBINED COMMUNICATION AND NAVIGATION FOR UNDERWATER VEHICLES

by

Sarah E. Webster

A dissertation submitted to The Johns Hopkins University in conformity with the requirements for the degree of Doctor of Philosophy.

Baltimore, Maryland

June, 2010

Abstract

This thesis reports the derivation and validation of two single-beacon acoustic navigation algorithms, as well as the development and experimental evaluation of a platform-independent acoustic communication (Acomms) system that enables combined communication and navigation. The navigation algorithms are centralized and decentralized formulations of single-beacon navigation, and employ range measurements from a single reference beacon to an underwater vehicle in addition to the vehicles Doppler velocity log, gyrocompass, and depth sensors to perform absolute (as opposed to relative) localization and navigation of the vehicle. The centralized single-beacon algorithm is based on the extended Kalman filter. We assume that the Kalman filter has simultaneous, real-time access to sensor measurements from both the vehicle and the beacon (e.g. the ship). The decentralized single-beacon algorithm is based on the information form of the extended Kalman filter. We assume that the information filter on the vehicle only has access to measurements from the vehicles on-board navigation sensors in real-time. The vehicle-based filter receives acoustic broadcasts from the reference beacon that contain information about the beacons position and sensor measurements. We show analytically and in simulation that the decentralized algorithm formulated herein yields an identical state estimate to the state estimate of the centralized algorithm at the instant of each range measurement; in addition we show that between range measurements the results from the two algorithms differ only by linearization errors and the effects of smoothing historic ship states. The Acomms system has been installed on the Wood Hole Oceanographic Institution vehicles *Puma*, *Jaguar*, and *Nereus*. The author and collaborators deployed the Acomms system in four sea trials in the North Pacific and South Atlantic Oceans, including the Mariana Trench. The performance of the navigation algorithms are evaluated using simulations and navigation data from these field trials. The benefit of single-beacon navigation and this implementation are that the decentralized formulation scales naturally to multiple vehicles and the use of a single, moving reference beacon eliminates the need for multiple, fixed beacons and their associated cost and range limitations.

ABSTRACT

Primary Thesis Adviser: Professor Louis L. Whitcomb, Johns Hopkins University
Secondary Thesis Adviser: Professor Ryan M. Eustice, University of Michigan

Thesis Committee:
Professor Noah J. Cowan, Johns Hopkins University
Professor Ryan M. Eustice, University of Michigan
Professor Daniel J. Stilwell, Virginia Polytechnic Institute and State University
Professor Louis L. Whitcomb, Johns Hopkins University

Acknowledgements

First I would like to thank my primary adviser, Louis L. Whitcomb. From Louis I have learned some of the finer points of getting research done (pretend you are out of town), writing research papers (my first was returned accompanied by a copy of Strunk and White), and how to not let the magic blue smoke out. He also have me the opportunity to be involved in the *Nereus* project, a once-in-a-lifetime opportunity. I would like to thank my co-adviser Ryan M. Eustice from the University of Michigan. Ryan helped me decide on my research focus and provided invaluable tutelage in the finer points of Kalman and information filters. He also provided a glimpse of life as a young faculty member, which is enough to cure anyone who likes sleep of her academic ambitions.

The research presented in this thesis was carried out in the context of two oceanographic research programs with which the author was fortunate to be involved. Field trials on the southern Mid-Atlantic Ridge with *Puma* and *Jaguar* were supported by the National Science Foundation under NSF Awards ATM-0427220 and ATM-0428122. *Nereus* field trials were supported by the National Science Foundation under award OCE-0334411, OCE-0453105, OCE-0452262, the Office of Naval Research under work order N0001409WX20051, the National Oceanic and Atmospheric Administration under award NA04OAR4300168, the Woods Hole Oceanographic Institution, and the Russell Family Foundation.

My own funding was provided by the generous support of several fellowships, including the Johns Hopkins University Mechanical Engineering Department Fellowship 2004-2005, the Johns Hopkins University Deans Fellowship 2004-2009, and the Link Foundation Doctoral Research Fellowship in Ocean Engineering and Instrumentation 2008-2009. These fellowships played a crucial role in enabling the research presented herein. I would like to especially thank the Dean's Office in the Whiting School of Engineering. Their generous funding made many things possible that are typically outside the scope of graduate student support, including my own equipment and funding for conferences and travel to Woods Hole Oceanographic Institution, which gave me the invaluable opportunity to interact with a wide variety of researchers in my field.

While at home, all of my labmates through the years—the ones who have already finished, including James Kinsey, Axel Krieger, Steve Martin, and Tabish Mustafa, and especially our current lab group, Amy Blank, Topher McFarland, Giancarlo Troni, and Hunter

Brown—have provided a wonderful lab environment with just the right mix of support, encouragement, harassment, and hilarity. I couldn't have had a better group of colleagues.

My others friends in the trenches of graduate school—Katherine, Lindsey, Netta, Eatai, Peter, the ladies from our impromptu *Anxious-to-Graduate Coffee Hour*, and many others—provided the kind of support that you can only get from those who know the ups and down of research. In contrast, my friends outside of graduate school—Julie, Thayne, Lucy, Ian, Carla, Britta, Camilla, Dave, Mike, and all of our other friends—provided the invaluable reminder that there is life outside of school and that it is pretty enjoyable! Thanks for all of the great excursions sailing, hiking, camping, biking, barbecuing, and rock climbing over the last six years. A few special shout-outs—to Lucy Acton for editing my entire thesis, I am eternally grateful; to Duncan for all of the awesome food and support provided during the final throes of thesis writing; to Netta, who's been here the whole time with me; to Lawton for the many late-night study sessions during the early years of graduate school; to the Gaines family, who provided my home away from home during all the time I spent in Woods Hole; to my terrific housemates past and present—Woody, Ian, Tom and especially Tomo; and last but not least to Dr. Locke, who first taught me to appreciate and celebrate the written word, and to the excellent and expert staff in the Mechanical Engineering Department and LCSR, without whose help none of this would have been possible.

Finally, I owe a huge debt of gratitude to my family—to my parents Gus and Anitra Webster for their unflagging encouragement and unfettered optimism throughout my academic career; to my brother Seth for caring what a Kalman filter is; to my sister-in-law Millie for putting up with, and even encouraging, Seth and me; to my nephew Ben for providing the entertainment at my defense and reminding me what's really important; to Grandpa Bard for the 1932 Johnson Sea Horse outboard engine; and to my cousin Stephanie for being a great friend. I am extraordinarily touched by how much you all celebrate my accomplishments; I could not have made it this far without your love and support.

Dedication

This dissertation is dedicated to my Grandfather.

Lawrence A. Bard
Industrial Engineer
Bryan, Ohio

Contents

List of Tables

List of Figures

List of Acronyms

CEIF centralized extended information filter

CEKF centralized extended Kalman filter

DEIF decentralized extended information filter

DOF degree-of-freedom

DVL Doppler velocity log

EIF extended information filter

EKF extended Kalman filter

GPS global positioning system

LBL long baseline

MLE maximum likelihood estimator

OWTT one-way travel-time

PPS pulse-per-second

TOA time-of-arrival

TOL time-of-launch

USBL ultra-short baseline

WHOI Woods Hole Oceanographic Institution

Chapter 1

Introduction

A great help also would be for the furtherance of skill, if those that are practisers in that Arte [of Navigation], and such as are Students of the Mathematikes, might often conferre together. For except there be a uniting of knowledge with practice, there can be nothing excellent.

William Barlow in *Navigator's Supply* (1597)

1.1 Motivation

The world's oceans cover more than 70% of our planet, but we presently know less about the submerged surface of the earth than we do about the surface of the moon. The oceans hold information that is important in basic research and our daily lives. They can provide clues to widely disparate areas of study, such as how species adapt to different depths and temperatures and how ocean circulation contributes to global climate regulation. To help understand these phenomena, we use underwater robotic vehicles to collect biological and geological samples, create accurate maps, and deploy and recover experiments. To enable these scientific activities, we must be able to accurately and repeatably measure vehicle position. The challenge, however, is that the global positioning system (GPS) does not work underwater.

In lieu of GPS, underwater navigation is most commonly accomplished using sound—for instance, garnering range measurements from the time-of-flight of acoustic signals. However, existing high-precision absolute acoustic navigation methods for underwater vehicles are impractical over long length scales (on the order of 10 km or more). Moreover, many existing acoustic navigation systems lack scalability for simultaneously navigating

multiple vehicles. In comparison to land-based radio frequency navigation and communication methods, underwater acoustic navigation and communication using underwater modems suffers from severely limited bandwidth and high latency [53]. Given the speed of sound in water ($\sim$1500 m/s), transmitting acoustic data over length scales on the order of kilometers results in latency on the order of seconds. Although the bandwidth of acoustic modem technology has increased dramatically in recent years, achieving throughput of up to 2400 bps [84], operationally the average throughput is on the order of 10-50 bps due to the low duty cycle with which acoustic messages are typically transmitted during underwater vehicle operations. As a result, existing multi-vehicle navigation algorithms that rely on high-bandwidth communication are of limited practical use underwater.

The goal of this thesis is to enable high-precision absolute navigation of multiple underwater vehicles over length scales on the order of 1 to 100 km. To support the simultaneous navigation of multiple underwater vehicles, we seek a flexible, scalable solution through a decentralized approach. This thesis focuses on a new navigation algorithm employing a single beacon that can be mounted on a ship. The algorithm is designed to work in a low-bandwidth environment, scale naturally to multiple vehicles, and avoid the geographical constraint imposed by fixed acoustic beacons.

1.2 Thesis Contributions and Roadmap

This thesis reports the development, implementation, and evaluation of a new navigation system for underwater vehicles, as well as the derivation of two navigation algorithms based on ranges from a single moving reference beacon (e.g. range-aided navigation). The navigation algorithms are a centralized implementation and a decentralized implementation of range-aided navigation based on the extended Kalman filter and the extended information filter respectively. The navigation system was tested in simulation and full-scale field trials. The centralized filter is experimentally validated with data collected during field trials and the decentralized filter is validated through simulation.

Review of Underwater Navigation and Previous Research

Chapter 2 reviews the current standard methods for underwater navigation, the previous research on the relatively unexploited method of single-beacon navigation, and the details of single-beacon one-way-travel-time (OWTT) navigation—the navigation method addressed in this thesis—which was first published in [27] and [28].

Acoustic Communications (Acomms) System

Chapter 3 reports the development of a novel navigation system for underwater vehicles that implements OWTT navigation, employing synchronous clocks and acoustic modems in addition to standard shipboard and vehicle-based navigation sensors to achieve simultaneous acoustic communication and navigation. Details of the Acomms system's performance and engineering accomplishments during four different oceanographic expeditions are presented. This work was published in part by the author and collaborators in [92].

System Models

Chapter 4 describes the process models for the vehicle and the ship and the observation models used in this thesis. These models are used in the formulation of both the Kalman filter and the information filter. These models are published in conjunction with the work in Chapter 5.

Centralized Extended Kalman Filter Algorithm and Benchmark

Chapter 5 reports the formulation and implementation of a centralized algorithm based on the extended Kalman filter and designed to estimate vehicle and ship position within the framework of single-beacon OWTT navigation. The centralized (CEKF) algorithm is designed to have simultaneous access to all sensor measurements from both the vehicle and the ship. Field results are reported from an autonomous underwater vehicle (AUV) survey carried out in 4000 m of water on the southern Mid-Atlantic Ridge while carrying out a near-bottom survey in search of hydrothermal vents. The experimental results presented demonstrate that single-beacon navigation is a viable alternative to traditional absolute acoustic navigation methods, and the CEKF is used as a benchmark for the decentralized algorithm discussed in Chapter 6. This CEKF work was published in part by the author and collaborators in [93].

Decentralized Extended Information Filter Algorithm

Chapter 6 reports the derivation of a decentralized algorithm based on the extended information filter for single-beacon OWTT navigation. The decentralized (DEIF) algorithm is designed to run locally on a submerged vehicle with real-time access to measurements from only the vehicle's on-board navigation sensors and with infrequent, asynchronous reception of acoustic broadcasts containing information from the ship. The DEIF algorithm is designed to be implemented in real time on one or more underwater vehicles. The DEIF is shown analytically to replicate exactly the state estimate of the CEKF immediately after each range measurement, and the analytical results are supported using a simulation of the deep-water experimental data set from Chapter 5. To the best knowledge of the author, this work is the first to formulate and test an extended information filter in the context of decentralized single-beacon navigation for underwater vehicles. This work has been accepted for publication in [94].

Future Work

Conclusions and future work are discussed in Chapter 7, including the extension of the decentralized algorithm to multi-vehicle operations employing inter-vehicle ranges.

Chapter 2

Underwater Vehicle Navigation

The ability to estimate the position of an underwater vehicle reliably, repeatably, and accurately is a necessary prerequisite for collecting high resolution oceanographic data, creating meaningful, high-resolution maps, and locating and relocating sites of interest in the ocean. This chapter reviews conventional underwater navigation methods as well as previous work reported in single-beacon and decentralized navigation. The remainder of the chapter is organized as follows: Section 2.1 reviews conventional navigation. Section 2.2 reviews previously reported results on single-beacon navigation and details of the implementation used in this thesis. Section 2.3 reviews previously reported results in decentralized estimation in the context of underwater navigation. Section 2.4 reviews previously reported navigation methods, both land- and water-based, that rely on the information filter. Section 2.5 concludes with a brief literature review of range-only simultaneous localization and mapping (RO-SLAM).

2.1 Conventional Navigation Methods

Conventional underwater navigation methods can be loosely categorized as either methods that provide bounded-error position estimates or methods that do not, resulting in position estimates with errors that are unbounded over time.

2.1.1 Dead Reckoning

Navigation based on velocity and heading, commonly referred to as dead reckoning, has long been a staple of nautical navigation [11]. Dead reckoning relies on an initial georeferenced position estimate, referred to as a position fix, and propagates this fix forward by

estimating the direction and distance traveled by the ship or vehicle. The distance traveled is estimated by integrating velocity or acceleration measurements to calculate relative displacement. In addition to these sensors, underwater vehicles typically have a depth sensor and a compass. The typical suite of vehicle-based navigation sensors available to underwater vehicles, depending on the vehicle size and budget, is shown in Table 2.1, where z denotes depth or altitude, $\ddot{x}$ denotes linear accelerations in the world frame, $\ddot{x}_{body}$ denotes linear accelerations in the body frame, ω denotes angular velocities, and $\dot{\omega}$ denotes angular accelerations.

Table 2.1: Navigation sensors commonly used in underwater vehicles.

Instrument	**Variable**	**Update Rate**	**Precision**	**Range**	**Drift**
Acoustic Altimeter	z (altitude)	0.1–10 Hz	0.01–1.0 m	varies w/ freq	—
Pressure Sensor	z (depth)	1 Hz	0.01–0.1%	11 km	—
Inclinometer	roll, pitch	1–10 Hz	0.1°–1°	$\pm 45°$	—
Magnetic Compass	heading	1–10 Hz	1–10°	360°	—
Gyro: Mechanical	heading	1–10 Hz	0.1°	360°	$10°/h$
Gyro: Ring-laser and Fiber-optic	heading	1–1600 Hz	0.01°–0.1°	360°	$0.1–10°/h$
Gyro: North Seeking	heading, pitch, roll,$\ddot{x}$,ω	1–100 Hz	0.01°–0.1°	360°	—
IMU	$\ddot{x}$,ω,$\dot{\omega}$	1–1000 Hz	0.01 m	varies	varies
Bottom-lock Doppler	$\dot{x}_{body}$	1–5 Hz	$\leq 0.3\%$	18–100 m	—

Source: Kinsey et al. [54]

In underwater vehicle navigation several methods for estimating vehicle velocity are common. A Doppler velocity log currently provides the most accurate estimate of linear velocity available to underwater vehicles. On torpedo-shaped vehicles the angular velocity of the propeller is sometimes used as a proxy for a forward velocity, and the direction of travel is assumed to be parallel to heading of the vehicle.

The advantage of dead reckoning is that it can be performed using only vehicle-based sensors. The disadvantage is that dead reckoning accrues error at a rate determined by the precision of these sensors and yields an estimate of local displacement with errors that are unbounded over time. In order to achieve bounded-error navigation, additional navigation information is required from an absolute georeferenced source.

2.1.2 Bounded-Error Navigation

Bounded-error navigation underwater is usually achieved with the aid of systems that rely on external sensors such as long baseline (LBL) or ultra-short baseline (USBL) navigation [68]. Table 2.2 shows a comparison between LBL, USBL, and global positioning

system (GPS) position measurements. Between position fixes, a vehicle estimates its position using velocity, acceleration, and attitude measurements as in dead reckoning. An extreme example of this is underwater gliders such as the Slocum glider that uses GPS to measure a position fix while on the surface, but navigates solely by dead reckoning between GPS fixes—typically for periods on the order of hours or days [91].

Table 2.2: Georeferenced navigation sensors used to measure XYZ position.

Instrument	**Variable**	**Update Rate**	**Precision**	**Range**
Global Positioning System	xyz	1–10 Hz	0.1–10 m in air	0 km in water
Long Baseline (300 kHz)	xyz	1–10 Hz	$\pm$0.007 m	0.1 km
Long Baseline (12 kHz)	xyz	0.1–1.0 Hz	0.1–10 m	5-10 km
Ultra-Short Baseline	range & bearing	0.02–0.5 Hz	0.1–2.0% of range	0.1-10 km

Source: Kinsey et al. [54]

LBL navigation relies on acoustic beacons that are typically deployed as subsurface moorings, 50-600 m above the seafloor, prior to vehicle deployment [68]. After deployment, the beacon locations are surveyed from the ship by collecting two-way travel times between the beacon and the ship's transducer as the ship navigates around the estimated beacon location. The position of the ship's transducer is known from GPS and the ship's gyrocompass so that, taking into account the sound velocity profile, a least squares estimate of the beacon position can be found. A careful beacon survey can result in residuals on the order of one meter or less in several thousand meters of water. Once the vehicle is deployed, it interrogates the beacons and the beacons respond with a fixed, known turnaround time. Using an estimate of sound velocity, the vehicle uses the two-way travel-time to estimate its range from each beacon and can thus triangulate its own position.

The principal advantage of LBL navigation is that it provides absolute geodetic navigation fixes. One of the disadvantages of LBL navigation is that, in most cases, the beacons are fixed, thus limiting the vehicle to a 5-10 km range for 12 kHz LBL. In addition, the beacons and the time required to deploy, survey, and recover them are costly in terms of the hardware, the cost of ship time, and the time lost during the expedition.[1]

USBL navigation relies on the calculation of a vehicle's *relative* displacement from a single external beacon typically mounted on a ship. Range, azimuth, and elevation are measured using an acoustic signal—the two-way travel time of the signal is used to determine range, a small transducer array is used to determine the azimuth and elevation of the incoming acoustic signal. Provided that the external beacon has a known location, it is possible to compute a geodetic fix for the vehicle. However, the vehicle position information is typically calculated at the external beacon, not on-board the vehicle, and is therefore

[1] Acoustic navigation beacons rated for full-ocean-depth operation typically cost more than $10k each. An acoustic beacon survey at full-ocean-depth takes $\sim$1–24 hours of ship time, and a large oceanographic ship such as an AGOR-25 class vessel, e.g. R/V *Atlantis* and R/V *Thomas G. Thompson*, costs $\sim$$30k/day.

not available to the vehicle unless the information is communicated acoustically or through some other means.

Because USBL navigation does not rely on a fixed external beacon, as is commonly the case with LBL navigation, the use of USBL does not constrain the vehicle to an area of the seafloor. However, the range limitations in a USBL system are more severe than LBL because a USBL system measures range and bearing, and error in the bearing measurement results in greater error in the position estimate of the vehicle at longer ranges. Thus the precision of the vehicle position estimate is a function of the range between the ship and the vehicle. This effectively depth-limits USBL systems depending on the desired precision.

2.2 Single-Beacon Navigation

In this thesis *range-aided navigation* refers to vehicle navigation that relies on ranges from one or more georeferenced sources *in addition to* supplementary non-georeferenced navigation information from additional sources such as inertial sensors. The term *range-only* navigation is reserved for navigation based solely on range measurements, possibly from multiple sources, with no additional navigation information. Single-beacon navigation is the minimal implementation of range-aided navigation, relying on range measurements from a single, georeferenced beacon to provide an absolute position reference. Conversely, long baseline could be considered the maximal implementation of range-aided navigation whereby ranges from multiple beacons are measured concurrently.

Compared to long baseline navigation, single-beacon navigation reduces the system complexity at the expense of reduced dimensionality of the constraint on vehicle position for each measurement. By virtue of requiring only one beacon, single-beacon navigation requires less equipment than traditional long-baseline. Additionally, the implementation of single-beacon navigation used in this thesis relies only on a ship-based beacon, eliminating the costly and time-consuming deployment and beacon survey. However, a single range measurement provides no position information in the direction orthogonal to the direction of the range measurement, relying on multiple measurements at different times and at different relative bearings to provide a fully observable solution.

Observability in single-beacon navigation has been covered from several perspectives as described in Appendix A.5. This thesis will not discuss the details of observability, but the consensus is that vehicle position is globally observable provided vehicle heading is known, the vehicle is not travelling directly towards or away from the beacon, and at least three range measurements have been made that are not along a linear vehicle trajectory (i.e. range measurements have been made at three non-collinear points).

The remainder of this section describes single-beacon one-way travel-time navigation, the implementation of single-beacon navigation advanced in this thesis, followed by a review of prior research on single-beacon navigation.

2.2.1 Single-Beacon One-Way-Travel-Time Navigation

Single-beacon one-way travel-time (OWTT) navigation relies on range estimation from the time-of-flight (TOF) of acoustic data packets propagating between a reference beacon with a known, though not necessarily stationary, location and the underwater vehicle to provide a reference to the world frame [27, 28]. The implementation of OWTT navigation, discussed in detail in Chapter 3, requires underwater acoustic modems on both the reference beacon and the underwater vehicle, as well as precision clocks to synchronize the modems. Figure 2.1 depicts a ship-based acoustic modem broadcasting acoustic data packets to multiple underwater vehicles. The acoustic data packets broadcast by the reference beacon (in this case a ship) encode both the time-of-launch (TOL) and information about the geodetic location of the sender's transducer at the TOL. The time-of-arrival (TOA) of this acoustic data packet at the receiver, combined with the decoded TOL and the position information in the acoustic data packet, are used to estimate range. A range measurement, in conjunction with the depth of the vehicle measured from a pressure sensor, constrains the vehicle position to a circle of solutions. Between range measurements, relative vehicle motion is estimated using velocity and attitude measurements.

The one-way time-of-flight is calculated from the difference between the TOL encoded in the acoustic packet, measured by a precision clock and modem system aboard the ship, and the TOA, measured by a precision clock and modem system aboard the underwater vehicle. The accuracy of this TOF measurements is limited by the accuracy of the precision clocks residing on the ship and the underwater vehicle. To ensure valid TOF measurements, it is crucial that the clocks on the sender and receiver remain synchronized throughout the dive to within an acceptable tolerance. The time-keeping problem and our solution are discussed in more detail in Section 3.2.2.

OWTT navigation provides bounded-error position estimates. Moreover, when the ship and vehicle navigate in concert, navigation can be conducted on an unbounded area. This is in contrast to a conventional 12 kHz LBL system using fixed beacons that provides navigation only within a range of a 5-10 km radius from the beacons. OWTT navigation provides scalability as well, allowing any vehicles within acoustic range to simultaneously use the same acoustic data packet broadcast independent of the number of vehicles.

2.2.2 Prior Single-Beacon Navigation Research

An in-depth review of selected single-beacon navigation papers—including a summary of the observation and process models used and a summary of the authors' conclusions—is provided in Appendix A. This section provides a more inclusive, though less detailed, overview of prior research in single-beacon navigation.

The majority of prior literature in single-beacon navigation reports estimation algorithms and the results of numerical simulations of these algorithms. Only a few report experimental evaluations of the proposed algorithms, and even fewer employ independent navigation methods to evaluate quantitatively the accuracy of the proposed methods.

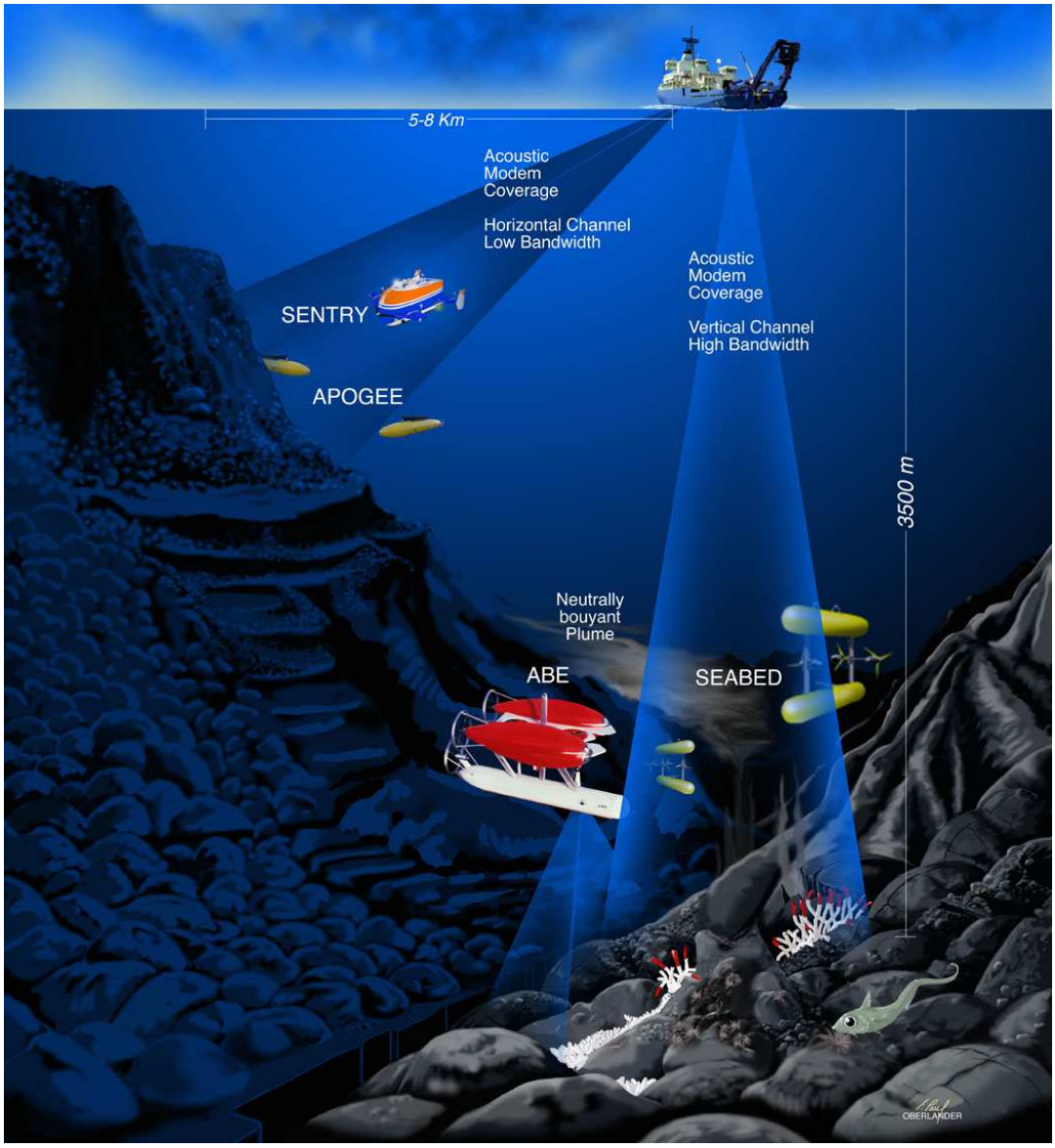

Figure 2.1: Acoustic data packet broadcast from the ship to multiple vehicles (RIP ABE). Photo credit: Paul Oberlander, WHOI.

The earliest formulation of vehicle navigation using ranges from a single beacon that is known to the authors is reported in [80]. This approach employs least-squares to estimate the unknown initial vehicle position and a constant-velocity unknown current; additionally, a linear algebra-based observability analysis is reported.

Range-only localization methods used for estimating the position of a target are addressed by [76] and [85]. In [76] the authors assume a constant-velocity, constant-bearing target trajectory and compute the theoretical Cramér-Rao bound and compare it to the per-

formance of a maximum-likelihood estimator (MLE), an extended Kalman filter (EKF), and a regularized particle filter during field tests. In [85] the author assumes a target with constant acceleration and addresses the observability of the target-tracker problem using the Fisher information matrix and reports simulation results using an EKF. In related work, [1] implements the EKF from [85] and reports simulation results.

Several different methods for addressing the observability of single-beacon navigation are reported in the literature. The papers [32–35] report an observability analysis employing limiting systems to assess uniform observability, and derive sufficient conditions for the existence of an observer with exponentially decaying estimation error for the cases of both known and unknown ambient currents. The authors report field results from their implementation of an EKF. In related work [62] extends the EKF reported in [32–35] to three-dimensional coordinates with simulation results.

A concise observability analysis in continuous time is reported in [77] using Lie derivatives to compute conditions for which the system has local weak observability. In [48] the authors report an algebraic analysis showing local uniform observability based on signal estimation techniques, though the lack of an estimation model disallows the computation of an updated position in the absence of a new measurement.

The use of EKFs for homing and single-beacon navigation, initialized by least-squares, is reported in [3,4,89] with both simulation and field trials. Similarly, in [18] the authors report an EKF initialized by a minimum mean squared error solution with simulation results. In [4] the authors also report a simulated two-vehicle system using a cascaded approach in which the second vehicle navigates relative to the first vehicle using inter-vehicle range measurements.

The papers [58–60] report an error state EKF for single-beacon navigation based on error models of the vehicle's inertial navigation system. The authors report results using a combination of field and simulation data.

More recent least-squares solutions are reported in [65], [42], and [57]. In [65] the authors report a nonlinear least mean square method for estimating a vehicle's initial position after which it relies on dead reckoning. In [42] the author reports an ad hoc iterative technique to estimate course. In [57] the author reports a method for advancing multiple single-beacon fixes along the vehicle's estimated trackline to simulate a multi-beacon fix.

An extended set-valued observer is reported in [63]. The authors show this observer provides bounds on the estimation error in the presence of non-linearities in the model and non-Gaussian noise, guaranteeing that the true vehicle position is contained within the estimator's predicted error covariance ellipsoid when linearization error and noise are correctly characterized.

Single-beacon navigation using differential Doppler measurements is reported in [17] with simulation results. Navigation using range-rate single-beacon measurements is discussed in [81]. In [83] the authors describe and provide experimental results for several methods of single- and multi-beacon navigation, including ranges based on one-way travel-time measurements from one or two beacons and the time-difference of arrival from multiple synchronized beacons.

This thesis is concerned with advancing the single-beacon navigation method first described in [27] and [28], in which the authors report the theory and first experimental results in single-beacon one-way-travel-time (OWTT) acoustic navigation with an acoustic modem and precision timing board. The authors employ a maximum-likelihood estimator and report field results from shallow-water sea trials. This thesis extends OWTT navigation to a centralized EKF and includes results from deep-water field trials as described in Chapter 5 and reported in part in [93]. This thesis also extends OWTT navigation to a decentralized extended information filter (EIF) and includes simulation results as described in Chapter 6 and reported in part in [94].

The single-beacon navigation method reported that most closely resembles the work presented in this thesis is [29]. In [29] the authors report a system employing a single moving georeferenced beacon to support the localization of multiple vehicles through asynchronous acoustic broadcasts. This work is a single-beacon implementation of the decentralized multi-vehicle navigation method reported in [5, 6], which is discussed briefly in Section 2.3 and in more detail in Section 6.4.3. The principal difference between [29] and the decentralized OWTT navigation algorithm reported herein is that [29] uses an ad hoc vehicle-based EKF to perform range measurement updates that rely on the absolute position and covariance broadcast from the reference beacon. In contrast, the decentralized method reported herein relies on incremental data broadcast from the reference beacon, allowing us to exactly recreate the results of a centralized EKF that has access to measurements from both the vehicle and the beacon's navigation sensors.

2.3 Decentralized Estimation in Navigation

Decentralized estimation in the context of underwater communication and navigation faces unique constraints in terms of low bandwidth and high latency, which renders many of the decentralized estimation solutions from land-based applications unsuitable. Until recently little research has been done on the topic of decentralized estimators and multi-vehicle navigation in the field of underwater robotics. However, as the cost of vehicles has decreased and their reliability improved, increased interest in multi-vehicle operations within the ocean science community has precipitated new research in this area.

The authors of [5, 6] address cooperative localization of multiple underwater and surface vehicles in a SLAM framework using ranges between multiple vehicles and reference beacons. The method presented allows a vehicle running a Bayes estimator to use range and position information broadcast from one or more moving beacons; the mechanics of the algorithm are discussed in more detail in Section 6.4. This work expands on the moving long baseline concept in [90] to encompass multiple range sources and real-time operation. The authors of [69] address a similar concept to moving long baseline and compare the effect of the use of the Kalman filter versus the particle filter on the vehicle's localization performance.

2.4 Navigation using Information Filters

To date, the information filter has not been widely used for navigation in the field of robotics. Derived in detail in [70], the extended information filter (EIF) has been employed for vehicle navigation [15] and SLAM algorithms [74, 87] in the context of land-based robotics. In the context of underwater vehicles, the EIF is most widely used for coordinated control, but there are a few examples of the EIF being employed in SLAM algorithms [22, 26].

2.5 Range-Only Simultaneous Localization and Mapping

Though not directly related to single-beacon navigation, range-only simultaneous localization and mapping (RO-SLAM) is briefly reviewed here. RO-SLAM is concerned with estimating vehicle position relying solely on range information from multiple beacons. The extension of RO-SLAM to multiple vehicles is similar to the future work proposed in this thesis—incorporating inter-vehicle ranges from multiple vehicles into a decentralized navigation solution.

The authors of [71, 72] address RO-SLAM for underwater vehicles and report experimental results. In this formulation multiple beacons are used but a priori beacon location is not known. Multi-beacon, range-only navigation for terrestrial vehicles in a SLAM framework is addressed in [23, 24, 51, 52, 55, 56] using radio-frequency beacons for range measurement, in [64] using audible sound, in [67, 86] using wireless sensor networks, and in [9, 10] with an unspecified range sensor. Specifically in the context of wireless networks, the author of [61] computes the Cramér-Rao bound on positioning accuracy using range measurements between multiple agents and illustrates with simulation.

Chapter 3

A Platform-Independent Acoustic Communication and Navigation System

3.1 Introduction

This chapter describes a platform-independent acoustic communication system, referred to as the Acomms system, designed by the author and collaborators to enable multiple nodes (any combination of underwater vehicles, surface ships, and fixed beacons) to simultaneously exchange data and calculate inter-node ranges with one meter accuracy with up to 10 km range. The Acomms system and field results herein are reported in part in [92].

Multi-vehicle operations are motivated by the desire to collect richer data sets, i.e. increased spatial extent, spatial resolution, and/or the variety of data types. The combined communication and navigation system described herein supports one-way-travel-time (OWTT) navigation, which enables one or more vehicles to use a single, georeferenced, moving beacon, e.g. the ship, to perform bounded-error navigation. As discussed in detail in Chapter 2, bounded-error navigation is achieved currently with the aid of systems such as long baseline (LBL) or ultra-short baseline (USBL) navigation. LBL navigation requires external, fixed reference beacons that have a range of only 5-10 km and require additional survey and recovery time, while the accuracy of USBL navigation is approximately 1% of range, which limits its usefulness over long ranges. Using the ship as a single reference beacon, OWTT navigation enables the vehicles to travel over tens of kilometers limited only by speed and endurance and removing the need for external beacons. In addi-

tion, the accuracy of the range measurements used in OWTT navigation is independent of range.

Advances in underwater communication systems promise improved communication and connectivity for underwater vehicles. Acoustic communication systems are increasingly employed on untethered underwater vehicles, which have historically had limited telemetry when submerged. The Acomms system supports two types of acoustic communication: *asynchronous* communication, which is the most commonly used for sending data, and *synchronous* communication, which in addition to communication enables navigation using inter-node ranges derived from the one-way travel-times of acoustic messages between nodes.

The Acomms system hardware is implemented with a dedicated software program, Linux host computers, acoustic underwater modems, and precision reference clocks. The acoustic communications software configures the modem, manages all acoustic communication traffic, and acts as an interface between the vehicle-specific software and the modems and clocks. While the communications and one-way travel time features are provided using the Woods Hole Oceanographic Institution (WHOI) Micro-Modems [30, 31] and the PPS-Board [27,28], the concepts have been developed in a hardware independent framework and can be used with any acoustic system or combination of systems that includes bidirectional communications with synchronous transmission and precision time-tagged reception.

The Acomms software and related hardware have been installed on the Woods Hole Oceanographic Institution vehicles *Puma*, *Jaguar*, and *Nereus*, and have been deployed successfully in sea trials at the southern Mid-Atlantic Ridge [93], the Mariana Trench [12, 13, 96], and the Cayman Trough [37]. This chapter covers the system architecture in detail and results from each of the field trials.

3.2 Acoustic Communication

The Acomms software, designed to operate symmetrically on all nodes, initializes the modem and issues a sequence of modem commands, defined by the user, to initiate data transmissions between nodes, transmit ranging pings, and interrogate acoustic navigation beacons. In addition, the Acomms software enables the user to specify modem configurations and ensures that the modem is properly configured after a vehicle or modem reboot. The Acomms software time-stamps and logs all modem communication traffic and Acomms-related data, provides basic format checking for messages sent to the modem, monitors the state of the modem, tracks message traffic and modem status, and reports modem statistics to the vehicle controller. Details of the Acomms software are discussed in Section 3.3.4.

3.2.1 Asynchronous Communication

The majority of vehicles that use underwater modems operate their modems asynchronously: the modems are used to transmit data and send commands between nodes—where a node can be an underwater vehicle, a ship, or a fixed entity such as a mooring—without the need for precision or synchronized time-keeping among the nodes. During asynchronous operation, a modem on one node is typically designated as the *master* modem. The master modem initiates acoustic communications for all nodes in a deployment, eliminating the potential for collisions between acoustic data transmissions.

3.2.2 Synchronous Communication and Navigation

In addition to asynchronous communication capabilities, the Acomms system enables synchronous communication and navigation when equipped with a precision clock. For synchronous communication, topside nodes, i.e. nodes that are not submerged, rely on a global positioning system (GPS) timeserver for their timing reference. Subsea each node is equipped with a free-running precision clock as a timing reference that is synchronized to a GPS timeserver prior to the start of the dive. Details of the implementation are covered in Section 3.3.

OWTT navigation, first proposed in [27], uses one-way travel times of acoustic messages to estimate range between subsea nodes and a surface node, such as a vehicle or ship equipped with a GPS receiver, that has knowledge of its position in the world frame [27, 28, 93]. OWTT navigation employs acoustic broadcasts of data packets that contain information about the transmitter's position and the time at which the message was transmitted. Because the transmitter and receiver clocks are synchronized, the receiver can calculate the time-of-flight of the acoustic broadcast using the time-of-arrival of the message and the time-of-launch that is encoded in the data packet. Time-of-flight information combined with the acoustically encoded position information from the transmitter provides a range measurement from a known position in the world frame. Between range measurements the vehicle performs dead reckoning. OWTT navigation is covered in detail in Chapter 2 and [27], [28], and [93].

The Acomms software supports OWTT navigation through a message packing function that precisely controls the timing of messages provided to the modem as specified in [39] and can thus properly anticipate and encode the time-of-launch of the data packet. The Acomms software and hardware also ensures that the modem's internal clock, which is used to measure the time-of-arrival of messages, is properly disciplined.

In addition to enabling OWTT navigation, synchronous communication provides further advantages over asynchronous communication by making it possible to accurately predict the timing of acoustic transmissions of other nodes, thereby enabling synchronized time-division multiple access (TDMA) cycles among nodes. Typically, to avoid collision of acoustic messages, a single node is designated as the master that commands data transmissions for all nodes in a deployment. Synchronous communication eliminates the need

for a single master node because messages originating at different nodes can be scheduled a priori to not overlap. This feature, which was used extensively during field trials as described in Section 3.4, enables a higher throughput of data while also retaining the ability for an operator to transmit additional acoustic messages from the ship. Using synchronous communication, an operator knows the exact timing of the vehicle's sequence of acoustic transmissions and can reliably predict when the acoustic channel is clear for transmission from the ship, such as an abort message that commands the vehicle to return to the surface. For example, a vehicle's modem could be programmed to run a two-minute-long cycle of data transmissions that starts on the even minutes but begins with a thirty-second period during which no acoustic transmissions are scheduled. The shipboard operator then knows that the thirty-second period after every even minute is clear to transmit acoustic transmission from the ship to the vehicle without risking message collision. We have further exploited this functionality to enable on-the-fly switching between different modem configurations (e.g. frequency band, modulation method, bandwidth, and bitrate) as described in more detail in Section 3.3.1, which requires simultaneously reconfiguring both the transmitting and receiving modems.

Previously reported acoustic modem drivers for synchronous communication, such as the modem drivers employed on the Massachusetts Institute of Technology (MIT) autonomous surface vehicles [20], and the WHOI Seabed vehicles [27, 28], are not portable due to the tight integration of these modem drivers into the vehicle-specific application code of their respective vehicle control and navigation systems. In contrast, the Acomms software reported herein is portable, employs a vehicle-independent interface based on user datagram protocol (UDP) messages, runs as a stand-alone daemon on a host Linux CPU, and operates symmetrically on all node types—e.g. underwater vehicles, fixed beacons, and surface ships.

3.3 System Architecture

For asynchronous communication the Acomms system requires an acoustic underwater modem, a transducer, and a host computer at each node. Synchronous communication additionally requires that each node's computer be synchronized within an acceptable tolerance for the duration of the mission. For example, assuming a sound speed of 1500 m/s, a 10 ms offset between the sender and receiver results in a 15 m error in the range measurement. The architecture of the Acomms system in a typical two-node setup is depicted in Figure 3.1, where the vehicle is referred to as the subsea node and the ship is referred to as the topside node. Topside the Acomms software runs on a laptop running Ubuntu Linux and communicates with the shipboard modem via the network using UDP messages through a MOXA^{TM}serial device server. Computers on the topside network are synchronized to a GPS timeserver through the Network Time Protocol (NTP). In addition, the timeserver supplies a pulse-per-second (PPS) signal to the topside modem, which consists of a 1 Hz square wave that has its rising edge synchronized with the start of the second. During the

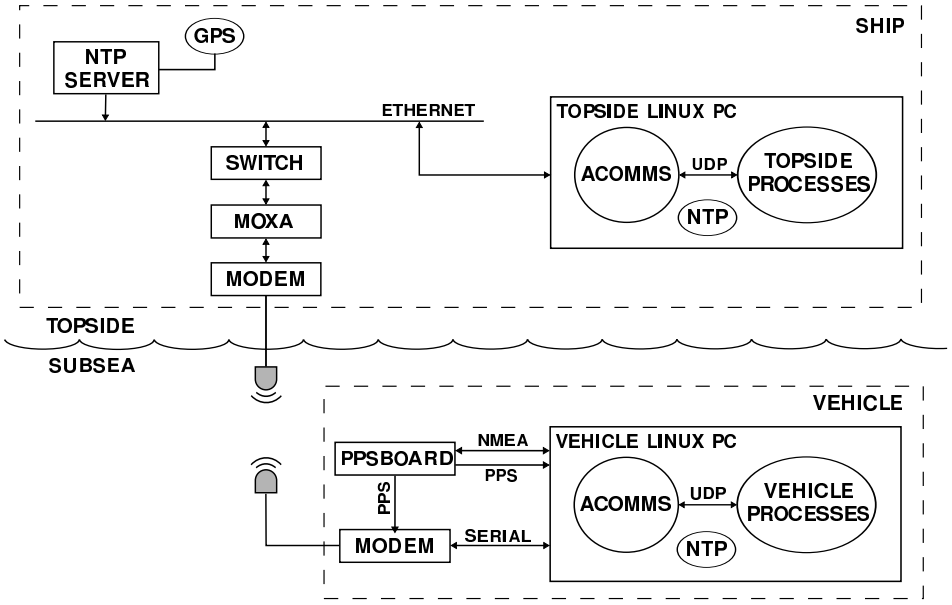

Figure 3.1: Typical sea-going architecture for a two-node deployment of the Acomms system.

field trials described here we used a Meinberg GPS/NTP shipboard timeserver [66].

Subsea, the Acomms software runs on the main vehicle computer, also running Ubuntu Linux, and communicates with the modem over a serial connection. Acomms communicates with the vehicle's controller and navigation processes over the vehicle's local network using UDP messages. At present, no commercially available precision clocks (such as the Meinberg noted above) are suitable for use on small autonomous underwater vehicles (AUVs) due to power and size constraints. To address this, we use the PPSBoard—a small, comparatively low-power, precision clock board suitable for AUV applications [27, 28]. The PPSBoard on the vehicle serves as the vehicle's on-board NTP timeserver and provides a PPS signal to the vehicle's modem. The acoustic modem used in the field trials described here is the WHOI Acoustic Micro-Modem. The individual components of the Acomms system are described in detail below.

3.3.1 WHOI Micro-Modem

The WHOI Micro-Modem is an acoustic modem capable of encoding and decoding acoustic data packets that it transmits through the water column [30, 31]. All Micro-Modems are able to transmit both frequency-shift keyed (FSK) and phase-shift keyed (PSK) encoded acoustic messages. All Micro-Modems are able to receive FSK encoded acoustic messages and, with the addition of a coprocessor board, are also able to receive PSK encoded messages. In Band A (8-12 kHz carrier frequency) 32-byte-long FSK-encoded data packets take 3-4 seconds to transmit. Mini-packets (32 bits long) take 840

ms to transmit. The range of the Micro-Modem varies with encoding, bandwidth, data-rate and the acoustic channel characteristics (horizontal/shallow channel versus vertical/deep channel). During recent trials in the Mariana Trench, the author and collaborators tested the modem's capabilities to the extremes of the vertical channel for a variety of combinations of encoding, bandwidth, and data-rates. PSK encoded data packets broadcast by the vehicle's modem at the lowest data-rate were reliably received by the ship's modem at up to 11 km [84].

The Micro-Modem employs its own internal clock to calculate the time-of-arrival of acoustic messages and the travel-time of ranging pings and replies from acoustic navigation beacons. When the modem is in synchronous navigation (SNV) mode, as described in [39], the modem's clock can be synchronized to a PPS signal using a NMEA clock message from the host. Once synchronized, the time-of-arrival (TOA) of each arriving message is reported to have an accuracy of $\pm$ 125 μs with respect to the PPS signal [31]. The accuracy of the PPS signals used topside and subsea are discussed in Sections 3.3.2 and 3.3.3 respectively. In SNV mode, all transmitted messages are initiated by the modem within $\pm$ 10 μs of the rising edge of the PPS signal [39].

3.3.2 PPSBoard

The PPSBoard provides a stable time reference that keeps the undersea vehicle's CPU clock and the vehicle's modem synchronized with the topside clock throughout the mission. The PPSBoard, described in detail in [27] and [28], was developed by Eustice and Whitcomb to provide a free-running, precision timing reference for use subsea that can be synchronized to a GPS timing signal. In addition to supplying a PPS signal to the Micro-Modem to enable its SNV mode described above, the PPSBoard is used to discipline the vehicle CPU's NTP server by providing a PPS signal and a NMEA-formatted clock message naming the upcoming second. The PPSBoard is synchronized to a GPS signal while the vehicle is on deck, and the drift characteristics of the board ($\sim$1 ms drift over 14 hours) ensure that the error introduced in the estimated range between the ship and the vehicle due to the relative drift between the two clocks is small—1 ms clock drift corresponds to 1.5 m error in the range between the ship and the vehicle assuming 1500 m/s sound velocity.

3.3.3 Topside NTP Timeserver

The Meinberg GPS/NTP timeserver, used during the field trials to provide a stable, shipboard timing reference, is a Stratum-1 NTP timeserver [66]. The topside computer stays synchronized with the timeserver over the network via NTP. The Meinberg also supplies a PPS signal, accurate to within 10 μs, to the topside modem.

3.3.4 Acomms Software

The Acomms software, written by the author with assistance from Louis L. Whitcomb, is a multi-threaded program written in C/C++ that uses modem driver code written by Matthew Grund. The Acomms software executes a state machine consisting of two sections: a modem initialization section and a TDMA sequence of commands. It is designed to act as a transport layer between the host computer and the modem, passing through all message traffic in both directions. All communications with the modem as well as various statistics on messages transmitted and received are time-stamped and logged. In addition, the Acomms software enables synchronous communication and navigation as described below.

The Acomms software is designed to run as a stand-alone process in either the foreground or the background, communicating with the modem and other processes via serial or network connections. The software is also able to run as a daemon thanks to Giancarlo Troni and Clayton Kunz. On *Nereus*, the Acomms daemon is started during the host computer boot-up process to ensure that the daemon is always running even in the event that the vehicle computer reboots.

Serial and Network Connections

The Acomms software allows the user to specify the connections to the modem and the host computer as shown in Figure 3.1. The Acomms software supports both serial I/O connection and network I/O connections. Network I/O connections use UDP and can either broadcast or unicast to a specified UDP port. A typical setup uses a serial connection to the modem on the vehicle and a network connection to the topside modem. On the vehicle the software typically communicates with the vehicle control and navigation processes over the network. The software is also able to route specific types of modem messages to different processes. For example one network I/O thread can communicate with the main vehicle process while a second network I/O thread communicates with the navigation process.

Modem Initialization

The Acomms software has a user-configurable initialization file that supports all of the WHOI Micro-Modem configurations. Configuration commands are sent to the modem when the Acomms process is started, and every time the Acomms process receives a message from the modem indicating that the modem has rebooted, in order to ensure that the modem stays properly configured.

TDMA Cycle

The Acomms software supports a user-configured TDMA cycle of modem commands that is executed continuously except when interrupted by the modem initialization process

or the clock watchdog (described below). The TDMA cycle is used to command the modem to transmit acoustic messages, interrogate long baseline (LBL) beacons, or change selective modem configurations on-the-fly such as the transmission frequency and bandwidth. Table 3.1 shows the TDMA commands currently available in the Acomms software.

Table 3.1: TDMA Cycle Command Summary

Command	Size	Addt'l Info
Configuration	n/a	supports all available cfgs
Ranging Ping	32 bits	returns OWTT between nodes
Mini-Packet	32 bits	user specified codes (e.g. Abort, UnAbort, etc.)
Cycle-Init	32 bits	initiates data TX between nodes
Data Packet	$32 - 2048$ bytes	user specified data, length varies by encoding type
LBL	n/a	listens on up to 4 frequencies
PAUSE	n/a	see Section 3.3.4
VLPAUSE	n/a	see Section 3.3.4

The commands PAUSE and VLPAUSE are special commands that pause the TDMA cycle before continuing to the next entry. PAUSE stops the TDMA cycle for a specified number of seconds, VLPAUSE pauses the TDMA cycle for a variable length of time in order to restart the TDMA cycle at an exactly specified interval (e.g. at the beginning of every even minute). These commands are used to insert time into the TDMA cycle so that the acoustic channel is clear for the modem to receive messages initiated at another node and, in the case of VLPAUSE, to synchronize the TDMA cycle with the vehicle clock.

Each entry in the TDMA cycle has an associated timeout period and a retry flag, such that if the step is not successfully completed by the end of the timeout period, the TDMA cycle will either proceed with sending the next message in the cycle or resend the current message as dictated by the retry flag. The Acomms software TDMA cycle is designed such that upon the successful completion of an entry in the TDMA cycle, the software can either proceed directly to the next entry, or it can wait for the full timeout specified for that entry (fixed interval timeout mode). For operations where higher message transmission rates are desired, the former is used. For operations where it is desirable to keep the TDMA cycle synchronized to the clock, the latter, in combination with a VLPAUSE, is used.

Synchronous Navigation Mode and Clock Watchdog

In order for the Acomms software to support the Micro-Modem's synchronous navigation (SNV) mode, the modem's clock must be initialized and monitored. This is accomplished by sending appropriately timed clock messages to the modem in conjunction with the PPS signal as described in [39]. The TDMA cycle sets the clock when Acomms is started, after every modem reboot, and whenever the clock watchdog is triggered by one of several indications that the modem clock needs to be set.

When the modem is in SNV mode, messages initiated by the modem are transmitted at the top-of-the-second, triggered by the rising edge of the PPS signal. The Acomms software monitors the timing of messages sent to the modem to ensure that the messages are provided adequately ahead of the top-of-the-second, as specified in [39], so that they can be transmitted at the top-of-the-second.

One potential pitfall of SNV mode is that in the event of the loss of the PPS signal, no acoustic messages will be initiated by the modem. To prevent a vehicle from losing all acoustic communications in this situation, a user-configurable timeout is provided such that after a given number of seconds without the PPS signal the state machine will send a command to take the modem out of SNV mode. Once the modem is not in SNV mode, messages will be sent regardless of the presence of the PPS signal. Message transmission will not be synchronized with the top of the second, making range measurements from the acoustic broadcasts impossible, but acoustic data transmission will resume.

Support for OWTT Navigation

To enable single-beacon one-way travel-time navigation as described in Section 3.2.2, the integer value of the top of the second at which a data packet will be transmitted must be encoded within the data packet. Because the Acomms process controls the timing of messages provided to the modem as described in Section 3.3.4, the Acomms process anticipates the time-of-launch of a data packet and over-writes a designated byte in the data packet's payload with the integer value of the anticipated time-of-launch. This is the only instance in which the Acomms process will modify a message sent from the host process before passing it to the modem.

3.4 Field Results

The Acomms system had been installed on three of WHOI's underwater vehicles—the hybrid remotely operated vehicle *Nereus* [13] and the *Puma* and *Jaguar* AUVs [82]. To date the system has been successfully deployed on four oceanographic expeditions, each one allowing us to develop and test new functionality for the Acomms system.

The Acomms system was first tested at sea in October 2007 during the deep-water field trials for *Nereus* near Oahu, Hawaii. During this expedition the Acomms system was used for asynchronous communication between the vehicle and the ship, enabling shipboard AUV operators to monitor the progress of and send commands to the new vehicle while it was submerged and operating autonomously [14]. In January 2008 the Acomms system was used for synchronous communication between the ship and the AUV *Puma* or *Jaguar* during an expedition to locate and map new hydrothermal vents on the southern Mid-Atlantic Ridge. The navigation results from this expedition provide experimental validation in post-processing for OWTT navigation [93]. In May-June 2009 the Acomms system provided synchronous communication between three nodes (*Nereus*, the ship, and a

depressor—described in more detail below) during *Nereus's* first dives to Challenger Deep in the Mariana Trench [12]. The depth of the site (10,903 m) and the expedition schedule precluded the use of a navigation ground truth such as LBL, but the multi-node configuration highlights the benefits of synchronous operation. In October 2009, the most recent Acomms deployment to date, the Acomms system was deployed with *Nereus* on an expedition to locate and map new hydrothermal vents in the Cayman Trough [37]. During this expedition, using two-node synchronous communication, not only were vehicle status updates sent from the vehicle to this ship, but also new mission plans and modifications to existing mission plans were sent from the ship to the vehicle, allowing shipboard AUV operators to modify the AUVs survey path in real time without recovering the vehicle.

3.4.1 November 2007, *Nereus*, Deep-Water Trials Asynchronous Two-Node Communication

The first full-scale at-sea deployment of the Acomms system was in November 2007 during field trials of the vehicle *Nereus* near the coast of Oahu, Hawaii. All Acomms-related hardware was installed on *Nereus* by Chris Taylor and John W. Bailey. The author installed the Acomms system software and was responsible for Acomms operations during the expedition. Christopher J. McFarland and Michael H. Brown assisted with the system install and testing. The Acomms system was used for asynchronous communication between the vehicle and the ship. Operations were conducted from the R/V *Kilo Moana*, a 185' small waterplane area, twin hull (SWATH) vessel operated by the University of Hawaii. Figures 3.2 and 3.3 show *Nereus* being lowered into the water from the R/V *Kilo Moana* configured as an AUV and an ROV respectively.

Nereus is a hybrid remotely operated vehicle (HROV) that is unique among full-ocean-depth underwater vehicles for two reasons: it can be configured as either a remotely operated vehicle or an autonomous underwater vehicle and it is designed to operate in up to 11 km of water [13]. *Nereus* has an EDO/Straza SP23 transducer mounted at the forward end of the starboard hull facing upwards. A second EDO/Straza SP23 transducer was lowered from the stern of the ship, facing downwards, in a baffled cage to reduce the ambient acoustic noise. During initial tests the transducer was lowered from the ship and held 1-2 meters below the surface of the water to keep it clear of the ship's propellers and other gear in the water. Later a bridle was used to reduce side-to-side motion and position the transducer 3-4 meters below the surface of the water. During two of the dives Benthos transponders were also lowered from the stern of the ship to test the modem's LBL functionality, though LBL beacons were not deployed at the site.

The Acomms software ran on the vehicle in both ROV and AUV mode. During this expedition, when the vehicle was in ROV mode, the Acomms software on the *ship* was typically designated as master using a TDMA cycle of modem messages consisting of a ranging ping to the vehicle, a request for a data packet to be transmitted from the vehicle to the ship, and an LBL ping if the LBL transducers were in the water. When the vehicle

Figure 3.2: The hybrid remotely operated vehicle *Nereus* configured as an AUV. Photo credit: Louis Whitcomb, JHU.

was in operation as an AUV, the Acomms software on the *vehicle* was typically designated as master using a TDMA cycle consisting of a data packet transmitted from the vehicle to the ship and a pause to allow for messages to be transmitted from the ship to the vehicle if necessary. There was no LBL ping because the LBL beacons were not deployed during the trials. The data packets transmitted from the vehicle to the ship contain vehicle status and health updates, including estimated position, speed, battery health, and the current goal or action. All messages were FSK-encoded. The synchronous navigation mode was not employed because the PPSBoard was not installed on the vehicle at that time.

During the expedition three successful ROV dives were completed to a maximum depth of 2257 m, with a total bottom time of 7 h 38 min. As an AUV the vehicle completed multiple shallow dives over a period of 11 h 33 min. The vehicle's maximum depth as an AUV was 22 m with 12 min of bottom time [14, 95]. Figure 3.4 shows the position data decoded in real time from acoustically transmitted status messages sent from the vehicle to the ship. These position data are overlaid on the full vehicle trackline that was retrieved after the conclusion of the dive. The real-time acoustic vehicle status updates allowed the AUV operators to monitor the vehicle's progress while it was submerged. In addition, we successfully tested an acoustic abort, where we sent an abort code to the vehicle using the Micro-Modems, commanding the vehicle to drop weights and return to the surface.

Figure 3.3: Lowering *Nereus* off the stern of the R/V *Kilo Moana*. Photo credit: Matthew Heintz, WHOI.

3.4.2 January 2008, *Puma* & *Jaguar*, Mid-Atlantic Ridge Synchronous Communication and Navigation

In January 2008 the Acomms system was deployed on the *Puma* and *Jaguar* AUVs during engineering trials for methods for locating and mapping new hydrothermal vents on the southern Mid-Atlantic Ridge in 4000 m of water. Chris Murphy assisted with the integration of the Acomms software on these AUVs. The author was responsible for the Acomms system operations during the expedition. Acoustic ranges and vehicle navigation data collected by the author and collaborators during Dive 03 with *Puma* were used by the author and collaborators in post-processing to experimentally validate the single-beacon one-way travel-time navigation methods described in Section 3.2.2. Figure 3.5 shows the AUV *Puma*; Figure 3.6 shows the trackline of the ship and the estimated trackline of the vehicle during Dive 03. This dive lasted 21 hours, of which 9 hours (the portion shown) were spent doing a gridded survey 200 m above the seafloor. Presented here is an analysis of the acoustic throughput of the Acomms system during this dive. The author's formulation of the OWTT navigation algorithm and the experimental navigation results from this expedition are covered in Chapter 5.

Both *Puma* and *Jaguar* have an upward-facing ITC-3013 [45] transducer mounted on the lower hull forward of the forward vertical yellow stanchion. An additional ITC-3013 was lowered over the side of the ship 3-6 m below the surface of the water facing down-

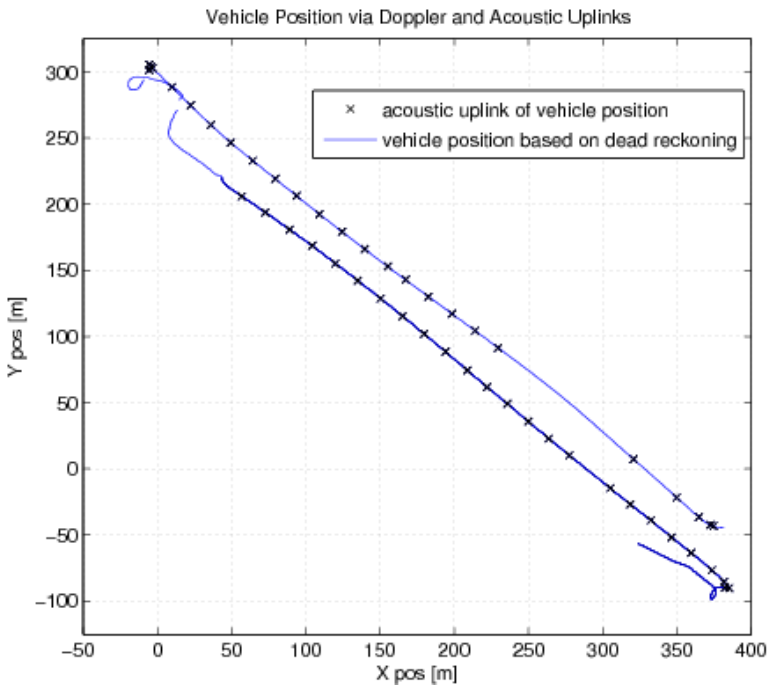

Figure 3.4: Real-time acoustically reported vehicle position overlaid on vehicle trackline.

Table 3.2: Two-minute TDMA cycle of modem messages during Dive 03.

Command	**Time [s]**
Data TX to ship	20
PING ship	10
LBL ping	20
Data RX from ship	20
PING ship	10
LBL ping	20
no acoustic TX	20
Total TDMA cycle time [s]	120

ward. Both vehicles also have PPSBoards installed, which enable the vehicle clocks to be synchronized with the topside clock. Three LBL transducers were deployed at the site. The Acomms software running on the vehicle was designated as the master and ran a two-minute TDMA cycle shown in Table 3.2. All modem communications were FSK-encoded. Travel times from the LBL interrogation were passed to the navigation process on the vehicle by the Acomms software.

During Dive 03, the vehicle modem had difficulty decoding messages it received once the vehicle's thrusters were enabled during the descent to the bottom and while the vehicle was at depth. We believe this difficulty was due to the location of the modem transducer on

Figure 3.5: AUV *Puma*. Photo credit: Louis Whitcomb, JHU.

the lower hull where the upper hull may have interfered with acoustic transmissions from the ship and/or due to electrical or acoustic noise from the vehicle thrusters. The successful throughput of messages was asymmetric and depended on the type of message (32-bit mini-packet versus full 32-byte data packet). For the dive shown here, 39% of mini packets transmitted from the vehicle to the ship were successfully received at the ship, whereas mini-packets transmitted from the ship to the vehicle were successfully received by the vehicle only 22% of the time. The successful receipt of 32-byte data packets is predicated on the success of the mini-packets: for a 32-byte message to be successfully received, a type of mini-packet called a cycle-init must first be successfully received. Because the vehicle was designated master, all cycle-inits originated from the vehicle. Thus, the maximum percent of data packet transmissions possible is limited by the 39% success rate of vehicle-to-ship mini-packets. Of the data transmissions that had successful cycle-inits, 59% of the data packets transmitted by the vehicle to the ship were successfully received and 25% of the ship-to-vehicle data packets were successfully received. This results in an overall success rate of 23% for vehicle-to-ship data packets and only 9.5% for ship-to-vehicle data packets. In addition to their sparsity, the messages received at the vehicle had time-of-flights that were largely inconsistent with the the time-of-flights of messages received at the ship. The cause of this discrepancy is still under investigation. The percentages presented here are based on a total of $\sim$ 2500 mini-packets (including ranging pings and cycle-inits) and $\sim$ 900 FSK-encoded data packets transmitted between the vehicle and the ship.

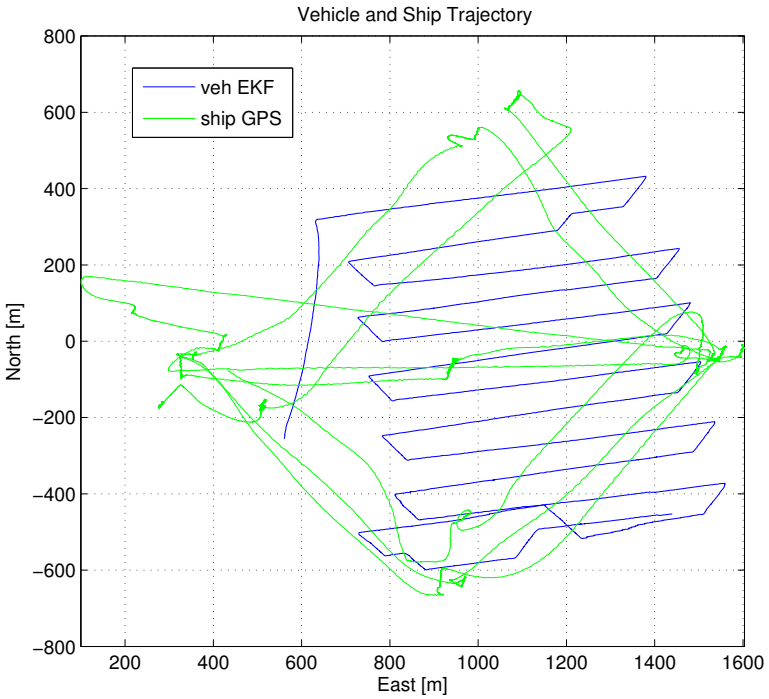

Figure 3.6: The ship trackline and estimated vehicle trackline during the 9-hour-long survey at 200m altitude.

3.4.3 May-June 2009, *Nereus*, Mariana Trench Synchronous Three-Node Communication

On May 31, 2009 *Nereus* completed the first of several dives to Challenger Deep in the Mariana Trench, reaching a maximum depth of 10,903 m. During these dives the Acomms software managed all acoustic communications between the vehicle, the depressor, and the ship. The author was responsible for the Acomms system operations. This was the first multi-node deployment with the Acomms system where we made use not only of the synchronized clocks on the vehicle and the ship to predict the vehicle's acoustic transmissions, but also actively initiated acoustic messages at each node as a regular part of the TDMA cycle in a true multi-master setup. Figure 3.7 shows the entire science and engineering team in front of Nereus with a bathymetric plot of Challenger Deep.

As described above, *Nereus* has an EDO/Straza SP23 transducer mounted at the forward end of the starboard hull facing upwards. Operations during this expedition were again conducted from the R/V *Kilo Moana* and the same bridle setup described in Section 3.4.1 was used for the shipboard EDO/Straza SP23 transducer. Figure 3.8 shows the author and the marine tech on the R/V *Kilo Moana*, Vic Polidoro, deploying the shipboard transducer. During this expedition, all dives were carried out with the vehicle in ROV mode with a depressor positioned around 5800 m deep for the deep dives. The depressor, shown in

Figure 3.7: The science and engineering team on board the R/V *Kilo Moana* after *Nereus* successfully completed three dives to Challenger Deep in the Mariana Trench. Photo credit: Barbara Fletcher, SPAWAR.

Figure 3.9, is the transition point between the standard steel-armored cable from the ship and the micro-fiber link to the vehicle. The depressor also carries a WHOI Micro-Modem, a PPSBoard, and a downward facing EDO/Straza SP23 transducer. The depressor modem is controlled from the ship and is intended to serve as an intermediate acoustic communication node for more reliable communication with the vehicle at full depth. LBL transducers were not deployed due to concerns over our ability to trigger the acoustic release mechanisms at 11 km deep from the ship. A detailed description of *Nereus* and the Mariana Trench deployment is reported in [12].

The six-minute TDMA cycle of messages used during the deep dives, shown in Table 3.3, consists of three two-minute schedules. Each schedule tests a different carrier frequency and bandwidth combination (referred to as Bands) using three different PSK data rates (see Table 3.4) and an FSK message when applicable (only Band A supports FSK). Each two-minute schedule includes a $\sim$30 second quiet time when an operator could initiate an acoustic message from the ship or the depressor, such as an Abort or a Ranging Ping. Sandipa Singh was responsible for the design of the TDMA cycle, while the author was responsible for its implementation and Acomms operations during the expedition. Because switching carrier frequencies and bandwidths requires changing the configuration on both the sending and receiving modems, this TDMA cycle would be impossible in practice without synchronized clocks on the vehicle, the depressor, and the ship.

As shown in Table 3.4.3 the successful throughput of messages versus range varied by

Figure 3.8: The author and shipboard marine tech deploying the Acomms transducer off the stern of the R/V *Kilo Moana*. Photo credit: Catherine Offinger, WHOI.

message types. Note that the carrier frequency is given for reference only—the acoustic range is not directly correlated to the carrier frequency. The operational range of the lower data-rate PSK messages, 11km, far exceeded the team's expectations, allowing direct communication from the vehicle to the ship throughout the deep dives. A complete analysis of acoustic communication performance during this expedition is reported in [84].

3.4.4 October 2009, *Nereus*, Cayman Trough On-The-Fly Subsea Mission Corrections

In October 2009 the Acomms system was again deployed with *Nereus* to the Cayman Trough in the western Caribbean Sea. The mission of this expedition was to locate and map new hydrothermal vents along the Mid-Cayman Rise, an ultra-slow spreading center with a maximum depth just over 6,800 m located at the center of the trough [7]. During this expedition Louis L. Whitcomb and James C. Kinsey were responsible for the Acomms system operations. During the first leg of the expedition *Nereus* was configured as an AUV; during the second leg of the expedition *Nereus* was operated as an ROV. The survey area in both cases was around 5200 m deep. During AUV operations, the vehicle operators used the Acomms system to monitor, in real time, both the vehicle position and health through navigation data packet uplinks and the science sensor data through science data packet uplinks. In addition, acoustic transmissions to the vehicle were used to modify the vehicle mission plan *in real time*. With this capability, the vehicle's path could be reprogrammed

Figure 3.9: The depressor shown on the aft deck of the R/V *Kilo Moana* with the depressor design team from SPAWAR. Photo credit: Catherine Offinger, WHOI.

from the surface without recovering and re-launching the vehicle—a lengthy process when the vehicle is operating at 5200 m. Figure 3.10 shows the science data that was acoustically sent to the ship from the vehicle, allowing the science and operations team to monitor the vehicle's progress in real time. Part way through the survey, the operations team acoustically broadcast new trackline information causing the vehicle to modify its mission plan in order to survey an area to the west of the original survey area. The new survey area contained strong evidence of hydrothermal activity as shown in the science data broadcast from the vehicle [37]. This functionality, not unique to the Acomms system, underscores the potential for acoustic communication to revolutionize autonomous vehicle operations.

3.5 Chapter Summary

The Acomms system has proven to be a valuable asset during autonomous vehicle operations, allowing AUV operators to monitor the status of the vehicle in real time, enabling multi-node systems to communicate efficiently without packet collision, and enabling on-the-fly mission corrections to the vehicle during subsea operations. In addition, one-way travel-time data collected by the author and collaborators using the Acomms system has experimentally validated single-beacon navigation in post-processing.

Table 3.3: Typical TDMA cycle of modem messages during Challenger Deep dives.

Command	**Description**	**Time [s]**
	Band A (10 kHz, 5kHz bandwidth)	
Configs	Set band, carrier freq, bandwidth	9
Ping	Topside pings Vehicle	21
Data Broadcast	Vehicle sends state data (FSK,0)	15
Data Broadcast	Vehicle sends state data (PSK,2)	15
Data Broadcast	Vehicle sends state data (PSK,4)	15
Data Broadcast	Vehicle sends state data (PSK,5)	15
Ping	Depressor pings Vehicle	20
Pause	Until the top of even minute	10
	Band 0 (12 kHz, 2kHz bandwidth)	
Configs	Set band, carrier freq, bandwidth	9
Ping	Topside pings Vehicle	21
Data Broadcast	Vehicle sends state data (PSK,2)	15
Data Broadcast	Vehicle sends state data (PSK,4)	15
Data Broadcast	Vehicle sends state data (PSK,5)	15
Ping	Depressor pings Vehicle	20
Pause	Until the top of even minute	25
	Band 0 (8 kHz, 1.25kHz bandwidth)	
Configs	Set band, carrier freq, bandwidth	9
Ping	Topside pings Vehicle	21
Data Broadcast	Vehicle sends state data (PSK,2)	15
Data Broadcast	Vehicle sends state data (PSK,4)	15
Data Broadcast	Vehicle sends state data (PSK,5)	15
Ping	Depressor pings Vehicle	20
Pause	Until the top of even minute	25
	Total TDMA Cycle Time [s] =	360

Table 3.4: Rate table for the WHOI Micro-Modem

Rate	**Max payload [bytes]**	**Burst rate [bps] per Bandwidth** *5000 Hz*	*2000 Hz*	*1250 Hz*
0	32	65	n/a	n/a
2	192	520	208	130
4	512	1300	520	325
5	2048	5380	2150	1340

Table 3.5: Approximate range for various PSK rates and bandwidth combinations through the vertical acoustic channel.

PSK rate	**Range @ Bandwidth (Carrier Frequency)**		
	1.25kHz (8kHz)	2kHz (12kHz)	5kHz (10kHz)
2	9 km	11 km	7 km
4	9 km	10 km	6 km
5	5 km	6 km	4 km

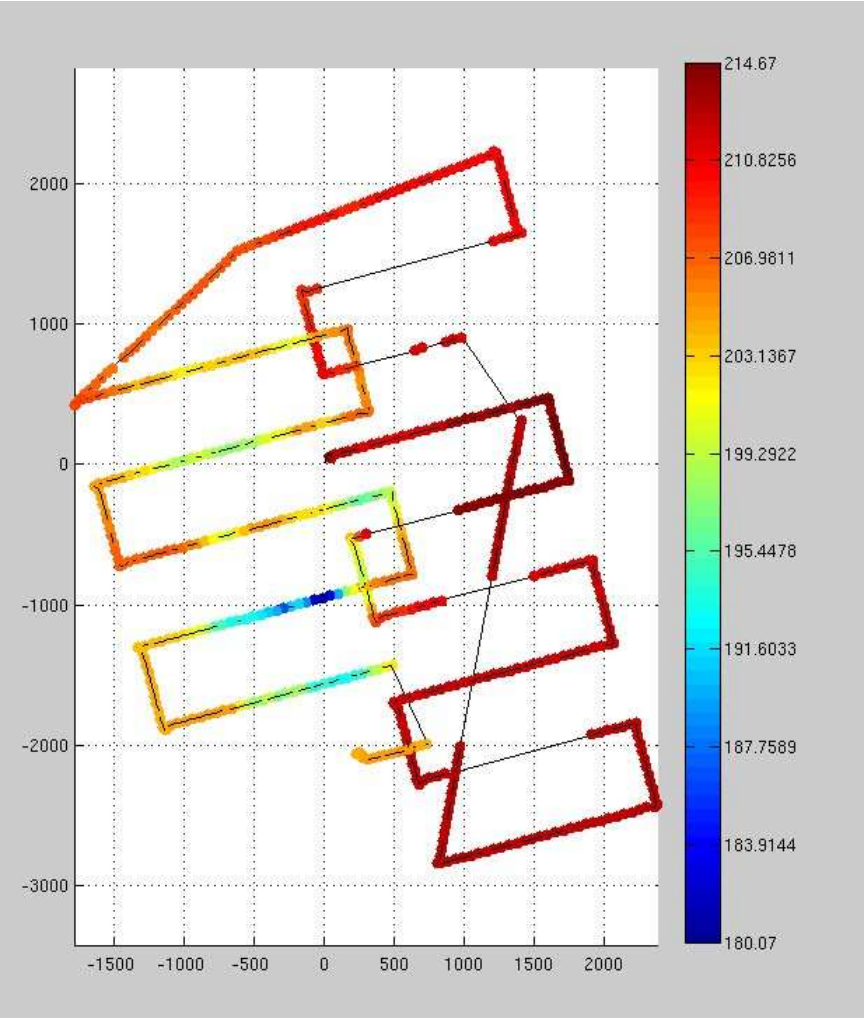

Figure 3.10: The vehicle track over the Mid-Cayman Rise with acoustically uplinked science data collected by the vehicle. The xy-axes are in meters and the color of the data points represents redox potential (Eh), the strength of the chemical signature in the water from the hydrothermal vent, where blue is strongest. The vehicle mission was reprogrammed acoustically from the surface to move the programmed survey to the west of the original survey as shown. Photo credit: WHOI.

Chapter 4

System Models

This chapter describes the process models for the vehicle and the ship and the observation models used in the formulation of both the Kalman filter and the information filter.

4.1 State Description

The complete state vector of the system, denoted with a different font $\mathbf{x}$, consists of the current vehicle estimate, $\boldsymbol{x}_v$, the current ship estimate, $\boldsymbol{x}_s$, and a fixed-length queue of historic states representing the ship and vehicle position at the beginning of the second (referred to as the top of the second) for the most recent n seconds, denoted $\boldsymbol{x}_{v-i}$ and $\boldsymbol{x}_{s-i}$ for $i \in [1, .., n]$.

$$\mathbf{x} = [\boldsymbol{x}_v^\top, \boldsymbol{x}_s^\top, \boldsymbol{x}_{v-1}^\top, \boldsymbol{x}_{s-1}^\top, \cdots, \boldsymbol{x}_{v-n}^\top, \boldsymbol{x}_{s-n}^\top]^\top \tag{4.1}$$

The current vehicle state contains local-level pose and attitude, as well as body-frame linear and angular velocities

$$\boldsymbol{x}_v = [\boldsymbol{s}^\top, \boldsymbol{\varphi}^\top, \boldsymbol{\upsilon}^\top, \boldsymbol{\omega}^\top]^\top \tag{4.2}$$

$$\boldsymbol{s} = \begin{bmatrix} x \\ y \\ z \end{bmatrix}, \quad \boldsymbol{\varphi} = \begin{bmatrix} \phi \\ \theta \\ \psi \end{bmatrix}, \quad \boldsymbol{\upsilon} = \begin{bmatrix} u \\ v \\ w \end{bmatrix}, \quad \boldsymbol{\omega} = \begin{bmatrix} p \\ q \\ r \end{bmatrix} \tag{4.3}$$

where $\boldsymbol{s}$ is the local-level vehicle pose in the local frame, $\boldsymbol{\varphi}$ is the local-level vehicle attitude (Euler roll, pitch, heading), $\boldsymbol{\upsilon}$ is the body-frame linear velocity, and $\boldsymbol{\omega}$ is the body-frame angular velocity. The current ship state contains x-y position, heading, and the respective velocities

$$\boldsymbol{x}_s = [x_s, y_s, \theta_s, \dot{x}_s, \dot{y}_s, \dot{\theta}_s]^\top. \tag{4.4}$$

Note that boldface math symbols, e.g. $\boldsymbol{x}$ and $\boldsymbol{R}$, represent vectors and matrices, while standard weight math symbols, e.g. t and θ, represent scalars.

The historic states contain full estimates of the vehicle state and the ship state from previous time steps. Historic states are necessary for causal processing of range measurements because of the time required for an acoustic data packet to propagate from the sender to the receiver. When the acoustic modems are in synchronous navigation mode (see Section 3.3.1) all acoustic transmissions are initiated at the top of the second. Thus, in order to ensure that the state vector contains the appropriate historic states needed to perform range measurement updates, the CEKF maintains an estimate of the state of the system at the top of the second for the previous n seconds. In practice $n = 6$ for this implementation, which enables the algorithm to accommodate range measurements with travel times of up to six seconds (i.e. 9000 m range assuming 1500 m/s sound velocity).

4.2 Vehicle Process Model

We seek a navigation algorithm that is independent of the vehicles on which it is employed. Thus, as is common for navigation algorithms, we use a constant-velocity kinematic model of the system that does not incorporate vehicle dynamics, drag models, or thrust or steering inputs. The constant-velocity assumption is valid in the context of underwater vehicles for several reasons. An autonomous vehicle survey typically consist of a "mowing-the-lawn" vehicle track consisting of long, straight, constant-velocity segments with short turns in between. In addition the vehicle is subject to low bandwidth control and moves slowly relative to the precision and frequency of measurement updates. During stops, starts, and turns the vehicle accrues bounded error, but the estimation error converges once the vehicle has returned to constant-velocity motion, as has been validated by [33].

The following formulation of the process model and the details of its linearization and discretization presented here are from [25]. As stated above, we use a constant-velocity process model for the vehicle

$$\dot{\boldsymbol{x}}_v = \underbrace{\begin{bmatrix} \mathbf{0} & \mathbf{0} & \boldsymbol{R}(\boldsymbol{\varphi}) & \mathbf{0} \\ \mathbf{0} & \mathbf{0} & \mathbf{0} & \boldsymbol{\mathcal{J}}(\boldsymbol{\varphi}) \\ \mathbf{0} & \mathbf{0} & \mathbf{0} & \mathbf{0} \\ \mathbf{0} & \mathbf{0} & \mathbf{0} & \mathbf{0} \end{bmatrix} \boldsymbol{x}_v}_{\boldsymbol{f}(\boldsymbol{x}_v(t))} + \underbrace{\begin{bmatrix} \mathbf{0} & \mathbf{0} \\ \mathbf{0} & \mathbf{0} \\ \boldsymbol{I} & \mathbf{0} \\ \mathbf{0} & \boldsymbol{I} \end{bmatrix}}_{\boldsymbol{G}_v} \boldsymbol{w}_v \tag{4.5}$$

where $\boldsymbol{R}(\boldsymbol{\varphi})$ is the transformation from body-frame to local-level linear velocities, $\boldsymbol{\mathcal{J}}(\boldsymbol{\varphi})$ is the transformation from body-frame angular velocities to Euler rates, and $\boldsymbol{w}_v \sim \mathcal{N}(0, \boldsymbol{Q}_v)$ is the independent zero-mean Gaussian process noise in the acceleration term. $\boldsymbol{R}(\boldsymbol{\varphi})$ and $\boldsymbol{\mathcal{J}}(\boldsymbol{\varphi})$ are found by solving

$$\boldsymbol{R}(\boldsymbol{\varphi}) = \boldsymbol{R}_\psi^\top \boldsymbol{R}_\theta^\top \boldsymbol{R}_\phi^\top \tag{4.6}$$

$$\boldsymbol{R}_\psi = \begin{bmatrix} \cos\psi & \sin\psi & 0 \\ -\sin\psi & \cos\psi & 0 \\ 0 & 0 & 1 \end{bmatrix}, \quad \boldsymbol{R}_\theta = \begin{bmatrix} \cos\theta & 0 & -\sin\theta \\ 0 & 1 & 0 \\ \sin\theta & 0 & \cos\theta \end{bmatrix}, \quad \boldsymbol{R}_\phi = \begin{bmatrix} 1 & 0 & 0 \\ 0 & \cos\phi & \sin\phi \\ 0 & -\sin\phi & \cos\phi \end{bmatrix}$$

and

$$\boldsymbol{\omega} = \begin{bmatrix} \dot{\phi} \\ 0 \\ 0 \end{bmatrix} + R_\phi \begin{bmatrix} 0 \\ \dot{\theta} \\ 0 \end{bmatrix} + R_\phi R_\theta \begin{bmatrix} 0 \\ 0 \\ \dot{\psi} \end{bmatrix} = \underbrace{\begin{bmatrix} 1 & 0 & -\sin\theta \\ 0 & \cos\phi & \sin\phi\cos\theta \\ 0 & -\sin\phi & \cos\phi\cos\theta \end{bmatrix}}_{\boldsymbol{\mathcal{J}}^{-1}} \dot{\varphi} \tag{4.7}$$

$$\boldsymbol{\mathcal{J}} = \begin{bmatrix} 1 & \sin\phi\tan\theta & \cos\phi\tan\theta \\ 0 & \cos\phi & -\sin\phi \\ 0 & \sin\phi\sec\theta & \cos\phi\sec\theta \end{bmatrix}. \tag{4.8}$$

Linearization: We linearize the vehicle process model (4.5) about $\boldsymbol{\mu}_t$, our estimate of the state at time t, using the Taylor series expansion

$$\dot{\boldsymbol{x}}_v(t) = \boldsymbol{f}(\boldsymbol{\mu}_t) + \boldsymbol{F}_x(\boldsymbol{x}_v(t) - \boldsymbol{\mu}_t) + HOT + \boldsymbol{G}_v\boldsymbol{w}_v(t) \tag{4.9}$$

where

$$\boldsymbol{F}_x = \left.\frac{\partial \boldsymbol{f}(\boldsymbol{x}_v)}{\partial \boldsymbol{x}_v}\right|_{\boldsymbol{x}_v(t)=\boldsymbol{\mu}_t} \tag{4.10}$$

and HOT denotes higher order terms. Dropping the HOT and rearranging we get

$$\dot{\boldsymbol{x}}_v(t) \approx \boldsymbol{F}_x\boldsymbol{x}_v(t) + \underbrace{\boldsymbol{f}(\boldsymbol{\mu}_t) - \boldsymbol{F}_x\boldsymbol{\mu}_t}_{\boldsymbol{u}(t)} + \boldsymbol{G}_v\boldsymbol{w}_v(t) \tag{4.11}$$

$$= \boldsymbol{F}_x\boldsymbol{x}_v(t) + \boldsymbol{u}(t) + \boldsymbol{G}_v\boldsymbol{w}_v(t) \tag{4.12}$$

where $\boldsymbol{f}(\boldsymbol{\mu}_t) - \boldsymbol{F}_x\boldsymbol{\mu}_t$ is treated as a constant input pseudo control $\boldsymbol{u}(t)$.

Discretization: In order to find a discrete-time model of the linearized vehicle process model we rewrite (4.12) as

$$\dot{\boldsymbol{x}}_v(t) = \boldsymbol{F}_x\boldsymbol{x}_v(t) + \boldsymbol{B}_v\boldsymbol{u}(t) + \boldsymbol{G}_v\boldsymbol{w}_v(t) \tag{4.13}$$

where $\boldsymbol{B}_v = \boldsymbol{I}$. Assuming zero-order hold and using the standard method [8] to discretize

over a time step T we solve for $\boldsymbol{F}_{v_k}$ and $\boldsymbol{B}_{v_k}$ in the discrete form of the process model:

$$\boldsymbol{x}_{v_{k+1}} = \boldsymbol{F}_{v_k}\boldsymbol{x}_{v_k} + \boldsymbol{B}_{v_k}\boldsymbol{u}_k + \boldsymbol{w}_{v_k} \tag{4.14}$$

$$\boldsymbol{F}_{v_k} = e^{\boldsymbol{F}_x T} \tag{4.15}$$

$$\begin{aligned}\boldsymbol{B}_{v_k} &= \int_0^T e^{\boldsymbol{F}_x(T-\tau)}\boldsymbol{B}_v d\tau \\ &= \int_0^T e^{\boldsymbol{F}_x(T-\tau)} d\tau \\ &= e^{\boldsymbol{F}_x T}\int_0^T e^{-\boldsymbol{F}_x\tau} d\tau.\end{aligned} \tag{4.16}$$

The discretized process noise $\boldsymbol{w}_{v_k}$ has the form

$$\boldsymbol{w}_{v_k} = \int_0^T e^{\boldsymbol{F}_x(T-\tau)}\boldsymbol{G}_v\boldsymbol{w}_v(\tau)d\tau \tag{4.17}$$

for which we can calculate the mean and variance as follows:

$$\begin{aligned}E\left[\boldsymbol{w}_{v_k}\right] &= E\left[\int_0^T e^{\boldsymbol{F}_x(T-\tau)}\boldsymbol{G}_v\boldsymbol{w}_v(\tau)d\tau\right] \\ &= \int_0^T e^{\boldsymbol{F}_x(T-\tau)}\boldsymbol{G}_v\underbrace{E[\boldsymbol{w}_v(\tau)]}_{0}d\tau \\ &= 0\end{aligned} \tag{4.18}$$

$$\begin{aligned}\boldsymbol{Q}_{v_k} &= E\left[\boldsymbol{w}_{v_k}\boldsymbol{w}_{v_k}^\top\right] \\ &= E\left[\int_0^T e^{\boldsymbol{F}_x(T-\tau)}\boldsymbol{G}_v\boldsymbol{w}_v(\tau)d\tau\int_0^T\left(e^{\boldsymbol{F}_x(T-\gamma)}\boldsymbol{G}_v\boldsymbol{w}_v(\gamma)\right)^\top d\gamma\right] \\ &= E\left[\int_0^T\int_0^T e^{\boldsymbol{F}_x(T-\tau)}\boldsymbol{G}_v\boldsymbol{w}_v(\tau)\boldsymbol{w}_v^\top(\gamma)\boldsymbol{G}_v^\top e^{\boldsymbol{F}_x^\top(T-\gamma)}d\tau d\gamma\right] \\ &= \int_0^T\int_0^T e^{\boldsymbol{F}_x(T-\tau)}\boldsymbol{G}_v\underbrace{E\left[\boldsymbol{w}_v(\tau)\boldsymbol{w}_v^\top(\gamma)\right]}_{\boldsymbol{Q}_v\delta(\tau-\gamma)}\boldsymbol{G}_v^\top e^{\boldsymbol{F}_x^\top(T-\gamma)}d\tau d\gamma \\ &= \int_0^T e^{\boldsymbol{F}_x(T-\tau)}\boldsymbol{G}_v\boldsymbol{Q}_v\boldsymbol{G}_v^\top e^{\boldsymbol{F}_x^\top(T-\tau)}d\tau.\end{aligned} \tag{4.19}$$

Note that we make use of the facts that the expected value can be brought inside the integral because it is a linear operator and the noise vector $\boldsymbol{w}_v$ is independent in time so that the covariance $E\left[\boldsymbol{w}_v(\tau)\boldsymbol{w}_v^\top(\gamma)\right]$ is zero except when $\gamma = \tau$.

4.3 Ship Process Model

Similar to the vehicle, we use a constant-velocity process model for the ship. As described for the vehicle process model, this is a valid assumption because of the typical ship operations, holding station or steaming at a constant speed, and the relative speed of the ship compared to the precision and frequency of GPS and gyro measurement updates.

$$\dot{\boldsymbol{x}}_s = \underbrace{\begin{bmatrix} \boldsymbol{0} & \boldsymbol{I} \\ \boldsymbol{0} & \boldsymbol{0} \end{bmatrix}}_{\boldsymbol{F}_s} \boldsymbol{x}_s + \underbrace{\begin{bmatrix} \boldsymbol{0} \\ \boldsymbol{I} \end{bmatrix}}_{\boldsymbol{G}_s} \boldsymbol{w}_s \tag{4.20}$$

where $\boldsymbol{w}_s \sim \mathcal{N}(0, \boldsymbol{Q}_s)$ is the independent zero-mean Gaussian process noise in the acceleration term. The ship process model (4.20) is already linear and does not require linearization. It is discretized in the same fashion as the vehicle model:

$$\boldsymbol{x}_{s_{k+1}} = \boldsymbol{F}_{s_k} \boldsymbol{x}_{s_k} + \boldsymbol{w}_{s_k} \tag{4.21}$$

$$\begin{aligned} \boldsymbol{F}_{s_k} &= e^{\boldsymbol{F}_s T} \\ &= \boldsymbol{I} + \boldsymbol{F}_s T + \frac{1}{2!}\boldsymbol{F}_s^2 T^2 + \frac{1}{3!}\boldsymbol{F}_s^3 T^3 + \cdots \\ &= \begin{bmatrix} \boldsymbol{I} & \boldsymbol{I}T \\ \boldsymbol{0} & \boldsymbol{I} \end{bmatrix} \end{aligned} \tag{4.22}$$

where the higher order terms are identically zero because of the structure of $\boldsymbol{F}_s$, resulting in a simple closed-form solution for $\boldsymbol{F}_{s_k}$. Note that $\boldsymbol{B}_{s_k} = \boldsymbol{0}$ because $\boldsymbol{B}_s = \boldsymbol{0}$. The discretized ship process noise

$$\boldsymbol{w}_{s_k} = \int_0^T e^{\boldsymbol{F}_s (T-\tau)} \boldsymbol{G}_s \boldsymbol{w}_s(\tau) d\tau, \tag{4.23}$$

can also be shown to be zero-mean Gaussian using formulas (4.18) and (4.19), such that $\boldsymbol{w}_{s_k} \sim \mathcal{N}(0, \boldsymbol{Q}_{s_k})$. Due to the structure of $\boldsymbol{F}_{s_k}$, the covariance matrix simplifies to

$$\boldsymbol{Q}_{s_k} = \begin{bmatrix} \frac{1}{3}T^3 & \frac{1}{2}T^2 \\ \frac{1}{2}T^2 & T \end{bmatrix} \boldsymbol{Q}_s. \tag{4.24}$$

4.4 Observation Model

The range measurement from the ship's modem transducer to the vehicle's modem transducer is a nonlinear function of the current vehicle state and an historic ship state. For simplicity of notation, we assume here that the transducers are located at the origin of their respective local frames and that the ship's transducer has a depth of 0 m.

The measurement equation for a range measurement made from an acoustic data packet sent from the ship to the vehicle is

$$z_{rng} = \sqrt{(\boldsymbol{x}_{v_{xyz}} - \boldsymbol{x}_{s_{xyz}})^\top (\boldsymbol{x}_{v_{xyz}} - \boldsymbol{x}_{s_{xyz}})} + v_{rng} \tag{4.25}$$

where $\boldsymbol{x}_{s_{xyz}}$ is the ship pose at the time of launch of the acoustic data packet, t_{TOL}, and $\boldsymbol{x}_{v_{xyz}}$ is the vehicle pose at the time of arrival of the acoustic data packet, t_{TOA}. We assume zero-mean Gaussian measurement noise, $v_{rng} \sim \mathcal{N}(0, R_{rng})$, which is in units of distance and represents the imprecision in timing multiplied by the speed of sound. The covariance R_{rng} is assumed to be identical for all range measurements and therefore does not have the time-dependent subscript k. We can rewrite (4.25) in terms of the state vector as

$$z_{rng} = (\mathbf{x}^\top \boldsymbol{M}^\top \boldsymbol{M} \mathbf{x})^{\frac{1}{2}} + v_{rng} \tag{4.26}$$

where

$$\boldsymbol{M} = \begin{bmatrix} \underbrace{\boldsymbol{J}_v}_{\boldsymbol{x}_{v_{xyz}}(t_{TOA})} & \mathbf{0} & \cdots & \mathbf{0} & \underbrace{\boldsymbol{J}_s}_{\boldsymbol{x}_{s_{xyz}}(t_{TOL})} & \mathbf{0} & \cdots & \mathbf{0} \end{bmatrix} \tag{4.27}$$

and $\boldsymbol{J}_v$ and $\boldsymbol{J}_s$ are defined to capture the pose information of the vehicle and ship[1]

$$\boldsymbol{J}_v \underbrace{\begin{bmatrix} (x,y,z)^\top \\ (\phi,\theta,\psi)^\top \\ (u,v,w)^\top \\ (p,q,r)^\top \end{bmatrix}}_{\boldsymbol{x}_v} = \begin{bmatrix} x \\ y \\ z \end{bmatrix} \tag{4.30}$$

$$\boldsymbol{J}_s \underbrace{\begin{bmatrix} (x_s,y_s,\theta_s)^\top \\ (\dot{x}_s,\dot{y}_s,\dot{\theta}_s)^\top \end{bmatrix}}_{\boldsymbol{x}_s} = \begin{bmatrix} x_s \\ y_s \\ 0 \end{bmatrix} \tag{4.31}$$

assuming that t_{TOA} is the current time and t_{TOL} is the the top of the second when the acoustic signal was broadcast from the ship.

The Jacobian of the measurement with respect to $\mathbf{x}$, $\boldsymbol{H}_{rng_k}$, is

$$\begin{aligned} \boldsymbol{H}_{rng_k} &= \left.\frac{\partial z_{rng}(\mathbf{x})}{\partial \mathbf{x}}\right|_{\mathbf{x}=\boldsymbol{\mu}_{k|k-1}} \\ &= (\boldsymbol{\mu}_{k|k-1}^\top \boldsymbol{M}^\top \boldsymbol{M} \boldsymbol{\mu}_{k|k-1})^{-\frac{1}{2}} \boldsymbol{\mu}_{k|k-1}^\top \boldsymbol{M}^\top \boldsymbol{M}. \end{aligned} \tag{4.32}$$

[1] $\boldsymbol{J}_v$ and $\boldsymbol{J}_s$ are defined explicitly as

$$\boldsymbol{J}_v = \begin{bmatrix} \boldsymbol{I}_{3\times3} & \mathbf{0}_{3\times9} \end{bmatrix} \tag{4.28}$$

$$\boldsymbol{J}_s = \begin{bmatrix} \boldsymbol{I}_{2\times2} & \begin{matrix} 0 \\ 0 \end{matrix} & \mathbf{0}_{3\times3} \\ \begin{matrix} 0 & 0 \end{matrix} & 0 & \end{bmatrix}. \tag{4.29}$$

Measurements from additional navigation sensors, e.g. depth sensor, gyrocompass, and Doppler velocity log, are processed asynchronously using standard observation models.

Chapter 5

Extended Kalman Filter for Single-Beacon Navigation

5.1 Introduction

This chapter describes the formulation and implementation of a centralized extended Kalman filter (CEKF) designed to estimate vehicle and ship position within the framework of one-way-travel-time (OWTT) navigation. The experimental results presented demonstrate that single-beacon navigation is a viable alternative to traditional absolute navigation methods such as long baseline (LBL) and ultra-short baseline (USBL) navigation (discussed in detail in Chapter 2). The CEKF is applicable in post-processing, where sensor measurements from both the ship and the vehicle are available simultaneously. The CEKF is used in Chapter 6 as a benchmark for the decentralized algorithm. The implementation described here is for a single surface node, the ship, and a single underwater vehicle, though the algorithm is trivially extensible to multiple vehicles.

This chapter describes the formulation of the extended Kalman filter designed by the author and collaborators for OWTT navigation and reports field results using data collected by the author and collaborators from an autonomous underwater vehicle (AUV) survey carried out in 4000 m of water on the southern Mid-Atlantic Ridge [93].

5.2 Centralized Extended Kalman Filter

An extended Kalman filter is employed to fuse depth, gyrocompass, and Doppler velocity measurements from the vehicle, position and attitude measurements from the ship, and range measurements between the vehicle and the ship. The CEKF is designed to estimate the current and previous states of both the ship and the vehicle and is applicable in post-processing of previously acquired dive data. This section briefly reviews the formulation of the extended Kalman filter followed by the details of the centralized implementation for OWTT navigation, summarized in Algorithm 1. A derivation of the linear Kalman filter is provided in Appendix B.

Algorithm 1 CEKF with state augmentation

loop {perform prediction and measurement update}
  $\Delta t = min$(time until top of the second; time until next measurement; 0.1s)
  if current time (before prediction) is the top of the second **then**
    augment state vector with prediction of current state forward Δt (5.12, 5.13)
  else
    predict current state forward Δt (5.15, 5.16)
  end if
  if $\exists$ measurements at this time step **then**
    perform measurement update (5.8, 5.9)
  end if
end loop

5.2.1 Review of EKF Formulation

The extended Kalman filter is a sub-optimal filter that recursively estimates system state. The EKF applies the general approach of the Kalman filter [50], the optimal linear estimator, to nonlinear plants by linearizing the plant process and observation models along the trajectory of the system. The formulation reported here is for a nonlinear plant with discrete observations [36]. Consider the general nonlinear plant process and observation model

$$\dot{\boldsymbol{x}}(t) = \boldsymbol{f}(\boldsymbol{x}(t), t) + \boldsymbol{G}(t)\boldsymbol{w}(t) \tag{5.1}$$
$$\boldsymbol{z}_k = \boldsymbol{h}(\boldsymbol{x}(t_k)) + \boldsymbol{v}_k, k = 1, 2, \cdots \tag{5.2}$$

where $\boldsymbol{x}(t)$ is the state in continuous time, $\boldsymbol{w}(t) \sim \mathcal{N}(0, \boldsymbol{Q}(t))$ is the independent zero-mean Gaussian process noise, $\boldsymbol{z}_k$ is the measurement at time step t_k in discrete time, and $\boldsymbol{v}_k \sim \mathcal{N}(0, \boldsymbol{R}_k)$ is the independent zero-mean Gaussian measurement noise. Note that boldface math symbols, e.g. $\boldsymbol{x}$ and $\boldsymbol{Q}$, represent vectors and matrices, while standard weight math symbols, e.g. t and k, represent scalars.

The CEKF reported herein employs a discrete-time linearization of the process model

$$\boldsymbol{x}_{k+1} = \boldsymbol{F}_k \boldsymbol{x}_k + \boldsymbol{B}_k \boldsymbol{u}_k + \boldsymbol{w}_k \tag{5.3}$$

to recursively estimates the mean, $\boldsymbol{\mu}$, and covariance, $\boldsymbol{\Sigma}$, of the state vector $\boldsymbol{x}$

$$\boldsymbol{\mu} = E\left[\boldsymbol{x}\right] \tag{5.4}$$
$$\boldsymbol{\Sigma} = E\left[(\boldsymbol{x} - \boldsymbol{\mu})(\boldsymbol{x} - \boldsymbol{\mu})^\top\right] \tag{5.5}$$

resulting in process prediction equations

$$\boldsymbol{\mu}_{k+1|k} = \boldsymbol{F}_k \boldsymbol{\mu}_{k|k} + \boldsymbol{B}_k \boldsymbol{u}_k \tag{5.6}$$
$$\boldsymbol{\Sigma}_{k+1|k} = \boldsymbol{F}_k \boldsymbol{\Sigma}_{k|k} \boldsymbol{F}_k^\top + \boldsymbol{Q}_k \tag{5.7}$$

where $\boldsymbol{F}_k$ is the discrete-time linear state transition matrix, $\boldsymbol{B}_k$ is the discrete-time linear input matrix, $\boldsymbol{Q}_k$ is the discrete-time process noise covariance, $\boldsymbol{u}_k$ is the piecewise-constant input at time step t_k, and we use $\top$ as the transpose operator.

The measurement update equations for the extended Kalman filter are

$$\boldsymbol{\mu}_{k|k} = \boldsymbol{\mu}_{k|k-1} + \boldsymbol{K}_k(\boldsymbol{z}_k - \boldsymbol{h}(\boldsymbol{\mu}_{k|k-1})) \tag{5.8}$$
$$\boldsymbol{\Sigma}_{k|k} = \boldsymbol{\Sigma}_{k|k-1} - \boldsymbol{K}_k \boldsymbol{H}_k \boldsymbol{\Sigma}_{k|k-1} \tag{5.9}$$

where $\boldsymbol{H}_k$ is the Jacobian of $\boldsymbol{h}$ at time step t_k

$$\boldsymbol{H}_k = \left.\frac{\partial \boldsymbol{h}(\boldsymbol{x}(t_k))}{\partial \boldsymbol{x}(t_k)}\right|_{\boldsymbol{x}(t_k)=\boldsymbol{\mu}_{k|k-1}} \tag{5.10}$$

and $\boldsymbol{K}_k$ is the Kalman gain at time step t_k, given by

$$\boldsymbol{K}_k = \boldsymbol{\Sigma}_{k|k-1} \boldsymbol{H}_k^\top (\boldsymbol{H}_k \boldsymbol{\Sigma}_{k|k-1} \boldsymbol{H}_k^\top + \boldsymbol{R}_k)^{-1}. \tag{5.11}$$

5.2.2 Process Prediction and Augmentation

The complete state process prediction for the EKF is written in terms of the full state vector of the system defined in (4.1). Combining the discrete-time linearized vehicle and ship process models (4.14) and (4.21), and substituting them into the discrete-time linearized Kalman process prediction equation (5.6), the complete state process prediction

becomes

$$\boldsymbol{\mu}_{k+1|k} = \underbrace{\begin{bmatrix} \boldsymbol{F}_{v_k} & 0 & 0 & \cdots & 0 \\ 0 & \boldsymbol{F}_{s_k} & 0 & \cdots & 0 \\ 0 & 0 & \boldsymbol{I} & \cdots & 0 \\ \vdots & \vdots & \vdots & \ddots & \vdots \\ 0 & 0 & 0 & \cdots & \boldsymbol{I} \end{bmatrix}}_{\boldsymbol{F}_k} \boldsymbol{\mu}_{k|k} + \begin{bmatrix} \boldsymbol{B}_{v_k}\boldsymbol{u}_k \\ 0 \\ 0 \\ \vdots \\ 0 \end{bmatrix} \tag{5.12}$$

$$\boldsymbol{\Sigma}_{k+1|k} = \boldsymbol{F}_k \boldsymbol{\Sigma}_{k|k} \boldsymbol{F}_k^\top + \boldsymbol{Q}_k. \tag{5.13}$$

where

$$\boldsymbol{Q}_k = \begin{bmatrix} \boldsymbol{Q}_{v_k} & 0 & 0 & \cdots & 0 \\ 0 & \boldsymbol{Q}_{s_k} & 0 & \cdots & 0 \\ 0 & 0 & 0 & \cdots & 0 \\ \vdots & \vdots & \vdots & \ddots & \vdots \\ 0 & 0 & 0 & \cdots & 0 \end{bmatrix}. \tag{5.14}$$

Note that the historic states do not change during this process update.

A modified process prediction is necessary at the top of the second when state augmentation is done in concert with the process prediction. During this modified prediction step, in addition to predicting forward the current vehicle state, the estimate of the current state (before the prediction) is added to the state vector while simultaneously marginalizing out the oldest historic state, i.e. $(\boldsymbol{x}_{v-n}, \boldsymbol{x}_{s-n})$

$$\boldsymbol{\mu}_{k+1|k} = \underbrace{\begin{bmatrix} \boldsymbol{F}_{v_k} & 0 & 0 & \cdots & 0 & 0 & 0 \\ 0 & \boldsymbol{F}_{s_k} & 0 & \cdots & 0 & 0 & 0 \\ \boldsymbol{I} & 0 & 0 & \cdots & 0 & 0 & 0 \\ 0 & \boldsymbol{I} & 0 & \cdots & 0 & 0 & 0 \\ 0 & 0 & \boldsymbol{I} & \cdots & 0 & 0 & 0 \\ \vdots & \vdots & \vdots & \ddots & \vdots & \vdots & \vdots \\ 0 & 0 & 0 & \cdots & \boldsymbol{I} & 0 & 0 \end{bmatrix}}_{\widetilde{\boldsymbol{F}}_k} \boldsymbol{\mu}_{k|k} + \begin{bmatrix} \boldsymbol{B}_{v_k}\boldsymbol{u}_k \\ 0 \\ 0 \\ 0 \\ \vdots \\ 0 \end{bmatrix} \tag{5.15}$$

$$\boldsymbol{\Sigma}_{k+1|k} = \widetilde{\boldsymbol{F}}_k \boldsymbol{\Sigma}_{k|k} \widetilde{\boldsymbol{F}}_k^\top + \boldsymbol{Q}_k. \tag{5.16}$$

and $\boldsymbol{Q}_k$ is as defined before.

5.2.3 Measurement Update

We find the extended Kalman filter measurement update equations for a range measurement by substituting the Jacobian of the range measurement (4.32) into (5.8) and (5.11)

$$\boldsymbol{\mu}_{k|k} = \boldsymbol{\mu}_{k|k-1} + \boldsymbol{K}_{rng_k}(\boldsymbol{z}_{rng_k} - (\boldsymbol{\mu}_{k|k-1}^\top \boldsymbol{M}^\top \boldsymbol{M} \boldsymbol{\mu}_{k|k-1})^{\frac{1}{2}}) \tag{5.17}$$

$$\boldsymbol{K}_{rng_k} = \boldsymbol{\Sigma}_{k|k-1} \boldsymbol{H}_{rng_k}^\top (\boldsymbol{H}_{rng_k} \boldsymbol{\Sigma}_{k|k-1} \boldsymbol{H}_{rng_k}^\top + R_{rng})^{-1}. \tag{5.18}$$

5.3 Field Results

Sea trials were conducted by the author and collaborators using the Acomms system with WHOI Micro-Modems and PPSBoards during an expedition on the R/V *Knorr* to the southern Mid-Atlantic Ridge in January 2008. The goal of the expedition was to test and evaluate engineering methods for locating and mapping new hydrothermal vents on the southern Mid-Atlantic Ridge. Navigation data collected by the author and collaborators during this expedition is used to experimentally validate the CEKF in post-processing. These results are reported here and were published in [93].

5.3.1 Site Description

The southern Mid-Atlantic Ridge (SMAR) is a divergent boundary between the South American Plate and the African Plate that is presently spreading at about 2.5 cm per year. The survey site, shown in Figure 5.1, is located near 04° S 12° W in a deep non-transform discontinuity whose maximum depth exceeds 4000 m [38]. Operations were conducted on a section of the SMAR to the north of the sites where active hydrothermal vents were first discovered by a combination of deep-tow and deep-submergence technologies culminating in photography by ABE [38] and subsequently sampled by the ROV Marum Quest [40].

5.3.2 Experimental Setup

The data presented here were collected by the author and collaborators using the autonomous underwater vehicle (AUV) *Puma*, developed at Woods Hole Oceanographic Institution [82]. *Puma* is a 5000 m rated AUV equipped with the following navigation sensors: a Paroscientific pressure depth sensor, an OCTANS fiber-optic gyrocompass for attitude and attitude rate measurements, and a 300 kHz RDI Doppler velocity log (DVL) for velocity measurements. The vehicle is also equipped with a WHOI Micro-Modem [31] and an ITC-3013 transducer [45] for acoustic communications and range measurements and a PPSBoard for precision timing [27,28]. The Micro-Modem and PPSBoard are described in more detail in Chapter 3. The author was responsible for the development and operations of the Acomms system during this expedition. Chris Murphy assisted with the integration of the Acomms software on *Puma*.

The R/V *Knorr* is a 279 ft oceanographic research vessel operated by WHOI. The ship has two azimuthing stern thrusters, a retractable azimuthing bow thruster, and dynamic positioning (DP) capability enabling it to hold station and maneuver in any direction [97]. For the ship's position information we used the C-Nav 2000 Real-Time GIPSY (RTG) GPS with a reported horizontal accuracy of 10 cm [19]. An Applanix POS/MV-320 provided heading, pitch, and roll data with a reported accuracy of 0.02° [2]. The ship was also equipped with a WHOI Micro-Modem [31] and an ITC-3013 transducer for sending and

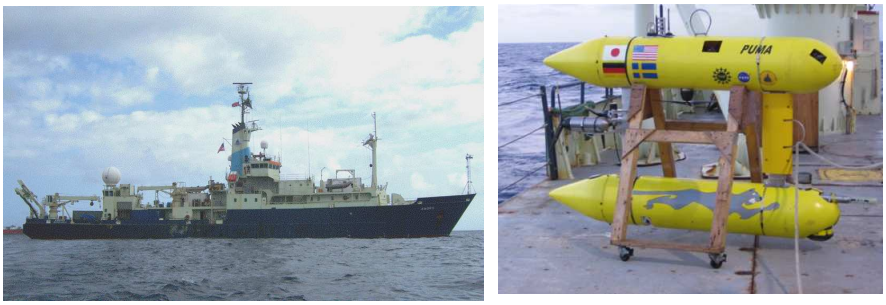

(a) (b)

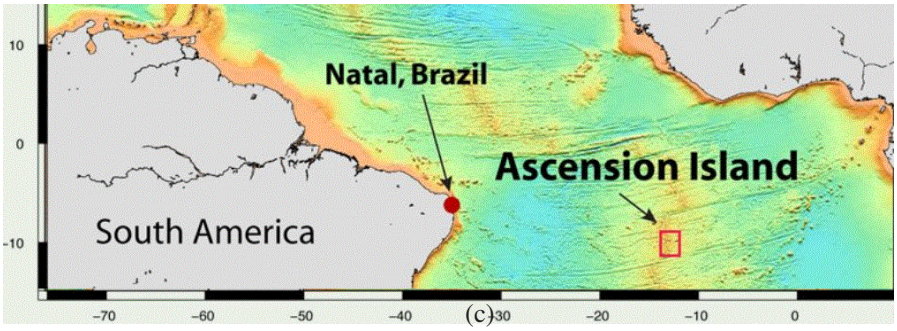

(c)

Figure 5.1: (a) R/V *Knorr* (b) AUV *Puma* (c) The survey site is shown by the red box near Ascension Island on the southern Mid-Atlantic Ridge. Photo credits: WHOI.

receiving acoustic data packets. Figure 5.1 shows the R/V *Knorr*, the AUV *Puma* and the survey area in the red box near Ascension Island.

On *Puma* Dive 03, the vehicle conducted a survey comprised of 12 tracklines approximately 65 meters apart and 700 meters long while maintaining an altitude of 200 m. While the vehicle carried out the survey mission, we repositioned the R/V *Knorr* around the survey site in a diamond shaped pattern, holding station at each apex. This was done to provide range measurements to the vehicle from different locations for increased observability. During these field trials we used two-way acoustic communication between the vehicle and the ship initiated by the vehicle. Acoustic data packets were sent from the vehicle to the ship and requested by the vehicle from the ship every 30 seconds.

5.3.3 Initialization

Because the EKF algorithm performs linearization along the system trajectories, an initial state estimate too far from the actual state could cause the algorithm to be unstable. In this implementation we initialize the CEKF with a maximum-likelihood estimate (MLE) of the vehicle state and covariance. For this implementation of the CEKF, the maximum-likelihood estimation is performed over the entire data set as previously reported in [28].

5.3.4 Sensor Offsets

The vehicle reference frame is defined to be coincident with the Doppler frame. Any angular offset between the OCTANS and the Doppler is accounted for as a mounting offset in the OCTANS. Doppler attitude measurements were not used by the CEKF, but, by comparing them to the OCTANS pitch and roll measurements in post-processing, we calculated the angular offset of the OCTANS to be -3.24° and 0.64° in pitch and roll respectively. The OCTANS heading offset was estimated by analyzing the mean and standard deviation of the error between the EKF-estimated vehicle position and the LBL vehicle position over the entire trackline for various OCTANS heading offsets, shown in Figure 5.2, assuming the previously stated roll and pitch offsets. Given these data a 3.5° heading offset in the gyrocompass was assumed and accounted for as a mounting offset in the OCTANS.

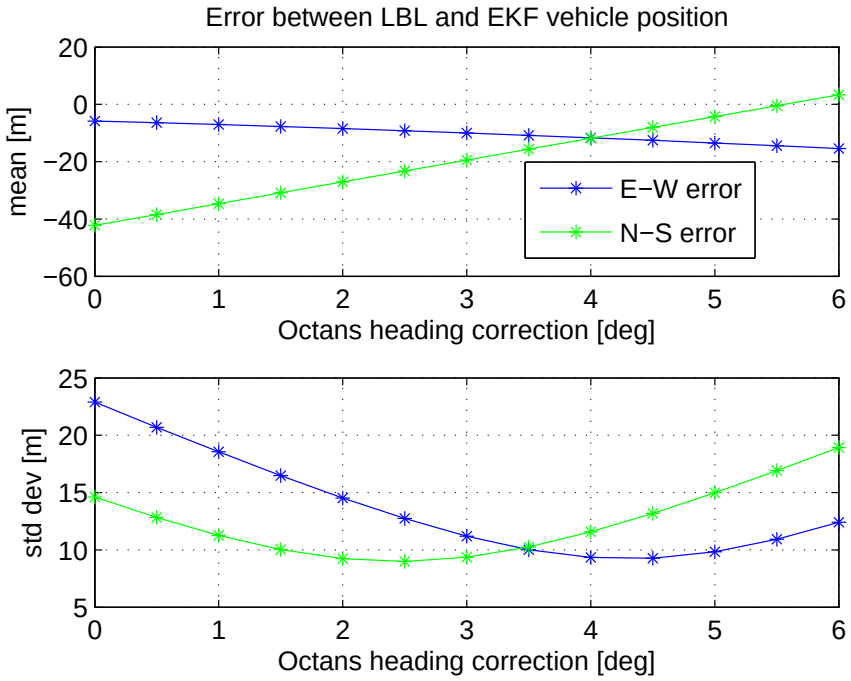

Figure 5.2: East-West and North-South components of the error between the EKF-estimated vehicle position and the LBL vehicle position. Errors are calculated over the entire trackline for a range of OCTANS heading offsets.

5.3.5 Results

The integrity of the vertical acoustic telemetry channel varied over the course of the dive. While the vehicle was surveying near the bottom, on average one acoustic data packet from which we could calculate range was successfully received every 90 seconds. Figure

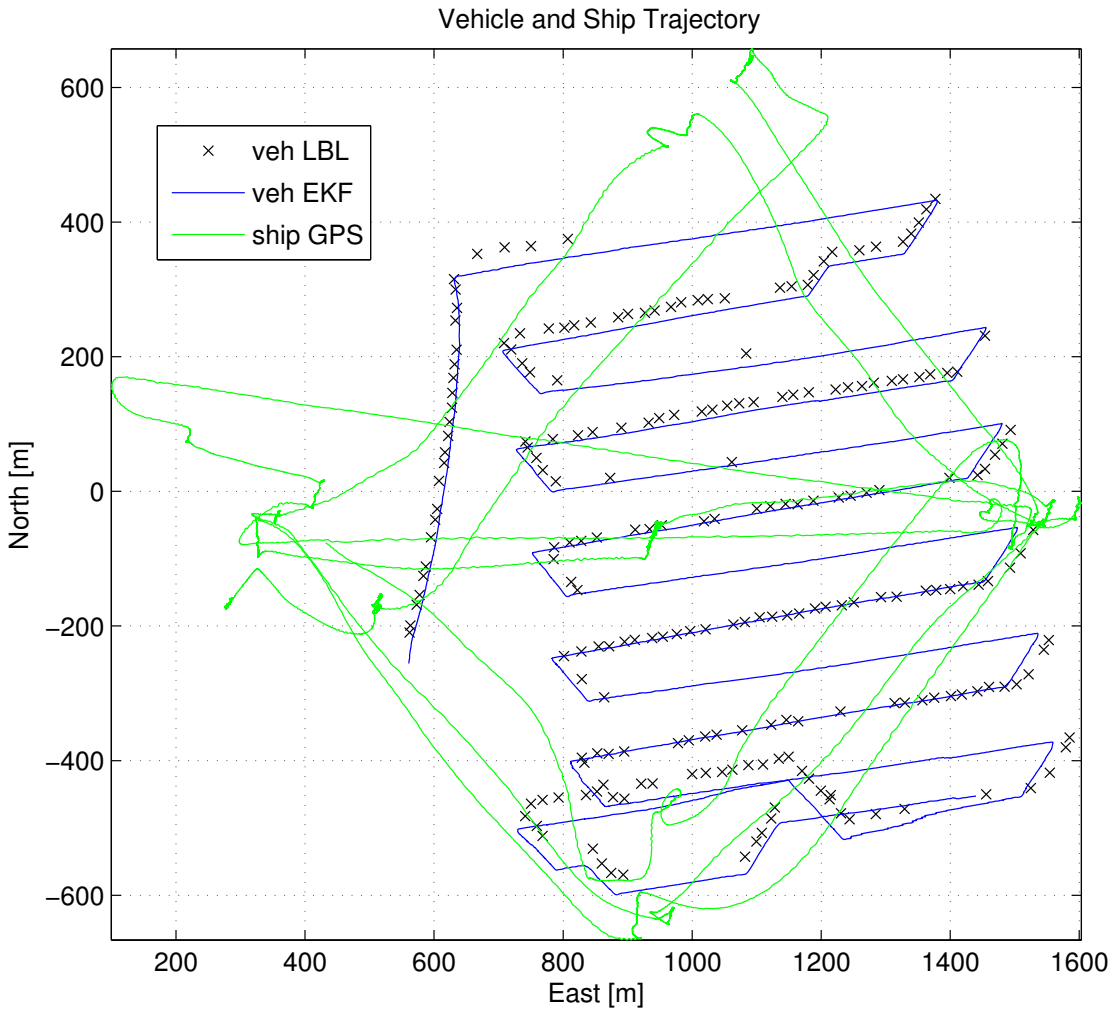

Figure 5.3: EKF estimate of vehicle position compared to LBL fixes with an overlay of the ship's track.

5.3 shows an XY plot of the vehicle trajectory as estimated by the CEKF compared with the vehicle position fixes from LBL. LBL fixes were largely unavailable on tracklines where the vehicle was heading east, most likely due to shadowing of the transducer by the vehicle frame at this vehicle heading. Calculating the difference between the LBL fixes and the corresponding CEKF estimated vehicle position in the East-West direction and the North-South direction, we find that error in the East-West direction has a mean of -10.3m and a standard deviation of 10.2 m, while the error in the North-South direction has a mean of -13.5 m and also a standard deviation of 10.2 m. These errors compare favorably with LBL, which has 1-10 m typical accuracy. However, the non-zero mean suggests the presence of systematic errors that are not accounted for in the reported sensor calibrations. The author and collaborators are currently pursuing a more rigorous evaluation of sensor calibration.

5.3.6 Sources of Error

Unmodelled non-zero-mean or non-Gaussian noise violates the assumptions of the Kalman filter and is a source of error in the filter's estimate. In addition to sensor offsets discussed above, other possible sources of error in this experiment are the estimate of the LBL beacon positions and the assumption of a constant sound velocity profile.

LBL Accuracy: While submerged, the vehicle used range information in the form of two-way travel times from three LBL beacons to estimate its absolute position in real time [44]. The accuracy of the vehicle position estimate from LBL ranges is predicated on the accuracy to which the position of the LBL beacons is known—uncertainty in beacon location translates directly to uncertainty in the vehicle position estimate in the radial direction from the beacon. The LBL beacon survey on this expedition, directed by Michael Jakuba, used the standard procedure of collecting two-way travel times from the ship to the individual beacons from 5-10 different ship locations after each beacon reaches the seafloor. The ship locations are spaced approximately equally around a circle with $\sim$1km horizontal radius from each beacon's estimated bottom location. Beacon location is then estimated using a least-squares algorithm after outliers have been manually rejected. Table 5.1 shows the position of the three LBL beacons used for this survey relative to the survey site and the residual root mean squared error of the estimated beacon position when surveyed in as described.

Table 5.1: LBL Beacon location and accuracy of position estimate.

Beacon	Approx. Location	RMS Error
A	3 km West	1.8 m
B	3 km North	3.8 m
C	2.5 km East	3.7 m

Sound Velocity Estimation: In this implementation, the CEKF uses a depth-weighted average sound velocity to calculate range from the travel time of acoustic data packets. The actual sound velocity profile, however, varies over depth as shown in Figure 5.4. Refraction due to the change in sound speed can cause ray bending in acoustic signals transmitted through the water column. As a result, the travel time of an acoustic signal is not directly proportional to slant range and is dependent on the horizontal displacement between the vehicle and the ship.

To quantify this error, we consider a range estimate between the vehicle and the ship when the ship is at the western-most apex of its diamond pattern and the vehicle is at the far eastern edge of its survey, thus incorporating the largest horizontal offset possible (1236 m horizontal offset). Calculating the difference in the range estimate found using ray-bending techniques [88] versus the depth-weighted average sound velocity, we find that assuming

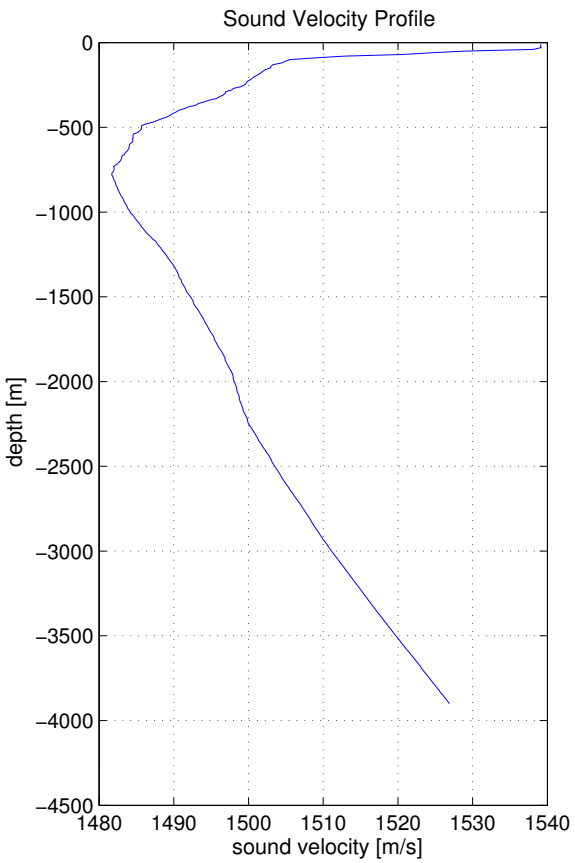

Figure 5.4: Sound velocity computed from data from the conductivity-temperature-depth (CTD) sensor on *Puma*.

a constant sound velocity equal to the depth-weighted average incurs an error in the range estimate on the order of one meter and therefore is not a substantial source of error in this data set.

5.4 Chapter Summary

This chapter reports results from deep-water sea trials evaluating a single-beacon one-way-travel-time navigation implemented with a centralized EKF. Results from the CEKF are compared to the ground truth absolute-navigation from LBL position fixes. The difference between the CEKF results and the LBL fixes is commensurate with the errors we typically expect from LBL, leading us to conclude that single-beacon navigation is a viable alternative to LBL navigation for deep-water applications where the ship or surface node can be moved around the survey site to provide appropriate geometric constraints on the vehicle position estimate.

Chapter 6

Extended Information Filter for Single-Beacon Navigation

6.1 Introduction

The information filter, originally conceived as a decentralized formulation of the Kalman filter [50], is a recursive estimator for linear systems that retains the properties of the Kalman filter (i.e. it is an unbiased, minimum variance estimator) with the additional benefits of additive measurement updates and, when formulated properly as discussed below, additive process predictions [26].

This chapter reports a brief overview of the extended information filter, a discussion of sparsity in the centralized implementation of the extended information filter (CEIF), and the derivation of a decentralized extended information filter (DEIF) for single-beacon one-way-travel-time (OWTT) navigation [27, 28, 93, 94]. The CEIF is formulated within the the same framework as that used in Chapter 5 for the CEKF, i.e. with access to all sensor data from both the vehicle and the ship. In contrast, the DEIF is designed to run locally on a submerged vehicle with real-time access to measurements from the vehicle's inertial sensors and infrequent, asynchronous access to acoustic broadcasts from a moving reference beacon. The DEIF does *not* have access to real-time global positioning system (GPS) measurements from the reference beacon or any other georeferenced information except that which is received acoustically. While the CEIF is applicable only in post-processing, the DEIF is designed to be implemented in real time on one or more vehicles. Both formulations reported here are for the nonlinear plant with discrete observations described in

Chapter 4. Note that the CEIF is identical to the CEKF by definition because they are formulated with identical constraints. The CEIF is simply based on a different, but equivalent, pair of statistics to describe the state of the system.

The remainder of this chapter is organized as follows: Section 6.2 reviews the extended information filter. Section 6.3 discusses the sparsity of the centralized information filter as it is formulated for OWTT navigation. Section 6.4 presents the derivation of the decentralized extended information filter and shows that analytically it produces identical results to those of a centralized extended Kalman filter at the time instant immediately following each range measurement. Section 6.5 presents the results of a numerical simulation used to validate the DEIF. Section 6.6 discusses the robustness of the proposed navigation method to packet loss and strategies for mitigating potential issues with packet loss. Section 6.7 concludes.

6.2 Extended Information Filter

The information filter is often referred to as the *dual* of the Kalman filter. The Kalman filter recursively estimates the mean, $\boldsymbol{\mu}$, and covariance, $\boldsymbol{\Sigma}$, of the random variable $\boldsymbol{x}$, which is the state vector of the system

$$\boldsymbol{\mu} = E[\boldsymbol{x}] \tag{6.1}$$
$$\boldsymbol{\Sigma} = E\left[(\boldsymbol{x}-\boldsymbol{\mu})(\boldsymbol{x}-\boldsymbol{\mu})^\top\right]. \tag{6.2}$$

The information filter is based on the explicit normalization of the random variable $\boldsymbol{x}$ by its covariance $\boldsymbol{\Sigma}$ such that the information filter recursively estimates the mean, $\boldsymbol{\eta}$, and covariance, $\boldsymbol{\Lambda}$, of the random variable $\boldsymbol{\Sigma}^{-1}\boldsymbol{x}$

$$\boldsymbol{\eta} = E[\boldsymbol{\Sigma}^{-1}\boldsymbol{x}] = \boldsymbol{\Sigma}^{-1}\boldsymbol{\mu} \tag{6.3}$$
$$\boldsymbol{\Lambda} = E\left[(\boldsymbol{\Sigma}^{-1}\boldsymbol{x}-\boldsymbol{\Sigma}^{-1}\boldsymbol{\mu})(\boldsymbol{\Sigma}^{-1}\boldsymbol{x}-\boldsymbol{\Sigma}^{-1}\boldsymbol{\mu})^\top\right] \tag{6.4}$$
$$= E\left[\boldsymbol{\Sigma}^{-1}\boldsymbol{x}\boldsymbol{x}^\top\boldsymbol{\Sigma}^{-1} - \boldsymbol{\Sigma}^{-1}\boldsymbol{x}\boldsymbol{\mu}^\top\boldsymbol{\Sigma}^{-1} - \boldsymbol{\Sigma}^{-1}\boldsymbol{\mu}\boldsymbol{x}^\top\boldsymbol{\Sigma}^{-1} + \boldsymbol{\Sigma}^{-1}\boldsymbol{\mu}\boldsymbol{\mu}^\top\boldsymbol{\Sigma}^{-1}\right] \tag{6.5}$$
$$= E\left[\boldsymbol{\Sigma}^{-1}\boldsymbol{x}\boldsymbol{x}^\top\boldsymbol{\Sigma}^{-1}\right] - \boldsymbol{\Sigma}^{-1}\boldsymbol{\mu}\boldsymbol{\mu}^\top\boldsymbol{\Sigma}^{-1} \tag{6.6}$$
$$= \boldsymbol{\Sigma}^{-1}\left(E\left[\boldsymbol{x}\boldsymbol{x}^\top\right] - \boldsymbol{\mu}\boldsymbol{\mu}^\top\right)\boldsymbol{\Sigma}^{-1} \tag{6.7}$$
$$= \boldsymbol{\Sigma}^{-1} \tag{6.8}$$

where $\boldsymbol{\eta}$ is referred to as the information vector, and $\boldsymbol{\Lambda}$ the information matrix [8, 70].

The information filter can be extended for use on nonlinear systems to form the extended information filter (EIF) in the same manner as the extended Kalman filter—by linearizing the process model and observation models along the trajectories of the system [36, 70]. A complete derivation of the linear information filter is provided in Appendix C. The process prediction and measurement update equations for the extended information filter are well known, and are provided here with references but without proof.

6.2.1 Conditioning and Marginalization

Assuming that we have a normal random variable $\boldsymbol{\xi}$ such that $p(\boldsymbol{\xi}) = \mathcal{N}(\boldsymbol{\mu}, \boldsymbol{\Sigma})$, partitioned $\boldsymbol{\xi} = [\boldsymbol{\alpha}^\top, \boldsymbol{\beta}^\top]^\top$ results in

$$p(\boldsymbol{\alpha}, \boldsymbol{\beta}) = \mathcal{N}\left(\begin{bmatrix} \boldsymbol{\mu}_\alpha \\ \boldsymbol{\mu}_\beta \end{bmatrix}, \begin{bmatrix} \boldsymbol{\Sigma}_{\alpha\alpha} & \boldsymbol{\Sigma}_{\alpha\beta} \\ \boldsymbol{\Sigma}_{\beta\alpha} & \boldsymbol{\Sigma}_{\beta\beta} \end{bmatrix}\right) \tag{6.9}$$

which in the information form results in the information vector and information matrix

$$\boldsymbol{\eta} = \begin{bmatrix} \boldsymbol{\eta}_\alpha \\ \boldsymbol{\eta}_\beta \end{bmatrix} \tag{6.10}$$

$$\boldsymbol{\Lambda} = \begin{bmatrix} \boldsymbol{\Lambda}_{\alpha\alpha} & \boldsymbol{\Lambda}_{\alpha\beta} \\ \boldsymbol{\Lambda}_{\beta\alpha} & \boldsymbol{\Lambda}_{\beta\beta} \end{bmatrix}. \tag{6.11}$$

Examining the probabilistic representation of the information filter compared to the Kalman filter, we see that the operations of marginalization and conditioning are performed by the dual calculations shown in Table 6.1.

Table 6.1: Kalman filter versus information filter

	Marginalization $p(\boldsymbol{\alpha}) = \int p(\boldsymbol{\alpha}, \boldsymbol{\beta}) d\boldsymbol{\beta}$	**Conditioning** $p(\boldsymbol{\alpha}\|\boldsymbol{\beta}) = p(\boldsymbol{\alpha}, \boldsymbol{\beta})/p(\boldsymbol{\beta})$
Kalman filter	$\boldsymbol{\mu} = \boldsymbol{\mu}_\alpha$ $\boldsymbol{\Sigma} = \boldsymbol{\Sigma}_{\alpha\alpha}$	$\boldsymbol{\mu}' = \boldsymbol{\mu}_\alpha + \boldsymbol{\Sigma}_{\alpha\beta}\boldsymbol{\Sigma}_{\beta\beta}^{-1}(\boldsymbol{\beta} - \boldsymbol{\mu}_\beta)$ $\boldsymbol{\Sigma}' = \boldsymbol{\Sigma}_{\alpha\alpha} - \boldsymbol{\Sigma}_{\alpha\beta}\boldsymbol{\Sigma}_{\beta\beta}^{-1}\boldsymbol{\Sigma}_{\beta\alpha}$
Information filter	$\boldsymbol{\eta} = \boldsymbol{\eta}_\alpha - \boldsymbol{\Lambda}_{\alpha\beta}\boldsymbol{\Lambda}_{\beta\beta}^{-1}\boldsymbol{\eta}_\beta$ $\boldsymbol{\Lambda} = \boldsymbol{\Lambda}_{\alpha\alpha} - \boldsymbol{\Lambda}_{\alpha\beta}\boldsymbol{\Lambda}_{\beta\beta}^{-1}\boldsymbol{\Lambda}_{\beta\alpha}$	$\boldsymbol{\eta}' = \boldsymbol{\eta}_\alpha - \boldsymbol{\Lambda}_{\alpha\beta}\boldsymbol{\beta}$ $\boldsymbol{\Lambda}' = \boldsymbol{\Lambda}_{\alpha\alpha}$

Source: Eustice et al. [26]

6.2.2 Process Prediction

We assume a general process model of the form

$$\dot{\boldsymbol{x}}(t) = \boldsymbol{f}(\boldsymbol{x}(t), t) + \boldsymbol{G}(t)\boldsymbol{w}(t) \tag{6.12}$$

where $\boldsymbol{x}(t)$ is the state vector and $\boldsymbol{w}(t) \sim \mathcal{N}(0, \boldsymbol{Q}(t))$ is independent zero-mean Gaussian process noise in the acceleration term. The discrete-time linearized process model is then

$$\boldsymbol{x}_{k+1} = \boldsymbol{F}_k\boldsymbol{x}_k + \boldsymbol{B}_k\boldsymbol{u}_k + \boldsymbol{w}_k \tag{6.13}$$

where $\boldsymbol{F}_k$ is the discrete-time linear state transition matrix, $\boldsymbol{u}_k$ is the piecewise-constant input, and $\boldsymbol{w}_k \sim \mathcal{N}(0, \boldsymbol{Q}_k)$ is independent zero-mean Gaussian process noise.

In the formulation of the information filter presented herein our state vector consists of both current and historic states of the plant defined in (6.13). Therefore we consider the state vector of the system, denoted by a different font $\mathbf{x}$, consisting of two plant states, the current plant state $\boldsymbol{x}_k$ and a previous plant state $\boldsymbol{x}_p$

$$\mathbf{x}_{k|k} = \begin{bmatrix} \boldsymbol{x}_k \\ \boldsymbol{x}_p \end{bmatrix} \tag{6.14}$$

with the information matrix and vector defined as

$$\boldsymbol{\Lambda}_{k|k} = \begin{bmatrix} \boldsymbol{\Lambda}_{kk} & \boldsymbol{\Lambda}_{kp} \\ \boldsymbol{\Lambda}_{pk} & \boldsymbol{\Lambda}_{pp} \end{bmatrix} \tag{6.15}$$

$$\boldsymbol{\eta}_{k|k} = \begin{bmatrix} \boldsymbol{\eta}_k \\ \boldsymbol{\eta}_p \end{bmatrix}. \tag{6.16}$$

In the information form, the process prediction equations for the system, conditioned on the vehicle sensor measurements up to time k, $\mathbf{Z}^{1:k}$, and the control inputs up to time k, $\mathbf{U}^{1:k}$, are

$$p(\boldsymbol{x}_{k+1}, \boldsymbol{x}_p | \mathbf{Z}^{1:k}, \mathbf{U}^{1:k}) : \tag{6.17}$$

$$\boldsymbol{\Lambda}_{k+1|k} = \begin{bmatrix} \Psi_k & \boldsymbol{Q}_k^{-1} \boldsymbol{F}_k \boldsymbol{\Omega}_k^{-1} \boldsymbol{\Lambda}_{kp} \\ \boldsymbol{\Lambda}_{pk} \boldsymbol{\Omega}_k^{-1} \boldsymbol{F}_k^\top \boldsymbol{Q}_k^{-1} & \boldsymbol{\Lambda}_{pp} - \boldsymbol{\Lambda}_{pk} \boldsymbol{\Omega}_k^{-1} \boldsymbol{\Lambda}_{kp} \end{bmatrix} \tag{6.18}$$

$$\boldsymbol{\eta}_{k+1|k} = \begin{bmatrix} \boldsymbol{Q}_k^{-1} \boldsymbol{F}_k \boldsymbol{\Omega}_k^{-1} \boldsymbol{\eta}_k + \Psi_k (\boldsymbol{f}(\boldsymbol{\mu}_{k|k}, \boldsymbol{u}_k) - \boldsymbol{F}_k \boldsymbol{\mu}_{k|k}) \\ \boldsymbol{\eta}_p - \boldsymbol{\Lambda}_{pk} \boldsymbol{\Omega}_k^{-1} \boldsymbol{\eta}_k^* \end{bmatrix} \tag{6.19}$$

where $\boldsymbol{f}(\cdot)$ is the nonlinear process model and

$$\Psi_k = (\boldsymbol{Q}_k + \boldsymbol{F}_k \boldsymbol{\Lambda}_{kk}^{-1} \boldsymbol{F}_k^\top)^{-1} \tag{6.20}$$

$$\boldsymbol{\Omega}_k = \boldsymbol{\Lambda}_{kk} + \boldsymbol{F}_k^\top \boldsymbol{Q}_k^{-1} \boldsymbol{F}_k \tag{6.21}$$

$$\boldsymbol{\eta}_k^* = \boldsymbol{\eta}_k - \boldsymbol{F}_k^\top \boldsymbol{Q}_k^{-1} (\boldsymbol{f}(\boldsymbol{\mu}_{k|k}, \boldsymbol{u}_k) - \boldsymbol{F}_k \boldsymbol{\mu}_{k|k}) \tag{6.22}$$

as derived in [26, 87].

6.2.3 Process Prediction with Augmentation

In equations (6.18) and (6.19), the current state at time k is propagated to time $k+1$, such that

$$\mathbf{x}_{k+1|k} = \begin{bmatrix} \boldsymbol{x}_{k+1} \\ \boldsymbol{x}_p \end{bmatrix}. \tag{6.23}$$

If, instead, we augment the state vector to include the state at time $k+1$ in addition to the original states

$$\mathbf{x}_{k+1|k} = \begin{bmatrix} \boldsymbol{x}_{k+1} \\ \boldsymbol{x}_k \\ \boldsymbol{x}_p \end{bmatrix} \tag{6.24}$$

the process prediction equations have a very different structure [26],

$$p(\boldsymbol{x}_{k+1}, \boldsymbol{x}_k, \boldsymbol{x}_p | \mathbf{Z}^{1:k}, \mathbf{U}^{1:k}) : \tag{6.25}$$

$$\boldsymbol{\Lambda}_{k+1|k} = \begin{bmatrix} \boldsymbol{Q}_k^{-1} & -\boldsymbol{Q}_k^{-1}\boldsymbol{F}_k & \mathbf{0} \\ -\boldsymbol{F}_k^\top \boldsymbol{Q}_k^{-1} & \boldsymbol{F}_k^\top \boldsymbol{Q}_k^{-1}\boldsymbol{F}_k + \boldsymbol{\Lambda}_{kk} & \boldsymbol{\Lambda}_{kp} \\ \mathbf{0} & \boldsymbol{\Lambda}_{pk} & \boldsymbol{\Lambda}_{pp} \end{bmatrix} \tag{6.26}$$

$$\boldsymbol{\eta}_{k+1|k} = \begin{bmatrix} \boldsymbol{Q}_k^{-1}(\boldsymbol{f}(\boldsymbol{\mu}_{k|k}, \boldsymbol{u}_k) - \boldsymbol{F}_k \boldsymbol{\mu}_{k|k}) \\ \boldsymbol{\eta}_k - \boldsymbol{F}_k^\top \boldsymbol{Q}_k^{-1}(\boldsymbol{f}(\boldsymbol{\mu}_{k|k}, \boldsymbol{u}_k) - \boldsymbol{F}_k \boldsymbol{\mu}_{k|k}) \\ \boldsymbol{\eta}_p \end{bmatrix} \tag{6.27}$$

where Equation (6.26) can be written as the sum of two matrices—one containing the process prediction information and the other containing the previous information matrix

$$\boldsymbol{\Lambda}_{k+1|k} = \begin{bmatrix} \boldsymbol{Q}_k^{-1} & -\boldsymbol{Q}_k^{-1}\boldsymbol{F}_k & \mathbf{0} \\ -\boldsymbol{F}_k^\top \boldsymbol{Q}_k^{-1} & \boldsymbol{F}_k^\top \boldsymbol{Q}_k^{-1}\boldsymbol{F}_k & \mathbf{0} \\ \mathbf{0} & \mathbf{0} & \mathbf{0} \end{bmatrix} + \begin{bmatrix} \mathbf{0} & \mathbf{0} & \mathbf{0} \\ \mathbf{0} & \boldsymbol{\Lambda}_{kk} & \boldsymbol{\Lambda}_{kp} \\ \mathbf{0} & \boldsymbol{\Lambda}_{pk} & \boldsymbol{\Lambda}_{pp} \end{bmatrix}. \tag{6.28}$$

As is noted in [26], this results in $\boldsymbol{\Lambda}$ having a sparse, block-tridiagonal structure. The sparsity of $\boldsymbol{\Lambda}$ is examined in greater detail in Section 6.3.

6.2.4 Measurement Update

Assuming that we have the discrete, nonlinear observation model

$$\boldsymbol{z}_k = \boldsymbol{h}(\boldsymbol{x}(t_k)) + \boldsymbol{v}_k, \ k = 1, 2, \cdots \tag{6.29}$$

where $\boldsymbol{z}_k$ is the measurement at time step t_k, $\boldsymbol{x}_k$ is the state vector, $\boldsymbol{h}(\cdot)$ is the observation model, and $\boldsymbol{v}_k \sim \mathcal{N}(0, \boldsymbol{R}_k)$ is independent zero-mean Gaussian measurement noise, the measurement update equations for the extended information filter are

$$\boldsymbol{\Lambda}_{k|k} = \boldsymbol{\Lambda}_{k|k-1} + \boldsymbol{H}_k^\top \boldsymbol{R}_k^{-1} \boldsymbol{H}_k \tag{6.30}$$

$$\boldsymbol{\eta}_{k|k} = \boldsymbol{\eta}_{k|k-1} + \boldsymbol{H}_k^\top \boldsymbol{R}_k^{-1}(\boldsymbol{z}_k - \boldsymbol{h}(\boldsymbol{\mu}_{k|k-1}) + \boldsymbol{H}_k \boldsymbol{\mu}_{k|k-1}) \tag{6.31}$$

where $\boldsymbol{H}_k$ is the Jacobian of the measurement with respect to $\boldsymbol{x}$

$$\boldsymbol{H}_k = \left. \frac{\partial \boldsymbol{h}(\boldsymbol{x}(t_k))}{\partial \boldsymbol{x}(t_k)} \right|_{\boldsymbol{x}(t_k) = \mu_{k|k-1}} \tag{6.32}$$

and $\boldsymbol{\mu}_{k|k-1}$ is the mean of the state vector [36,70,87]. Note that one of the useful properties of the information filter, shown clearly in (6.30) and (6.31), is that the measurement update equation is additive.

6.3 Sparsity in the Centralized Filter

The purpose of using the information filter is to enable a tractable decentralized implementation for one-way-travel-time navigation. Before deriving the decentralized information filter, however, we briefly explore sparsity in the centralized extended information filter (CEIF) within the context of OWTT navigation.

The CEIF uses the identical model described in chapter 4. As described in [26], the information matrix can be represented graphically using undirected graphical models. Figure 6.1 depicts two such models of the vehicle and the ship, where the nodes, $\boldsymbol{x}_{v_i}$ and $\boldsymbol{x}_{s_i}$ for $i \in [1, \cdots, n]$, represent the pose of the vehicle or ship at a different time step and the edges represent constraints between poses. Note that, though the graph is undirected, arrows are used for the convenience of the readers to represent the temporal dependence of the poses. All of the poses shown are included in the state vector of the system

$$\mathbf{x} = [\boldsymbol{x}_{v_0}^\top, \cdots, \boldsymbol{x}_{v_6}^\top, \boldsymbol{x}_{s_0}^\top, \cdots, \boldsymbol{x}_{s_6}^\top]^\top. \tag{6.33}$$

In the information form, constraints also represent non-zero entries in the corresponding information matrix. In the information matrices shown, the vehicle poses are grouped together in the upper left sub-block and the ship poses are grouped together in the bottom right sub-block as shown in (6.33). The *current* ship and vehicle states, $\boldsymbol{x}_{v_6}$ and $\boldsymbol{x}_{s_6}$, are in the top left corner of their respective sub-blocks.

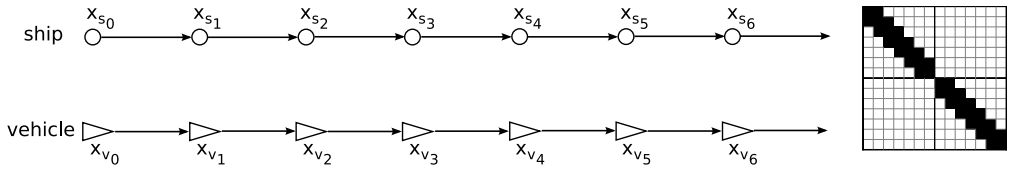

(a) Undirected graphical models for the vehicle and ship, where x_{v_n} and x_{s_n} are the vehicle and ship states respectively at time step n. The associated information matrix is sparse and tridiagonal.

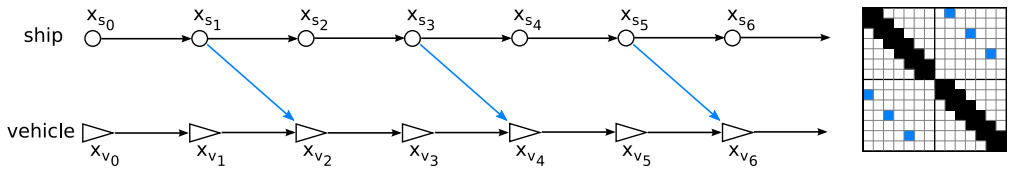

(b) Range measurements between the ship and vehicle add additional constraints shown in blue.

Figure 6.1: Example undirected graphical models and their corresponding information matrices.

As is noted in [26] and shown in Section 6.2.3, when the information filter is formulated such that the state vector contains an estimate of multiple poses, the resulting information matrix, $\mathbf{\Lambda}$, has a sparse, tridiagonal structure. This tridiagonal structure is clearly visible from the graphical model because each pose is only connected to the pose immediately before it in time and the pose immediately after it in time. Mathematically this represents the *conditional* independence of the current pose, given the previous pose, of all other historic poses—a property of first-order Markov processes [78].

In Figure 6.1, the graphical model in (a) shows the vehicle and ship independent of each other. The addition of range measurements in (b) adds constraints between the vehicle and ship and adds non-zero off-diagonal entries to the information matrix. Because every ship or vehicle pose has at most one range measurement associated with it (in the single-vehicle implementation), the range measurements add only a single diagonal above and below the tridiagonal. Measurements from other vehicle or ship sensors do not add additional constraints because they only add information to the current vehicle or ship state.

The marginalization of states in the system has the potential to reduce sparsity by causing fill-in. Graphically, when a state is marginalized out, every state linked to it in the pose graph becomes simply connected as shown in Figure 6.2. When marginalizing out a state that does not have a range measurement associated with it, as in (a), the tridiagonal structure of the information matrix is not altered. However, when the ship and vehicle states associated with one of the range measurement are marginalized out, as in (b), the resulting graphical has a densely connected subset of states. In the CEIF we avoid this problem by marginalizing out only the oldest vehicle and ship states as shown in (c). In this case, when marginalizing out both the ship and vehicle states associated with the oldest time step that has a range measurement associated with it, the constraint from the original range measurement is replaced by a link between the oldest remaining vehicle and ship states, but no additional links are added to the graphical model.

6.4 Decentralized Implementation

In this section we present the derivation of the vehicle-based decentralized extended information filter (DEIF), designed to enable the simultaneous navigation of multiple underwater vehicles in real time using only vehicle-based navigation sensors and acoustic broadcasts from the ship or other georeferenced node. The implementation of the DEIF relies on two separate filters, a ship-based filter and a vehicle-based filter, both of which process sensor data causally and asynchronously. The information filter on the ship has access to ship sensor data but not range measurements. The ship-based filter is used to calculate the change, or delta, in the ship information vector and information matrix between acoustic broadcasts, and this delta information is acoustically transmitted to the vehicle. Figure 6.3 shows a schematic of the delta ship information transmitted from the ship to the vehicle. The decentralized vehicle-based filter, the DEIF, has real-time access to vehicle sensor data and the asynchronous acoustic broadcasts from the ship, but does *not* have di-

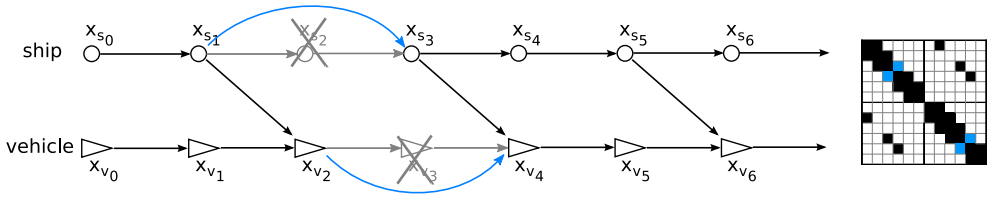

(a) The marginalization of a state that is only serially connected with the states before and after it has no effect on the sparsity or tridiagonal structure of the information matrix.

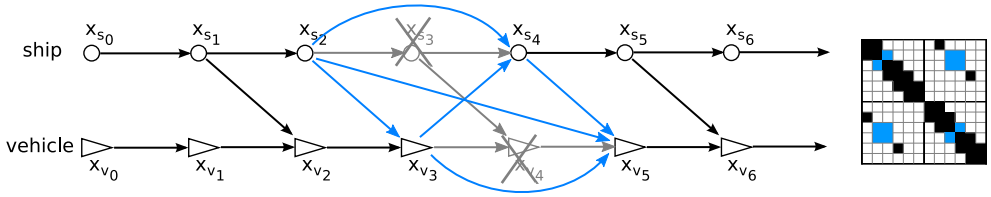

(b) During the marginalization of the states associated with a range measurement, fill-in occurs in the information matrix.

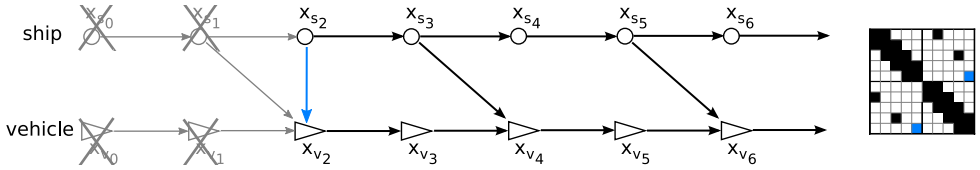

(c) The marginalization of only the oldest states prevents fill-in in the information matrix, even in the presence of range measurements.

Figure 6.2: Undirected graphical models illustrating the effects of marginalization. Vehicle and ship states are shown for every t_{TOL} and t_{TOA}.

rect access to the ship sensor measurements apart from the delta information transmissions.

6.4.1 DEIF State Vector

The DEIF, the filter on the vehicle, maintains an estimate of the *current vehicle state* as well as estimates of *historic ship states* reconstructed from the delta information received acoustically from the ship

$$\mathbf{x}_{k|k} = \begin{bmatrix} \boldsymbol{x}_{v_k} \\ \boldsymbol{x}_{s_{TOL_n}} \\ \vdots \\ \boldsymbol{x}_{s_{TOL_1}} \end{bmatrix} \tag{6.34}$$

where $\mathbf{x}_{k|k}$ denotes the entire vehicle state vector, $\boldsymbol{x}_{v_k}$ denotes the current vehicle state, and $\boldsymbol{x}_{s_{TOL_n}}$ denotes the ship state at the time-of-launch (TOL) of the n$^{\text{th}}$ acoustic data packet. In practice it is undesirable and unnecessary to keep every ship state, causing the state vector to grow without bound. Instead we maintain a fixed-length queue of ship states by

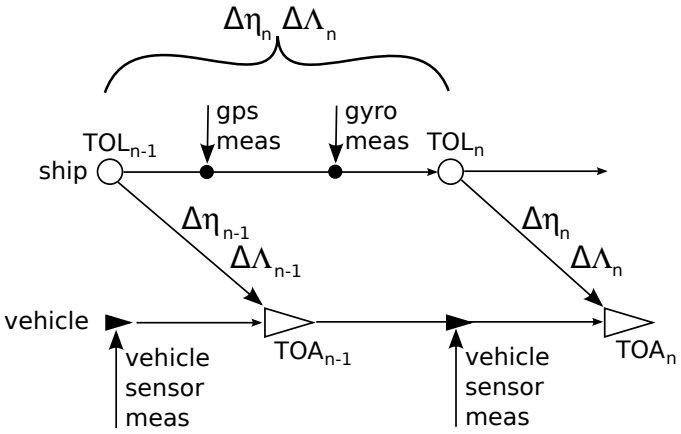

Figure 6.3: A schematic of the information contained in the acoustic data packet transmitted from the ship to the vehicle.

marginalizing out the oldest ship state when a new state is appended to the state vector. Note that, because acoustic broadcasts have a non-negligible time delay associated with them, the DEIF state vector cannot contain information about the *current* ship state, it only contains information about *historic* ship states (see Figure 6.3).

The reconstructed ship states are not subjected to process predictions or measurement updates other than range measurements, because the DEIF has no knowledge of the ship process model or measurement from ship sensors. The ship states remain unchanged over time except when new information from acoustic broadcasts is incorporated and range measurement updates are performed.

6.4.2 Independent Ship Filter

The ship-based filter maintains an estimate of the current ship state as well as estimates of previous ship states at the time-of-launch (TOL) of each acoustic data packet. Assuming n data packets have been broadcast, this results in a state vector of the form

$$\mathbf{x}_{s_{k|k}} = \begin{bmatrix} \boldsymbol{x}_{s_k} \\ \boldsymbol{x}_{s_{TOL_n}} \\ \vdots \\ \boldsymbol{x}_{s_{TOL_2}} \\ \boldsymbol{x}_{s_{TOL_1}} \end{bmatrix} \tag{6.35}$$

where $\mathbf{x}_{s_{k|k}}$ denotes the entire state vector at time k, $\boldsymbol{x}_{s_k}$ denotes the current ship state, and $\boldsymbol{x}_{s_{TOL_n}}$ denotes the ship state when the n$^{\text{th}}$ acoustic data packet was broadcast. In practice it is undesirable and unnecessary to keep every ship state, causing the state vector to grow without bound. Instead we maintain a fixed-length queue of ship states by marginalizing out the oldest ship state when a new state is appended to the state vector.

6.4.3 Acoustic Range Measurements

To initiate a range measurement, the ship broadcasts an acoustic data packet containing information about the ship state. When a data packet packet arrives at the vehicle, the ship information included in the data packet is incorporated into the DEIF in order to recreate the ship's filter. After the ship information is incorporated, the range measurement update, (6.30) and (6.31), is performed using the range information garnered from the acoustic broadcast.

What differentiates the DEIF from other estimators used in decentralized single-beacon navigation is the information that is transmitted with the range measurements and how that information is incorporated into the decentralized vehicle navigation filter in conjunction with the range measurement. In other formulations of single-beacon navigation, the acoustic data packet contains the mean and covariance of the ship's current x-y position, which is used by the filter on the vehicle to perform a range measurement update. In [5] and [29] in particular, which are the works that most closely resemble the work presented in this thesis, range measurements are incorporated in an ad hoc fashion where multiple hypotheses for current and historic vehicle states are found based on the intersection of the current range measurement and a given number of historic range measurements are forward propagated using the vehicle's dead-reckoned track. The likelihood of the vehicle's path through each combination of these possible states is evaluated with a cost function based on the Kullback-Leibler divergence distance metric. Over-confidence is addressed by maintaining multiple filters on each vehicle that selectively exclude data from every combination of other vehicles. The acoustic broadcast from a vehicle contains the estimates from all of these filters so that the receiving vehicle is able to choose an estimate that does not result in an over-confident solution. As a result, the proposed algorithm is somewhat cumbersome and difficult or impossible to compare analytically to a centralized filter.

In contrast, in the formulation presented here, the acoustic data packet contains the *change* in $\mathbf{\Lambda}_s$ and $\boldsymbol{\eta}_s$ between the time of the current acoustic broadcast, TOL_n, and the time of the previous acoustic broadcast, TOL_{n-1},

$$\Delta\mathbf{\Lambda}_{TOL_n} = \mathbf{\Lambda}_{s_{TOL_n}} - \mathbf{\Lambda}_{s_{TOL_{n-1}}} \tag{6.36}$$

$$\Delta\boldsymbol{\eta}_{TOL_n} = \boldsymbol{\eta}_{s_{TOL_n}} - \boldsymbol{\eta}_{s_{TOL_{n-1}}} \tag{6.37}$$

where, for conformability, $\mathbf{\Lambda}_{s_{TOL_{n-1}}}$ and $\boldsymbol{\eta}_{s_{TOL_{n-1}}}$ have been padded with zeros to match the size of $\mathbf{\Lambda}_{s_{TOL_n}}$ and $\boldsymbol{\eta}_{s_{TOL_n}}$ respectively. These data packets are reassembled subsea in the DEIF to recreate the ship's filter and, as discussed in more detail in Section 6.4.4, enable the vehicle-based filter to exactly replicate the results of the centralized filter immediately after each range measurement. The structure of the ship-based filter is the key to making this replication possible.

Because of the linear ship model and the linear observation models for GPS and gyrocompass measurements, no linearization is necessary to calculate the process prediction or

the measurement update. The process prediction

$$\boldsymbol{\Lambda}_{s_{k+1|k}} = \begin{bmatrix} \boldsymbol{Q}_{s_k}^{-1} & -\boldsymbol{Q}_{s_k}^{-1}\boldsymbol{F}_{s_k} \\ -\boldsymbol{F}_{s_k}^{\top}\boldsymbol{Q}_{s_k}^{-1} & \boldsymbol{F}_{s_k}^{\top}\boldsymbol{Q}_{s_k}^{-1}\boldsymbol{F}_{s_k} \end{bmatrix} + \begin{bmatrix} \mathbf{0} & \mathbf{0} \\ \mathbf{0} & \boldsymbol{\Lambda}_{s_{k|k}} \end{bmatrix} \tag{6.38}$$

$$= \begin{bmatrix} \boldsymbol{Q}_{s_k}^{-1} & -\boldsymbol{Q}_{s_k}^{-1}\boldsymbol{F}_{s_k} \\ -\boldsymbol{F}_{s_k}^{\top}\boldsymbol{Q}_{s_k}^{-1} & \boldsymbol{F}_{s_k}^{\top}\boldsymbol{Q}_{s_k}^{-1}\boldsymbol{F}_{s_k} + \boldsymbol{\Lambda}_{s_{k|k}} \end{bmatrix} \tag{6.39}$$

is additive and independent of the ship state—$\boldsymbol{F}_{s_k}$ is constant and $\boldsymbol{Q}_{s_k}$ is dependent only on the size of the time step. The measurement update

$$\boldsymbol{\Lambda}_{s_{k+1|k+1}} = \boldsymbol{\Lambda}_{s_{k+1|k}} + \begin{bmatrix} \boldsymbol{H}_{k+1}^{\top}\boldsymbol{R}_{k+1}^{-1}\boldsymbol{H}_{k+1} & \mathbf{0} \\ \mathbf{0} & \mathbf{0} \end{bmatrix} \tag{6.40}$$

$$= \begin{bmatrix} \boldsymbol{Q}_{s_k}^{-1} & -\boldsymbol{Q}_{s_k}^{-1}\boldsymbol{F}_{s_k} \\ -\boldsymbol{F}_{s_k}^{\top}\boldsymbol{Q}_{s_k}^{-1} & \boldsymbol{F}_{s_k}^{\top}\boldsymbol{Q}_{s_k}^{-1}\boldsymbol{F}_{s_k} + \boldsymbol{\Lambda}_{s_{k|k}} \end{bmatrix} + \begin{bmatrix} \boldsymbol{H}_{k+1}^{\top}\boldsymbol{R}_{k+1}^{-1}\boldsymbol{H}_{k+1} & \mathbf{0} \\ \mathbf{0} & \mathbf{0} \end{bmatrix} \tag{6.41}$$

$$= \begin{bmatrix} \boldsymbol{Q}_{s_k}^{-1} + \boldsymbol{H}_{k+1}^{\top}\boldsymbol{R}_{k+1}^{-1}\boldsymbol{H}_{k+1} & -\boldsymbol{Q}_{s_k}^{-1}\boldsymbol{F}_{s_k} \\ -\boldsymbol{F}_{s_k}^{\top}\boldsymbol{Q}_{s_k}^{-1} & \boldsymbol{F}_{s_k}^{\top}\boldsymbol{Q}_{s_k}^{-1}\boldsymbol{F}_{s_k} + \boldsymbol{\Lambda}_{s_{k|k}} \end{bmatrix} \tag{6.42}$$

is also additive and depends only on the observation models and the measurement noise. In the case of the ship's GPS and gyrocompass observation models, both are linear because they are directly measuring elements in the state vector (x-y position and heading) and we assume a constant measurement noise covariance $\boldsymbol{R}$ for each that does not vary with time.

The delta information after a process prediction and measurement update

$$\Delta\boldsymbol{\Lambda}_{TOL_{k+1}} = \boldsymbol{\Lambda}_{s_{k+1|k+1}} - \boldsymbol{\Lambda}_{s_{k|k}} \tag{6.43}$$

$$= \begin{bmatrix} \boldsymbol{Q}_{s_k}^{-1} + \boldsymbol{H}_{k+1}^{\top}\boldsymbol{R}_{k+1}^{-1}\boldsymbol{H}_{k+1} & -\boldsymbol{Q}_{s_k}^{-1}\boldsymbol{F}_{s_k} \\ -\boldsymbol{F}_{s_k}^{\top}\boldsymbol{Q}_{s_k}^{-1} & \boldsymbol{F}_{s_k}^{\top}\boldsymbol{Q}_{s_k}^{-1}\boldsymbol{F}_{s_k} \end{bmatrix} \tag{6.44}$$

is thus completely independent of the ship state because every element in the matrix is constant. In addition, a single delta measurement encapsulates all of the ship sensor information gained since the last acoustic data packet was transmitted.

At the vehicle, when the delta information is received, it is incorporated into the DEIF by addition after accounting for conformability. We assume that the range measurement was broadcast at the ship at $t = k+1$ and arrives at the vehicle at $t = m+1$ where $m > k$. Let $\boldsymbol{\Lambda}_{m+1|m}^{-}$ represent the DEIF information matrix before the addition of the delta ship information and $\boldsymbol{\Lambda}_{m+1|m}^{+}$ represent the DEIF information matrix after the addition of the delta ship information. We assume that

$$\boldsymbol{\Lambda}_{m+1|m}^{-} = \begin{bmatrix} \boldsymbol{\Lambda}_{v_{m+1|m}} & \boldsymbol{\Lambda}_{rng_m}^{\top} \\ \boldsymbol{\Lambda}_{rng_m} & \boldsymbol{\Lambda}_{s_{k|k}} \end{bmatrix} \tag{6.45}$$

before the delta ship information is incorporated, where $\boldsymbol{\Lambda}_{rng_m}$ is the term from the previous range measurement at $t = m$ that correlates the current vehicle state and the ship state at

$t = k$. After the delta ship information is incorporated

$$\boldsymbol{\Lambda}^{+}_{m+1|m} = \boldsymbol{\Lambda}^{-}_{m+1|m} + \Delta\boldsymbol{\Lambda}_{TOL_{k+1}} \tag{6.46}$$

$$= \begin{bmatrix} \boldsymbol{\Lambda}_{v_{m+1|m}} & \mathbf{0} & \boldsymbol{\Lambda}^{\top}_{rng_m} \\ \mathbf{0} & \mathbf{0} & \mathbf{0} \\ \boldsymbol{\Lambda}_{rng_m} & \mathbf{0} & \boldsymbol{\Lambda}_{s_{k|k}} \end{bmatrix} + \begin{bmatrix} \mathbf{0} & \mathbf{0} & \mathbf{0} \\ \mathbf{0} & \boldsymbol{Q}^{-1}_{s_k} + \boldsymbol{H}^{\top}_{k+1}\boldsymbol{R}^{-1}_{k+1}\boldsymbol{H}_{k+1} & -\boldsymbol{Q}^{-1}_{s_k}\boldsymbol{F}_{s_k} \\ \mathbf{0} & -\boldsymbol{F}^{\top}_{s_k}\boldsymbol{Q}^{-1}_{s_k} & \boldsymbol{F}^{\top}_{s_k}\boldsymbol{Q}^{-1}_{s_k}\boldsymbol{F}_{s_k} \end{bmatrix} \tag{6.47}$$

$$= \begin{bmatrix} \boldsymbol{\Lambda}_{v_{m+1|m}} & \mathbf{0} & \boldsymbol{\Lambda}^{\top}_{rng} \\ \mathbf{0} & \boldsymbol{Q}^{-1}_{s_k} + \boldsymbol{H}^{\top}_{k+1}\boldsymbol{R}^{-1}_{k+1}\boldsymbol{H}_{k+1} & -\boldsymbol{Q}^{-1}_{s_k}\boldsymbol{F}_{s_k} \\ \boldsymbol{\Lambda}_{rng_m} & -\boldsymbol{F}^{\top}_{s_k}\boldsymbol{Q}^{-1}_{s_k} & \boldsymbol{F}^{\top}_{s_k}\boldsymbol{Q}^{-1}_{s_k}\boldsymbol{F}_{s_k} + \boldsymbol{\Lambda}_{s_{k|k}} \end{bmatrix}. \tag{6.48}$$

Incorporating the new range measurement that is made at $t = m + 1$ when the delta ship information arrives

$$\boldsymbol{\Lambda}_{m+1|m+1} = \boldsymbol{\Lambda}^{+}_{m+1|m} + \boldsymbol{H}^{\top}_{rng_{m+1}} R^{-1}_{rng}\boldsymbol{H}_{rng_{m+1}} \tag{6.49}$$

where

$$\boldsymbol{H}^{\top}_{rng_{m+1}} R^{-1}_{rng}\boldsymbol{H}_{rng_{m+1}} = \begin{bmatrix} \boldsymbol{\Lambda}_{rng;v_{m+1}} & \boldsymbol{\Lambda}^{\top}_{rng_{m+1}} & \mathbf{0} \\ \boldsymbol{\Lambda}_{rng_{m+1}} & \boldsymbol{\Lambda}_{rng;s_{k+1}} & \mathbf{0} \\ \mathbf{0} & \mathbf{0} & \mathbf{0} \end{bmatrix} \tag{6.50}$$

correlates the current vehicle state and the ship state at $k + 1$ such that

$$\boldsymbol{\Lambda}_{m+1|m+1} = \boldsymbol{\Lambda}^{+}_{m+1|m} + \boldsymbol{H}^{\top}_{rng_{m+1}} R^{-1}_{rng}\boldsymbol{H}_{rng_{m+1}} \tag{6.51}$$

$$= \begin{bmatrix} \boldsymbol{\Lambda}_{v_{m+1|m}} & \mathbf{0} & \boldsymbol{\Lambda}^{\top}_{rng_m} \\ \mathbf{0} & \boldsymbol{Q}^{-1}_{s_k} + \boldsymbol{H}^{\top}_{k+1}\boldsymbol{R}^{-1}_{k+1}\boldsymbol{H}_{k+1} & -\boldsymbol{Q}^{-1}_{s_k}\boldsymbol{F}_{s_k} \\ \boldsymbol{\Lambda}_{rng_m} & -\boldsymbol{F}^{\top}_{s_k}\boldsymbol{Q}^{-1}_{s_k} & \boldsymbol{F}^{\top}_{s_k}\boldsymbol{Q}^{-1}_{s_k}\boldsymbol{F}_{s_k} + \boldsymbol{\Lambda}_{s_{k|k}} \end{bmatrix} \tag{6.52}$$

$$+ \begin{bmatrix} \boldsymbol{\Lambda}_{rng;v_{m+1}} & \boldsymbol{\Lambda}^{\top}_{rng_{m+1}} & \mathbf{0} \\ \boldsymbol{\Lambda}_{rng_{m+1}} & \boldsymbol{\Lambda}_{rng;s_{k+1}} & \mathbf{0} \\ \mathbf{0} & \mathbf{0} & \mathbf{0} \end{bmatrix} \tag{6.53}$$

$$= \begin{bmatrix} \boldsymbol{\Lambda}_{v_{m+1|m+1}} & \boldsymbol{\Lambda}^{\top}_{rng_{m+1}} & \boldsymbol{\Lambda}^{\top}_{rng_m} \\ \boldsymbol{\Lambda}_{rng_{m+1}} & \boldsymbol{\Lambda}_{s_{k+1|k+1}} & -\boldsymbol{Q}^{-1}_{s_k}\boldsymbol{F}_{s_k} \\ \boldsymbol{\Lambda}_{rng_m} & -\boldsymbol{F}^{\top}_{s_k}\boldsymbol{Q}^{-1}_{s_k} & \boldsymbol{F}^{\top}_{s_k}\boldsymbol{Q}^{-1}_{s_k}\boldsymbol{F}_{s_k} + \boldsymbol{\Lambda}_{s_{k|k}} \end{bmatrix} \tag{6.54}$$

where

$$\boldsymbol{\Lambda}_{v_{m+1|m+1}} = \boldsymbol{\Lambda}_{v_{m+1|m}} + \boldsymbol{\Lambda}_{rng;v_{m+1}} \tag{6.55}$$

$$\boldsymbol{\Lambda}_{s_{k+1|k+1}} = \boldsymbol{Q}^{-1}_{s_k} + \boldsymbol{H}^{\top}_{k+1}\boldsymbol{R}^{-1}_{k+1}\boldsymbol{H}_{k+1} + \boldsymbol{\Lambda}_{rng;s_{k+1}}. \tag{6.56}$$

Because the elements that comprise the delta information are constant, i.e. independent of the actual ship state, the independent ship filter and the centralized filter will calculate identical information from process predictions and measurement updates. Thus $\Delta\boldsymbol{\Lambda}_{TOL_{k+1}}$

and $\Delta\boldsymbol{\eta}_{TOL_{k+1}}$ calculated from the ship-based filter, which has no knowledge of the vehicle and is not subject to range measurement updates, is *identical* to the CEIF even though the two filters have different estimates of the ship's current state. The simplicity of this computation is one of the advantages of the information filter.

6.4.4 Comparison between DEIF and CEKF

The centralized extended Kalman filter (CEKF) that has simultaneous, real-time access to both vehicle and ship sensor data is used as a benchmark for state estimation performance. The goal of the DEIF is for the current state of the vehicle recovered from the DEIF to exactly reproduce the vehicle state recovered from the CEKF. The DEIF accomplishes this immediately after each range measurement update, but there are several subtleties to this operation that we address here.

The range measurement is a nonlinear measurement. In order for the range measurement update made by the DEIF to match that made by the CEKF, both filters must be linearizing the range observation model about the same vehicle state. At the TOA of the acoustic data packet, the range measurement is made between $\boldsymbol{x}_{v_{TOA}}$ and $\boldsymbol{x}_{s_{TOL}}$. Comparing the probability distributions of the two filters immediately after the range measurement update, we find that they are *not* identical because, as shown in Figure 6.4, the centralized filter has access to the ship-based measurements shown in blue, while the decentralized filter does not,

$$\text{DEIF: } p\left(\boldsymbol{x}_{v_k}, \boldsymbol{x}_{s_{TOL}} | z_{rng}^{TOA}, \mathbf{Z}_v^{1:TOA}, \mathbf{U}_v^{1:TOA}, \boxed{\mathbf{Z}_s^{1:TOL}}\right) \tag{6.57}$$

$$\text{CEKF: } p\left(\boldsymbol{x}_{v_k}, \boldsymbol{x}_{s_{TOL}} | z_{rng}^{TOA}, \mathbf{Z}_v^{1:TOA}, \mathbf{U}_v^{1:TOA}, \boxed{\mathbf{Z}_s^{1:TOA}}\right) \tag{6.58}$$

where z_{rng}^{TOA} is the most recent range measurement, $\mathbf{Z}_v^{1:TOA}$ are the vehicle sensor measurements up to the TOA, $\mathbf{U}_v^{1:TOA}$ are the vehicle control inputs up to the TOA, and $\mathbf{Z}_s^{1:TOL}$ are the ship sensor measurements up to the TOL. The ramifications of this are that the DEIF

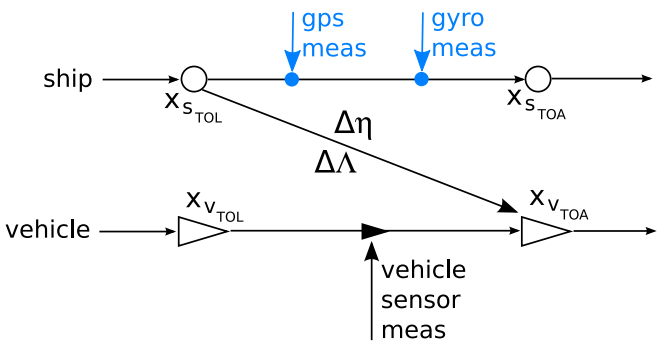

Figure 6.4: The centralized filter has access to ship sensor measurements, shown in blue, that are unavailable to the decentralized filter when the range measurement is received.

performs a range measurement between the current vehicle state and the best estimate of the ship state at the TOL given ship sensor measurements *only up to the TOL*. In contrast, the CEKF performs a range measurement between the current vehicle state and the best estimate of the ship state at the TOL given ship sensor measurement *up to the TOA*. The CEKF is essentially performing a smoothing operation on the ship state at the TOL, because it has additional information from the ship sensors after the data packet was broadcast.

In order to properly compare the CEKF and the DEIF, we use a two-step delayed measurement update in the CEKF, first performing a measurement update for the range measurement that only includes ship measurements up until the TOL, (6.59), and then performing another measurement update for the ship measurements that happened between the TOL and the TOA, (6.60)

$$\text{CEKF (step 1): } p(\boldsymbol{x}_{v_k}, \boldsymbol{x}_{s_{TOL}} | z_{rng}^{TOA}, \mathbf{Z}_v^{1:TOA}, \mathbf{U}_v^{1:TOA}, \boxed{\mathbf{Z}_s^{1:TOL}}) \tag{6.59}$$

$$\text{CEKF (step 2): } p(\boldsymbol{x}_{v_k}, \boldsymbol{x}_{s_{TOL}} | z_{rng}^{TOA}, \mathbf{Z}_v^{1:TOA}, \mathbf{U}_v^{1:TOA}, \mathbf{Z}_s^{1:TOL}, \boxed{\mathbf{Z}_s^{TOL:TOA}}). \tag{6.60}$$

Now the DEIF distribution in (6.57) is identical to the CEKF distribution in (6.59), without compromising the CEKF's final distribution, i.e. (6.60) is identical to (6.58).

Between range measurements, the CEKF and DEIF estimates of the vehicle state will not be identical because of linearization errors, as seen in (6.57) versus (6.58). However, at the instant of every range measurement, through the two-step delayed update, the filter estimates will be made identical again.

6.5 Simulation

The performance of the DEIF in comparison to the CEKF is demonstrated using a simulated 6-hour survey at 3800m depth. The CEKF has access to the sensor measurements from both the ship and the vehicle simultaneously. The DEIF has real-time access to vehicle sensor data and asynchronous acoustic broadcasts from the ship that are used to make range measurements. The DEIF does *not* have access to the ship sensor measurements apart from these acoustic broadcasts. To test the validity of the DEIF, we compare the state estimate recovered from it to that obtained from the CEKF using the two-step delayed measurement update as described in Section 6.4.3.

6.5.1 Simulation Setup

This simulation is designed to mimic the experimental setup of the deep water survey described in Section 5.3 and [93]. In the simulated mission presented here, the vehicle drives ten 700 m tracklines spaced 80 m apart at a velocity of 0.35 m/s. The vehicle depth is constant at 3800 m. The vehicle takes approximately 6 hours to complete the survey, during which time the ship drives around the vehicle survey area in a diamond pattern at

Table 6.2: Simulated navigation sensor sampling frequency and noise.

Sensor	Frequency	Noise
OCTANS	3 Hz	ψ: 0.1° ϕ, θ: 0.01° r: 0.5°/s p, q: 0.25°/s
depth sensor	0.9 Hz	5 cm
DVL	3.0 Hz	1 cm/s
GPS	1.0 Hz	0.5 m
gyrocompass	2.0 Hz	0.1°
modem	every 2.5 min	4 m

0.5 m/s, broadcasting acoustic data packets every 2.5 minutes.

We assume that the ship is equipped with a differential global positioning system (DGPS) receiver and a gyrocompass to measure heading. The vehicle has an OCTANS fiber-optic gyrocompass to measure attitude and attitude rates; a Paroscientific pressure sensor to measure depth; and an RDI Doppler velocity log (DVL) to measure bottom-referenced velocities. Acoustic modems are used to measure the range between the ship and the vehicle. The vehicle and ship navigation sensors, their sampling frequencies, and the noise statistics for each sensor are given in Table 6.2, where ψ, θ, and ϕ are local-level heading, pitch, and roll respectively; r, q, and p are body-frame angular rates in heading, pitch, and roll.

In order to compare the CEKF and the DEIF, we must initialize them to the same point. In this simulation, for comparison purposes we initialize the vehicle state to the true vehicle position with a large covariance for both filters. During an actual mission this would, of course, not be possible. Instead the vehicle would estimate its initial own position using a method such as a maximum likelihood estimate over the first few range measurements.

6.5.2 DEIF Results

A comparison between the DEIF and the CEKF for the simulated dive is shown in Figures 6.6, 6.7, and 6.5. Figure 6.5 shows the estimated vehicle trajectory overlaid with the 3-sigma covariance of the vehicle position as estimated by the DEIF. The GPS-reported position of the ship as it moves around the vehicle survey area is also shown. Figure 6.6 shows the difference between the true vehicle position and the estimate from the DEIF of the vehicle position over the course of the simulated dive. The 3-sigma error bars are included to show that the filter maintains consistency over the course of the dive. The error at the end of the dive between the DEIF's estimate of the vehicle position and the true vehicle position is 3.7 m cross-track and 0.2 m along-track both with 3.1 m standard deviation. For comparison, had the vehicle relied solely on dead reckoning throughout the dive with no range measurements, the error at the end of the dive between the estimated and

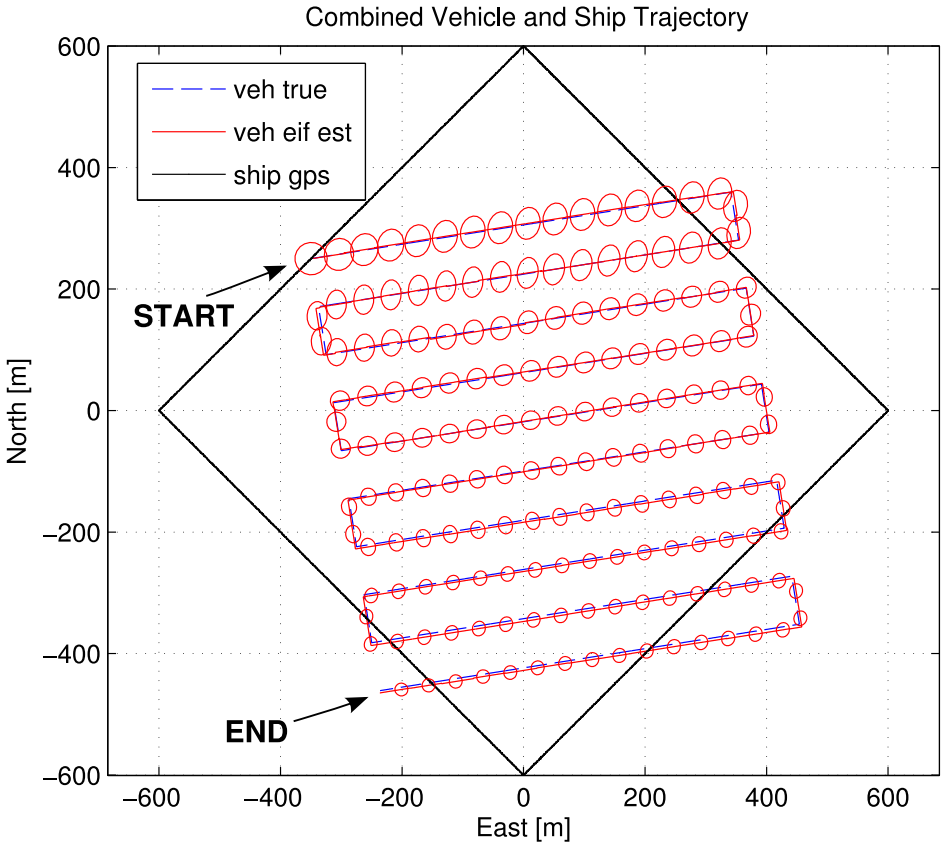

Figure 6.5: Ship and vehicle trajectories. The ship moved counter-clockwise around the diamond starting at the eastern-most apex.

true vehicle position would have been 8.8 m cross-track and 5.6 m along-track with a 7.8 m standard deviation. Comparing the estimated mean of the 12 DOF vehicle state vector from the DEIF versus the CEKF, Figure 6.7 shows the norm of the difference of the state vector, $(\Delta\mathbf{x}^\top\Delta\mathbf{x})^{-1/2}$ where $\Delta\mathbf{x} = \mathbf{x}_{DEIF} - \mathbf{x}_{CEKF}$, over the course of the simulation. The lower plot highlights the norm of the difference immediately after the range measurements marked by asterisks. Note that the y-axis on the lower plot has been scaled down by two orders of magnitude to show the precision with which the DEIF is able to reproduce the results of the CEKF. As expected, the x-y position error dominates the norm. The average difference between the filters across the entire dive is 5.68e-3 m (5.7 mm) in x-y position and 3.35e-8 in the other state elements. The average difference immediately after a range measurement is 8.27e-5 m in x-y position and 1.70e-10 in the other vehicle states.

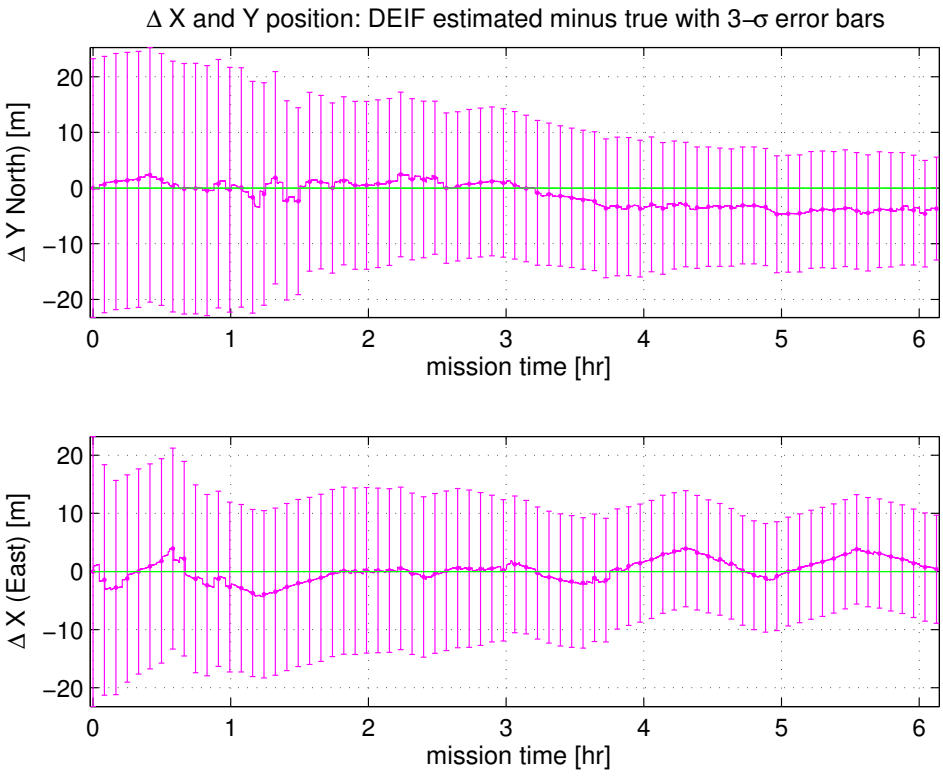

Figure 6.6: The difference between the true vehicle position and estimate from the DEIF over time. The error bars are 3 times the standard deviation in each degree of freedom.

6.5.3 Discussion

As discussed in Section 6.4.4, we expect the DEIF to produce state estimates that are comparable to the CEKF: *immediately after* each range update the results should be identical; *between* range updates, the results should differ only due to linearization errors. The results from the simulation shown in Figure 6.7 support this within the tolerance of numerical precision. Over the course of the 6-hour simulated dive the difference in x-y position between the DEIF and the CEKF is, on average, 8.27e-5 m immediately after each range update. In addition, the difference between the filters due to linearization errors (averaged over the entire dive) is 5.7 mm on average with a maximum difference of 4.9 cm.

Because these results are based on a simulated data set, there are several possible discrepancies compared to experimental data. The assumed noise characteristics of the navigation sensors in Table 6.2 are used both in the simulation of noisy sensor data and in the observation models in the DEIF and CEKF. As a result the observation models exactly predict the performance of the navigation sensors. In addition, the noise for every sensor is assumed to be Gaussian. While these assumptions may be reasonable for common vehicle navigation sensors that have been tested extensively in the field [54], acoustic range mea-

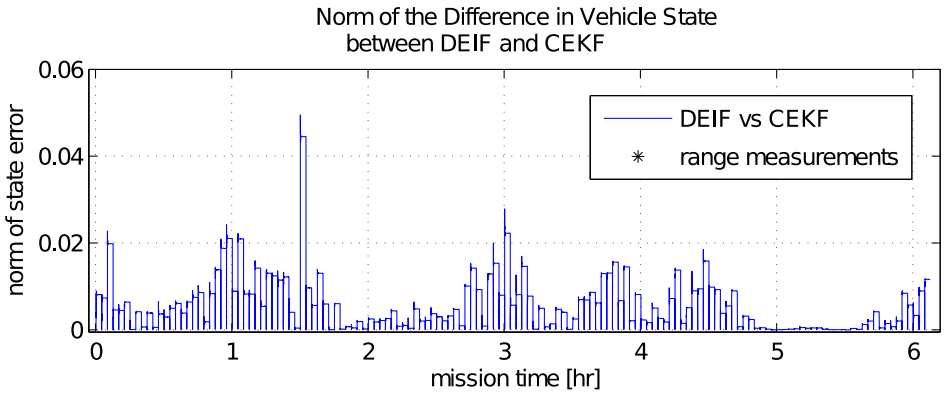

(a)

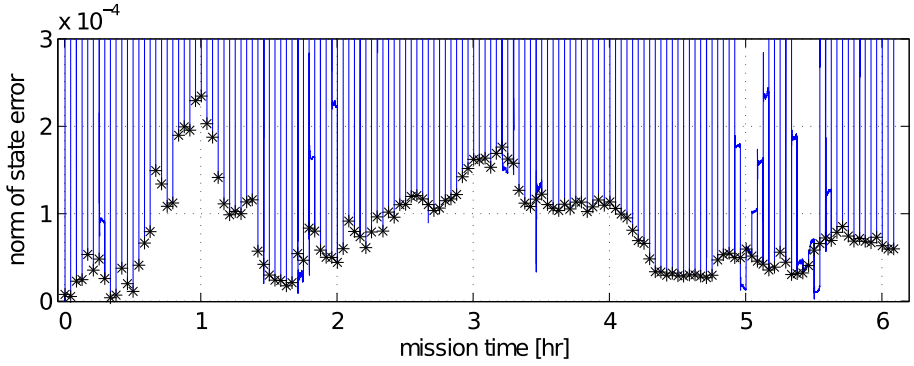

(b)

Figure 6.7: (a) The sum of the squared error between the mean vehicle position as estimated by the DEIF versus the CEKF. (b) The same plot as (a) but with a zoomed view of the y-axis highlighting the norm immediately after the range measurements.

surements suffer from highly-variable, non-Gaussian noise sources including multi-path and ray-bending errors. In an attempt to account for this, we use a large assumed variance for the range measurements. In a real-world context, outlier filtering of the range data would be necessary.

6.6 Robustness to Acoustic Data Packet Loss

Packet loss occurs when acoustically transmitted data packets are not successfully received and decoded by the vehicle. Packet loss can occur for a variety of reasons, including poor signal-to-noise ratio, attenuation due to range, or acoustic collision because of an acoustic multi-path or other acoustic transmissions. Packet loss is a legitimate operational concern given the structure of the algorithm presented here, whereby incremental information about the ship's filter is acoustically broadcast by the ship and reconstructed by the

vehicle.

Operationally there exist several possible implementations that address packet loss. Contingent on the available bandwidth, the $\Delta\Lambda$ for the last k broadcasts can be included in each acoustic broadcast. In addition, in the field vehicle operations are typically monitored via acoustic broadcasts from the vehicle that contain basic vehicle health and status updates. To mitigate the possibility of packet loss, the vehicle status updates will include the time of the last range measurement successfully received at the vehicle, allowing the surface beacon to adjust its delta measurement broadcasts accordingly. We are also continuing to investigate alternate structuring of the delta information that is broadcast from the ship in order to enable the DEIF to exactly recreate the delta information regardless of packet loss. Robustness to packet loss and fully exploring the ramifications of packet loss on the DEIF's estimate of vehicle position over time are both areas for further research.

6.7 Chapter Summary

The structure of the information filter makes it a natural choice for a decentralized implementation where the available bandwidth for sending data between nodes is limited. Delayed ship updates are simply additive and require a minimal amount of information to be acoustically transmitted that is well within the functional limits of available acoustic modems [30, 31]. In this chapter we have derived a vehicle-based extended information filter that is able to estimate a vehicle's state, including x-y position, using only vehicle-based inertial sensors and asynchronous acoustic broadcasts from a single, moving, georeferenced beacon. The DEIF is able to locally recreate vehicle state estimates that are commensurate with the results from a centralized extended Kalman filter within a margin of numerical error, and the filter did so over the course of a simulation that is representative of an actual, deep-water survey in both physical scale and the frequency of measurements. In addition, the filter in its current form can be utilized on multiple underwater vehicles where each vehicle simultaneously receives acoustic data broadcasts from the reference beacon. Given the favorable results in simulation of the DEIF, we look forward to experimentally validating this algorithm and continuing to work towards a full multi-vehicle implementation.

Chapter 7

Conclusion

The chirp of the underwater modem heralds a new age of communication, navigation, and control for underwater vehicles. The ability of a shipboard science and operations team to communicate with an autonomous vehicle that is underway thousands of meters deep has the potential to revolutionize autonomous vehicle operations. Receiving science data in near real time or sending commands and new mission plans to the vehicle acoustically without risking the hazards or wasting the time of recovery and launch provides improvements in the duty-cycle of vehicle operations, flexibility in mission programming, and the ability to monitor in detail the progress of the vehicle both operationally and scientifically. The emerging field of acoustic underwater communications also has the potential to enable collective or collaborative multi-vehicle behavior that has thus far been the purview of land, air, and space vehicles because of their access to wireless networks for inter-vehicle communication. The contributions of this thesis are based on combining acoustic communication with navigation in order to eliminate the need for costly external acoustic beacons while providing a distributed, scalable precision navigation system.

7.1 Summary

This thesis presents the hardware, software, and algorithms designed to perform decentralized single-beacon one-way-travel-time navigation for underwater vehicles. The Acomms system, consisting of the hardware and software necessary for single-beacon one-way-travel-time navigation, has proven its effectiveness for managing acoustic communication on four oceanographic expeditions to date, including multiple dives to more than 10,900 m depth in the Challenger Deep in the Mariana Trench with the HROV *Nereus*.

We verified the ability of the centralized single-beacon navigation algorithm to pro-

vide vehicle state estimates that have an accuracy commensurate with that of long baseline acoustic navigation in deep water using navigation data collected by the author and collaborators with the Acomms system during an AUV survey in 4000 m of water. The state estimate of the decentralized vehicle-based single-beacon navigation algorithm was shown to be *identical* to the state estimate from the centralized filter at the instant of each range measurement, and to differ by only linearization errors between range measurements. This conclusion is supported by the results from a simulation of a deep-water AUV survey.

7.2 Future Work

The decentralized vehicle-based algorithm extends naturally to multiple vehicles—any vehicle within acoustic range of the ship can execute its own independent local vehicle-based filter. A natural extension of the decentralized algorithm is to incorporate acoustic broadcasts from *other vehicles* in addition to broadcasts from the ship. Inter-vehicle range measurements made from inter-vehicle acoustic broadcasts would further constrain the navigation solution and improve each vehicle's own state estimate. However, as mentioned in Section 6.4.3, in order to maintain consistency between the decentralized filter and the centralized filter the process model of the node broadcasting the acoustic data (i.e. the ship) must be *linear*. A linear process model ensures that measurement updates and process predictions in the ship filter are independent of the ship's current state. Thus, the calculation of the information that is broadcast from the ship is identical to that of the centralized filter, despite the fact that the state estimate of the ship from the centralized filter differs from the state estimate of the ship from the independent ship filter. (The state estimates are different because the centralized filter's estimate is conditioned on previous range measurements that are not accessible to the independent ship filter. This is true regardless of the linearity of the ship process model.) If the ship process model is *not* linear, measurement updates and process predictions, which require a linearization about the filter's estimated current state, will be different in the centralized filter compared to the independent ship filter. So while we believe that assuming a linear ship process model is both reasonable and principled, the vehicle process model is not linear as defined herein. This presents a challenge for extending the decentralized algorithm to include inter-vehicle ranges. In addition, the problem of over-confidence associated with double-counting information passed between the vehicles must be addressed.

Appendix A

Review of Single-Beacon Navigation Literature

This appendix provides an overview of the selection of significant papers shown in Table A.1 in the area of single beacon navigation published through 2006. I have included a summary of the measurement and process models used in each paper as well as a summary of the authors' conclusions. Unless noted otherwise, the vehicle coordinate frame is assumed to be defined with x forward, y lateral and z vertical, and the body-frame velocities u, v and w are defined in the x, y and z directions respectively. Thus the vehicle body-frame velocity u is in the direction of the vehicle heading.

A.1 Least Squares Approach

Scherbatyuk, 1995 [80]

This paper is the earliest formulation of the single-beacon navigation problem with unknown currents that we know of. The author proposes to use least squares to solve for the initial vehicle position and unknown current velocity. The author also reports a linear algebra-based observability analysis.

Vehicle Process Model: The author assumes a simple kinematic model for the vehicle in Cartesian coordinates in which the vehicle perfectly maintains a piecewise constant heading and forward velocity through the water using dead reckoning. The author assumes the vehicle operates at a constant depth with no side slip, i.e. $u \neq 0, v = 0, w = 0$ in body frame

Table A.1: Single-beacon navigation papers reviewed in this Appendix.

Least Squares Approach		
A. Scherbatyuk	1995	[80]
C. Hartsfield	2005	[42]
C. LaPointe	2006	[57]
Least Squares Seeded Extended Kalman Filter Approach		
J. Vaganay, P. Baccou, B. Jovencel	2000	[89]
P. Baccou, B. Jovencel	2002	[3]
P. Baccou, B. Jovencel	2003	[4]
Extended Kalman Filter Approach		
M. Larsen	2000	[58]
M. Larsen	2001	[59]
M. Larsen	2002	[60]
Extended Set-Valued Observer Approach		
J. Marçal, J. Jouffroy, T. Fossen	2005	[63]
Observability Analysis		
A. Gadre, D. Stilwell	2004	[33]
A. Gadre, D. Stilwell	2005	[34]
A. Gadre, D. Stilwell	2005	[35]
A. Gadre	2007	[32]
A. Ross, J. Jouffroy	2005	[77]
J. Jouffroy, J. Reger	2006	[48]
T. Song	1999	[85]
B. Ristic, S. Arulampalam, J. McCarthy	2002	[76]
Multi-Beacon Range-Only SLAM		
P. Newman, J. Leonard	2003	[71]
E. Olson, J. Leonard, S. Teller	2006	[72]
G. Kantor and S. Singh	2002	[51]

coordinates. The vehicle's world position is affected only by the unknown current and its unknown starting position. After the first three legs when the the first current estimate is made, this estimate is used in subsequent dead reckoning and updated after each leg.

Observation Model: The observation model is also formulated in Cartesian coordinates. Process inputs are range to the single beacon, vehicle yaw (heading), and the vehicle's relative velocity through the water. The x, y, z location of the beacon is assumed fixed and known and the vehicle depth is assumed known without noise, reducing the problem to two dimensions. Range measurement errors are modelled as symmetrical mutually independent uniform random variables in the interval [-0.1,0.1]. The vehicle yaw and relative velocity errors are modelled as mutually independent zero-mean Gaussian noise with dispersions 2% of parameter values. All of these quantities are assumed known at each time step without additional measurement noise.

Method: The least squares method is used to determine the coefficients that arise in the quadratic formulation of the squared range: $r^2(k) = A(k\tau)^2 + B(k\tau) + C$ where k is the time step, τ is the time step interval, $r(k)$ is the range at time step k and A, B, and C are unknown coefficients that are functions of the vehicle position, heading and velocity and the beacon position. Once the coefficients are found for three separate legs, the unknown current and initial vehicle position is calculated using simple linear algebra

techniques. This estimate is used in subsequent dead reckoning estimates and updated after each successive leg is completed.

The statistical characterization of the evaluation of each of the four unknown parameters (initial vehicle x, y position and x, y components of the current) was explored using the Monte Carlo method.

Observability: The author reports that the algorithm requires the vehicle to traverse three distinct steady straight-line trajectories in order to uniquely detect the current velocity and the initial vehicle position. Trajectories directly towards or away from the beacon are viable trajectories.

Hartsfield, 2005 [42]

This paper presents a single-beacon navigation algorithm, the Single Transponder Range Only Navigation Geometry (STRONG) algorithm, and details of its implementation on a REMUS vehicle. The author employs an iterative technique to determine vehicle course (in the world frame) and position over a sequence of four transponder-to-vehicle ranges. Unknown currents are permissible but are not estimated.

Vehicle Process Model: The vehicle process model is formulated in Cartesian coordinates. For the least squares solution, either vehicle velocity or heading is assumed constant between each received range depending on whether a speed or course correction is to be done (see below). The effects of unknown currents are assumed to be subsumed in the constant bias error of the vehicle heading and velocity.

Observation Model: The observation model is formulated in Cartesian coordinates. The x, y, z location of a single beacon is assumed precisely known, as well as the vehicle depth, resulting in a two-dimensional problem. Ranges between the transponder and the vehicle are measured from a single beacon and are assumed accurate (no measurement noise). Variable-length time steps are defined by the receipt of these acoustic ranges. The body frame vehicle velocity with respect to the ground is known from a Doppler Velocity Log (DVL). Vehicle heading is known from a magnetic compass.

The author assumes that either the estimated vehicle velocity or the estimated vehicle heading is constant between successive ranges. Thus the estimated vehicle path consist of a series of either constant bearing or constant speed path segments, as described below.

Method: The author uses ad hoc iterative techniques to assess different possible velocities, headings and initial positions for each path segment independently. Either a course correction (heading and initial position) or speed correction (velocity and initial position) is performed depending on the user's choice. In the case of the course correction, velocity is assumed to be measured accurately (no measurement noise or bias). Heading and initial position are then assessed by minimizing the squared error between the proposed path and the four most recent range measurements. The process iterates between heading and initial position until a solution with a suitably small covariance is achieved. The speed correction is performed similarly, assuming heading is measured accurately without measurement noise and iterating between velocity and initial position.

Conclusions: The author concludes that this algorithm is a viable method for localizing a REMUS or similarly equipped vehicle using ranges from a single beacon.

LaPointe, 2006 [57]

This paper presents a single-beacon navigation algorithm, the Virtual Long Baseline (VLBL) algorithm, and its simulation. The author proposes a method for time-aligning current and previous range fixes and uses least squares to solve for the vehicle position. The robustness of the method with respect to two model parameters is tested in simulation. The effects of loss of observability are noted where manifested in the simulated results.

Vehicle Process Model: The vehicle process and noise models are not addressed in detail, except to note that the vehicle's body-frame velocity, from a Doppler velocity log, heading, from a magnetic compass, and depth are known inputs to the model. In simulation the author assumes a deterministic vehicle model, i.e. no process noise, such that the vehicle follows an exact path.

Observation Model: The observation model is formulated in Cartesian coordinates. The measured output of the system is transponder-vehicle ranges, which are received asynchronously. The transponder is assumed to be at a fixed, known location. Combined with the known vehicle depth this makes the problem two-dimensional.

Method: The VLBL method relies on interrogating a single transponder multiple times and "virtually" advancing each transponder along the estimated vehicle trackline to simulate multiple simultaneous transponder fixes from different locations.

Simulations: Simulations were performed using both synthesized data and real-world data from Autonomous Benthic Explorer (ABE) Dive 162. The author nominally uses four transponder ranges for the least squares solution of the vehicle position. For the simulated data set no noise was included. Also, the navigation fixes are plotted as calculated without filtering or processing. Fixes with large discontinuities over short periods of time are allowed in simulation.

Observability: The author notes the effects of loss of observability as indicated by the degradation of simulated vehicle navigation fixes. Degradation in vehicle fixes is seen at corners in the survey pattern and along tracklines with a nearly constant bearing to the transponder. The lack of global observability for constant heading trajectories as manifest in the existence of a parallel indistinguishable trackline is also observable in the simulated data.

Range Sampling Rate: The author assess the range sampling rate, n, for its effect on the performance of the algorithm using simulated data. The author tests four values of n, ($n = 1, n = 4, n = 10, n = 25$), where n is the number of data points received for each sample taken, e.g. for $n = 4$, the range data used to solve for the vehicle position is every 4th range data point received. Because the simulated data contains no noise, the author is careful to point out that the experimental results can potentially significantly overestimate the observability of the system, especially in a scenario where the transponder lies very close to the vehicle trackline. The author also notes the need to balance the trade-offs

between faster sampling rates (smaller n's), which could render the least squares solution impossible to calculate due to too small of a baseline and therefore an uninvertible state matrix, versus slower sampling rates (larger n's), which could result in vehicle position estimates that are too infrequent. Simulations using real-world data show the effect of range sampling rate and the degradation that occurs at slower sampling rates.

Outlier Rejections: The effect of varying the "outlier rejection factor" was tested in simulation using real-world data from ABE Dive 162. The outlier rejection factor represents a radius from the last position fix outside which position estimates are rejected. The radius is calculated based on a percentage of the expected distance travelled based on dead reckoning. The tests ranged from 1.1 to 2.5 (i.e. 110% to 250% of the expected distance travelled from the last navigation fix) and showed divergence when the radius was either too small or too large.

Conclusions: The author concludes that the VLBL method is appropriate as a redundant navigation system for use with traditional Long baseline. Future work suggested by the author includes automating parameter tuning and careful transponder location selection to ensure observability of the system.

A.2 Least Squares Seeded Extended Kalman Filter Approach

Vaganay, Baccou, and Jovencel, 2000 [89]; Baccou and Jovencel, 2002 [3]; Baccou and Jovencel, 2003 [4]

These papers present a method for implementing single-beacon navigation using Least Squares to generate an initial position estimate for the vehicle from a specific trajectory (a circle) and an extended Kalman filter to update the vehicle position estimate over time. The authors assume the presence of an unknown, constant current and a vehicle without a Doppler Velocity Log (DVL) sensor (no direct speed-over-ground measurements). A two-vehicle system is explored in [4] that is in essence a cascaded version of the original algorithm. Results of simulations using simulated data and real-world data are presented. Observability is not addressed.

These three papers address successive reports by the same authors on one problem and are discussed together herein. The first paper provides an overview of the methods, which are refined for the second and third papers. Thus only the methods employed for [3] and [4] are discussed here.

Vehicle Process Model: The vehicle motion is simulated using a kinematic vehicle model formulated in Cartesian coordinates. The state vector for the model is defined as $s = [x, y, z, v_x, v_y, du]$, where x, y, z are the vehicle position in world coordinates, v_x and v_y are the x and y components of the the current (assumed constant), and du is an assumed constant vehicle speed bias. The inputs are the vehicle heading ψ, pitch θ, and speed

through the water u, where vehicle velocity through the water is derived from an a priori propeller rpm to water velocity calibration. A DVL is not used.

Kalman Filter: The extended Kalman filter is formulated in discrete time using the vehicle process model. The state noise vector, v_k, is assumed to be zero-mean Gaussian with a covariance matrix of Q_k. The authors assume that the x,y,z position of the beacon is known a priori without error. The depth of the vehicle is also assumed known without error, making the problem two-dimensional.

The only observation is of the acoustic ping's round-trip time of flight, T, between the vehicle and the beacon. T is a function of the vehicle state when the ping was sent, the vehicle state when it was received, and the speed of sound. The measurement noise, w_k, is assumed to be zero-mean Gaussian with a variance of R_k.

Method: The authors use a two-part approach to solving the problem of vehicle homing in the presence of unknown currents. First, least squares is employed to calculate an initial estimate of the vehicle position and the current plus vehicle speed bias during strategic vehicle maneuvers. Second, a Kalman filter is then used to continually update the vehicle-beacon relative position and the current estimate while the vehicle is homing in on the beacon.

LS Initialization: The vehicle is commanded to maneuver in a circle collecting range data to the beacon. After pre-filtering (see [3]), the authors select fourteen (14) randomly selected ranges N different times and find the group that produces the smallest median residual (N = 70 in the simulations). Using these 14 data points, the system of equations for the vehicle position versus range and current are then solved by least squares using the Levenburg-Marquardt algorithm to estimate the vehicle's x-y position and the x,y components of the current. To calculate an initial position estimate sufficiently close to the actual initial position and thus avoid the problem of the existence of many local minima, the problem is first solved for position only (assuming no current). That position is then used as an initial estimate for the least squares problem with an unknown current.

EKF Homing: The non-linear least squares solution to the initialization problem was used to seed the Kalman filter for the homing phase. During the homing phase the vehicle uses an extended Kalman filter to update the beacon-vehicle relative position estimate and the current estimate. The vehicle drives in a spiral pattern in order to minimize the covariance while approaching the beacon.

Simulations: Baccou and Jovencel in [3] test the above method in simulation and also in post-processing with real vehicle data that was validated by LBL. The authors report that the differences between LBL and their method "converge to zero" despite the added perturbation of an unmodelled heading bias. The authors conclude that the navigation method is "robust and efficient" and that single-beacon navigation using an EKF is worthy of further study.

Baccou and Jovencel in [4] present the work discussed in the previous paper and add a simulation of two vehicle operations. The vehicles are assumed to act in a leader/follower arrangement, where the leader knows its precise position (is not affected by currents, etc.) and the follower receives periodic range and state information from the leader via acoustic

modem link. The setup is, in essence, a cascaded one-vehicle, single-beacon problem where each vehicle only has one ranging source. The difference between the vehicles is that the ranging source for the fist vehicle is stationary and its position is known with certainty. The ranging source for the second vehicle is the first vehicle, which is moving and in reality its position is not known with certainty, though the algorithm assumes that it is.

A.3 Extended Kalman Filter Approach

Larsen, 2000 [58]; Larsen, 2001 [59]; Larsen, 2002 [60]

These papers present the implementation of a single-beacon navigation solution using an error state Kalman filter. A MARPOS®-aided dead reckoning navigation system is assumed, which includes a Doppler velocity log for body-frame velocities and a gyrocompass for vehicle heading. The author's thesis [59] contains in-depth information about the concepts presented in [58] and [60] as well as a detailed dynamic model of vehicle motion. The author briefly discusses the use of Doppler frequency shift in addition to or instead of range to improve dead reckoning position estimation in [58], but does not pursue the idea.

Vehicle Process Model: The author assumes a MARPOS® dead reckoning system, which includes a Doppler velocity log (DVL) in bottom-lock mode and a gyrocompass, providing body-frame vehicle velocities and heading respectively. The derivation of the dynamic model will be covered only in a most cursory manner here. The reader is urged to consult [59] for significantly more detail. Briefly, the dynamics are governed by $\dot{\delta x} = A\delta x + G\delta u$, where the state vector, δx, is comprised of various inertial navigation-dependent states and δu is comprised of inertial navigation-related angular velocities and specific forces. A is a matrix valued coefficient consisting of time-varying functions of position, velocity, attitude and specific force. G is also a matrix-valued coefficient that maps the body frame inertial sensor noise into the navigation frame. See [59] for a complete treatment of the definitions and derivations of these quantities.

Kalman Filter: The x, y, z location of the single beacon is known exactly. Vehicle depth is also assumed to be known, thus reducing the problem to two dimensions. The author assumes a random walk model to describe x, y position estimate error drift from the MARPOS®. Range to the beacon is measured with noise.

An error state Kalman filter in Cartesian coordinates is used to estimate the accrued dead reckoning error state (and possibly errors in the beacon x, y position at each time step). The state vector is the error state vector, $\delta\mathbf{x} = [\theta_{\mathbf{dr}}, \theta_{\mathbf{tp}}]$ where $\theta_{\mathbf{dr}} = [\delta x_v, \delta y_v]$, the vehicle position error from dead reckoning, and $\theta_{\mathbf{tp}}$ is a vector of the measurement errors of each range measurement. The process noise is assumed to be zero-mean Gaussian.

For the observation equation of the Kalman filter, a linearized range error is used with the addition of zero-mean Gaussian measurement noise. The true vehicle and beacon positions are approximated by their corresponding estimates since they are not known. Range

measurement noise is assumed to be uncorrelated white Gaussian noise with a standard deviation of 0.3 m.

Observability: Observability is not directly addressed. The author notes that there is some asymmetry in the position accuracy related to the trajectory and suggests a trajectory perpendicular to the bearing of the transponder for best results.

Simulations: The results from two simulations are presented.

Survey Grid Simulation: The first simulation uses real data from a 600 m by 600 m survey grid. The vehicle travels at a speed of 6 km/hr (3.2 knots) for 180 minutes resulting in $\sim$18.5 km of linear travel. A single simulated beacon is placed at the center of the grid with an initial position error of $\sim$11m (5 m N, 10 m E). Ranges to the beacon are provided at 10-second intervals.

Survey Line Simulation: The second simulation uses real data from an 8km long linear track. With an average speed of roughly 6 km/hr (3.2 knots) the trackline took approximately 80 minutes. Two simulated transponders are placed along the trackline near the beginning, roughly 1.5 km apart. There is no uncertainty modelled in the transponders locations. The transponders are interrogated only when the vehicle is within 600 meters of them at a rate of once per minute.

Conclusions: The author reports that in the survey grid simulation the position error at the end of the test is reduced from $\sim$18 m to $\sim$2 m when ranges to the transponders are included in the position estimate. In addition, the position error appears to converge within the first few minutes despite the induced error in the initial position of the beacon. In the survey line simulation the position error at the end of the test is reduced from $\sim$18 m to $\sim$5 m when ranges to the transponders are included in the position estimate.

A.4 Extended Set-Valued Observer Approach

Marçal, Jouffroy, and Fossen, 2005 [63]

These papers describe the implementation of an extended set-valued observer instead of the commonly used Kalman filter to estimate vehicle position using ranges from a single beacon. The set-valued estimator assumes the presence of measurement noise that is bounded but not necessarily Gaussian, in contrast to the Kalman filter, which assumes Gaussian noise. According to the authors, the impetus behind this observer choice was to provide an estimation technique that would provide bounds on the estimation error even in the presence of strong non-linearities in model and non-Gaussian noise. The output of the observer is not as "smooth" as the Kalman filter but it is reported to guarantee that the true position is always within the predicted covariance or confidence ellipsoid.

Vehicle Process Model: The vehicle model has state variables, in polar coordinates, of $[\rho(t)\ \theta(t)\ \psi(t)]$ corresponding to the vehicle's range from the beacon, bearing from the beacon, and heading. Yaw rate and velocity, $[r(t)\ v(t)]$, are inputs; range and heading, $[\rho(t)\ \psi(t)]$, are measured.

Observability: The authors assess the observability of the system in polar coordinates by proving the existence of an admissible control, subject to certain conditions, in order to guarantee the distinguishability of two non-identical states [75] (reference [17] in the paper). The authors accomplish this using the Lie derivatives of the measurement equation along the solutions of the state equation (all in polar coordinates). They show that a trajectory where yaw rate $r(t) = 0$ is not uniquely distinguishable. The authors also discuss the condition when yaw rate $r(t)$ is small leading to two possible trajectories that are in close spatial proximity to each other. While in theory the trajectory is distinguishable, the authors claim that in practice the measurement noise may lead to the observer "settling" on the wrong track, especially if the true location is outside of the 3σ-ellipsoid confidence region as is possible with the EKF.

Set-Valued Observer: The authors implement the observer in Cartesian coordinates using the linear matrix inequalities framework as described in [79] and [16] (references [3], [5] in the paper). The sampling dynamics include an unknown but bounded noise vector, w, multiplied by a scaling matrix, B, for the state equation. The measurement equation also includes an unknown but bounded noise vector multiplied by a scaling matrix, v and D respectively. The prediction step is defined such that the bounding error ellipsoid is guaranteed to contain the true vehicle position provided proper noise and linearization errors are chosen. The update step, similar to a Kalman filter, provides a method for fusing information with different statistics. The result is an estimator with larger error bounds than a Kalman filter but that guarantees the inclusion of the true vehicle position.

Comparison with EKF: The observer performance was compared to that of an extended Kalman filter (EKF) in three anecdotal simulations using a straight line trajectory, a "lawn-mowing" trajectory, and a "lawn-moving" trajectory with bad measurements (measurements with non-Gaussian error). Note that despite the assumption of the presence of not-necessarily-Gaussian noise, the range measurements are assumed to have Gaussian noise for the simulations. In particular, the authors show an example where the set-valued observer's covariance ellipsoid contains the true state while the EKF's 3-σ covariance ellipsoid does not. The relative lack of smoothness of the set-valued observer compared to the EKF was also noted by the authors.

A.5 Observability Analysis

Gadre and Stilwell, 2004 [33]; Gadre and Stilwell, 2005 [34]; Gadre and Stilwell, 2005 [35]; Gadre, 2007 [32]

These papers address the problem of navigation from range measurements in the presence of either known or unknown currents. A novel observability analysis for linear time-varying systems is performed for the system with no current, with a known current, and with an unknown current. The authors employ limiting systems to assess uniform observability, and then formulate sufficient conditions for the existence of an observer with

exponentially decaying estimation error for the cases of both known and unknown currents. The performance of the observers is demonstrated using real field data.

Vehicle Process Model: The authors use a kinematic model in Cartesian coordinates of the AUV, assuming that the vehicle operates at a constant depth with no side-slip, i.e. $u \neq 0, v = 0, w = 0$ in body-frame coordinates. The authors note that there will be error between the estimated and the true motion of the vehicle during turning maneuvers and when the change in currents is not significantly slower than the estimation time constant. Vehicle depth and transponder depth are assumed known; thus the authors solve the two-dimensional problem in which the vehicle and the transponder are in the same horizontal plane. Transponder location (x,y) is assumed known and coincident with the origin of the world frame.

In the case of known or zero current, the state vector of the system is defined by $s(t) = [x(t), y(t), \varphi(t)]^\top$ where $x(t)$ and $y(t)$ are the vehicle position and $\varphi(t)$ is the vehicle heading. In the case of unknown currents, the state vector is defined by $s(t) = [x(t), y(t), \varphi(t), \upsilon_x(t), \upsilon_y(t)]^\top$ where $\upsilon_x(t)$ and $\upsilon_y(t)$ are the x and y components of the unknown current. Both models take as inputs the heading rate of change (from a MEMs gyrocompass) and vehicle velocity through the water (based on a pre-determined mapping from steady-state propeller angular velocity). The measurement vector is the same in both cases, $h(t) = [\sqrt{x^2(t) + y^2(t)}, \varphi(t)]^\top$. Output measurements are made via magnetic compass for vehicle heading and acoustic beacon for range.

Observability: For all three systems (no current, known current, unknown current) local observability was addressed by linearizing the system about arbitrary potential trajectories and assessing the observability of the linearized time-varying (LTV) system.

For the system with known currents (including zero current), the authors use the standard rank test for observability of LTV systems and conclude that it is locally observable [33] excluding the case of $\dot{\theta} = 0$ where θ is the bearing from the transponder to the vehicle. Using the observability grammian of a subsystem, Gadre shows that the system is uniformly observable [32] also excluding the case $\dot{\theta} = 0$.

For the system with unknown currents, uniform observability is shown over a finite time interval of length δ. This, combined with the requirement for observability over all sliding intervals $[t - \delta, t]$ in $[t_o + \delta, t_f]$, proves uniform observability for δ over the finite interval $[t_o, t_f]$.

Using this result, the authors formulate a specific condition on the vehicle trajectory that is sufficient to guarantee the existence of an observer with asymptotically stable error dynamics—specifically a Luenberger observer. The condition shows straight-line trajectories that do not pass through the origin to be observable. Gadre also shows in his thesis that uniform observability over a finite interval is sufficient to guarantee the existence of a stabilizing Kalman gain over a finite interval [32].

All of these observability results are local and depend on the estimated initial state being sufficiently close to the actual initial state. For example, straight line trajectories are locally observable but not globally observable due to the existence of a parallel indistinguishable trajectory. Straight line trajectories that pass through the origin are not observable, but

trajectories including but not exclusively consisting of a trajectory whose extension passes through the origin are observable.

The authors also simulate the effect of a non-zero angle of attack such as is present during turning maneuvers and changing currents. The authors conclude that bounded estimation error will occur but exponentially decay towards zero during straight line trajectories.

Kalman Filter: Although a Luenberger observer is used for the stability analysis, a discrete-time extended Kalman filter in Cartesian coordinates is used for the implementation of the observer in post-processing simulations. The authors assume that the vehicle velocity is parallel to its heading (i.e. a no-slip condition). The implementation is referred to as "standard" by the authors except for the process noise covariance matrix, which varies with time to allow for a larger process noise during turning maneuvers.

Testing: Testing was carried out using the Virginia Tech (VT) Miniature AUV in a lake for the system with no current and on a river for the systems with known or unknown currents. The vehicle successfully localized its position in the presence of both zero and known non-zero current. The vehicle successfully localized its position and estimated the current in the presence of unknown and varying currents. The authors conclude that slowly varying unknown currents introduce negligible errors; therefore this algorithm is suitable for real-time analysis.

Ross and Jouffroy, 2005 [77]

This paper provides a concise treatment of the observability of a single-beacon, single-vehicle measurement system in continuous time. The authors use Lie derivatives to compute the conditions for which the system has local weak observability.

Vehicle Process Model: The kinematic vehicle model is formulated in continuous time in both Cartesian and polar coordinates. In Cartesian coordinates the model has a state vector of $[x(t), y(t)]$, the vehicle's horizontal position. Inputs to the system are fixed body velocities, u, v, from a bottom-lock Doppler sonar, and heading, ψ, from a gyrocompass. The measurement vector consists of the range to the vehicle from the beacon (assumed to be at the origin of the world frame).

Observability: In polar coordinates, using an analysis of the Lie derivatives of the output function and the observability rank condition for nonlinear systems [43] (reference [6] in the authors' paper), the authors show that the system is locally weakly observable provided that the vehicle is not travelling directly towards or away from the beacon. Further, for any trajectory to be distinct the vehicle must change course at least once during the trajectory.

Kalman Filter: The authors propose an observer based on a modified EKF to give a prescribed degree of stability as presented in [49]. The state vector of the observer is $z(t) = [R(t), \gamma(t)]^\top$ where $R(t)$ and γ are the vehicle's range and bearing to the beacon (the origin in this analysis). The measurement vector is simply the first entry in the state vector, $R(t)$, the range. Process and measurement noise characteristics are not mentioned.

Simulations: Results are presented from four simulations: a straight-line trajectory with good initialization where the observer converges; a straight-line trajectory with bad initialization where the observer converges on the parallel indistinguishable trajectory; a maneuvering trajectory where the observer initially converges on the parallel indistinguishable trajectory and then after the maneuver onto the correct trajectory; and finally an unobservable trajectory where the observer fails to converge.

Jouffroy and Reger, 2006 [48]

The authors address the observability of a single-vehicle, single-beacon system using what the authors call an "algebraic method", by expressing the state as a function of the input, the measured output, and a finite number of their derivatives to show local uniform observability. The authors also present an "algebraic estimator" that relies on fitting a second order polynomial to the signal over a sliding time window. The estimated signal and its derivatives are used with the proposed observability mapping to estimate the state of the system. This technique lacks an estimation model however, which disallows the computation of an updated position without a measurement.

Vehicle Process Model: The system model, in polar coordinates, has a state vector of $[R(t), \gamma(t)]^\top$, the range and bearing from the beacon to the vehicle. Inputs to the system are u and v, the vehicle velocity in body-frame coordinates from bottom-lock Doppler measurements, and ψ, the vehicle heading measured by a gyrocompass. The angular velocity $\dot{\psi} = r$ is intentionally omitted by the authors because it is assumed measured by an Inertial Measurement Unit (IMU). The measurement vector, though not explicitly defined, consists of the beacon-vehicle range, $R(t)$.

Observability: The authors assess the observability of the system in polar coordinates using an algebraic approach developed by [21] (reference [1] in the paper). The authors analyze the conditions for which the state can be expressed as a function of the input, the measured output, and a finite number of their derivatives, which is equivalent to local uniform observability. The authors show that the system is not globally observable for constant heading trajectories because every straight line trajectory that does not extend through the beacon location has a parallel indistinguishable trajectory. They also show that the system is unobservable for trajectories directly towards or away from the beacon and when the vehicle velocity is zero, $\rho = \sqrt{u^2 + v^2} = 0$.

Estimation Technique: The authors use time-derivative estimation techniques from [46] and [47] (references [9], [10] in the paper) to estimate a polynomial representation of the desired signal using multiple integrations of the desired signal. The derivatives of the signal are estimated by simply differentiating the polynomial estimation. The authors point out that multiple integrals of the signal are "readily and practically available...since integrators will augment the signal/noise ratio." In order to ease the computational burden of performing multiple time integrals at every time step, the authors suggest utilizing the differential relationship between the time integrals.

To address the problem of fitting a second order polynomial to a real signal over con-

stantly increasing time scale (0 to t), the authors suggest fitting a polynomial over a fixed length time interval ($t - T$ to t). The authors re-derive the time-derivative estimation technique for this sliding time window assumption.

Finally, the authors combine the derived estimation technique and the conditions on observability to create an "algebraic estimator" for $\dot{R}(t)$ and $\gamma(t)$. In the estimator, $\rho(t)$ and $\alpha(t)$ (from the Doppler sensor) and $\psi(t)$ are all assumed to be corrupted by measurement noise, the nature of which is not defined. The range measurement $R(t)$ is also assumed to be corrupted by Gaussian white noise.

Simulations: Two 400 second-long simulations are conducted using the proposed estimator: a "well-behaved" straight trajectory that moves the vehicle past the beacon and a straight trajectory that moves the vehicle directly away from the beacon. In the results from the first simulation the estimator appears to converge on the actual vehicle state after about 50 seconds of transient behavior. The results from the second simulation, according to the text, show that the curves are very noisy, but the related figure does not appear to reflect the stated simulated vehicle path or the stated results, i.e. the figure does not show $\gamma = constant$ and $\dot{R} = u$ as one would expect for a vehicle on a constant-bearing trajectory from the beacon.

Future work suggested, but not pursued by the authors, includes taking into account the time delays inherent in acoustic systems as well as different update rates for different inputs. An improvement in noise reduction is also suggested.

Song, 1999 [85]

This paper addresses target tracking using only range measurements in the which the target is assumed to be moving with constant acceleration. The problem set-up differs from the vehicle navigation papers that model a vehicle estimating its own position from range measurements. Here an observer, the tracker, is estimating the position of a target relative to itself, using only target-tracker range information. The heading of the target is not used. The author derives necessary and sufficient conditions for local system observability using the Fisher information matrix in "modified polar coordinates."

Target Process Model: The target is modeled as a dynamic system in continuous time using Cartesian coordinates. The state vector is $x = [X, Y, \dot{X}, \dot{Y}, A_{T_X}, A_{T_Y}]$, where X and Y are the target position relative to the tracker, $\dot{X}$ and $\dot{Y}$ are the relative velocity, and A_{T_X} and A_{T_Y} are the assumed constant world frame accelerations of the target. The input is $A_m = (A_{m_X}, A_{m_X})$, the tracker acceleration vector. The author assumes that the dynamics are modelled perfectly with no process noise.

Observation Model: Measurements are taken in polar coordinates at discrete times. The only measurement in the system, $z(t)$, is the tracker-target range, $r(t)$. The author assumes zero-mean Gaussian measurement noise, $v(t)$, with variance σ^2 such that $z(t_i) = r(t_i) + v(t_i)$ at discrete time $t = t_i$.

Observability: The observability analysis first requires a reformulation of the state vector in polar coordinates. The state vector is redefined as $y(t) = [\dot{\beta}, \dot{r}/r, \beta, 1/r, A_{T_\beta}, A_{T_r}]$

where β is the target-tracker bearing, r is the target-tracker range, and A_{T_β} and A_{T_r} are the bearing and range accelerations respectively. The observability criteria are derived from the requirement that the Fisher information matrix be positive definite and result in a necessary and sufficient condition for local observability.

This observability condition dictates that tracker/target trajectories resulting in constant relative bearing are globally unobservable. More specifically, when the target is on a course directly towards or away from the tracker (in the tracker's frame) the target's course is globally and locally unobservable. Also, when the the target and tracker both have constant bearing (regardless of direction) and constant acceleration (including zero), the target has a linear trajectory with respect to the tracker, resulting in a locally observable but not globally observable trajectory (i.e, a parallel indistinguishable trajectory exists). The author suggests that the tracker's trajectory should contain non-zero jerk in order to track a target with constant acceleration and a non-zero acceleration to track a target with constant velocity.

Simulation: The author uses an extended Kalman filter in Cartesian coordinates with the state and observation models discussed above. A 0.2 Hz update rate and a measurement noise with $\sigma^2 = 0.1m^2$ are used for simulations. The structure of the EKF is not discussed in detail. The author reports that the simulation results "indicate good tracking performance for target states including position, velocity, and acceleration."

Ristic, Arulampalam, and McCarthy, 2002 [76]

The authors make several limiting assumptions concerning the problem statement and the dynamic models of the target and tracker as detailed below. They then compute the theoretical Cramer-Rao lower bound and compare that to the results from three different estimators using Monte Carlo simulations. The three estimators analyzed are a maximum likelihood estimator, an angle-parameterized extended Kalman filter, and a regularized particle filter.

The authors make several limiting assumptions for the dynamic model of the system. The authors assume that the target is on a constant velocity, constant bearing trajectory. The target kinematic state is defined as $\mathbf{s}_k^t = [x_k^t, \dot{x}_k^t, y_k^t, \dot{y}_k^t]^\top$. The observer state is defined as $\mathbf{s}_k^o = [x_k^o, \dot{x}_k^o, y_k^o, \dot{y}_k^o]^\top$. Thus the relative state vector is $\mathbf{s}_k = \mathbf{s}_k^t - \mathbf{s}_k^o = [x_k, \dot{x}_k, y_k, \dot{y}_k]^\top$. The authors further assume that the target's initial position at time t_0 is known and that the tracker is on a constant velocity circular trajectory. Range measurements to the target are made at regular intervals, T_s, starting at some time delay, T_d, after the initial detection, t_0, where $T_d >> T_s$. This represents the target position acquisition by the Ingara radar in Scan mode at time t_0, the time delay, T_d, to switch the instrument to ISAR mode, and then regular range measurements at intervals of T_s thereafter. Because of these assumptions, I believe that the observability analysis and the estimation method comparison may not be applicable to single-beacon OWTT navigation.

A.6 Simultaneous Localization and Mapping:

Navigating with range-only measurements to multiple beacons with no a priori knowledge of beacon location

Newman and J. Leonard, 2003 [71]

This paper addresses the topic of range-only navigation using multiple acoustic beacons but without the use of any additional navigation aids (i.e. no Doppler velocity log or inertial measurement unit) and without a priori knowledge of the location of the acoustic navigation beacons. The authors use a non-linear least squares method to solve for a concatenation of the last N vehicle positions and the beacon locations and present simulation results based on data collected in the field.

Process/Trajectory Model: The state vector of the system consists of some predetermined number, N, of the most recent vehicle pose states as well as the location of i acoustic beacons.

$$\mathbf{X} = [x_A, x_B, x_C, \cdots, x_N, x_1, x_2, x_3, \cdots, x_i]^\top$$

In place of an explicit process model, the authors use a trajectory function, $f(\mathbf{X}) = 0$, to constrain the trajectory of the vehicle to a constant velocity. Vehicle acceleration is modelled as a zero-mean Gaussian random variable, $\ddot{x}(\cdot) \sim \mathcal{N}(0, Q)$. This leads to a linear relationship between any three consecutive vehicle positions: $x_{(\cdot)-1} - 2x_{(\cdot)} + x_{(\cdot)+1} = 0$.

Observation Model: The acoustic time of flight between the vehicle and each of the i^{th} beacons is concatenated into a measurement vector $Z_t = h(\mathbf{X})$. The covariance of Z_t, R, is a diagonal matrix consisting of the variance of each observation. The authors model the observation error as a Cauchy distribution with half maximum width σ.

Least Squares Solution: The combination of observations and constraint equations is solved using a non-linear least-squares approach. Z is the stacked vector consisting of the observations and the trajectory constraints.

$$\begin{bmatrix} Z_t \\ 0 \end{bmatrix} = \begin{bmatrix} h(\mathbf{X}) \\ f(\mathbf{X}) \end{bmatrix}$$

$$Z = h(\mathbf{X})$$

Given Z, the authors use the large-scale non-linear optimization method presented in [41] to solve the linearized system of Gauss-Newton equations, $\mathbf{H}\delta x = \mathbf{J}^\top \mathbf{W} \delta \mathbf{z}$, where $\mathbf{H}$ is the Hessian and $\mathbf{J}$ is the Jacobian of Z evaluated at the current $\hat{\mathbf{X}}$. The measurement residual is $\delta \mathbf{z} = Z - h(\hat{\mathbf{X}})$ and $\mathbf{W}$ is the observation weight matrix, $\mathbf{W} = diag(R^{-1}, Q^{-1})$.

Experiments: Data was collected for simulation during an experiment in shallow water ($\sim$11m depth) using an Odyssey III class vehicle. Acoustic beacons were dropped onto the seafloor and their surface release positions marked with a DGPS. These beacons were used to independently calculate the absolute position of the vehicle and compared to the results

of the algorithm. The vehicle navigated using an extended Kalman filter (EKF) with LBL (and a priori knowledge of the beacon locations) as well as compass and Doppler velocity. The survey consisted of parallel tracklines approximately 75 m apart and 350 m long.

Due to a synthetic aperture sonar on the vehicle whose frequency overlaps the frequency band of the acoustic beacons, the range measurement data were extremely noisy with a significant number of outliers and non-Gaussian noise. To counter this, the data were filtered to reject outliers using a series of ad hoc algorithms. The filtered range information for approximately 1 km of the survey was used in post-processing as input to the range-only algorithm.

Results: Due to the nature of the range-only navigation problem presented, i.e. a solution found without any additional navigation aids, the range-only navigation solution produced is relative to the beacons without a world-frame reference. Thus the solution is unconstrained in x, y and θ and must be rotated and translated in order to compare it to the EKF solution. The authors accomplish this by choosing a rotation and translation that collocates the position of the transponder labelled "T1" and aligns the baseline between T1 and T2. The results show baseline length errors between 1.3% and 2.3% with trackline following within 5-10 m of the EKF solution except when the trackline was in a geometrically undesirable position with respect to the acoustic beacons. During these periods the off-track error between the EKF and the range-only solution deteriorated to 20-30 m.

Olson, Leonard, and Teller, 2006 [72]

This paper addresses vehicle position estimation using only range measurements to multiple beacons without a priori knowledge of beacon locations. The main result presented in this paper is an outlier rejection algorithm for extremely noisy range data with a large number of non-Gaussian outliers. The authors also present an algorithm for the determination of the initial estimate of a beacon's position, in this case to seed an extended Kalman filter (EKF). Finally, the authors present the optimal vehicle trajectory for disambiguating between two possible beacon locations. The authors use an EKF to estimate vehicle and beacon locations and they present a method for dynamically increasing the size of the state vector (and covariance matrix) as new beacons are identified and initialized.

Pre-Filtering Range Data: The authors present an outlier rejection algorithm using a form of spectral graph partitioning denoted Single Cluster Graph Partitioning (SCGP). This algorithm relies solely on pairs of concurrent range measurements and vehicle position estimates requiring no a priori knowledge of beacon locations. This review will not cover the outlier rejection algorithm in detail because it is not the focus of the review, but readers interested in more information about the algorithm are encouraged to read both the paper reviewed here [72] and the previous paper published by the authors on the subject [73].

Process Model: The process model is not explicitly addressed except to define the state vector $x_n = [r_x, r_y, r_t, b_x, b_y]$, where r_x, r_y, r_t are the vehicle x,y position and heading in world coordinates respectively, and b_x and b_y are a beacon location in world coordinates (one (b_z, b_y) pair exists for every beacon). As new beacons are detected and initialized,

they are added to the state vector and the state covariance matrix is updated. Neither the authors' assumptions concerning vehicle dynamics nor the existence or characteristics of process noise are reported in the paper.

Observation Model: The observation model is not explicitly defined. However, the estimated measurement, as calculated from the current state, is defined as $\hat{z}_n = [(r_x - b_x)^2 + (r_y - b_y)^2]^{1/2}$. The existence of measurement noise is not addressed in the paper.

Extended Kalman Filter: To estimate vehicle and beacon positions, the authors implement an extended Kalman filter with the state vector defined above. The authors propose an algorithm for obtaining the initial estimate of a beacon position by comparing every possible pair of data points, where a data point consists of a vehicle location and a range to the beacon. Using a "voting scheme", each intersection of possible beacon locations among all of the pairs of data points is recorded as a "vote" for that location. As soon as the difference in the number of votes between any two locations exceeds a preset number of votes, the location with the most votes is chosen as the approximate beacon location used to seed the extended Kalman filter.

During this voting process, two distinct candidate beacon positions may appear to be equally likely. The authors present a simple calculation based on the gradient of the absolute difference in range between the two candidate positions to determine the optimal vehicle trajectory to disambiguate the true beacon position.

Experiments: Data used for simulation was collected during an experiment in shallow water ($\sim$11m depth) using an Odyssey III class vehicle. Acoustic beacons were dropped onto the seafloor and their surface release positions marked with a DGPS. These positions were used as ground truth for the algorithm. The vehicle navigated using an EKF with LBL (and a priori knowledge of the beacon locations) as well as compass and Doppler velocity. The survey consisted of parallel tracklines approximately 75 m apart and 350 m long. This is the same data set used by Newman and J. Leonard in [71].

Due to a synthetic aperture sonar whose frequency overlaps the frequency band of the acoustic beacons, the range measurement data were extremely noisy with a significant number of outliers and non-Gaussian noise.

Navigation Results: Because the navigation solution is calculated only relative to the beacons without a world frame reference, the solution is unconstrained in x, y and θ and must be rotated and translated in order to compare it to the EKF solution. The authors used one beacon to determine the global alignment and found errors for the remaining three beacon positions between 1.5m and 3m. The authors note that because a ground truth beacon position was used to determine the global alignment, the beacon position error may be underestimated.

Kantor and Singh, 2002 [51]

This paper presents several estimation methods applied to the problem of robot localization using range measurements from multiple beacons. The authors address three separate

topics in mobile robot localization: static localization, position tracking, and simultaneous localization and tracking.

Static localization is accomplished using Markovian probability grid methods and tested experimentally. For position tracking, the authors compare simulation results from an extended Kalman filter (EKF) and a Monte Carlo particle filter. For both the static localization and the position tracking, the authors assume that the beacon locations are known precisely. Finally, assuming that precise beacon locations are not known a priori, the authors present simulation results for a simultaneous localization and mapping (SLAM) algorithm that utilizes an extended Kalman filter.

Static Localization with Probability Grids: To test static localization, the authors use a Markovian probability grid method. Using a 50'x50' test area divided into 1'x1' squares, each square is assigned a real number, P_s, equal to the probability that the robot is occupying that square. Given a measurement from a beacon, m_i, and that beacon's location, x_b, the probability for each square is calculated by $P_s = p(r_s|m_i)/(2\pi r_s \beta)$, where $r_s = ||x_b - x_s||$ and x_s is the location of the center of the square. β is a constant normalizing factor to ensure that the total probability over the test area adds to 1.

Given a probability grid for every measurement from each beacon, the authors combine the probability grids using point-wise multiplication and re-normalize. This combined probability grid is then used to calculate a weighted average of the estimated vehicle position and covariance.

Experimentally, the authors selected approximately 100 different vehicle locations distributed across a 50'x50' test area with eight radio-frequency beacons. Each radio frequency beacon provides range measurements in feet discretized to a values in the set {0,6,12,18,25,31,37,43,50}. The authors experimentally determined the probability density function for each measurement.

Using the probability grid method of localization, the authors found an average estimation error of 1.62 feet.

Position Tracking: For the purpose of position tracking the authors compare an extended Kalman filter (EKF) and a Monte Carlo particle filter.

Extended Kalman Filter: The EKF is based on the discrete-time process model

$$x(k+1) = x(k) + T \begin{bmatrix} u_1(k) \\ u_2(k) \end{bmatrix} + w(k),$$

where $u_1(k), u_2(k)$ are the vehicle x and y velocities in world coordinates and $w(k)$ is a zero-mean, independent and identically distributed Gaussian random vector with covariance R. The static solution described above is used as the seed for the EKF.

The authors create an ad hoc Gaussian distribution to represent a pseudo-measurement of vehicle position. The pseudo-measurement is based on the actual range measurement such that the vehicle position lies at the measured range and the angle to the beacon is based on the prior:

$$\hat{z} = x_b + \begin{bmatrix} \bar{r}_m \cos\theta \\ \bar{r}_m \sin\theta \end{bmatrix},$$

where $\bar{r}_m$ is the mean of the range measurement and θ is the angle between the x axis and the line between the beacon and the prior estimated vehicle location. Instead of modelling measurement noise, the authors assign a covariance matrix C to the pseudo-measurement such that

$$C = \Phi \begin{bmatrix} v_r & 0 \\ 0 & 10 * v_r \end{bmatrix} \Phi^\top,$$

where v_r is the measurement variance (along the direction of the measurement) and

$$\Phi = \begin{bmatrix} \cos\theta & -\sin\theta \\ \sin\theta & \cos\theta \end{bmatrix}.$$

Monte Carlo Particle Filter: In comparison to the EKF, the authors construct a Monte Carlo particle filter. Following similar "prediction" and "update" steps as the EKF, the authors start with N_p particles and compute $\tilde{x}_p(k)$ for each p using the process model given above. Each particle, p, is assigned a weight, $w(p)$ such that $w(p) = p(r_p|m(k))$, where r_p is the distance between $x_b(k)$ and the projected position. After computing weights for all of the points, the weights are rescaled such that the sum of the weights for all points equals 1. Finally, for each p, $x_p(k+1)$ is randomly chosen from the prescribed collection.

Comparison: The authors found that using identical beacon locations, beacon returns, robot trajectories and noise covariance matrices, the average estimation error from the Kalman filter simulation is slightly better than the Monte Carlo simulation (0.73 feet versus 0.93 feet), and the Kalman filter only requires $O(N_b)$ computations while the Monte Carlo simulation requires $O(N_b N_p)$ computations. The authors conclude that this is a significant difference in computation cost because the smallest N_p that gives reasonable results is approximately 200.

Simultaneous Localization and Mapping with EKF: The authors extend the EKF described above to the situation where beacon locations are approximately but not exactly known. The state vector consists of the vehicle position as well as the beacon locations and the process model is updated accordingly assuming the beacon locations do not move. The authors assume that range measurements are transformed into a position measurement with zero-mean Gaussian noise as described above.

In simulation, the range measurements noise variance is $v = 1$ and the variance of the initial robot and beacon estimates is set to 25 (i.e. an expected error of 5 feet). In the simulation shown in the paper, the average error improved from 5.13 feet initially to 0.77 feet after travelling approximately 60 feet.

Appendix B

Linear Kalman Filter Derivation

The following is a brief derivation of the prediction and update equations for the Kalman filter. We assume that we have a discrete-time process model and observation model of the form

$$\boldsymbol{x}_{k+1} = \boldsymbol{F}\boldsymbol{x}_k + \boldsymbol{B}\boldsymbol{u}_k + \boldsymbol{w}_k \tag{B.1}$$
$$\boldsymbol{z}_k = \boldsymbol{H}\boldsymbol{x}_k + \boldsymbol{v}_k \tag{B.2}$$

where $\boldsymbol{x}$ is the state vector, $\boldsymbol{u}_k$ is the input, $\boldsymbol{z}_k$ is the measurement, and $\boldsymbol{w} \sim \mathcal{N}(0, \boldsymbol{Q})$ and $\boldsymbol{v}_k \sim \mathcal{N}(0, \boldsymbol{R})$ are independent zero-mean Gaussian noise.

B.1 Assumptions

In deriving the Kalman filter we seek a recursive *unbiased* estimator for the plant state

$$\boldsymbol{\mu}_{k+1|k} = E[\boldsymbol{x}_{k+1}] \tag{B.3}$$
$$\boldsymbol{\mu}_{k|k} = E[\boldsymbol{x}_k] \tag{B.4}$$

such that the sum of the *variance* of the state estimate

$$E[(\boldsymbol{x}_k - \boldsymbol{\mu}_{k|k})^\top (\boldsymbol{x}_k - \boldsymbol{\mu}_{k|k})] \tag{B.5}$$

is minimized.

B.2 Process Prediction

Using the unbiased estimator assumption (B.3) we compute the prediction equation for $\boldsymbol{\mu}$, the mean of $\boldsymbol{x}$, as follows,

$$\begin{aligned}\boldsymbol{\mu}_{k+1|k} &= E[\boldsymbol{x}_{k+1}] \\ &= E[\boldsymbol{F}\boldsymbol{x}_k + \boldsymbol{B}\boldsymbol{u}_k + \boldsymbol{w}_k] \\ &= \boldsymbol{F}E[\boldsymbol{x}_k] + \boldsymbol{B}\boldsymbol{u}_k + \cancelto{0}{E[\boldsymbol{w}_k]} \\ \boldsymbol{\mu}_{k+1|k} &= \boldsymbol{F}\boldsymbol{\mu}_{k|k} + \boldsymbol{B}\boldsymbol{u}_k\end{aligned} \tag{B.6}$$

$$\tag{B.7}$$

where we rely on the fact that $\boldsymbol{x}_k$ and $\boldsymbol{w}_k$ are uncorrelated. Using (B.7) we can solve for the prediction equation for $\boldsymbol{\Sigma}$, the covariance of $\boldsymbol{x}$, as follows,

$$\begin{aligned}\boldsymbol{\Sigma}_{k+1|k} &= cov(\boldsymbol{x}_{k+1} - \boldsymbol{\mu}_{k+1|k}) \\ &= cov(\boldsymbol{F}\boldsymbol{x}_k + \cancel{\boldsymbol{B}\boldsymbol{u}_k} - \boldsymbol{F}\boldsymbol{\mu}_{k|k} - \cancel{\boldsymbol{B}\boldsymbol{u}_k} - \boldsymbol{w}_k) \\ &= cov(\boldsymbol{F}(\boldsymbol{x}_k - \boldsymbol{\mu}_{k|k}) - \boldsymbol{w}_k) \\ &= cov(\boldsymbol{F}(\boldsymbol{x}_k - \boldsymbol{\mu}_{k|k}) + cov(\boldsymbol{w}_k) \\ &= \boldsymbol{F}cov((\boldsymbol{x}_k - \boldsymbol{\mu}_{k|k}))\boldsymbol{F}^\top + cov(\boldsymbol{w}_k) \\ \boldsymbol{\Sigma}_{k+1|k} &= \boldsymbol{F}\boldsymbol{\Sigma}_{k|k}\boldsymbol{F}^\top + \boldsymbol{Q}\end{aligned} \tag{B.8}$$

$$\tag{B.9}$$

where we use the fact that $\boldsymbol{F}(\boldsymbol{\mu}_{k|k} - \boldsymbol{x}_k)$ and $\boldsymbol{w}_k$ are uncorrelated.

B.3 Measurement Update

We assume when deriving the measurement update equations that the update is a linear combination of the previous state estimate and the measurement:

$$\boldsymbol{\mu}_{k|k} = \boldsymbol{A}\boldsymbol{\mu}_{k|k-1} + \boldsymbol{K}\boldsymbol{z}_k \tag{B.10}$$

where both $\boldsymbol{A}$ and $\boldsymbol{K}$ are unknown. Using equation B.4 to solve for $\boldsymbol{A}$:

$$\begin{aligned}\boldsymbol{0} &= E[\boldsymbol{x}_k - \boldsymbol{\mu}_{k|k}] \\ &= E[\boldsymbol{x}_k - \boldsymbol{A}\boldsymbol{\mu}_{k|k-1} - \boldsymbol{K}\boldsymbol{z}_k] \\ &= E[\boldsymbol{x}_k - \boldsymbol{A}\boldsymbol{\mu}_{k|k-1} - \boldsymbol{K}(\boldsymbol{H}\boldsymbol{x}_k + \boldsymbol{v}_k)] \\ &= E[\boldsymbol{x}_k - \boldsymbol{K}\boldsymbol{H}\boldsymbol{x}_k] - \cancelto{0}{E[\boldsymbol{K}\boldsymbol{v}_k]} - E[\boldsymbol{A}\boldsymbol{\mu}_{k|k-1}] \\ \boldsymbol{0} &= (\boldsymbol{I} - \boldsymbol{K}\boldsymbol{H})E[\boldsymbol{x}_k] - \boldsymbol{A}\boldsymbol{\mu}_{k|k-1} \\ \boldsymbol{A} &= \boldsymbol{I} - \boldsymbol{K}\boldsymbol{H}\end{aligned} \tag{B.11}$$

$$\tag{B.12}$$

Substituting (B.12) into equation (B.10) we arrive at the measurement update equation for the mean of $\boldsymbol{x}$ in terms of $\boldsymbol{K}$:

$$\boldsymbol{\mu}_{k|k} = \boldsymbol{\mu}_{k|k-1} + \boldsymbol{K}(\boldsymbol{z}_k - \boldsymbol{H}\boldsymbol{\mu}_{k|k-1}) \tag{B.13}$$

We compute the measurement update equation for the covariance of $\boldsymbol{x}$ in terms of $\boldsymbol{K}$

$$\begin{aligned}
\boldsymbol{\Sigma}_{k|k} &= cov(\boldsymbol{x}_k - \boldsymbol{\mu}_{k|k}) && \text{(B.14)}\\
&= cov(\boldsymbol{x}_k - \boldsymbol{\mu}_{k|k-1} + \boldsymbol{K}\boldsymbol{H}\boldsymbol{\mu}_{k|k-1} - \boldsymbol{K}\boldsymbol{z}_k)\\
&= cov(\boldsymbol{x}_k - \boldsymbol{\mu}_{k|k-1} + \boldsymbol{K}\boldsymbol{H}\boldsymbol{\mu}_{k|k-1} - \boldsymbol{K}\boldsymbol{H}\boldsymbol{x}_k - \boldsymbol{K}\boldsymbol{v}_k)\\
&= cov((\boldsymbol{I} - \boldsymbol{K}\boldsymbol{H})(\boldsymbol{x}_k - \boldsymbol{\mu}_{k|k-1}) - \boldsymbol{K}\boldsymbol{v}_k)\\
&= cov((\boldsymbol{I} - \boldsymbol{K}\boldsymbol{H})(\boldsymbol{x}_k - \boldsymbol{\mu}_{k|k-1})) + cov(\boldsymbol{K}\boldsymbol{v}_k)\\
&= (\boldsymbol{I} - \boldsymbol{K}\boldsymbol{H})cov(\boldsymbol{x}_k - \boldsymbol{\mu}_{k|k-1})(\boldsymbol{I} - \boldsymbol{K}\boldsymbol{H})^\top + \boldsymbol{K}cov(\boldsymbol{v}_k)\boldsymbol{K}^\top\\
\boldsymbol{\Sigma}_{k|k} &= (\boldsymbol{I} - \boldsymbol{K}\boldsymbol{H})\boldsymbol{\Sigma}_{k|k-1}(\boldsymbol{I} - \boldsymbol{K}\boldsymbol{H})^\top + \boldsymbol{K}\boldsymbol{R}\boldsymbol{K}^\top. && \text{(B.15)}
\end{aligned}$$

B.4 Kalman Gain

To solve for the Kalman gain, $\boldsymbol{K}$, we use the fact that we are seeking a recursive estimator that minimizes the sum of the variance of the state estimate, and we note that minimizing the sum of the variance is identical to minimize the trace of the covariance matrix,

$$\begin{aligned}
E[(\boldsymbol{x}_k - \boldsymbol{\mu}_{k|k})^\top(\boldsymbol{x}_k - \boldsymbol{\mu}_{k|k})] &= trE[(\boldsymbol{x}_k - \boldsymbol{\mu}_{k|k})(\boldsymbol{x}_k - \boldsymbol{\mu}_{k|k})^\top] && \text{(B.16)}\\
&= tr\boldsymbol{\Sigma}_{k|k}. && \text{(B.17)}
\end{aligned}$$

Substituting the measurement update equation (B.15) for the covariance, we minimize the trace by setting the partial derivative equal to zero and note that the trace of the partial derivative equals the partial derivative of the trace:

$$0 = \frac{\partial}{\partial \boldsymbol{K}}\{tr\boldsymbol{\Sigma}_{k|k}\} = tr\frac{\partial}{\partial \boldsymbol{K}}\{\boldsymbol{\Sigma}_{k|k}\}. \tag{B.18}$$

Substituting the definition of $\boldsymbol{\Sigma}_{k|k}$ from (B.15) into (B.18) we obtain

$$\begin{aligned}
0 &= tr\frac{\partial}{\partial \boldsymbol{K}}\{(\boldsymbol{I} - \boldsymbol{K}\boldsymbol{H})\boldsymbol{\Sigma}_{k|k-1}(\boldsymbol{I} - \boldsymbol{K}\boldsymbol{H})^\top + \boldsymbol{K}\boldsymbol{R}\boldsymbol{K}^\top\}\\
&= tr\frac{\partial}{\partial \boldsymbol{K}}\{\boldsymbol{\Sigma}_{k|k-1} - \boldsymbol{K}\boldsymbol{H}\boldsymbol{\Sigma}_{k|k-1} - \boldsymbol{\Sigma}_{k|k-1}\boldsymbol{H}^\top\boldsymbol{K}^\top\\
&+ \boldsymbol{K}\boldsymbol{H}\boldsymbol{\Sigma}_{k|k-1}\boldsymbol{H}^\top\boldsymbol{K}^\top + \boldsymbol{K}\boldsymbol{R}\boldsymbol{K}^\top\}\\
&= tr\{-\boldsymbol{\Sigma}_{k|k-1}^\top\boldsymbol{H}^\top - \boldsymbol{\Sigma}_{k|k-1}\boldsymbol{H}^\top + \boldsymbol{K}\boldsymbol{H}\boldsymbol{\Sigma}_{k|k-1}^\top\boldsymbol{H}^\top\\
&+ \boldsymbol{K}\boldsymbol{H}\boldsymbol{\Sigma}_{k|k-1}\boldsymbol{H}^\top + \boldsymbol{K}\boldsymbol{R} + \boldsymbol{K}\boldsymbol{R}^\top\}. && \text{(B.19)}
\end{aligned}$$

Because $\boldsymbol{\Sigma}_{k|k-1}$ and $\boldsymbol{R}$ are symmetric by definition we can further simplify (B.19)

$$0 = tr\{-2\boldsymbol{\Sigma}_{k|k-1}\boldsymbol{H}^\top + 2\boldsymbol{K}\boldsymbol{H}\boldsymbol{\Sigma}_{k|k-1}\boldsymbol{H}^\top + 2\boldsymbol{K}\boldsymbol{R}\}. \tag{B.20}$$

The constraint (B.20) is satisfied by setting the argument of the trace equal to zero

$$0 = -2\boldsymbol{\Sigma}_{k|k-1}\boldsymbol{H}^\top + 2\boldsymbol{K}\boldsymbol{H}\boldsymbol{\Sigma}_{k|k-1}\boldsymbol{H}^\top + 2\boldsymbol{K}\boldsymbol{R} \tag{B.21}$$

which allows us to solve for the Kalman gain

$$\boldsymbol{K} = \boldsymbol{\Sigma}_{k|k-1}\boldsymbol{H}^\top(\boldsymbol{H}\boldsymbol{\Sigma}_{k|k-1}\boldsymbol{H}^\top + \boldsymbol{R})^{-1}. \tag{B.22}$$

Appendix C

Linear Information Filter Derivation

The following is a brief derivation of the linear information filter in the context of a linear, one degree-of-freedom plant model. The information filter is often referred to as the *dual* of the Kalman filter. The Kalman filter recursively estimates the mean, $\boldsymbol{\mu}$, and covariance, $\boldsymbol{\Sigma}$, of the random variable $\boldsymbol{x}$, where

$$\boldsymbol{\mu} = E[\boldsymbol{x}] \tag{C.1}$$
$$\boldsymbol{\Sigma} = E\left[(\boldsymbol{x} - \boldsymbol{\mu})(\boldsymbol{x} - \boldsymbol{\mu})^\top\right]. \tag{C.2}$$

The information filter is based on the explicit normalization of the random variable $\boldsymbol{x}$ by its covariance $\boldsymbol{\Sigma}$ such that the information filter recursively estimates the mean, $\boldsymbol{\eta}$, and covariance, $\boldsymbol{\Lambda}$, of the normalized random variable $\boldsymbol{\Sigma}^{-1}\boldsymbol{x}$

$$\boldsymbol{\eta} = E[\boldsymbol{\Sigma}^{-1}\boldsymbol{x}] = \boldsymbol{\Sigma}^{-1}\boldsymbol{\mu} \tag{C.3}$$
$$\boldsymbol{\Lambda} = E\left[(\boldsymbol{\Sigma}^{-1}\boldsymbol{x} - \boldsymbol{\Sigma}^{-1}\boldsymbol{\mu})(\boldsymbol{\Sigma}^{-1}\boldsymbol{x} - \boldsymbol{\Sigma}^{-1}\boldsymbol{\mu})^\top\right] = \boldsymbol{\Sigma}^{-1} \tag{C.4}$$

where $\boldsymbol{\eta}$ is referred to as the information vector, and $\boldsymbol{\Lambda}$ the information matrix [8, 70].

C.1 Kalman Filter Review

The derivation of the information filter is presented in the context of the Kalman filter. Thus we start with a brief overview of the Kalman filter. For this derivation we will assume that $\boldsymbol{B} = 0$.

The Kalman filter prediction equations from Appendix B are

$$\boldsymbol{\mu}_{k+1|k} = \boldsymbol{F}_k\boldsymbol{\mu}_{k|k} + \cancelto{0}{\boldsymbol{B}_k\boldsymbol{u}_k} \tag{C.5}$$
$$\boldsymbol{\Sigma}_{k+1|k} = \boldsymbol{F}_k\boldsymbol{\Sigma}_{k|k}\boldsymbol{F}_k^\top + \boldsymbol{Q}_k. \tag{C.6}$$

The Kalman filter measurement update equations from Appendix B are

$$\boldsymbol{\mu}_{k|k} = \boldsymbol{\mu}_{k|k-1} + \boldsymbol{K}(\boldsymbol{z}_k - \boldsymbol{H}\boldsymbol{\mu}_{k|k-1}) \tag{C.7}$$
$$\boldsymbol{\Sigma}_{k|k} = (\boldsymbol{I} - \boldsymbol{K}_k\boldsymbol{H}_k)\boldsymbol{\Sigma}_{k|k-1} \tag{C.8}$$
$$\boldsymbol{K}_k = \boldsymbol{\Sigma}_{k|k-1}\boldsymbol{H}_k^\top(\boldsymbol{H}_k\boldsymbol{\Sigma}_{k|k-1}\boldsymbol{H}_k^\top + \boldsymbol{R}_k)^{-1} \tag{C.9}$$

where (C.8) is derived from the form of $\boldsymbol{\Sigma}_{k|k}$ given in (B.15) as follows

$$\begin{aligned}
\boldsymbol{\Sigma}_{k|k} &= (\boldsymbol{I} - \boldsymbol{K}_k\boldsymbol{H}_k)\boldsymbol{\Sigma}_{k|k-1}(\boldsymbol{I} - \boldsymbol{K}_k\boldsymbol{H}_k)^\top + \boldsymbol{K}_k\boldsymbol{R}_k\boldsymbol{K}_k^\top \qquad \text{(C.10)}\\
&= \boldsymbol{\Sigma}_{k|k-1} - \boldsymbol{K}_k\boldsymbol{H}_k\boldsymbol{\Sigma}_{k|k-1} - \boldsymbol{\Sigma}_{k|k-1}\boldsymbol{H}_k^\top\boldsymbol{K}_k^\top + \boldsymbol{K}_k\boldsymbol{H}_k\boldsymbol{\Sigma}_{k|k-1}\boldsymbol{H}_k^\top\boldsymbol{K}_k^\top + \boldsymbol{K}_k\boldsymbol{R}_k\boldsymbol{K}_k^\top\\
&= \boldsymbol{\Sigma}_{k|k-1} - \boldsymbol{K}_k\boldsymbol{H}_k\boldsymbol{\Sigma}_{k|k-1} - \boldsymbol{\Sigma}_{k|k-1}\boldsymbol{H}_k^\top\boldsymbol{K}_k^\top + \boldsymbol{K}_k(\boldsymbol{H}_k\boldsymbol{\Sigma}_{k|k-1}\boldsymbol{H}_k^\top + \boldsymbol{R}_k)\boldsymbol{K}_k^\top\\
&= \boldsymbol{\Sigma}_{k|k-1} - \boldsymbol{\Sigma}_{k|k-1}\boldsymbol{H}_k^\top(\boldsymbol{H}_k\boldsymbol{\Sigma}_{k|k-1}\boldsymbol{H}_k^\top + \boldsymbol{R}_k)^{-1}\boldsymbol{H}_k\boldsymbol{\Sigma}_{k|k-1}\\
&\quad - \boldsymbol{\Sigma}_{k|k-1}\boldsymbol{H}_k^\top(\boldsymbol{H}_k\boldsymbol{\Sigma}_{k|k-1}\boldsymbol{H}_k^\top + \boldsymbol{R}_k)^{-1}\boldsymbol{H}_k\boldsymbol{\Sigma}_{k|k-1}\\
&\quad + \cancel{\boldsymbol{\Sigma}_{k|k-1}\boldsymbol{H}_k^\top(\boldsymbol{H}_k\boldsymbol{\Sigma}_{k|k-1}\boldsymbol{H}_k^\top + \boldsymbol{R}_k)^{-1}(\boldsymbol{H}_k\boldsymbol{\Sigma}_{k|k-1}\boldsymbol{H}_k^\top + \boldsymbol{R}_k)}\\
&\quad \cancel{(\boldsymbol{H}_k\boldsymbol{\Sigma}_{k|k-1}\boldsymbol{H}_k^\top + \boldsymbol{R}_k)^{-1}\boldsymbol{H}_k\boldsymbol{\Sigma}_{k|k-1}}\\
&= \boldsymbol{\Sigma}_{k|k-1} - \boldsymbol{\Sigma}_{k|k-1}\boldsymbol{H}_k^\top(\boldsymbol{H}_k\boldsymbol{\Sigma}_{k|k-1}\boldsymbol{H}_k^\top + \boldsymbol{R}_k)^{-1}\boldsymbol{H}_k\boldsymbol{\Sigma}_{k|k-1}\\
&\quad \cancel{- \boldsymbol{\Sigma}_{k|k-1}\boldsymbol{H}_k^\top(\boldsymbol{H}_k\boldsymbol{\Sigma}_{k|k-1}\boldsymbol{H}_k^\top + \boldsymbol{R}_k)^{-1}\boldsymbol{H}_k\boldsymbol{\Sigma}_{k|k-1}}\\
&\quad \cancel{+ \boldsymbol{\Sigma}_{k|k-1}\boldsymbol{H}_k^\top(\boldsymbol{H}_k\boldsymbol{\Sigma}_{k|k-1}\boldsymbol{H}_k^\top + \boldsymbol{R}_k)^{-1}\boldsymbol{H}_k\boldsymbol{\Sigma}_{k|k-1}}\\
&= \cancel{\boldsymbol{\Sigma}_{k|k-1} - \boldsymbol{K}_k\boldsymbol{H}_k\boldsymbol{\Sigma}_{k|k-1}}\\
&= (\boldsymbol{I} - \boldsymbol{K}_k\boldsymbol{H}_k)\boldsymbol{\Sigma}_{k|k-1}
\end{aligned}$$

noting that $(\boldsymbol{H}_k\boldsymbol{\Sigma}_{k|k-1}\boldsymbol{H}_k^\top + \boldsymbol{R}_k)^{-1}$ is symmetric.

C.2 Plant Process Model

We assume a 1 degree-of-freedom constant-velocity linear process model for the plant

$$\dot{\boldsymbol{x}} = \underbrace{\begin{bmatrix} 0 & 1 \\ 0 & 0 \end{bmatrix}}_{\boldsymbol{F}}\boldsymbol{x} + \underbrace{\begin{bmatrix} 0 \\ 1 \end{bmatrix}}_{\boldsymbol{G}} w \tag{C.11}$$

where the state vector $\boldsymbol{x}$ is position and velocity along the y-axis

$$\boldsymbol{x} = \begin{bmatrix} y \\ \dot{y} \end{bmatrix} \tag{C.12}$$

and w is independent zero-mean Gaussian process noise in the acceleration term.

$$w \sim \mathcal{N}(0, q) \tag{C.13}$$

The process model is discretized according to standard methods [8], resulting in the discrete-time linear process model

$$\boldsymbol{x}_{k+1} = \boldsymbol{F}_k \boldsymbol{x}_k + \boldsymbol{w}_k \tag{C.14}$$

$$\boldsymbol{F}_k = e^{\boldsymbol{F}T} = \begin{bmatrix} 1 & T \\ 0 & 1 \end{bmatrix} \tag{C.15}$$

where $\boldsymbol{F}$ is defined in (C.11), T is the discrete time step and

$$\boldsymbol{x}_k = \begin{bmatrix} y_k \\ \dot{y}_k \end{bmatrix} \tag{C.16}$$

is the discrete state vector. The discretized process noise, $\boldsymbol{w}_k$ is zero-mean Gaussian

$$\boldsymbol{w}_k \sim \mathcal{N}(0, \boldsymbol{Q}) \tag{C.17}$$

$$\tag{C.18}$$

where the covariance matrix is

$$\boldsymbol{Q} = \begin{bmatrix} \frac{1}{3}T^3 & \frac{1}{2}T^2 \\ \frac{1}{2}T^2 & T \end{bmatrix} q. \tag{C.19}$$

Note that even though $\boldsymbol{F}_k$ and $\boldsymbol{w}_k$ are shown with a subscript denoting the time step k, they are in fact constant and do not depend on time.

C.3 Process Prediction

To derive the prediction equations for the information matrix, we start with the definition of Λ,

$$\begin{aligned} \boldsymbol{\Lambda}_{k|k-1} &= \boldsymbol{\Sigma}_{k|k-1}^{-1} \\ &= (\underbrace{\boldsymbol{F}_{k-1}\boldsymbol{\Sigma}_{k-1|k-1}\boldsymbol{F}_{k-1}^{\top}}_{\boldsymbol{A}_{k-1}^{-1}} + \boldsymbol{Q}_{k-1})^{-1} \\ &= (\boldsymbol{A}_{k-1}^{-1} + \boldsymbol{Q}_{k-1})^{-1} \end{aligned} \tag{C.20}$$

$$\boldsymbol{\Lambda}_{k|k-1} = \boldsymbol{A}_{k-1} - \boldsymbol{A}_{k-1}\left(\boldsymbol{A}_{k-1} + \boldsymbol{Q}_{k-1}^{-1}\right)^{-1}\boldsymbol{A}_{k-1} \tag{C.21}$$

where we define $\boldsymbol{A}_{k-1}^{-1}$ such that $\boldsymbol{A}_{k-1} = \boldsymbol{F}_{k-1}^{\top^{-1}} \boldsymbol{\Sigma}_{k-1|k-1}^{-1} \boldsymbol{F}_{k-1}^{-1}$ and we invoke the matrix inversion lemma from Bar-Shalom [8, p. 23]

$$(A + BCB^\top)^{-1} = A^{-1} - A^{-1}B(B^\top A^{-1}B + C^{-1})^{-1}B^\top A^{-1}. \tag{C.22}$$

Similarly for $\boldsymbol{\eta}$,

$$\begin{aligned}
\boldsymbol{\eta}_{k|k-1} &= \boldsymbol{\Sigma}_{k|k-1}^{-1}\boldsymbol{\mu}_{k|k-1} \qquad \text{(C.23)}\\
&= \left[\boldsymbol{F}_{k-1}\boldsymbol{\Sigma}_{k-1|k-1}\boldsymbol{F}_{k-1}^\top + \boldsymbol{Q}_{k-1}\right]^{-1}\boldsymbol{F}_{k-1}\boldsymbol{\mu}_{k-1|k-1}\\
&= \left[\boldsymbol{F}_{k-1}(\boldsymbol{\Sigma}_{k-1|k-1} + \boldsymbol{F}_{k-1}^{-1}\boldsymbol{Q}_{k-1}\boldsymbol{F}_{k-1}^{\top^{-1}})\boldsymbol{F}_{k-1}^\top\right]^{-1}\boldsymbol{F}_{k-1}\boldsymbol{\mu}_{k-1|k-1}\\
&= \boldsymbol{F}_{k-1}^{\top^{-1}}\underbrace{(\boldsymbol{\Sigma}_{k-1|k-1} + \boldsymbol{F}_{k-1}^{-1}\boldsymbol{Q}_{k-1}\boldsymbol{F}_{k-1}^{\top^{-1}})^{-1}}_{\textit{matrix inversion lemma}}\cancel{\boldsymbol{F}_{k-1}^{-1}\boldsymbol{F}_{k-1}}\boldsymbol{I}\boldsymbol{\mu}_{k-1|k-1}\\
&= \boldsymbol{F}_{k-1}^{\top^{-1}}\Big[\boldsymbol{\Sigma}_{k-1|k-1}^{-1} - \boldsymbol{\Sigma}_{k-1|k-1}^{-1}\boldsymbol{F}_{k-1}^{-1}(\boldsymbol{F}_{k-1}^{\top^{-1}}\boldsymbol{\Sigma}_{k-1|k-1}^{-1}\boldsymbol{F}_{k-1}^{-1} + \boldsymbol{Q}_{k-1}^{-1})^{-1}\cdots\\
&\qquad \cdots\boldsymbol{F}_{k-1}^{\top^{-1}}\boldsymbol{\Sigma}_{k-1|k-1}^{-1}\Big]\boldsymbol{\mu}_{k-1|k-1}\\
&= \Big[\boldsymbol{F}_{k-1}^{\top^{-1}} - \underbrace{\boldsymbol{F}_{k-1}^{\top^{-1}}\boldsymbol{\Sigma}_{k-1|k-1}^{-1}\boldsymbol{F}_{k-1}^{-1}}_{\boldsymbol{A}_{k-1}}(\underbrace{\boldsymbol{F}_{k-1}^{\top^{-1}}\boldsymbol{\Sigma}_{k-1|k-1}^{-1}\boldsymbol{F}_{k-1}^{-1}}_{\boldsymbol{A}_{k-1}} + \boldsymbol{Q}_{k-1}^{-1})^{-1}\,\boldsymbol{F}_{k-1}^{\top^{-1}}\Big]\cdots\\
&\qquad \cdots\underbrace{\boldsymbol{\Sigma}_{k-1|k-1}^{-1}\boldsymbol{\mu}_{k-1|k-1}}_{\boldsymbol{\eta}_{k-1|k-1}}\\
\boldsymbol{\eta}_{k|k-1} &= \left[\boldsymbol{I} - \boldsymbol{A}_{k-1}(\boldsymbol{A}_{k-1} + \boldsymbol{Q}_{k-1}^{-1})^{-1}\right]\boldsymbol{F}_{k-1}^{\top^{-1}}\boldsymbol{\eta}_{k-1|k-1}. \qquad \text{(C.24)}
\end{aligned}$$

C.4 Process Prediction with Augmentation

In this example, the *system* state is augmented with the newly predicted *plant* state for every prediction, so that all historic states are retained and the system state vector grows over time. To avoid ambiguity, we will use $\mathbf{x}_t$ to denote the *system* state, which is the entire state of the system including current and historic states. The system state consists of the current plant state $\boldsymbol{x}_k$ and a collection of historic plant states $\boldsymbol{x}_p$

$$\mathbf{x}_t = \begin{bmatrix} \boldsymbol{x}_k \\ \boldsymbol{x}_p \end{bmatrix}. \tag{C.25}$$

For this derivation we will assume that $\boldsymbol{x}_p$ consists of a single historic plant state. During each prediction, the process model for the system augments the system state with a new plant state, $\boldsymbol{x}_{k+1}$. Thus the system state vector grows at each time step to include not only the collection of historic states and the current plant state $\boldsymbol{x}_k$, but also the prediction of the next plant state $\boldsymbol{x}_{k+1}$ as governed by the plant process model in equation C.14. We will drop the subscript k on $\boldsymbol{F}$ and $\boldsymbol{w}$ for clarity of notation for the remainder of the derivation.

We can now write the process model for the system as

$$\mathbf{x}_{t+1} = \underbrace{\begin{bmatrix} \boldsymbol{F} & \mathbf{0} \\ \boldsymbol{I} & \mathbf{0} \\ 0 & \boldsymbol{I} \end{bmatrix}}_{\boldsymbol{F}_t} \mathbf{x}_t + \underbrace{\begin{bmatrix} \boldsymbol{I} \\ \mathbf{0} \\ \mathbf{0} \end{bmatrix}}_{\boldsymbol{G}_t} \boldsymbol{w} \tag{C.26}$$

where

$$\mathbf{x}_{t+1} = \begin{bmatrix} \boldsymbol{x}_{k+1} \\ \boldsymbol{x}_k \\ \boldsymbol{x}_p \end{bmatrix}. \tag{C.27}$$

We define the mean and covariance of the system state estimate before prediction as

$$\boldsymbol{\mu}_t = \begin{bmatrix} \boldsymbol{\mu}_k \\ \boldsymbol{\mu}_p \end{bmatrix} \tag{C.28}$$

$$\boldsymbol{\Sigma}_t = \begin{bmatrix} \boldsymbol{\Sigma}_{kk} & \boldsymbol{\Sigma}_{kp} \\ \boldsymbol{\Sigma}_{pk} & \boldsymbol{\Sigma}_{pp} \end{bmatrix} \tag{C.29}$$

which, in the information form, are

$$\boldsymbol{\Lambda}_t = \boldsymbol{\Sigma}_t^{-1} = \begin{bmatrix} \boldsymbol{\Lambda}_{kk} & \boldsymbol{\Lambda}_{kp} \\ \boldsymbol{\Lambda}_{pk} & \boldsymbol{\Lambda}_{pp} \end{bmatrix} \tag{C.30}$$

$$\boldsymbol{\eta}_t = \boldsymbol{\Lambda}_t \boldsymbol{\mu}_t = \begin{bmatrix} \boldsymbol{\Lambda}_{kk}\boldsymbol{\mu}_k + \boldsymbol{\Lambda}_{kp}\boldsymbol{\mu}_p \\ \boldsymbol{\Lambda}_{pk}\boldsymbol{\mu}_k + \boldsymbol{\Lambda}_{pp}\boldsymbol{\mu}_p \end{bmatrix} = \begin{bmatrix} \boldsymbol{\eta}_k \\ \boldsymbol{\eta}_p \end{bmatrix}. \tag{C.31}$$

The mean and covariance of the system state estimate after prediction are

$$\boldsymbol{\mu}_{t+1} = \boldsymbol{F}_t \boldsymbol{\mu}_t \tag{C.32}$$

$$= \begin{bmatrix} \boldsymbol{F} & \mathbf{0} \\ \boldsymbol{I} & \mathbf{0} \\ \mathbf{0} & \boldsymbol{I} \end{bmatrix} \begin{bmatrix} \boldsymbol{\mu}_k \\ \boldsymbol{\mu}_p \end{bmatrix}$$

$$= \begin{bmatrix} \boldsymbol{F}\boldsymbol{\mu}_k \\ \boldsymbol{\mu}_k \\ \boldsymbol{\mu}_p \end{bmatrix} \tag{C.33}$$

$$\boldsymbol{\Sigma}_{t+1} = \boldsymbol{F}_t \boldsymbol{\Sigma}_t \boldsymbol{F}_t^\top + \boldsymbol{G}_t \boldsymbol{Q} \boldsymbol{G}_t^\top \tag{C.34}$$

$$= \begin{bmatrix} \boldsymbol{F} & \mathbf{0} \\ \boldsymbol{I} & \mathbf{0} \\ 0 & \boldsymbol{I} \end{bmatrix} \begin{bmatrix} \boldsymbol{\Sigma}_{kk} & \boldsymbol{\Sigma}_{kp} \\ \boldsymbol{\Sigma}_{pk} & \boldsymbol{\Sigma}_{pp} \end{bmatrix} \begin{bmatrix} \boldsymbol{F}^\top & \boldsymbol{I} & 0 \\ \mathbf{0} & \mathbf{0} & \boldsymbol{I} \end{bmatrix} + \begin{bmatrix} \boldsymbol{I} \\ \mathbf{0} \\ \mathbf{0} \end{bmatrix} \boldsymbol{Q} \begin{bmatrix} \boldsymbol{I} & \mathbf{0} & \mathbf{0} \end{bmatrix}$$

$$= \begin{bmatrix} \boldsymbol{F}\boldsymbol{\Sigma}_{kk}\boldsymbol{F}^\top + \boldsymbol{Q} & \boldsymbol{F}\boldsymbol{\Sigma}_{kk} & \boldsymbol{F}\boldsymbol{\Sigma}_{kp} \\ \boldsymbol{\Sigma}_{kk}\boldsymbol{F}^\top & \boldsymbol{\Sigma}_{kk} & \boldsymbol{\Sigma}_{kp} \\ \boldsymbol{\Sigma}_{pk}\boldsymbol{F}^\top & \boldsymbol{\Sigma}_{pk} & \boldsymbol{\Sigma}_{pp} \end{bmatrix} \tag{C.35}$$

which, in the information form [25], are

$$\begin{aligned}
\boldsymbol{\Lambda}_{t+1} &= \boldsymbol{\Sigma}_{t+1}^{-1} \\
&= \begin{bmatrix} \boldsymbol{F}\boldsymbol{\Sigma}_{kk}\boldsymbol{F}^\top + \boldsymbol{Q} & \boldsymbol{F}\boldsymbol{\Sigma}_{kk} & \boldsymbol{F}\boldsymbol{\Sigma}_{kp} \\ \boldsymbol{\Sigma}_{kk}\boldsymbol{F}^\top & \boldsymbol{\Sigma}_{kk} & \boldsymbol{\Sigma}_{kp} \\ \boldsymbol{\Sigma}_{pk}\boldsymbol{F}^\top & \boldsymbol{\Sigma}_{pk} & \boldsymbol{\Sigma}_{pp} \end{bmatrix}^{-1} \\
&= \begin{bmatrix} \boldsymbol{Q}^{-1} & -\boldsymbol{Q}^{-1}\boldsymbol{F} & \boldsymbol{0} \\ -\boldsymbol{F}^\top\boldsymbol{Q}^{-1} & \boldsymbol{F}^\top\boldsymbol{Q}^{-1}\boldsymbol{F} + \boldsymbol{\Lambda}_{kk} & \boldsymbol{\Lambda}_{kp} \\ \boldsymbol{0} & \boldsymbol{\Lambda}_{pk} & \boldsymbol{\Lambda}_{pp} \end{bmatrix} \qquad \text{(C.36)} \\
\boldsymbol{\eta}_{t+1} &= \boldsymbol{\Lambda}_{t+1}\boldsymbol{\mu}_{t+1} \qquad \text{(C.37)} \\
&= \begin{bmatrix} \boldsymbol{Q}^{-1} & -\boldsymbol{Q}^{-1}\boldsymbol{F} & \boldsymbol{0} \\ -\boldsymbol{F}^\top\boldsymbol{Q}^{-1} & \boldsymbol{F}^\top\boldsymbol{Q}^{-1}\boldsymbol{F} + \boldsymbol{\Lambda}_{kk} & \boldsymbol{\Lambda}_{kp} \\ \boldsymbol{0} & \boldsymbol{\Lambda}_{pk} & \boldsymbol{\Lambda}_{pp} \end{bmatrix} \begin{bmatrix} \boldsymbol{F}\boldsymbol{\mu}_k \\ \boldsymbol{\mu}_k \\ \boldsymbol{\mu}_p \end{bmatrix} \\
&= \begin{bmatrix} \boldsymbol{0} \\ \boldsymbol{\Lambda}_{kk}\boldsymbol{\mu}_k + \boldsymbol{\Lambda}_{kp}\boldsymbol{\mu}_p \\ \boldsymbol{\Lambda}_{pk}\boldsymbol{\mu}_k + \boldsymbol{\Lambda}_{pp}\boldsymbol{\mu}_p \end{bmatrix} \\
&= \begin{bmatrix} \boldsymbol{0} \\ \boldsymbol{\eta}_k \\ \boldsymbol{\eta}_p \end{bmatrix} \qquad \text{(C.38)}
\end{aligned}$$

for a linear plant, where, as noted in [26], prediction with augmentation results in (C.36) having a sparse tridiagonal structure. As noted in [25], the derivation of (C.36) through the inversion of $\boldsymbol{\Sigma}_{t+1}$ is tedious, but the result can easily be validated by matrix multiplication to show that $\boldsymbol{\Lambda}_{t+1}\boldsymbol{\Sigma}_{t+1} = \boldsymbol{I}$. Note that (C.36) can be written as the sum of a two matrices consisting of a constant matrix plus the previous information matrix

$$\boldsymbol{\Lambda}_{t+1} = \begin{bmatrix} \boldsymbol{Q}^{-1} & -\boldsymbol{Q}^{-1}\boldsymbol{F} & \boldsymbol{0} \\ -\boldsymbol{F}^\top\boldsymbol{Q}^{-1} & \boldsymbol{F}^\top\boldsymbol{Q}^{-1}\boldsymbol{F} & \boldsymbol{0} \\ \boldsymbol{0} & \boldsymbol{0} & \boldsymbol{0} \end{bmatrix} + \begin{bmatrix} \boldsymbol{0} & \boldsymbol{0} & \boldsymbol{0} \\ \boldsymbol{0} & \boldsymbol{\Lambda}_{kk} & \boldsymbol{\Lambda}_{kp} \\ \boldsymbol{0} & \boldsymbol{\Lambda}_{pk} & \boldsymbol{\Lambda}_{pp} \end{bmatrix}. \qquad \text{(C.39)}$$

C.5 Measurement Update

The measurement update equation for the information matrix is straightforward to derive using the matrix inversion lemma,

$$\begin{aligned}
\boldsymbol{\Lambda}_{k|k} &= \boldsymbol{\Sigma}_{k|k}^{-1} \qquad \text{(C.40)} \\
&= \left[(\boldsymbol{I} - \boldsymbol{K}_k\boldsymbol{H}_k)\boldsymbol{\Sigma}_{k|k-1}\right]^{-1} \\
&= \left[\boldsymbol{\Sigma}_{k|k-1} - \boldsymbol{\Sigma}_{k|k-1}\boldsymbol{H}_k^\top(\boldsymbol{H}_k\boldsymbol{\Sigma}_{k|k-1}\boldsymbol{H}_k^\top + \boldsymbol{R}_k)^{-1}\boldsymbol{H}_k\boldsymbol{\Sigma}_{k|k-1}\right]^{-1} \\
&= \boldsymbol{\Sigma}_{k|k-1}^{-1} + \boldsymbol{H}_k^\top\boldsymbol{R}_k^{-1}\boldsymbol{H}_k \\
\boldsymbol{\Lambda}_{k|k} &= \boldsymbol{\Lambda}_{k|k-1} + \boldsymbol{H}_k^\top\boldsymbol{R}_k^{-1}\boldsymbol{H}_k \qquad \text{(C.41)}
\end{aligned}$$

where z_k is the measurement, H_k is the linear measurement matrix, and R_k is the covariance matrix of the measurement noise.

To derive the measurement update equation for the information vector, we will use the fact that $\boldsymbol{K}_k = \boldsymbol{\Sigma}_{k|k}\boldsymbol{H}_k^\top \boldsymbol{R}_k^{-1}$,

$$\begin{aligned}
\boldsymbol{K}_k &= \boldsymbol{\Sigma}_{k|k-1}\boldsymbol{H}_k^\top(\boldsymbol{H}_k\boldsymbol{\Sigma}_{k|k-1}\boldsymbol{H}_k^\top + \boldsymbol{R}_k)^{-1} && \text{(C.42)}\\
\boldsymbol{K}_k(\boldsymbol{H}_k\boldsymbol{\Sigma}_{k|k-1}\boldsymbol{H}_k^\top + \boldsymbol{R}_k) &= \boldsymbol{\Sigma}_{k|k-1}\boldsymbol{H}_k^\top \\
\boldsymbol{K}_k\boldsymbol{R}_k &= (\boldsymbol{I} - \boldsymbol{K}_k\boldsymbol{H}_k)\boldsymbol{\Sigma}_{k|k-1}\boldsymbol{H}_k^\top \\
\boldsymbol{K}_k &= (\boldsymbol{I} - \boldsymbol{K}_k\boldsymbol{H}_k)\boldsymbol{\Sigma}_{k|k-1}\boldsymbol{H}_k^\top\boldsymbol{R}_k^{-1} \\
\boldsymbol{K}_k &= (\boldsymbol{\Sigma}_{k|k-1} - \boldsymbol{K}_k\boldsymbol{H}_k\boldsymbol{\Sigma}_{k|k-1})\cancel{\boldsymbol{\Sigma}_{k|k-1}^{-1}}\cancel{\boldsymbol{\Sigma}_{k|k-1}}\boldsymbol{H}_k^\top\boldsymbol{R}_k^{-1} \\
\boldsymbol{K}_k &= \boldsymbol{\Sigma}_{k|k}\boldsymbol{H}_k^\top\boldsymbol{R}_k^{-1}. && \text{(C.43)}
\end{aligned}$$

The derivation for the information vector is then

$$\begin{aligned}
\boldsymbol{\eta}_{k|k} &= \boldsymbol{\Sigma}_{k|k}^{-1}\boldsymbol{\mu}_{k|k} && \text{(C.44)}\\
&= \boldsymbol{\Sigma}_{k|k}^{-1}\left[\boldsymbol{\mu}_{k|k-1} + \boldsymbol{K}_k(\boldsymbol{z}_k - \boldsymbol{H}_k\boldsymbol{\mu}_{k|k-1})\right] \\
&= \boldsymbol{\Sigma}_{k|k}^{-1}\boldsymbol{\mu}_{k|k-1} - \boldsymbol{\Sigma}_{k|k}^{-1}\boldsymbol{K}_k\boldsymbol{H}_k\boldsymbol{\mu}_{k|k-1} + \boldsymbol{\Sigma}_{k|k}^{-1}\boldsymbol{K}_k\boldsymbol{z}_k \\
&= (\boldsymbol{\Lambda}_{k|k-1} + \boldsymbol{H}_k^\top\boldsymbol{R}_k^{-1}\boldsymbol{H}_k)\boldsymbol{\mu}_{k|k-1} - \cancel{\boldsymbol{\Sigma}_{k|k}^{-1}}\cancel{\boldsymbol{\Sigma}_{k|k}}\boldsymbol{H}_k^\top\boldsymbol{R}_k^{-1}\boldsymbol{H}_k\boldsymbol{\mu}_{k|k-1} + \cancel{\boldsymbol{\Sigma}_{k|k}^{-1}}\cancel{\boldsymbol{\Sigma}_{k|k}}\boldsymbol{H}_k^\top\boldsymbol{R}_k^{-1}\boldsymbol{z}_k \\
&= \boldsymbol{\Lambda}_{k|k-1}\boldsymbol{\mu}_{k|k-1} + \boldsymbol{H}_k^\top\boldsymbol{R}_k^{-1}\boldsymbol{H}_k\boldsymbol{\mu}_{k|k-1} - \boldsymbol{H}_k^\top\boldsymbol{R}_k^{-1}\boldsymbol{H}_k\boldsymbol{\mu}_{k|k-1} + \boldsymbol{H}_k^\top\boldsymbol{R}_k^{-1}\boldsymbol{z}_k \\
\boldsymbol{\eta}_{k|k} &= \boldsymbol{\eta}_{k|k-1} + \boldsymbol{H}_k^\top\boldsymbol{R}_k^{-1}z_k. && \text{(C.45)}
\end{aligned}$$

C.6 Marginalization

The derivation for the generalized equations for marginalization are adapted from [25]. This derivation uses the result for the inverse of a nonsingular block 2×2 matrix from Bar-Shalom [8, p.21], which is repeated here for convenience.

The inverse of a nonsingular block 2×2 is

$$\begin{bmatrix} P_{11} & P_{12} \\ P_{21} & P_{22} \end{bmatrix}^{-1} = \begin{bmatrix} V_{11} & V_{12} \\ V_{21} & V_{22} \end{bmatrix} \tag{C.46}$$

where

$$\begin{aligned}
V_{11} &= P_{11}^{-1} + P_{11}^{-1}P_{12}V_{22}P_{21}P_{11}^{-1} = (P_{11} - P_{12}P_{22}^{-1}P_{21})^{-1} && \text{(C.47)}\\
V_{12} &= -P_{11}^{-1}P_{12}V_{22}^{-1} = -V_{11}P_{12}P_{22}^{-1} && \text{(C.48)}\\
V_{21} &= -V_{22}P_{21}P_{11}^{-1} = -P_{22}^{-1}P_{21}V_{11} && \text{(C.49)}\\
V_{22} &= P_{22}^{-1} + P_{22}^{-1}P_{21}V_{11}P_{12}P_{22}^{-1} = (P_{22} - P_{21}P_{11}^{-1}P_{12})^{-1}. && \text{(C.50)}
\end{aligned}$$

Replacing P with Λ and V with Σ

$$\begin{bmatrix} \Lambda_{\alpha\alpha} & \Lambda_{\alpha\beta} \\ \Lambda_{\beta\alpha} & \Lambda_{\beta\beta} \end{bmatrix}^{-1} = \begin{bmatrix} \Sigma_{\alpha\alpha} & \Sigma_{\alpha\beta} \\ \Sigma_{\beta\alpha} & \Sigma_{\beta\beta} \end{bmatrix} \tag{C.51}$$

we solve for the elements of Σ because in the covariance form if

$$\Sigma(\alpha, \beta) = \begin{bmatrix} \Sigma_{\alpha\alpha} & \Sigma_{\alpha\beta} \\ \Sigma_{\beta\alpha} & \Sigma_{\beta\beta} \end{bmatrix} \tag{C.52}$$

then

$$\Sigma(\alpha) = \Sigma_{\alpha\alpha} \tag{C.53}$$

and thus

$$\Lambda(\alpha) = \Sigma(\alpha)^{-1} = \Sigma_{\alpha\alpha}^{-1} \tag{C.54}$$

where α are the states to be kept and β are the states to be marginalized out. Thus marginalizing out β results in

$$\eta(\alpha) = \eta_\alpha - \Lambda_{\alpha\beta}\Lambda_{\beta\beta}^{-1}\eta_\beta \tag{C.55}$$

$$\Lambda(\alpha) = \Lambda_{\alpha\alpha} - \Lambda_{\alpha\beta}\Lambda_{\beta\beta}^{-1}\Lambda_{\beta\alpha}. \tag{C.56}$$

Appendix D

Linear Information Filter Example

Presented here is an example implementation of the linear information filter in the context of a strictly linear, one-degree-of-freedom system. The linear information filter equations are used here without derivation. Readers are referred to Appendix C for the linear information filter derivation.

This example consists of a two-node system, the nodes labelled *ship* and *vehicle* respectively. Each nodes has one degree of freedom, moving along the y-axis. Both the ship and the vehicle have a linear, constant-velocity process model. Three types of measurements are possible, position measurements for the ship, velocity measurements for the vehicle, and range measurements between the ship and the vehicle.

The goal of this example is to explore the differences between a centralized filter that has access to all sensor measurements from both the ship and the vehicle in real-time and a decentralized vehicle-based filter that only has access to vehicle sensor measurements in real time. In the decentralized filter the vehicle receives asynchronous data transmissions from the ship concurrent with range measurements from the ship, but does not have access to ship measurements of the ship state estimate in real time.

D.1 Process Model

We assume a constant-velocity process model for both the vehicle and the ship

$$\dot{\boldsymbol{x}}_v = \underbrace{\begin{bmatrix} 0 & 1 \\ 0 & 0 \end{bmatrix}}_{\boldsymbol{F}_v} \boldsymbol{x}_v + \underbrace{\begin{bmatrix} 0 \\ 1 \end{bmatrix}}_{\boldsymbol{G}_v} \boldsymbol{w}_v \tag{D.1}$$

$$\dot{\boldsymbol{x}}_s = \underbrace{\begin{bmatrix} 0 & 1 \\ 0 & 0 \end{bmatrix}}_{\boldsymbol{F}_s} \boldsymbol{x}_s + \underbrace{\begin{bmatrix} 0 \\ 1 \end{bmatrix}}_{\boldsymbol{G}_s} \boldsymbol{w}_s \tag{D.2}$$

where the state vectors $\boldsymbol{x}_v$ and $\boldsymbol{x}_s$ contain the position and velocity along the y-axis of the vehicle and the ship respectively

$$\boldsymbol{x}_v = \begin{bmatrix} y_v \\ \dot{y}_v \end{bmatrix} \tag{D.3}$$

$$\boldsymbol{x}_s = \begin{bmatrix} y_s \\ \dot{y}_s \end{bmatrix} \tag{D.4}$$

and $\boldsymbol{w}_v$ and $\boldsymbol{w}_s$ are independent zero-mean Gaussian process noise in the respective acceleration terms

$$\boldsymbol{w}_v \sim \mathcal{N}(0, q_v) \tag{D.5}$$

$$\boldsymbol{w}_s \sim \mathcal{N}(0, q_s). \tag{D.6}$$

The process models are discretized according to standard methods [8]. The resulting discrete-time linear process models are

$$\boldsymbol{x}_{v_{k+1}} = \boldsymbol{F}_{v_k} \boldsymbol{x}_{v_k} + \boldsymbol{w}_{v_k} \tag{D.7}$$

$$\boldsymbol{F}_{v_k} = e^{\boldsymbol{F}_v T} = \begin{bmatrix} 1 & T \\ 0 & 1 \end{bmatrix} \tag{D.8}$$

$$\boldsymbol{x}_{s_{k+1}} = \boldsymbol{F}_{s_k} \boldsymbol{x}_{s_k} + \boldsymbol{w}_{s_k} \tag{D.9}$$

$$\boldsymbol{F}_{s_k} = e^{\boldsymbol{F}_s T} = \begin{bmatrix} 1 & T \\ 0 & 1 \end{bmatrix} \tag{D.10}$$

where $\boldsymbol{F}_v$ and $\boldsymbol{F}_s$ are defined in (D.1) and (D.2) respectively and T is the discrete time step. The discretized process noise, $\boldsymbol{w}_{v_k}$ and $\boldsymbol{w}_{s_k}$, are zero-mean Gaussian

$$\boldsymbol{w}_{v_k} \sim \mathcal{N}(0, \boldsymbol{Q}_v) \tag{D.11}$$

$$\boldsymbol{w}_{s_k} \sim \mathcal{N}(0, \boldsymbol{Q}_s) \tag{D.12}$$

where the covariance matrices are

$$\boldsymbol{Q}_v = \begin{bmatrix} \frac{1}{3}T^3 & \frac{1}{2}T^2 \\ \frac{1}{2}T^2 & T \end{bmatrix} q_v \tag{D.13}$$

$$\boldsymbol{Q}_s = \begin{bmatrix} \frac{1}{3}T^3 & \frac{1}{2}T^2 \\ \frac{1}{2}T^2 & T \end{bmatrix} q_s. \tag{D.14}$$

Note that even though $\boldsymbol{F}_{v_k}$, $\boldsymbol{F}_{s_k}$, $\boldsymbol{w}_{v_k}$, and $\boldsymbol{w}_{s_k}$ are shown with a subscript denoting the time step k, they are in fact constant and do not depend on time.

D.2 Process Prediction and Augmentation

The ship and vehicle process models have identical process prediction and augmentation equations. *For simplicity of notation I will derive a general form of the equations without either the s or v subscripts.* This system is formulated such that the complete state vector consists of both current and historic states. For every prediction, the current state is augmented with the newly predicted state, thus all historic states are retained and the state vector grows over time. To avoid ambiguity, I will use $\boldsymbol{x}_k$ to denote current *plant* states, $\boldsymbol{x}_p$ to denote historic *plant* states, and a different font $\mathbf{x}_t$ to denote the *system* state, which is the entire state of the system including both current and historic plant states

$$\mathbf{x}_k = \begin{bmatrix} \boldsymbol{x}_k \\ \boldsymbol{x}_p \end{bmatrix}. \tag{D.15}$$

Consider a system in which the *plant* state is governed by the following constant-velocity, discrete-time, linear process model similar to (D.7) and (D.9)

$$\boldsymbol{x}_{k+1} = \underbrace{\begin{bmatrix} 1 & T \\ 0 & 1 \end{bmatrix}}_{\boldsymbol{F}} \boldsymbol{x}_k + \boldsymbol{w} \tag{D.16}$$

$$\boldsymbol{x}_k = \begin{bmatrix} y_k \\ \dot{y}_k \end{bmatrix} \tag{D.17}$$

where $w \sim \mathcal{N}(0, \boldsymbol{Q})$, $\boldsymbol{Q} = \begin{bmatrix} \frac{1}{3}T^3 & \frac{1}{2}T^2 \\ \frac{1}{2}T^2 & T \end{bmatrix} q$ and T is the discrete time step.

The process model for the *system* augments the system state with a new plant state, $\boldsymbol{x}_{k+1}$, which is the prediction forward of the current plant state

$$\mathbf{x}_{k+1} = \underbrace{\begin{bmatrix} \boldsymbol{F} & \mathbf{0} \\ \boldsymbol{I} & \mathbf{0} \\ 0 & \boldsymbol{I} \end{bmatrix}}_{\boldsymbol{F}_k} \mathbf{x}_k + \begin{bmatrix} \boldsymbol{I} \\ \mathbf{0} \\ \mathbf{0} \end{bmatrix} \boldsymbol{w} \tag{D.18}$$

where

$$\mathbf{x}_{k+1} = \begin{bmatrix} \boldsymbol{x}_{k+1} \\ \boldsymbol{x}_k \\ \boldsymbol{x}_p \end{bmatrix}. \tag{D.19}$$

The mean and covariance of the system state estimate before prediction are

$$\tilde{\boldsymbol{\mu}}_{k|k} = E[\mathbf{x}_k] = \begin{bmatrix} \boldsymbol{\mu}_k \\ \boldsymbol{\mu}_p \end{bmatrix} \tag{D.20}$$

$$\tilde{\boldsymbol{\Sigma}}_{k|k} = E[(\mathbf{x}_k - \tilde{\boldsymbol{\mu}}_{k|k})(\mathbf{x}_k - \tilde{\boldsymbol{\mu}}_{k|k})^\top] = \begin{bmatrix} \boldsymbol{\Sigma}_{kk} & \boldsymbol{\Sigma}_{kp} \\ \boldsymbol{\Sigma}_{pk} & \boldsymbol{\Sigma}_{pp} \end{bmatrix} \tag{D.21}$$

which, in the information form, are

$$\tilde{\boldsymbol{\Lambda}}_{k|k} = \tilde{\boldsymbol{\Sigma}}_{k|k}^{-1} = \begin{bmatrix} \boldsymbol{\Lambda}_{kk} & \boldsymbol{\Lambda}_{kp} \\ \boldsymbol{\Lambda}_{pk} & \boldsymbol{\Lambda}_{pp} \end{bmatrix} \tag{D.22}$$

$$\tilde{\boldsymbol{\eta}}_{k|k} = \tilde{\boldsymbol{\Lambda}}_{k|k}\tilde{\boldsymbol{\mu}}_{k|k} = \begin{bmatrix} \boldsymbol{\Lambda}_{kk}\boldsymbol{\mu}_k + \boldsymbol{\Lambda}_{kp}\boldsymbol{\mu}_p \\ \boldsymbol{\Lambda}_{pk}\boldsymbol{\mu}_k + \boldsymbol{\Lambda}_{pp}\boldsymbol{\mu}_p \end{bmatrix}. \tag{D.23}$$

The mean and covariance of the system state estimate after prediction are

$$\tilde{\boldsymbol{\mu}}_{k+1|k} = \begin{bmatrix} \boldsymbol{F}\boldsymbol{\mu}_k \\ \boldsymbol{\mu}_k \\ \boldsymbol{\mu}_p \end{bmatrix} \tag{D.24}$$

$$\tilde{\boldsymbol{\Sigma}}_{k+1|k} = \begin{bmatrix} \boldsymbol{F}\boldsymbol{\Sigma}_{kk}\boldsymbol{F}^\top + \boldsymbol{Q} & \boldsymbol{F}\boldsymbol{\Sigma}_{kk} & \boldsymbol{F}\boldsymbol{\Sigma}_{kp} \\ \boldsymbol{\Sigma}_{kk}\boldsymbol{F}^\top & \boldsymbol{\Sigma}_{kk} & \boldsymbol{\Sigma}_{kp} \\ \boldsymbol{\Sigma}_{pk}\boldsymbol{F}^\top & \boldsymbol{\Sigma}_{pk} & \boldsymbol{\Sigma}_{pp} \end{bmatrix} \tag{D.25}$$

which, in the information form [25], are

$$\begin{aligned} \tilde{\boldsymbol{\Lambda}}_{k+1|k} &= \tilde{\boldsymbol{\Sigma}}_{k+1|k}^{-1} \\ &= \begin{bmatrix} \boldsymbol{Q}^{-1} & -\boldsymbol{Q}^{-1}\boldsymbol{F} & \mathbf{0} \\ -\boldsymbol{F}^\top\boldsymbol{Q}^{-1} & \boldsymbol{F}^\top\boldsymbol{Q}^{-1}\boldsymbol{F} + \boldsymbol{\Lambda}_{kk} & \boldsymbol{\Lambda}_{kp} \\ \mathbf{0} & \boldsymbol{\Lambda}_{pk} & \boldsymbol{\Lambda}_{pp} \end{bmatrix} \end{aligned} \tag{D.26}$$

$$\tilde{\boldsymbol{\eta}}_{k+1|k} = \tilde{\boldsymbol{\Lambda}}_{k+1|k}\tilde{\boldsymbol{\mu}}_{k+1|k} = \begin{bmatrix} \mathbf{0} \\ \boldsymbol{\eta}_t \end{bmatrix}. \tag{D.27}$$

Note that (D.26) can be written as the sum of a two matrices consisting of a constant matrix plus the previous information matrix

$$\tilde{\boldsymbol{\Lambda}}_{k+1|k} = \begin{bmatrix} \boldsymbol{Q}^{-1} & -\boldsymbol{Q}^{-1}\boldsymbol{F} & \mathbf{0} \\ -\boldsymbol{F}^\top\boldsymbol{Q}^{-1} & \boldsymbol{F}^\top\boldsymbol{Q}^{-1}\boldsymbol{F} & \mathbf{0} \\ \mathbf{0} & \mathbf{0} & \mathbf{0} \end{bmatrix} + \begin{bmatrix} \mathbf{0} & \mathbf{0} & \mathbf{0} \\ \mathbf{0} & \boldsymbol{\Lambda}_{kk} & \boldsymbol{\Lambda}_{kp} \\ \mathbf{0} & \boldsymbol{\Lambda}_{pk} & \boldsymbol{\Lambda}_{pp} \end{bmatrix}. \tag{D.28}$$

D.3 Marginalization

In this example, states that do not have range measurements associated with them are marginalized out after a given time. For completeness, the generalized marginaliza-

tion equations are shown here for two scenarios. The first scenario is when the one or more states at the bottom of the system information vector (i.e. the oldest states) are to be marginalized out. In this case the information vector can be split into two partitions, one associated with the states to keep, $\boldsymbol{\eta}_\alpha$, and the other associated with the states to be marginalized out, $\boldsymbol{\eta}_\beta$

$$\boldsymbol{\eta}(\alpha,\beta) = \begin{bmatrix} \boldsymbol{\eta}_\alpha \\ \boldsymbol{\eta}_\beta \end{bmatrix} \tag{D.29}$$

$$\boldsymbol{\Lambda}(\alpha,\beta) = \begin{bmatrix} \boldsymbol{\Lambda}_{\alpha\alpha} & \boldsymbol{\Lambda}_{\alpha\beta} \\ \boldsymbol{\Lambda}_{\beta\alpha} & \boldsymbol{\Lambda}_{\beta\beta} \end{bmatrix}. \tag{D.30}$$

Marginalizing out β results in

$$\boldsymbol{\eta}(\alpha) = \boldsymbol{\eta}_\alpha - \boldsymbol{\Lambda}_{\alpha\beta}\boldsymbol{\Lambda}_{\beta\beta}^{-1}\boldsymbol{\eta}_\beta \tag{D.31}$$

$$\boldsymbol{\Lambda}(\alpha) = \boldsymbol{\Lambda}_{\alpha\alpha} - \boldsymbol{\Lambda}_{\alpha\beta}\boldsymbol{\Lambda}_{\beta\beta}^{-1}\boldsymbol{\Lambda}_{\beta\alpha}. \tag{D.32}$$

Note that $\boldsymbol{\eta}(\alpha) \neq \boldsymbol{\eta}_\alpha$ after marginalization.

In the second scenario, one or more states in the middle of the state vector are to be marginalized out. In this scenario the information vector is split into three partitions, where the states associated with $\boldsymbol{\eta}_\beta$ are again to be marginalized out.

$$\boldsymbol{\eta}(\alpha,\beta,\gamma) = \begin{bmatrix} \boldsymbol{\eta}_\alpha \\ \boldsymbol{\eta}_\beta \\ \boldsymbol{\eta}_\gamma \end{bmatrix} \tag{D.33}$$

$$\boldsymbol{\Lambda}(\alpha,\beta,\gamma) = \begin{bmatrix} \boldsymbol{\Lambda}_{\alpha\alpha} & \boldsymbol{\Lambda}_{\alpha\beta} & \boldsymbol{\Lambda}_{\alpha\gamma} \\ \boldsymbol{\Lambda}_{\beta\alpha} & \boldsymbol{\Lambda}_{\beta\beta} & \boldsymbol{\Lambda}_{\beta\gamma} \\ \boldsymbol{\Lambda}_{\gamma\alpha} & \boldsymbol{\Lambda}_{\gamma\beta} & \boldsymbol{\Lambda}_{\gamma\gamma} \end{bmatrix} \tag{D.34}$$

Marginalizing out β results in

$$\boldsymbol{\eta}(\alpha,\gamma) = \begin{bmatrix} \boldsymbol{\eta}_\alpha \\ \boldsymbol{\eta}_\gamma \end{bmatrix} - \begin{bmatrix} \boldsymbol{\Lambda}_{\alpha\beta} \\ \boldsymbol{\Lambda}_{\gamma\beta} \end{bmatrix} \boldsymbol{\Lambda}_{\beta\beta}^{-1}\boldsymbol{\eta}_\beta \tag{D.35}$$

$$\boldsymbol{\Lambda}(\alpha,\gamma) = \begin{bmatrix} \boldsymbol{\Lambda}_{\alpha\alpha} & \boldsymbol{\Lambda}_{\alpha\gamma} \\ \boldsymbol{\Lambda}_{\gamma\alpha} & \boldsymbol{\Lambda}_{\gamma\gamma} \end{bmatrix} - \begin{bmatrix} \boldsymbol{\Lambda}_{\alpha\beta} \\ \boldsymbol{\Lambda}_{\gamma\beta} \end{bmatrix} \boldsymbol{\Lambda}_{\beta\beta}^{-1} \begin{bmatrix} \boldsymbol{\Lambda}_{\beta\alpha} & \boldsymbol{\Lambda}_{\beta\gamma} \end{bmatrix}. \tag{D.36}$$

Note that the second scenario, and indeed any general case concerning the partitioning of $\boldsymbol{\eta}$ and $\boldsymbol{\Lambda}$, reduces to the two-partition scenario, because $\boldsymbol{\eta}$ and $\boldsymbol{\Lambda}$ can be reordered into two partitions using an appropriate orthonormal permutation matrix. See [25] for more details.

D.4 Measurement Update

Given a generalized observation model for a scalar measurement

$$z_k = H_k\mathbf{x}_k + v_k \tag{D.37}$$

where z_k is the measurement, H_k is the linear measurement matrix, and $v_k \sim \mathcal{N}(0, r_k)$ is the measurement noise, the measurement update equations for the information filter are

$$\boldsymbol{\eta}_{k|k} = \boldsymbol{\eta}_{k|k-1} + H_k^\top r_k^{-1} z_k \tag{D.38}$$
$$\boldsymbol{\Lambda}_{k|k} = \boldsymbol{\Lambda}_{k|k-1} + H_k^\top r_k^{-1} H_k. \tag{D.39}$$

D.5 Observation Models

The full state vector for this system contains current and historic states for both the vehicle and the ship. However, for simplicity of notation, the observation models below are written in terms of a simplified state vector consisting of only the current vehicle and current ship states except where otherwise noted.

D.5.1 Ship GPS Measurement

The position measurement for the ship mimics a GPS measurement. The position measurement equation is

$$z_{gps} = y_s + v_{gps} \tag{D.40}$$

where $v_{gps} \sim \mathcal{N}(0, r_{gps})$. We can rewrite (D.40) in matrix notation as

$$z_{gps} = \underbrace{\begin{bmatrix} 0 & 0 & 1 & 0 \end{bmatrix}}_{\boldsymbol{H}_{gps}} \begin{bmatrix} \boldsymbol{x}_v \\ \boldsymbol{x}_s \end{bmatrix} + v_{gps}. \tag{D.41}$$

D.5.2 Vehicle Velocity Measurement

The velocity measurement for the vehicle mimics a Doppler velocity log measurement. The velocity measurement equation is

$$z_{vel} = \dot{y}_v + v_{vel} \tag{D.42}$$

where $v_{vel} \sim \mathcal{N}(0, r_{vel})$. We can rewrite (D.42) in matrix notation as

$$z_{vel} = \underbrace{\begin{bmatrix} 0 & 1 & 0 & 0 \end{bmatrix}}_{\boldsymbol{H}_{vel}} \begin{bmatrix} \boldsymbol{x}_v \\ \boldsymbol{x}_s \end{bmatrix} + v_{vel}. \tag{D.43}$$

D.5.3 Range Measurement

The range measurement between the vehicle and ship in this example is chosen to mimic a range measurement made underwater using the time-of-flight of an acoustic signal, except that the measurement here is linear. The range measurements in this example are

always made from the ship to the vehicle. Because the travel time of an acoustic signal underwater is non-negligible, the range measurement is made between the receiver (the vehicle) at the current time step and the sender (the ship) at an earlier time step.

The range measurement equation between the ship and the vehicle in this problem is

$$z_{rng} = y_{v_k} - y_{s_{k-1}} + v_{rng} \tag{D.44}$$

where $t_k - t_{k-1}$ is the time-of-fight of the acoustic transmission and the noise $v_{rng} \sim \mathcal{N}(0, r_{rng})$ represents the imprecision in the distance measurement. Note that the range measurement is a signed number in this model in order to disambiguate which side of the ship the vehicle is on. We can rewrite (D.44) in matrix notation as

$$z_{rng} = \underbrace{\begin{bmatrix} 1 & 0 & -1 & 0 \end{bmatrix}}_{\boldsymbol{H}_{rng}} \begin{bmatrix} \boldsymbol{x}_{v_k} \\ \boldsymbol{x}_{s_{k-1}} \end{bmatrix} + v_{rng}. \tag{D.45}$$

D.6 Centralized Implementation

In the centralized implementation, the filter estimates the current and historic states of both the vehicle and the ship. We assume that the filter has access to all vehicle and ship sensor measurements in real time. The ship and the vehicle start at t_0 and the filter is initialized to

$$\eta_{0|0} = \begin{bmatrix} \eta_{v_0} \\ \eta_{s_0} \end{bmatrix} \tag{D.46}$$

$$\Lambda_{0|0} = \begin{bmatrix} \Lambda_{v_0 v_0} & \mathbf{0} \\ \mathbf{0} & \Lambda_{s_0 s_0} \end{bmatrix}. \tag{D.47}$$

Figure D.1 shows the example system used here to compare the centralized and the decentralized implementations of the information filter. In addition to the measurements shown, the vehicle state at t_0 and the ship state at t_1 are marginalized out after the t_1 to t_2 prediction with augmentation step.

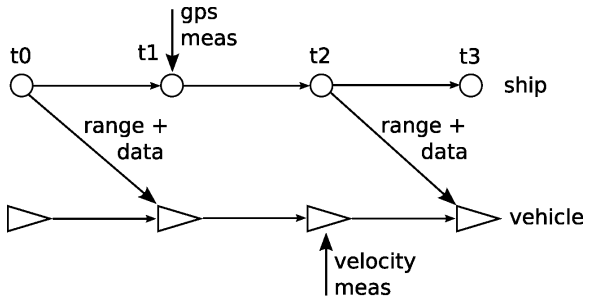

Figure D.1: Vehicle and ship trajectories with sensor measurements.

Prediction with Augmentation $t_0 \rightarrow t_1$

A prediction with augmentation step transitions the state from t_0 to t_1:

$$\eta_{1|0} = \begin{bmatrix} 0 \\ \eta_{v_0} \\ 0 \\ \eta_{s_0} \end{bmatrix} \tag{D.48}$$

$$\begin{aligned} \Lambda_{1|0} &= \begin{bmatrix} \boldsymbol{Q}_v^{-1} & -\boldsymbol{Q}_v^{-1}\boldsymbol{F}_v & 0 & 0 \\ -\boldsymbol{F}_v^\top \boldsymbol{Q}_v^{-1} & \boldsymbol{F}_v^\top \boldsymbol{Q}_v^{-1}\boldsymbol{F}_v & 0 & 0 \\ 0 & 0 & \boldsymbol{Q}_s^{-1} & -\boldsymbol{Q}_s^{-1}\boldsymbol{F}_s \\ 0 & 0 & -\boldsymbol{F}_s^\top \boldsymbol{Q}_s^{-1} & \boldsymbol{F}_s^\top \boldsymbol{Q}_s^{-1}\boldsymbol{F}_s \end{bmatrix} + \begin{bmatrix} 0 & 0 & 0 & 0 \\ 0 & \Lambda_{v_0 v_0} & 0 & 0 \\ 0 & 0 & 0 & 0 \\ 0 & 0 & 0 & \Lambda_{s_0 s_0} \end{bmatrix} \\ &= \begin{bmatrix} \boldsymbol{Q}_v^{-1} & -\boldsymbol{Q}_v^{-1}\boldsymbol{F}_v & 0 & 0 \\ -\boldsymbol{F}_v^\top \boldsymbol{Q}_v^{-1} & \boldsymbol{F}_v^\top \boldsymbol{Q}_v^{-1}\boldsymbol{F}_v + \Lambda_{v_0 v_0} & 0 & 0 \\ 0 & 0 & \boldsymbol{Q}_s^{-1} & -\boldsymbol{Q}_s^{-1}\boldsymbol{F}_s \\ 0 & 0 & -\boldsymbol{F}_s^\top \boldsymbol{Q}_s^{-1} & \boldsymbol{F}_s^\top \boldsymbol{Q}_s^{-1}\boldsymbol{F}_s + \Lambda_{s_0 s_0} \end{bmatrix}. \end{aligned} \tag{D.49}$$

Range Measurement at t_1

Incorporating the range measurement $z_{rng}(t_1)$ gives us

$$\eta_{1|z_{rng_1}} = \eta_{1|0} + H_{rng}^\top r_{rng}^{-1} z_{rng}(t_1) \tag{D.50}$$

$$\begin{aligned} &= \begin{bmatrix} 0 \\ \eta_{v_0} \\ 0 \\ \eta_{s_0} \end{bmatrix} + \begin{bmatrix} \begin{bmatrix} 1 \\ 0 \end{bmatrix} \\ 0 \\ 0 \\ \begin{bmatrix} -1 \\ 0 \end{bmatrix} \end{bmatrix} \frac{z_{rng}(t_1)}{r_{rng}} \\ &= \begin{bmatrix} 0 \\ \eta_{v_0} \\ 0 \\ \eta_{s_0} \end{bmatrix} + \begin{bmatrix} z_{r_1} \\ 0 \\ 0 \\ -z_{r_1} \end{bmatrix} \\ &= \begin{bmatrix} z_{r_1} \\ \eta_{v_0} \\ 0 \\ \eta_{s_0} - z_{r_1} \end{bmatrix} \end{aligned} \tag{D.51}$$

where we define $z_{r_1} = \begin{bmatrix} 1 \\ 0 \end{bmatrix} \frac{z_{rng}(t_1)}{r_{rng}}$.

$$\Lambda_{1|z_{rng_1}} = \Lambda_{1|0} + H_{rng}^\top r_{rng}^{-1} H_{rng} \tag{D.52}$$

$$\begin{aligned}
&= \Lambda_{1|0} + \begin{bmatrix} \begin{bmatrix} 1 \\ 0 \end{bmatrix} \\ 0 \\ 0 \\ \begin{bmatrix} -1 \\ 0 \end{bmatrix} \end{bmatrix} r_{rng}^{-1} \begin{bmatrix} \begin{bmatrix} 1 & 0 \end{bmatrix} & 0 & 0 & \begin{bmatrix} -1 & 0 \end{bmatrix} \end{bmatrix} \\
&= \Lambda_{1|0} + \begin{bmatrix} \begin{bmatrix} \frac{1}{r_{rng}} & 0 \\ 0 & 0 \end{bmatrix} & 0 & 0 & \begin{bmatrix} \frac{-1}{r_{rng}} & 0 \\ 0 & 0 \end{bmatrix} \\ 0 & 0 & 0 & 0 \\ 0 & 0 & 0 & 0 \\ \begin{bmatrix} \frac{-1}{r_{rng}} & 0 \\ 0 & 0 \end{bmatrix} & 0 & 0 & \begin{bmatrix} \frac{1}{r_{rng}} & 0 \\ 0 & 0 \end{bmatrix} \end{bmatrix} \\
&= \Lambda_{1|0} + \begin{bmatrix} R_r & 0 & 0 & -R_r \\ 0 & 0 & 0 & 0 \\ 0 & 0 & 0 & 0 \\ -R_r & 0 & 0 & R_r \end{bmatrix} \\
&= \begin{bmatrix} \boldsymbol{Q}_v^{-1} + \boldsymbol{R}_r & -\boldsymbol{Q}_v^{-1}\boldsymbol{F}_v & 0 & -\boldsymbol{R}_r \\ -\boldsymbol{F}_v^\top \boldsymbol{Q}_v^{-1} & \boldsymbol{F}_v^\top \boldsymbol{Q}_v^{-1}\boldsymbol{F}_v + \Lambda_{v_0 v_0} & 0 & 0 \\ 0 & 0 & \boldsymbol{Q}_s^{-1} & -\boldsymbol{Q}_s^{-1}\boldsymbol{F}_s \\ -\boldsymbol{R}_r & 0 & -\boldsymbol{F}_s^\top \boldsymbol{Q}_s^{-1} & \boldsymbol{F}_s^\top \boldsymbol{Q}_s^{-1}\boldsymbol{F}_s + \Lambda_{s_0 s_0} + \boldsymbol{R}_r \end{bmatrix}
\end{aligned} \tag{D.53}$$

where we define $R_r = \begin{bmatrix} \frac{1}{r_{rng}} & 0 \\ 0 & 0 \end{bmatrix}$.

Ship GPS Measurement at t_1

Next we incorporate the ship GPS measurement $z_{gps}(t_1)$.

$$\eta_{1|z_{rng_1}, z_{gps_1}} = \eta_{1|z_{rng_1}} + H_{gps}^\top r_{gps}^{-1} z_{gps}(t_1) \tag{D.54}$$

$$\begin{aligned}
&= \begin{bmatrix} z_{r_1} \\ \eta_{v_0} \\ 0 \\ \eta_{s_0} - z_{r_1} \end{bmatrix} + \begin{bmatrix} 0 \\ 0 \\ \begin{bmatrix} 1 \\ 0 \end{bmatrix} \\ 0 \end{bmatrix} \frac{z_{gps}(t_1)}{r_{gps}} \\
&= \begin{bmatrix} z_{r_1} \\ \eta_{v_0} \\ 0 \\ \eta_{s_0} - z_{r_1} \end{bmatrix} + \begin{bmatrix} 0 \\ 0 \\ z_{g_1} \\ 0 \end{bmatrix} \\
&= \begin{bmatrix} z_{r_1} \\ \eta_{v_0} \\ z_{g_1} \\ \eta_{s_0} - z_{r_1} \end{bmatrix}
\end{aligned} \tag{D.55}$$

where we define $z_{g_1} = \begin{bmatrix} 1 \\ 0 \end{bmatrix} \frac{z_{gps}(t_1)}{r_{gps}}$.

$$\Lambda_{1|z_{rng_1},z_{gps_1}} = \Lambda_{1|z_{rng_1}} + H_{gps}^\top r_{gps}^{-1} H_{gps} \tag{D.56}$$

$$\begin{aligned}
&= \Lambda_{1|z_{rng_1}} + \begin{bmatrix} 0 \\ 0 \\ \begin{bmatrix} 1 \\ 0 \end{bmatrix} \\ 0 \end{bmatrix} r_{gps}^{-1} \begin{bmatrix} 0 & 0 & \begin{bmatrix} 1 & 0 \end{bmatrix} & 0 \end{bmatrix} \\
&= \Lambda_{1|z_{rng_1}} + \begin{bmatrix} 0 & 0 & 0 & 0 \\ 0 & 0 & 0 & 0 \\ 0 & 0 & \begin{bmatrix} \frac{1}{r_{gps}} & 0 \\ 0 & 0 \end{bmatrix} & 0 \\ 0 & 0 & 0 & 0 \end{bmatrix} \\
&= \Lambda_{1|z_{rng_1}} + \begin{bmatrix} 0 & 0 & 0 & 0 \\ 0 & 0 & 0 & 0 \\ 0 & 0 & R_g & 0 \\ 0 & 0 & 0 & 0 \end{bmatrix} \\
&= \begin{bmatrix} \boldsymbol{Q}_v^{-1} + \boldsymbol{R}_r & -\boldsymbol{Q}_v^{-1}\boldsymbol{F}_v & 0 & -\boldsymbol{R}_r \\ -\boldsymbol{F}_v^\top \boldsymbol{Q}_v^{-1} & \boldsymbol{F}_v^\top \boldsymbol{Q}_v^{-1}\boldsymbol{F}_v + \Lambda_{v_0 v_0} & 0 & 0 \\ 0 & 0 & \boldsymbol{Q}_s^{-1} + \boldsymbol{R}_g & -\boldsymbol{Q}_s^{-1}\boldsymbol{F}_s \\ -\boldsymbol{R}_r & 0 & -\boldsymbol{F}_s^\top \boldsymbol{Q}_s^{-1} & \boldsymbol{F}_s^\top \boldsymbol{Q}_s^{-1}\boldsymbol{F}_s + \Lambda_{s_0 s_0} + \boldsymbol{R}_r \end{bmatrix}
\end{aligned} \tag{D.57}$$

where we define $R_g = \begin{bmatrix} 0 & 0 \\ 0 & \frac{1}{r_{gps}} \end{bmatrix}$.

After incorporating all of the measurements for this time step we let

$$\eta_{1|1} = \begin{bmatrix} \eta_{1|1_v} \\ \eta_{1|1_s} \end{bmatrix} = \eta_{1|z_{rng_1},z_{gps_1}} \tag{D.58}$$

$$\Lambda_{1|1} = \begin{bmatrix} \Lambda_{1|1_{vv}} & \Lambda_{1|1_{vs}} \\ \Lambda_{1|1_{sv}} & \Lambda_{1|1_{ss}} \end{bmatrix} = \Lambda_{1|z_{rng_1},z_{gps_1}}. \tag{D.59}$$

Prediction with Augmentation $t_1 \rightarrow t_2$

A prediction with augmentation step transitions the state from t_1 to t_2:

$$\eta_{2|1} = \begin{bmatrix} 0_{1x1} \\ \eta_{1|1_{v\,2x1}} \\ 0_{1x1} \\ \eta_{1|1_{s\,2x1}} \end{bmatrix} = \begin{bmatrix} 0 \\ z_{r_1} \\ \eta_{v_0} \\ 0 \\ z_{g_1} \\ \eta_{s_0} - z_{r_1} \end{bmatrix} \tag{D.60}$$

$$\begin{aligned}
\Lambda_{2|1} = &\begin{bmatrix} \boldsymbol{Q}_v^{-1} & -\boldsymbol{Q}_v^{-1}\boldsymbol{F}_v & 0 & 0 & 0 & 0 \\ -\boldsymbol{F}_v^\top \boldsymbol{Q}_v^{-1} & \boldsymbol{F}_v^\top \boldsymbol{Q}_v^{-1}\boldsymbol{F}_v & 0 & 0 & 0 & 0 \\ 0 & 0 & 0 & 0 & 0 & 0 \\ 0 & 0 & 0 & \boldsymbol{Q}_s^{-1} & -\boldsymbol{Q}_s^{-1}\boldsymbol{F}_s & 0 \\ 0 & 0 & 0 & -\boldsymbol{F}_s^\top \boldsymbol{Q}_s^{-1} & \boldsymbol{F}_s^\top \boldsymbol{Q}_s^{-1}\boldsymbol{F}_s & 0 \\ 0 & 0 & 0 & 0 & 0 & 0 \end{bmatrix} \\
&+ \begin{bmatrix} 0 & 0 & 0 & 0 & 0 & 0 \\ 0 & \boldsymbol{\Lambda}_{1|1_{vv}} & 0 & \boldsymbol{\Lambda}_{1|1_{vs}} & & \\ 0 & & 0 & & & \\ 0 & 0 & 0 & 0 & 0 & 0 \\ 0 & \boldsymbol{\Lambda}_{1|1_{sv}} & 0 & \boldsymbol{\Lambda}_{1|1_{ss}} & & \\ 0 & & 0 & & & \end{bmatrix}
\end{aligned} \tag{D.61}$$

$$= \begin{bmatrix} \boldsymbol{Q}_v^{-1} & -\boldsymbol{Q}_v^{-1}\boldsymbol{F}_v & 0 \\ -\boldsymbol{F}_v^\top \boldsymbol{Q}_v^{-1} & \boldsymbol{F}_v^\top \boldsymbol{Q}_v^{-1}\boldsymbol{F}_v + \boldsymbol{Q}_v^{-1} + \boldsymbol{R}_r & -\boldsymbol{Q}_v^{-1}\boldsymbol{F}_v \\ 0 & -\boldsymbol{F}_v^\top \boldsymbol{Q}_v^{-1} & \boldsymbol{F}_v^\top \boldsymbol{Q}_v^{-1}\boldsymbol{F}_v + \Lambda_{v_0 v_0} \quad \cdots \\ 0 & 0 & 0 \\ 0 & 0 & 0 \\ 0 & -\boldsymbol{R}_r & 0 \end{bmatrix}$$

$$\begin{bmatrix} 0 & 0 & 0 \\ 0 & 0 & -\boldsymbol{R}_r \\ \cdots \quad 0 & 0 & 0 \\ \boldsymbol{Q}_s^{-1} & -\boldsymbol{Q}_s^{-1}\boldsymbol{F}_s & 0 \\ -\boldsymbol{F}_s^\top \boldsymbol{Q}_s^{-1} & \boldsymbol{F}_s^\top \boldsymbol{Q}_s^{-1}\boldsymbol{F}_s + \boldsymbol{Q}_s^{-1} + \boldsymbol{R}_g & -\boldsymbol{Q}_s^{-1}\boldsymbol{F}_s \\ 0 & -\boldsymbol{F}_s^\top \boldsymbol{Q}_s^{-1} & \boldsymbol{F}_s^\top \boldsymbol{Q}_s^{-1}\boldsymbol{F}_s + \Lambda_{s_0 s_0} + \boldsymbol{R}_r \end{bmatrix} \tag{D.61}$$

Marginalize out $\boldsymbol{x}_v(t_0)$, Vehicle State at t_0

Starting with the information vector after the prediction to t_2, equation (D.60),

$$\eta_{2|1}(\boldsymbol{x}_{v_2}, \boldsymbol{x}_{v_1}, \boldsymbol{x}_{v_0}, \boldsymbol{x}_{s_2}, \boldsymbol{x}_{s_1}, \boldsymbol{x}_{s_0},) = \begin{bmatrix} 0 \\ z_{r_1} \\ \eta_{v_0} \\ 0 \\ z_{g_1} \\ \eta_{s_0} - z_{r_1} \end{bmatrix}, \tag{D.62}$$

we marginalize out the vehicle state at t_0 using equations (D.35) and (D.36),

$$\eta_{2|1}(\boldsymbol{x}_{v_2}, \boldsymbol{x}_{v_1}, \boldsymbol{x}_{s_2}, \boldsymbol{x}_{s_1}, \boldsymbol{x}_{s_0}) = \begin{bmatrix} 0 \\ z_{r_1} \\ 0 \\ z_{g_1} \\ \eta_{s_0} - z_{r_1} \end{bmatrix} - \begin{bmatrix} 0 \\ -\boldsymbol{Q}_v^{-1}\boldsymbol{F}_v \\ 0 \\ 0 \\ 0 \end{bmatrix} (\boldsymbol{F}_v^\top \boldsymbol{Q}_v^{-1}\boldsymbol{F}_v + \boldsymbol{\Lambda}_{v_0 v_0})^{-1}\eta_{v_0} \tag{D.63}$$

$$= \begin{bmatrix} 0 \\ \tilde{\eta}_{v_1} \\ 0 \\ z_{g_1} \\ \eta_{s_0} - z_{r_1} \end{bmatrix} \tag{D.64}$$

where

$$\tilde{\eta}_{v_1} = z_{r_1} + \boldsymbol{Q}_v^{-1}\boldsymbol{F}_v(\boldsymbol{F}_v^\top \boldsymbol{Q}_v^{-1}\boldsymbol{F}_v + \boldsymbol{\Lambda}_{v_0 v_0})^{-1}\eta_{v_0} \tag{D.65}$$

Similarly for the information matrix,

$$\Lambda_{2|1}(\boldsymbol{x}_{v_2}, \boldsymbol{x}_{v_1}, \boldsymbol{x}_{s_2}, \boldsymbol{x}_{s_1}, \boldsymbol{x}_{s_0}) \tag{D.66}$$

$$= \begin{bmatrix} \boldsymbol{Q}_v^{-1} & -\boldsymbol{Q}_v^{-1}\boldsymbol{F}_v & & & \\ -\boldsymbol{F}_v^\top \boldsymbol{Q}_v^{-1} & \boldsymbol{F}_v^\top \boldsymbol{Q}_v^{-1}\boldsymbol{F}_v + \boldsymbol{Q}_v^{-1} + \boldsymbol{R}_r & \cdots & & \\ 0 & 0 & & & \\ 0 & 0 & & & \\ 0 & -\boldsymbol{R}_r & & & \end{bmatrix}$$

$$\begin{bmatrix} 0 & 0 & 0 \\ 0 & 0 & -\boldsymbol{R}_r \\ \cdots & \boldsymbol{Q}_s^{-1} & -\boldsymbol{Q}_s^{-1}\boldsymbol{F}_s & 0 \\ & -\boldsymbol{F}_s^\top \boldsymbol{Q}_s^{-1} & \boldsymbol{F}_s^\top \boldsymbol{Q}_s^{-1}\boldsymbol{F}_s + \boldsymbol{Q}_s^{-1} + \boldsymbol{R}_g & -\boldsymbol{Q}_s^{-1}\boldsymbol{F}_s \\ & 0 & -\boldsymbol{F}_s^\top \boldsymbol{Q}_s^{-1} & \boldsymbol{F}_s^\top \boldsymbol{Q}_s^{-1}\boldsymbol{F}_s + \Lambda_{s_0 s_0} + \boldsymbol{R}_r \end{bmatrix}$$

$$- \begin{bmatrix} 0 \\ -\boldsymbol{Q}_v^{-1}\boldsymbol{F}_v \\ 0 \\ 0 \\ 0 \end{bmatrix} (\boldsymbol{F}_v^\top \boldsymbol{Q}_v^{-1}\boldsymbol{F}_v + \boldsymbol{\Lambda}_{v_0 v_0})^{-1} \begin{bmatrix} 0 & -\boldsymbol{F}_v^\top \boldsymbol{Q}_v^{-1} & 0 & 0 & 0 \end{bmatrix} \tag{D.67}$$

$$= \begin{bmatrix} \boldsymbol{Q}_v^{-1} & -\boldsymbol{Q}_v^{-1}\boldsymbol{F}_v & 0 & & \\ -\boldsymbol{F}_v^\top \boldsymbol{Q}_v^{-1} & \tilde{\boldsymbol{\Lambda}}_{v_1 v_1} & 0 & & \\ 0 & 0 & \boldsymbol{Q}_s^{-1} & \cdots & \\ 0 & 0 & -\boldsymbol{F}_s^\top \boldsymbol{Q}_s^{-1} & & \\ 0 & -\boldsymbol{R}_r & 0 & & \end{bmatrix}$$

$$\begin{bmatrix} 0 & 0 \\ 0 & -\boldsymbol{R}_r \\ \cdots & -\boldsymbol{Q}_s^{-1}\boldsymbol{F}_s & 0 \\ & \boldsymbol{F}_s^\top \boldsymbol{Q}_s^{-1}\boldsymbol{F}_s + \boldsymbol{Q}_s^{-1} + \boldsymbol{R}_g & -\boldsymbol{Q}_s^{-1}\boldsymbol{F}_s \\ & -\boldsymbol{F}_s^\top \boldsymbol{Q}_s^{-1} & \boldsymbol{F}_s^\top \boldsymbol{Q}_s^{-1}\boldsymbol{F}_s + \Lambda_{s_0 s_0} + \boldsymbol{R}_r \end{bmatrix} \tag{D.68}$$

where

$$\tilde{\boldsymbol{\Lambda}}_{v_1 v_1} = \boldsymbol{F}_v^\top \boldsymbol{Q}_v^{-1}\boldsymbol{F}_v + \boldsymbol{Q}_v^{-1} + \boldsymbol{R}_r - \boldsymbol{Q}_v^{-1}\boldsymbol{F}_v(\boldsymbol{F}_v^\top \boldsymbol{Q}_v^{-1}\boldsymbol{F}_v + \Lambda_{v_0 v_0})^{-1}\boldsymbol{F}_v^\top \boldsymbol{Q}_v^{-1}. \tag{D.69}$$

Marginalize out $\boldsymbol{x}_s(t_1)$, Ship State at t_1

Starting with $\boldsymbol{x}_{v_0}$ already marginalized out, equations (D.64) and (D.68), we marginalize out the ship state at t_1, again using equations (D.35) and (D.36),

$$\eta_{2|1}(\boldsymbol{x}_{v_2}, \boldsymbol{x}_{v_1}, \boldsymbol{x}_{s_2}, \boldsymbol{x}_{s_0}) = \begin{bmatrix} 0 \\ \tilde{\eta}_{v_1} \\ 0 \\ \eta_{s_0} - z_{r_1} \end{bmatrix} - \begin{bmatrix} 0 \\ 0 \\ -\boldsymbol{Q}_s^{-1}\boldsymbol{F}_s \\ -\boldsymbol{F}_s^\top \boldsymbol{Q}_s^{-1} \end{bmatrix} (\boldsymbol{F}_s^\top \boldsymbol{Q}_s^{-1}\boldsymbol{F}_s + \boldsymbol{Q}_s^{-1} + \boldsymbol{R}_g)^{-1} z_{g_1} \tag{D.70}$$

$$= \begin{bmatrix} 0 \\ \tilde{\eta}_{v_1} \\ \tilde{\eta}_{s_2} \\ \tilde{\eta}_{s_0} \end{bmatrix} \tag{D.71}$$

where $\tilde{\eta}_{v_1}$ was defined in equation (D.65) and

$$\tilde{\eta}_{s_2} = \boldsymbol{Q}_s^{-1}\boldsymbol{F}_s(\boldsymbol{F}_s^\top \boldsymbol{Q}_s^{-1}\boldsymbol{F}_s + \boldsymbol{Q}_s^{-1} + \boldsymbol{R}_g)^{-1} z_{g_1} \tag{D.72}$$

$$\tilde{\eta}_{s_0} = \eta_{s_0} - z_{r_1} + \boldsymbol{F}_s^\top \boldsymbol{Q}_s^{-1}(\boldsymbol{F}_s^\top \boldsymbol{Q}_s^{-1}\boldsymbol{F}_s + \boldsymbol{Q}_s^{-1} + \boldsymbol{R}_g)^{-1} z_{g_1}. \tag{D.73}$$

Similarly for the information matrix,

$$\Lambda_{2|1}(\boldsymbol{x}_{v_2}, \boldsymbol{x}_{v_1}, \boldsymbol{x}_{s_2}, \boldsymbol{x}_{s_0}) = \begin{bmatrix} \boldsymbol{Q}_v^{-1} & -\boldsymbol{Q}_v^{-1}\boldsymbol{F}_v & 0 & 0 \\ -\boldsymbol{F}_v^\top \boldsymbol{Q}_v^{-1} & \tilde{\boldsymbol{\Lambda}}_{v_1 v_1} & 0 & -\boldsymbol{R}_r \\ 0 & 0 & \boldsymbol{Q}_s^{-1} & 0 \\ 0 & -\boldsymbol{R}_r & 0 & \boldsymbol{F}_s^\top \boldsymbol{Q}_s^{-1}\boldsymbol{F}_s + \Lambda_{s_0 s_0} + \boldsymbol{R}_r \end{bmatrix}$$
$$- \begin{bmatrix} 0 \\ 0 \\ -\boldsymbol{Q}_s^{-1}\boldsymbol{F}_s \\ -\boldsymbol{F}_s^\top \boldsymbol{Q}_s^{-1} \end{bmatrix} (\boldsymbol{F}_s^\top \boldsymbol{Q}_s^{-1}\boldsymbol{F}_s + \boldsymbol{Q}_s^{-1} + \boldsymbol{R}_g)^{-1} \begin{bmatrix} 0 & 0 & -\boldsymbol{F}_s^\top \boldsymbol{Q}_s^{-1} & -\boldsymbol{Q}_s^{-1}\boldsymbol{F}_s \end{bmatrix}$$
$$= \begin{bmatrix} \boldsymbol{Q}_v^{-1} & -\boldsymbol{Q}_v^{-1}\boldsymbol{F}_v & 0 & 0 \\ -\boldsymbol{F}_v^\top \boldsymbol{Q}_v^{-1} & \tilde{\boldsymbol{\Lambda}}_{v_1 v_1} & 0 & -\boldsymbol{R}_r \\ 0 & 0 & \tilde{\boldsymbol{\Lambda}}_{s_2 s_2} & \tilde{\boldsymbol{\Lambda}}_{s_2 s_0} \\ 0 & -\boldsymbol{R}_r & \tilde{\boldsymbol{\Lambda}}_{s_0 s_2} & \tilde{\boldsymbol{\Lambda}}_{s_0 s_0} \end{bmatrix} \tag{D.74}$$

where $\tilde{\boldsymbol{\Lambda}}_{v_1 v_1}$ was defined in equation (D.69) and

$$\tilde{\boldsymbol{\Lambda}}_{s_2 s_2} = \boldsymbol{Q}_s^{-1} - \boldsymbol{Q}_s^{-1}\boldsymbol{F}_s(\boldsymbol{F}_s^\top \boldsymbol{Q}_s^{-1}\boldsymbol{F}_s + \boldsymbol{Q}_s^{-1} + \boldsymbol{R}_g)^{-1}\boldsymbol{F}_s^\top \boldsymbol{Q}_s^{-1} \tag{D.75}$$
$$\tilde{\boldsymbol{\Lambda}}_{s_2 s_0} = -\boldsymbol{Q}_s^{-1}\boldsymbol{F}_s(\boldsymbol{F}_s^\top \boldsymbol{Q}_s^{-1}\boldsymbol{F}_s + \boldsymbol{Q}_s^{-1} + \boldsymbol{R}_g)^{-1}\boldsymbol{Q}_s^{-1}\boldsymbol{F}_s \tag{D.76}$$
$$\tilde{\boldsymbol{\Lambda}}_{s_0 s_2} = -\boldsymbol{F}_s^\top \boldsymbol{Q}_s^{-1}(\boldsymbol{F}_s^\top \boldsymbol{Q}_s^{-1}\boldsymbol{F}_s + \boldsymbol{Q}_s^{-1} + \boldsymbol{R}_g)^{-1}\boldsymbol{F}_s^\top \boldsymbol{Q}_s^{-1} \tag{D.77}$$
$$\tilde{\boldsymbol{\Lambda}}_{s_0 s_0} = \boldsymbol{F}_s^\top \boldsymbol{Q}_s^{-1}\boldsymbol{F}_s + \Lambda_{s_0 s_0} + \boldsymbol{R}_r - \boldsymbol{F}_s^\top \boldsymbol{Q}_s^{-1}(\boldsymbol{F}_s^\top \boldsymbol{Q}_s^{-1}\boldsymbol{F}_s + \boldsymbol{Q}_s^{-1} + \boldsymbol{R}_g)^{-1}\boldsymbol{Q}_s^{-1}\boldsymbol{F}_s \tag{D.78}$$

Vehicle Velocity Measurement at t_2

Next we incorporate the vehicle velocity measurement $z_{vel}(t_2)$.

$$\eta_{2|z_{vel_2}} = \eta_{2|1} + H_{vel}^\top r_{vel}^{-1} z_{vel}(t_2) \tag{D.79}$$
$$= \begin{bmatrix} 0 \\ \tilde{\eta}_{v_1} \\ \tilde{\eta}_{s_2} \\ \tilde{\eta}_{s_0} \end{bmatrix} + \begin{bmatrix} \begin{bmatrix} 0 \\ 1 \end{bmatrix} \\ 0 \\ 0 \\ 0 \end{bmatrix} \frac{z_{vel}(t_2)}{r_{vel}}$$
$$= \begin{bmatrix} 0 \\ \tilde{\eta}_{v_1} \\ \tilde{\eta}_{s_2} \\ \tilde{\eta}_{s_0} \end{bmatrix} + \begin{bmatrix} z_{v_2} \\ 0 \\ 0 \\ 0 \end{bmatrix}$$
$$= \begin{bmatrix} z_{v_2} \\ \tilde{\eta}_{v_1} \\ \tilde{\eta}_{s_2} \\ \tilde{\eta}_{s_0} \end{bmatrix} \tag{D.80}$$

where we define $z_{v_2} = \begin{bmatrix} 0 \\ 1 \end{bmatrix} \frac{z_{vel}(t_2)}{r_{vel}}$.

$$\Lambda_{2|z_{vel_2}} = \Lambda_{2|1} + H_{vel}^{\top} r_{vel}^{-1} H_{vel} \tag{D.81}$$

$$\begin{aligned}
&= \Lambda_{2|1} + \begin{bmatrix} \begin{bmatrix} 0 \\ 1 \end{bmatrix} \\ 0 \\ 0 \\ 0 \\ 0 \end{bmatrix} r_{vel}^{-1} \begin{bmatrix} \begin{bmatrix} 0 & 1 \end{bmatrix} & 0 & 0 & 0 & 0 \end{bmatrix} \\
&= \Lambda_{2|1} + \begin{bmatrix} \begin{bmatrix} 0 & 0 \\ 0 & \frac{1}{r_{vel}} \end{bmatrix} & 0 & 0 & 0 \\ 0 & 0 & 0 & 0 \\ 0 & 0 & 0 & 0 \\ 0 & 0 & 0 & 0 \end{bmatrix} \\
&= \Lambda_{2|1} + \begin{bmatrix} R_v & 0 & 0 & 0 \\ 0 & 0 & 0 & 0 \\ 0 & 0 & 0 & 0 \\ 0 & 0 & 0 & 0 \end{bmatrix} \\
&= \begin{bmatrix} \boldsymbol{Q}_v^{-1} + \boldsymbol{R}_v & -\boldsymbol{Q}_v^{-1}\boldsymbol{F}_v & 0 & 0 \\ -\boldsymbol{F}_v^{\top}\boldsymbol{Q}_v^{-1} & \boldsymbol{\Lambda}_{v_1 v_1} & 0 & -\boldsymbol{R}_r \\ 0 & 0 & \tilde{\boldsymbol{\Lambda}}_{s_2 s_2} & \tilde{\boldsymbol{\Lambda}}_{s_2 s_0} \\ 0 & -\boldsymbol{R}_r & \tilde{\boldsymbol{\Lambda}}_{s_0 s_2} & \tilde{\boldsymbol{\Lambda}}_{s_0 s_0} \end{bmatrix}
\end{aligned} \tag{D.82}$$

where we define $R_v = \begin{bmatrix} 0 & 0 \\ 0 & \frac{1}{r_{vel}} \end{bmatrix}$.

After completing the marginalizations and incorporating all of the measurements for this time step we let

$$\eta_{2|2} = \begin{bmatrix} \eta_{2|2_v} \\ \eta_{2|2_s} \end{bmatrix} = \eta_{2|z_{vel_2}} \tag{D.83}$$

$$\Lambda_{2|2} = \begin{bmatrix} \Lambda_{2|2_{vv}} & \Lambda_{2|2_{vs}} \\ \Lambda_{2|2_{sv}} & \Lambda_{2|2_{ss}} \end{bmatrix} = \Lambda_{2|z_{vel_2}}. \tag{D.84}$$

Prediction with Augmentation $t_2 \rightarrow t_3$

A prediction with augmentation step transitions the state from t_2 to t_3:

$$\eta_{3|2} = \begin{bmatrix} 0_{1x1} \\ \eta_{2|2_{v\,2x1}} \\ 0_{1x1} \\ \eta_{2|2_{s\,2x1}} \end{bmatrix} = \begin{bmatrix} 0 \\ z_{v_2} \\ \tilde{\eta}_{v_1} \\ 0 \\ \tilde{\eta}_{s_2} \\ \tilde{\eta}_{s_0} \end{bmatrix} \tag{D.85}$$

$$\Lambda_{3|2} = \begin{bmatrix} \boldsymbol{Q}_v^{-1} & -\boldsymbol{Q}_v^{-1}\boldsymbol{F}_v & 0 & 0 & 0 & 0 \\ -\boldsymbol{F}_v^\top \boldsymbol{Q}_v^{-1} & \boldsymbol{F}_v^\top \boldsymbol{Q}_v^{-1}\boldsymbol{F}_v & 0 & 0 & 0 & 0 \\ 0 & 0 & 0 & 0 & 0 & 0 \\ 0 & 0 & 0 & \boldsymbol{Q}_s^{-1} & -\boldsymbol{Q}_s^{-1}\boldsymbol{F}_s & 0 \\ 0 & 0 & 0 & -\boldsymbol{F}_s^\top \boldsymbol{Q}_s^{-1} & \boldsymbol{F}_s^\top \boldsymbol{Q}_s^{-1}\boldsymbol{F}_s & 0 \\ 0 & 0 & 0 & 0 & 0 & 0 \end{bmatrix} + \begin{bmatrix} 0 & 0 & 0 & 0 & 0 & 0 \\ 0 & \boldsymbol{\Lambda}_{2|2_{vv}} & 0 & \boldsymbol{\Lambda}_{2|2_{vs}} & & \\ 0 & & 0 & & & \\ 0 & 0 & 0 & 0 & 0 & 0 \\ 0 & \boldsymbol{\Lambda}_{2|2_{sv}} & 0 & \boldsymbol{\Lambda}_{2|2_{ss}} & & \\ 0 & & 0 & & & \end{bmatrix}$$

$$= \begin{bmatrix} \boldsymbol{Q}_v^{-1} & -\boldsymbol{Q}_v^{-1}\boldsymbol{F}_v & 0 & \cdots \\ -\boldsymbol{F}_v^\top \boldsymbol{Q}_v^{-1} & \boldsymbol{F}_v^\top \boldsymbol{Q}_v^{-1}\boldsymbol{F}_v + \boldsymbol{Q}_v^{-1} + \boldsymbol{R}_v & -\boldsymbol{Q}_v^{-1}\boldsymbol{F}_v & \\ 0 & -\boldsymbol{F}_v^\top \boldsymbol{Q}_v^{-1} & \tilde{\boldsymbol{\Lambda}}_{v_1 v_1} & \\ 0 & 0 & 0 & \\ 0 & 0 & 0 & \\ 0 & 0 & -\boldsymbol{R}_r & \end{bmatrix}$$

$$\begin{bmatrix} 0 & 0 & 0 \\ 0 & 0 & 0 \\ 0 & 0 & -\boldsymbol{R}_r \\ \boldsymbol{Q}_s^{-1} & -\boldsymbol{Q}_s^{-1}\boldsymbol{F}_s & 0 \\ -\boldsymbol{F}_s^\top \boldsymbol{Q}_s^{-1} & \boldsymbol{F}_s^\top \boldsymbol{Q}_s^{-1}\boldsymbol{F}_s + \tilde{\boldsymbol{\Lambda}}_{s_2 s_2} & \tilde{\boldsymbol{\Lambda}}_{s_2 s_0} \\ 0 & \tilde{\boldsymbol{\Lambda}}_{s_0 s_2} & \tilde{\boldsymbol{\Lambda}}_{s_0 s_0} \end{bmatrix}. \tag{D.86}$$

Range Measurement at t_3

Incorporating the range measurement $z_{rng}(t_3)$ gives us

$$\eta_{3|z_{rng_3}} = \eta_{3|2} + H_{rng}^\top r_{rng}^{-1} z_{rng}(t_3) \tag{D.87}$$

$$= \begin{bmatrix} 0 \\ z_{v_2} \\ \tilde{\eta}_{v_1} \\ 0 \\ \tilde{\eta}_{s_2} \\ \tilde{\eta}_{s_0} \end{bmatrix} + \begin{bmatrix} z_{r_3} \\ 0 \\ 0 \\ 0 \\ -z_{r_3} \\ 0 \end{bmatrix}$$

$$= \begin{bmatrix} z_{r_3} \\ z_{v_2} \\ \tilde{\eta}_{v_1} \\ 0 \\ \tilde{\eta}_{s_2} - z_{r_3} \\ \tilde{\eta}_{s_0} \end{bmatrix} \tag{D.88}$$

where we define $z_{r_3} = \begin{bmatrix} 1 \\ 0 \end{bmatrix} \frac{z_{rng}(t_3)}{r_{rng}}$.

Similarly for the information matrix,

$$\Lambda_{3|z_{rng_3}} = \Lambda_{3|2} + H_{rng}^\top r_{rng}^{-1} H_{rng} \tag{D.89}$$

$$= \Lambda_{3|2} + \begin{bmatrix} R_r & 0 & 0 & 0 & -R_r & 0 \\ 0 & 0 & 0 & 0 & 0 & 0 \\ 0 & 0 & 0 & 0 & 0 & 0 \\ 0 & 0 & 0 & 0 & 0 & 0 \\ -R_r & 0 & 0 & 0 & R_r & 0 \\ 0 & 0 & 0 & 0 & 0 & 0 \end{bmatrix}$$

$$= \begin{bmatrix} \boldsymbol{Q}_v^{-1} + \boldsymbol{R}_r & -\boldsymbol{Q}_v^{-1}\boldsymbol{F}_v & 0 \\ -\boldsymbol{F}_v^\top \boldsymbol{Q}_v^{-1} & \boldsymbol{F}_v^\top \boldsymbol{Q}_v^{-1}\boldsymbol{F}_v + \boldsymbol{Q}_v^{-1} + \boldsymbol{R}_v & -\boldsymbol{Q}_v^{-1}\boldsymbol{F}_v \\ 0 & -\boldsymbol{F}_v^\top \boldsymbol{Q}_v^{-1} & \tilde{\boldsymbol{\Lambda}}_{v_1 v_1} \\ 0 & 0 & 0 \\ -\boldsymbol{R}_r & 0 & 0 \\ 0 & 0 & -\boldsymbol{R}_r \end{bmatrix} \quad \cdots$$

$$\begin{bmatrix} 0 & -\boldsymbol{R}_r & 0 \\ 0 & 0 & 0 \\ 0 & 0 & -\boldsymbol{R}_r \\ \boldsymbol{Q}_s^{-1} & -\boldsymbol{Q}_s^{-1}\boldsymbol{F}_s & 0 \\ -\boldsymbol{F}_s^\top \boldsymbol{Q}_s^{-1} & \boldsymbol{F}_s^\top \boldsymbol{Q}_s^{-1}\boldsymbol{F}_s + \tilde{\boldsymbol{\Lambda}}_{s_2 s_2} + \boldsymbol{R}_r & \tilde{\boldsymbol{\Lambda}}_{s_2 s_0} \\ 0 & \tilde{\boldsymbol{\Lambda}}_{s_0 s_2} & \tilde{\boldsymbol{\Lambda}}_{s_0 s_0} \end{bmatrix} \tag{D.90}$$

where we define $R_r = \begin{bmatrix} \frac{1}{r_{rng}} & 0 \\ 0 & 0 \end{bmatrix}$.

For ease of notation let

$$\eta_{3|3} = \eta_{3|z_{rng_3}} \tag{D.91}$$

$$\Lambda_{3|3} = \Lambda_{3|z_{rng_3}}. \tag{D.92}$$

Marginalize out $\boldsymbol{x}_s(t_0)$, Ship State at t_0

We will now marginalize out the ship state at t_0. This will illustrate what happens when a state associated with a range measurement is marginalized out, and allow is to verify that the solution is reproducible in the decentralized implementation.

Using equations (D.35) and (D.36),

$$\eta_{3|3}(\boldsymbol{x}_{v_3}, \boldsymbol{x}_{v_2}, \boldsymbol{x}_{v_1}, \boldsymbol{x}_{s_3}, \boldsymbol{x}_{s_2}) = \begin{bmatrix} z_{r_3} \\ z_{v_2} \\ \tilde{\eta}_{v_1} \\ 0 \\ \tilde{\eta}_{s_2} - z_{r_3} \end{bmatrix} - \begin{bmatrix} 0 \\ 0 \\ -\boldsymbol{R}_r \\ 0 \\ \tilde{\boldsymbol{\Lambda}}_{s_2 s_0} \end{bmatrix} \tilde{\boldsymbol{\Lambda}}_{s_0 s_0}^{-1} \tilde{\eta}_{s_0} \tag{D.93}$$

$$= \begin{bmatrix} z_{r_3} \\ z_{v_2} \\ \hat{\eta}_{v_1} \\ 0 \\ \hat{\eta}_{s_2} \end{bmatrix} \tag{D.94}$$

where

$$\hat{\eta}_{v_1} = \tilde{\eta}_{v_1} + \boldsymbol{R}_r \tilde{\boldsymbol{\Lambda}}_{s_0 s_0}^{-1} \tilde{\eta}_{s_0} \tag{D.95}$$

$$\hat{\eta}_{s_2} = \tilde{\eta}_{s_2} - z_{r_3} - \tilde{\boldsymbol{\Lambda}}_{s_2 s_0} \tilde{\boldsymbol{\Lambda}}_{s_0 s_0}^{-1} \tilde{\eta}_{s_0}. \tag{D.96}$$

Similarly for the information matrix,

$$\Lambda_{3|3}(\boldsymbol{x}_{v_3}, \boldsymbol{x}_{v_2}, \boldsymbol{x}_{v_1}, \boldsymbol{x}_{s_3}, \boldsymbol{x}_{s_2}) = \begin{bmatrix} \boldsymbol{Q}_v^{-1} + \boldsymbol{R}_r & -\boldsymbol{Q}_v^{-1}\boldsymbol{F}_v & 0 & \\ -\boldsymbol{F}_v^\top \boldsymbol{Q}_v^{-1} & \boldsymbol{F}_v^\top \boldsymbol{Q}_v^{-1}\boldsymbol{F}_v + \boldsymbol{Q}_v^{-1} + \boldsymbol{R}_v & -\boldsymbol{Q}_v^{-1}\boldsymbol{F}_v & \\ 0 & -\boldsymbol{F}_v^\top \boldsymbol{Q}_v^{-1} & \tilde{\boldsymbol{\Lambda}}_{v_1 v_1} & \cdots \\ 0 & 0 & 0 & \\ -\boldsymbol{R}_r & 0 & 0 & \end{bmatrix}$$

$$\cdots \begin{bmatrix} 0 & -\boldsymbol{R}_r \\ 0 & 0 \\ 0 & 0 \\ \boldsymbol{Q}_s^{-1} & -\boldsymbol{Q}_s^{-1}\boldsymbol{F}_s \\ -\boldsymbol{F}_s^\top \boldsymbol{Q}_s^{-1} & \boldsymbol{F}_s^\top \boldsymbol{Q}_s^{-1}\boldsymbol{F}_s + \tilde{\boldsymbol{\Lambda}}_{s_2 s_2} + \boldsymbol{R}_r \end{bmatrix} - \begin{bmatrix} 0 \\ 0 \\ -\boldsymbol{R}_r \\ 0 \\ \tilde{\boldsymbol{\Lambda}}_{s_2 s_0} \end{bmatrix} \tilde{\boldsymbol{\Lambda}}_{s_0 s_0}^{-1} \begin{bmatrix} 0 & 0 & -\boldsymbol{R}_r & 0 & \tilde{\boldsymbol{\Lambda}}_{s_0 s_2} \end{bmatrix}$$

$$= \begin{bmatrix} \boldsymbol{Q}_v^{-1} + \boldsymbol{R}_r & -\boldsymbol{Q}_v^{-1}\boldsymbol{F}_v & 0 & 0 & -\boldsymbol{R}_r \\ -\boldsymbol{F}_v^\top \boldsymbol{Q}_v^{-1} & \boldsymbol{F}_v^\top \boldsymbol{Q}_v^{-1}\boldsymbol{F}_v + \boldsymbol{Q}_v^{-1} + \boldsymbol{R}_v & -\boldsymbol{Q}_v^{-1}\boldsymbol{F}_v & 0 & 0 \\ 0 & -\boldsymbol{F}_v^\top \boldsymbol{Q}_v^{-1} & \hat{\boldsymbol{\Lambda}}_{v_1 v_1} & 0 & \hat{\boldsymbol{R}}_{r_{v_1 s_0}} \\ 0 & 0 & 0 & \boldsymbol{Q}_s^{-1} & -\boldsymbol{Q}_s^{-1}\boldsymbol{F}_s \\ -\boldsymbol{R}_r & 0 & \hat{\boldsymbol{R}}_{r_{s_0 v_1}} & -\boldsymbol{F}_s^\top \boldsymbol{Q}_s^{-1} & \hat{\boldsymbol{\Lambda}}_{s_2 s_2} \end{bmatrix} \tag{D.97}$$

where

$$\hat{\boldsymbol{\Lambda}}_{v_1 v_1} = \tilde{\boldsymbol{\Lambda}}_{v_1 v_1} - \boldsymbol{R}_r \tilde{\boldsymbol{\Lambda}}_{s_0 s_0}^{-1} \boldsymbol{R}_r \tag{D.98}$$

$$\hat{\boldsymbol{\Lambda}}_{s_2 s_2} = \boldsymbol{F}_s^\top \boldsymbol{Q}_s^{-1} \boldsymbol{F}_s + \tilde{\boldsymbol{\Lambda}}_{s_2 s_2} + \boldsymbol{R}_r - \tilde{\boldsymbol{\Lambda}}_{s_2 s_0} \tilde{\boldsymbol{\Lambda}}_{s_2 s_2}^{-1} \tilde{\boldsymbol{\Lambda}}_{s_0 s_2} \tag{D.99}$$

$$\hat{\boldsymbol{R}}_{r_{v_1 s_0}} = \boldsymbol{R}_r \tilde{\boldsymbol{\Lambda}}_{s_0 s_0}^{-1} \tilde{\boldsymbol{\Lambda}}_{s_0 s_2} \tag{D.100}$$

$$\hat{\boldsymbol{R}}_{r_{s_0 v_1}} = \tilde{\boldsymbol{\Lambda}}_{s_2 s_0} \tilde{\boldsymbol{\Lambda}}_{s_0 s_0}^{-1} \boldsymbol{R}_r. \tag{D.101}$$

D.7 Decentralized Implementation

The decentralized implementation relies on two separate information filters, one on the vehicle and one on the ship. The ship filter has no knowledge of the vehicle or the range measurements. The vehicle filter receives data transmissions from the ship concurrent with range measurements from the ship, but does not have access to the ship measurements directly or the ship state estimate in real time. The data transmissions contains the delta change in the ship information vector and matrix since the last transmission to the vehicle (i.e. when the last range measurement was sent). For the example presented here, the initial ship state at t_0 is transmitted to the vehicle at t_0 and received at t_1, and the delta change in the ship state from t_0 to t_1 is transmitted at $t_1$to the vehicle and received at t_2.

D.7.1 Ship Filter

Because the ship has no knowledge of the vehicle state or the range measurements we compute its trajectory estimate first. To differentiate this filter from the vehicle filter we will use $\hat{y}$ and Y to represent the information form of the ship filter.

Initial Conditions The ship starts at t_0 and we assume that

$$\hat{y}_{0|0} = \eta_{s_0} \tag{D.102}$$
$$Y_{0|0} = \Lambda_{s_0 s_0}. \tag{D.103}$$

Prediction with Augmentation $t_0 \rightarrow t_1$

$$\hat{y}_{1|0} = \begin{bmatrix} 0 \\ \eta_{s_0} \end{bmatrix} \tag{D.104}$$
$$Y_{1|0} = \begin{bmatrix} \boldsymbol{Q}_s^{-1} & -\boldsymbol{Q}_s^{-1}\boldsymbol{F}_s \\ -\boldsymbol{F}_s^\top \boldsymbol{Q}_s^{-1} & \boldsymbol{F}_s^\top \boldsymbol{Q}_s^{-1}\boldsymbol{F}_s \end{bmatrix} + \begin{bmatrix} 0 & 0 \\ 0 & \Lambda_{s_0 s_0} \end{bmatrix} \tag{D.105}$$
$$= \begin{bmatrix} \boldsymbol{Q}_s^{-1} & -\boldsymbol{Q}_s^{-1}\boldsymbol{F}_s \\ -\boldsymbol{F}_s^\top \boldsymbol{Q}_s^{-1} & \boldsymbol{F}_s^\top \boldsymbol{Q}_s^{-1}\boldsymbol{F}_s + \Lambda_{s_0 s_0} \end{bmatrix} \tag{D.106}$$

Ship GPS Measurement at t_1

$$\hat{y}_{1|z_{gps_1}} = \hat{y}_{1|0} + H_{gps}^\top r_{gps}^{-1} z_{gps}(t_1) \tag{D.107}$$
$$= \begin{bmatrix} 0 \\ \eta_{s_0} \end{bmatrix} + \begin{bmatrix} z_{g_1} \\ 0 \end{bmatrix}$$
$$= \begin{bmatrix} z_{g_1} \\ \eta_{s_0} \end{bmatrix} \tag{D.108}$$
$$Y_{1|gps_1} = Y_{1|1} + H_{gps}^\top r_{gps}^{-1} H_{gps} \tag{D.109}$$
$$= Y_{1|1} + \begin{bmatrix} R_g & 0 \\ 0 & 0 \end{bmatrix}$$
$$= \begin{bmatrix} \boldsymbol{Q}_s^{-1} + \boldsymbol{R}_g & -\boldsymbol{Q}_s^{-1}\boldsymbol{F}_s \\ -\boldsymbol{F}_s^\top \boldsymbol{Q}_s^{-1} & \boldsymbol{F}_s^\top \boldsymbol{Q}_s^{-1}\boldsymbol{F}_s + \Lambda_{s_0 s_0} \end{bmatrix} \tag{D.110}$$

where

$$R_v = \begin{bmatrix} 0 & 0 \\ 0 & \frac{1}{r_{rng}} \end{bmatrix} \tag{D.111}$$

Once we are finished with all of the measurements at time step t_1 we assign

$$\hat{y}_{1|1} = \hat{y}_{1|z_{gps_1}} \tag{D.112}$$
$$Y_{1|1} = Y_{1|gps_1}. \tag{D.113}$$

Prediction with Augmentation $t_1 \rightarrow t_2$

$$\hat{y}_{2|1} = \begin{bmatrix} 0_{1x1} \\ \hat{y}_{1|1_{2x1}} \end{bmatrix} = \begin{bmatrix} 0 \\ z_{g_1} \\ \eta_{s_0} \end{bmatrix} \tag{D.114}$$
$$Y_{2|1} = \begin{bmatrix} \boldsymbol{Q}_s^{-1} & -\boldsymbol{Q}_s^{-1}\boldsymbol{F}_s & 0 \\ -\boldsymbol{F}_s^\top \boldsymbol{Q}_s^{-1} & \boldsymbol{F}_s^\top \boldsymbol{Q}_s^{-1}\boldsymbol{F}_s & 0 \\ 0 & 0 & 0 \end{bmatrix} + \begin{bmatrix} 0 & 0 & 0 \\ 0 & \boldsymbol{Y}_{1|1} & \\ 0 & & \end{bmatrix} \tag{D.115}$$
$$= \begin{bmatrix} \boldsymbol{Q}_s^{-1} & -\boldsymbol{Q}_s^{-1}\boldsymbol{F}_s & 0 \\ -\boldsymbol{F}_s^\top \boldsymbol{Q}_s^{-1} & \boldsymbol{F}_s^\top \boldsymbol{Q}_s^{-1}\boldsymbol{F}_s + \boldsymbol{Q}_s^{-1} + \boldsymbol{R}_g & -\boldsymbol{Q}_s^{-1}\boldsymbol{F}_s \\ 0 & -\boldsymbol{F}_s^\top \boldsymbol{Q}_s^{-1} & \boldsymbol{F}_s^\top \boldsymbol{Q}_s^{-1}\boldsymbol{F}_s + \Lambda_{s_0 s_0} \end{bmatrix} \tag{D.116}$$

There are no measurements to include at time step t_2 so

$$\hat{y}_{2|2} = \hat{y}_{2|1} \tag{D.117}$$
$$Y_{2|2} = Y_{2|1} \tag{D.118}$$

Prediction with Augmentation $t_2 \rightarrow t_3$

$$\hat{y}_{3|2} = \begin{bmatrix} 0_{1x1} \\ \hat{y}_{2|2_{3x1}} \end{bmatrix} = \begin{bmatrix} 0 \\ 0 \\ z_{g_1} \\ \eta_{s_0} \end{bmatrix} \tag{D.119}$$

$$Y_{3|2} = \begin{bmatrix} \boldsymbol{Q}_s^{-1} & -\boldsymbol{Q}_s^{-1}\boldsymbol{F}_s & 0 & 0 \\ -\boldsymbol{F}_s^{\top}\boldsymbol{Q}_s^{-1} & \boldsymbol{F}_s^{\top}\boldsymbol{Q}_s^{-1}\boldsymbol{F}_s & 0 & 0 \\ 0 & 0 & 0 & 0 \\ 0 & 0 & 0 & 0 \end{bmatrix} + \begin{bmatrix} 0 & 0 & 0 & 0 \\ 0 & & & \\ 0 & & \boldsymbol{Y}_{2|2} & \\ 0 & & & \end{bmatrix} \tag{D.120}$$

$$= \begin{bmatrix} \boldsymbol{Q}_s^{-1} & -\boldsymbol{Q}_s^{-1}\boldsymbol{F}_s & 0 & 0 \\ -\boldsymbol{F}_s^{\top}\boldsymbol{Q}_s^{-1} & \boldsymbol{F}_s^{\top}\boldsymbol{Q}_s^{-1}\boldsymbol{F}_s + \boldsymbol{Q}_s^{-1} & -\boldsymbol{Q}_s^{-1}\boldsymbol{F}_s & 0 \\ 0 & -\boldsymbol{F}_s^{\top}\boldsymbol{Q}_s^{-1} & \boldsymbol{F}_s^{\top}\boldsymbol{Q}_s^{-1}\boldsymbol{F}_s + \boldsymbol{Q}_s^{-1} + \boldsymbol{R}_g & -\boldsymbol{Q}_s^{-1}\boldsymbol{F}_s \\ 0 & 0 & -\boldsymbol{F}_s^{\top}\boldsymbol{Q}_s^{-1} & \boldsymbol{F}_s^{\top}\boldsymbol{Q}_s^{-1}\boldsymbol{F}_s + \Lambda_{s_0 s_0} \end{bmatrix} \tag{D.121}$$

D.7.2 Vehicle Filter

For the vehicle filter we will use the η and Λ variables for the information filter vector and matrix respectively. The ship and the vehicle start at t_0 but we assume that initially we only have knowledge of the vehicle state.

Initial Conditions

$$\eta_{0|v_0} = \eta_{v_0} \tag{D.122}$$
$$\Lambda_{0|v_0} = \Lambda_{v_0 v_0} \tag{D.123}$$

Vehicle-Only Prediction with Augmentation $t_0 \rightarrow t_1$

$$\eta_{1|v_0} = \begin{bmatrix} 0 \\ \eta_{v_0} \end{bmatrix} \tag{D.124}$$

$$\Lambda_{1|v_0} = \begin{bmatrix} \boldsymbol{Q}_v^{-1} & -\boldsymbol{Q}_v^{-1}\boldsymbol{F}_v \\ -\boldsymbol{F}_v^{\top}\boldsymbol{Q}_v^{-1} & \boldsymbol{F}_v^{\top}\boldsymbol{Q}_v^{-1}\boldsymbol{F}_v \end{bmatrix} + \begin{bmatrix} 0 & 0 \\ 0 & \Lambda_{v_0 v_0} \end{bmatrix} \tag{D.125}$$

$$= \begin{bmatrix} \boldsymbol{Q}_v^{-1} & -\boldsymbol{Q}_v^{-1}\boldsymbol{F}_v \\ -\boldsymbol{F}_v^{\top}\boldsymbol{Q}_v^{-1} & \boldsymbol{F}_v^{\top}\boldsymbol{Q}_v^{-1}\boldsymbol{F}_v + \Lambda_{v_0 v_0} \end{bmatrix} \tag{D.126}$$

Incorporate Initial Ship Data from Data Transmission at t_0

The ship information transmitted with the first range measurement is just the initial conditions of the ship:

$$\hat{y}_{0|0} = \eta_{s_0} \tag{D.127}$$
$$Y_{0|0} = \Lambda_{s_0 s_0}. \tag{D.128}$$

We add these new states to the vehicle filter:

$$\eta_{1|v_0,s_0} = \begin{bmatrix} \eta_{1|v_0{}_{2x1}} \\ \hat{y}_{0|0}{}_{1x1} \end{bmatrix} = \begin{bmatrix} 0 \\ \eta_{v_0} \\ \eta_{s_0} \end{bmatrix} \tag{D.129}$$

$$\Lambda_{1|v_0,s_0} = \begin{bmatrix} \Lambda_{1|v_0{}_{2x2}} & 0 \\ 0 & Y_{0|0}{}_{1x1} \end{bmatrix} \tag{D.130}$$

$$= \begin{bmatrix} \boldsymbol{Q}_v^{-1} & -\boldsymbol{Q}_v^{-1}\boldsymbol{F}_v & 0 \\ -\boldsymbol{F}_v^\top \boldsymbol{Q}_v^{-1} & \boldsymbol{F}_v^\top \boldsymbol{Q}_v^{-1}\boldsymbol{F}_v + \Lambda_{v_0v_0} & 0 \\ 0 & 0 & \Lambda_{s_0s_0} \end{bmatrix}. \tag{D.131}$$

After adding the ship states let

$$\eta_{1|0} = \eta_{1|v_0,s_0} \tag{D.132}$$

$$\Lambda_{1|0} = \Lambda_{1|v_0,s_0}. \tag{D.133}$$

Range Measurement at t_1

$$\eta_{1|z_{rng_1}} = \eta_{1|0} + H_{rng}^\top r_{rng}^{-1} z_{rng}(t_1) \tag{D.134}$$

$$= \begin{bmatrix} 0 \\ \eta_{v_0} \\ \eta_{s_0} \end{bmatrix} + \begin{bmatrix} z_{r_1} \\ 0 \\ -z_{r_1} \end{bmatrix}$$

$$= \begin{bmatrix} z_{r_1} \\ \eta_{v_0} \\ \eta_{s_0} - z_{r_1} \end{bmatrix} \tag{D.135}$$

where

$$z_{r_1} = \begin{bmatrix} 1 \\ 0 \end{bmatrix} \frac{z_{rng}(t_1)}{r_{rng}}. \tag{D.136}$$

$$\Lambda_{1|z_{rng_1}} = \Lambda_{1|0} + H_{rng}^\top r_{rng}^{-1} H_{rng} \tag{D.137}$$

$$= \Lambda_{1|0} + \begin{bmatrix} R_r & 0 & -R_r \\ 0 & 0 & 0 \\ -R_r & 0 & R_r \end{bmatrix}$$

$$= \begin{bmatrix} \boldsymbol{Q}_v^{-1} + \boldsymbol{R}_r & -\boldsymbol{Q}_v^{-1}\boldsymbol{F}_v & -\boldsymbol{R}_r \\ -\boldsymbol{F}_v^\top \boldsymbol{Q}_v^{-1} & \boldsymbol{F}_v^\top \boldsymbol{Q}_v^{-1}\boldsymbol{F}_v + \Lambda_{v_0v_0} & 0 \\ -\boldsymbol{R}_r & 0 & \Lambda_{s_0s_0} + \boldsymbol{R}_r \end{bmatrix} \tag{D.138}$$

where

$$R_r = \begin{bmatrix} \frac{1}{r_{rng}} & 0 \\ 0 & 0 \end{bmatrix}. \tag{D.139}$$

With all of the measurements incorporated for this time step, let

$$\eta_{1|1} = \eta_{1|z_{rng_1}} \tag{D.140}$$

$$\Lambda_{1|1} = \begin{bmatrix} \boldsymbol{\Lambda}_{1|1_{vv}} & \boldsymbol{\Lambda}_{1|1_{vs}} \\ \boldsymbol{\Lambda}_{1|1_{sv}} & \boldsymbol{\Lambda}_{1|1_{ss}} \end{bmatrix} = \Lambda_{1|z_{rng_1}}. \tag{D.141}$$

Vehicle-Only Prediction with Augmentation $t_1 \rightarrow t_2$

$$\eta_{2|v_1,s_0} = \begin{bmatrix} 0_{1x1} \\ \eta_{1|1_{3x1}} \end{bmatrix} = \begin{bmatrix} 0 \\ z_{r_1} \\ \eta_{v_0} \\ \eta_{s_0} - z_{r_1} \end{bmatrix} \tag{D.142}$$

$$\Lambda_{2|v_1,s_0} = \begin{bmatrix} \boldsymbol{Q}_v^{-1} & -\boldsymbol{Q}_v^{-1}\boldsymbol{F}_v & 0 & 0 \\ -\boldsymbol{F}_v^\top \boldsymbol{Q}_v^{-1} & \boldsymbol{F}_v^\top \boldsymbol{Q}_v^{-1}\boldsymbol{F}_v & 0 & 0 \\ 0 & 0 & 0 & 0 \\ 0 & 0 & 0 & 0 \end{bmatrix} + \begin{bmatrix} 0 & 0 & 0 & 0 \\ 0 & \boldsymbol{\Lambda}_{1|1_{vv}} & \boldsymbol{\Lambda}_{1|1_{vs}} \\ 0 & \boldsymbol{\Lambda}_{1|1_{sv}} & \boldsymbol{\Lambda}_{1|1_{ss}} \end{bmatrix} \tag{D.143}$$

$$= \begin{bmatrix} \boldsymbol{Q}_v^{-1} & -\boldsymbol{Q}_v^{-1}\boldsymbol{F}_v & 0 & 0 \\ -\boldsymbol{F}_v^\top \boldsymbol{Q}_v^{-1} & \boldsymbol{F}_v^\top \boldsymbol{Q}_v^{-1}\boldsymbol{F}_v + \boldsymbol{Q}_v^{-1} + \boldsymbol{R}_r & -\boldsymbol{Q}_v^{-1}\boldsymbol{F}_v & -\boldsymbol{R}_r \\ 0 & -\boldsymbol{F}_v^\top \boldsymbol{Q}_v^{-1} & \boldsymbol{F}_v^\top \boldsymbol{Q}_v^{-1}\boldsymbol{F}_v + \Lambda_{v_0 v_0} & 0 \\ 0 & -\boldsymbol{R}_r & 0 & \Lambda_{s_0 s_0} + \boldsymbol{R}_r \end{bmatrix} \tag{D.144}$$

For simplicity of notation let

$$\eta_{2|1} = \eta_{2|v_1,s_0} \tag{D.145}$$

$$\Lambda_{2|1} = \Lambda_{2|v_1,s_0}. \tag{D.146}$$

Marginalize out Vehicle State at t_0

We marginalize out the vehicle state at t_0 using equations (D.35) and (D.36),

$$\eta_{2|1}(\boldsymbol{x}_{v_2}, \boldsymbol{x}_{v_1}, \boldsymbol{x}_{s_0}) = \begin{bmatrix} 0 \\ z_{r_1} \\ \eta_{s_0} - z_{r_1} \end{bmatrix} - \begin{bmatrix} 0 \\ -\boldsymbol{Q}_v^{-1}\boldsymbol{F}_v \\ 0 \end{bmatrix} (\boldsymbol{F}_v^\top \boldsymbol{Q}_v^{-1}\boldsymbol{F}_v + \boldsymbol{\Lambda}_{v_0 v_0})^{-1} \eta_{v_0} \tag{D.147}$$

$$= \begin{bmatrix} 0 \\ \tilde{\eta}_{v_1} \\ \eta_{s_0} - z_{r_1} \end{bmatrix} \tag{D.148}$$

where

$$\tilde{\eta}_{v_1} = z_{r_1} + \boldsymbol{Q}_v^{-1}\boldsymbol{F}_v(\boldsymbol{F}_v^\top \boldsymbol{Q}_v^{-1}\boldsymbol{F}_v + \boldsymbol{\Lambda}_{v_0 v_0})^{-1}\eta_{v_0} \tag{D.149}$$

Similarly for the information matrix,

$$\Lambda_{2|1}(\boldsymbol{x}_{v_2}, \boldsymbol{x}_{v_1}, \boldsymbol{x}_{s_0}) = \begin{bmatrix} \boldsymbol{Q}_v^{-1} & -\boldsymbol{Q}_v^{-1}\boldsymbol{F}_v & 0 \\ -\boldsymbol{F}_v^\top \boldsymbol{Q}_v^{-1} & \boldsymbol{F}_v^\top \boldsymbol{Q}_v^{-1}\boldsymbol{F}_v + \boldsymbol{Q}_v^{-1} + \boldsymbol{R}_r & -\boldsymbol{R}_r \\ 0 & -\boldsymbol{R}_r & \Lambda_{s_0 s_0} + \boldsymbol{R}_r \end{bmatrix} - \begin{bmatrix} 0 \\ -\boldsymbol{Q}_s^{-1}\boldsymbol{F}_s \\ 0 \end{bmatrix} (\boldsymbol{F}_v^\top \boldsymbol{Q}_v^{-1}\boldsymbol{F}_v + \boldsymbol{\Lambda}_{v_0 v_0})^{-1} \begin{bmatrix} 0 & -\boldsymbol{F}_s^\top \boldsymbol{Q}_s^{-1} & 0 \end{bmatrix} \tag{D.150}$$

$$= \begin{bmatrix} \boldsymbol{Q}_v^{-1} & -\boldsymbol{Q}_v^{-1}\boldsymbol{F}_v & 0 \\ -\boldsymbol{F}_v^\top \boldsymbol{Q}_v^{-1} & \tilde{\boldsymbol{\Lambda}}_{v_1 v_1} & -\boldsymbol{R}_r \\ 0 & -\boldsymbol{R}_r & \Lambda_{s_0 s_0} + \boldsymbol{R}_r \end{bmatrix} \tag{D.151}$$

where

$$\tilde{\boldsymbol{\Lambda}}_{v_1 v_1} = \boldsymbol{F}_v^\top \boldsymbol{Q}_v^{-1}\boldsymbol{F}_v + \boldsymbol{Q}_v^{-1} + \boldsymbol{R}_r - \boldsymbol{Q}_v^{-1}\boldsymbol{F}_v(\boldsymbol{F}_v^\top \boldsymbol{Q}_v^{-1}\boldsymbol{F}_v + \Lambda_{v_0 v_0})^{-1}\boldsymbol{F}_v^\top \boldsymbol{Q}_v^{-1}. \tag{D.152}$$

Note: Unlike the centralized implementation we only have information for the ship state at t_0 at this time, so we must delay marginalizing out the ship state at t_1.

Vehicle Velocity Measurement at t_2

$$\begin{aligned}\eta_{2|z_{vel_2}} &= \eta_{2|1} + H_{vel}^{\top} r_{vel}^{-1} z_{vel}(t_2) && \text{(D.153)}\\ &= \begin{bmatrix} 0 \\ \tilde{\eta}_{v_1} \\ \eta_{s_0} - z_{r_1} \end{bmatrix} + \begin{bmatrix} \begin{bmatrix} 0 \\ 1 \end{bmatrix} \\ 0 \\ 0 \end{bmatrix} \frac{z_{vel}(t_2)}{r_{vel}} \\ &= \begin{bmatrix} 0 \\ \tilde{\eta}_{v_1} \\ \eta_{s_0} - z_{r_1} \end{bmatrix} + \begin{bmatrix} z_{v_2} \\ 0 \\ 0 \end{bmatrix} \\ &= \begin{bmatrix} z_{v_2} \\ \tilde{\eta}_{v_1} \\ \eta_{s_0} - z_{r_1} \end{bmatrix} && \text{(D.154)}\end{aligned}$$

where

$$z_{v_2} = \begin{bmatrix} 0 \\ 1 \end{bmatrix} \frac{z_{vel}(t_2)}{r_{vel}}. \tag{D.155}$$

$$\begin{aligned}\Lambda_{2|z_{vel_2}} &= \Lambda_{2|1} + H_{vel}^{\top} r_{vel}^{-1} H_{vel} && \text{(D.156)}\\ &= \Lambda_{2|1} + \begin{bmatrix} \begin{bmatrix} 0 \\ 1 \end{bmatrix} \\ 0 \\ 0 \end{bmatrix} r_{vel}^{-1} \begin{bmatrix} \begin{bmatrix} 0 & 1 \end{bmatrix} & 0 & 0 \end{bmatrix} \\ &= \Lambda_{2|1} + \begin{bmatrix} \begin{bmatrix} 0 & 0 \\ 0 & \frac{1}{r_{vel}} \end{bmatrix} & 0 & 0 \\ 0 & 0 & 0 \\ 0 & 0 & 0 \end{bmatrix} \\ &= \Lambda_{2|1} + \begin{bmatrix} R_v & 0 & 0 \\ 0 & 0 & 0 \\ 0 & 0 & 0 \end{bmatrix} \\ &= \begin{bmatrix} \boldsymbol{Q}_v^{-1} + \boldsymbol{R}_v & -\boldsymbol{Q}_v^{-1}\boldsymbol{F}_v & 0 \\ -\boldsymbol{F}_v^{\top}\boldsymbol{Q}_v^{-1} & \tilde{\boldsymbol{\Lambda}}_{v_1 v_1} & -\boldsymbol{R}_r \\ 0 & -\boldsymbol{R}_r & \Lambda_{s_0 s_0} + \boldsymbol{R}_r \end{bmatrix} && \text{(D.157)}\end{aligned}$$

where

$$R_v = \begin{bmatrix} 0 & 0 \\ 0 & \frac{1}{r_{vel}} \end{bmatrix} \tag{D.158}$$

With all of the measurements incorporated for this time step, let

$$\eta_{2|2} = \eta_{2|z_{vel_2}} \tag{D.159}$$

$$\Lambda_{2|2} = \begin{bmatrix} \boldsymbol{\Lambda}_{2|2_{vv}} & \boldsymbol{\Lambda}_{2|2_{vs}} \\ \boldsymbol{\Lambda}_{2|2_{sv}} & \boldsymbol{\Lambda}_{2|2_{ss}} \end{bmatrix} \Lambda_{2|z_{vel_2}}. \tag{D.160}$$

Vehicle-Only Prediction with Augmentation $t_2 \rightarrow t_3$

$$\eta_{3|v_2,s_0} = \begin{bmatrix} 0_{1x1} \\ \eta_{2|2_{3x1}} \end{bmatrix} = \begin{bmatrix} 0 \\ z_{v_2} \\ \tilde{\eta}_{v_1} \\ \eta_{s_0} - z_{r_1} \end{bmatrix} \tag{D.161}$$

$$\Lambda_{3|v_2,s_0} = \begin{bmatrix} \boldsymbol{Q}_v^{-1} & -\boldsymbol{Q}_v^{-1}\boldsymbol{F}_v & 0 & 0 \\ -\boldsymbol{F}_v^\top \boldsymbol{Q}_v^{-1} & \boldsymbol{F}_v^\top \boldsymbol{Q}_v^{-1}\boldsymbol{F}_v & 0 & 0 \\ 0 & 0 & 0 & 0 \\ 0 & 0 & 0 & 0 \end{bmatrix} + \begin{bmatrix} 0 & 0 & 0 & 0 \\ 0 & \boldsymbol{\Lambda}_{2|2_{vv}} & \boldsymbol{\Lambda}_{2|2_{vs}} \\ 0 & \boldsymbol{\Lambda}_{2|2_{sv}} & \boldsymbol{\Lambda}_{2|2_{ss}} \end{bmatrix} \tag{D.162}$$

$$= \begin{bmatrix} \boldsymbol{Q}_v^{-1} & -\boldsymbol{Q}_v^{-1}\boldsymbol{F}_v & 0 & 0 \\ -\boldsymbol{F}_v^\top \boldsymbol{Q}_v^{-1} & \boldsymbol{F}_v^\top \boldsymbol{Q}_v^{-1}\boldsymbol{F}_v + \boldsymbol{Q}_v^{-1} + \boldsymbol{R}_v & -\boldsymbol{Q}_v^{-1}\boldsymbol{F}_v & 0 \\ 0 & -\boldsymbol{F}_v^\top \boldsymbol{Q}_v^{-1} & \Lambda_{v_1 v_1} & -\boldsymbol{R}_r \\ 0 & 0 & -\boldsymbol{R}_r & \Lambda_{s_0 s_0} + \boldsymbol{R}_r \end{bmatrix} \tag{D.163}$$

Incorporate Delta Ship Data t_0 to t_2 from Data Transmission at t_2

The ship information transmitted with the second range measurement is the change in the ship state from t_0 to t_2, taking into account conformability.

$$\Delta\hat{y} = \hat{y}_{2|2} - \begin{bmatrix} 0 \\ 0 \\ \hat{y}_{0|0} \end{bmatrix} \tag{D.164}$$

$$= \begin{bmatrix} 0 \\ z_{g_1} \\ \eta_{s_0} \end{bmatrix} - \begin{bmatrix} 0 \\ 0 \\ \eta_{s_0} \end{bmatrix} \tag{D.165}$$

$$= \begin{bmatrix} 0 \\ z_{g_1} \\ 0 \end{bmatrix} \tag{D.166}$$

$$\Delta Y = Y_{2|2} - \begin{bmatrix} 0 & 0 & 0 \\ 0 & 0 & 0 \\ 0 & 0 & Y_{0|0} \end{bmatrix} \tag{D.167}$$

$$= \begin{bmatrix} \boldsymbol{Q}_s^{-1} & -\boldsymbol{Q}_s^{-1}\boldsymbol{F}_s & 0 \\ -\boldsymbol{F}_s^\top \boldsymbol{Q}_s^{-1} & \boldsymbol{F}_s^\top \boldsymbol{Q}_s^{-1}\boldsymbol{F}_s + \boldsymbol{Q}_s^{-1} + \boldsymbol{R}_g & -\boldsymbol{Q}_s^{-1}\boldsymbol{F}_s \\ 0 & -\boldsymbol{F}_s^\top \boldsymbol{Q}_s^{-1} & \boldsymbol{F}_s^\top \boldsymbol{Q}_s^{-1}\boldsymbol{F}_s + \Lambda_{s_0 s_0} \end{bmatrix} - \begin{bmatrix} 0 & 0 & 0 \\ 0 & 0 & 0 \\ 0 & 0 & \Lambda_{s_0 s_0} \end{bmatrix} \tag{D.168}$$

$$= \begin{bmatrix} \boldsymbol{Q}_s^{-1} & -\boldsymbol{Q}_s^{-1}\boldsymbol{F}_s & 0 \\ -\boldsymbol{F}_s^\top \boldsymbol{Q}_s^{-1} & \boldsymbol{F}_s^\top \boldsymbol{Q}_s^{-1}\boldsymbol{F}_s + \boldsymbol{Q}_s^{-1} + \boldsymbol{R}_g & -\boldsymbol{Q}_s^{-1}\boldsymbol{F}_s \\ 0 & -\boldsymbol{F}_s^\top \boldsymbol{Q}_s^{-1} & \boldsymbol{F}_s^\top \boldsymbol{Q}_s^{-1}\boldsymbol{F}_s \end{bmatrix} \tag{D.169}$$

The delta ship states are added to the vehicle filter, again taking info account conformability.

$$\begin{aligned}\eta_{3|v_2,s_2} &= \begin{bmatrix} 1 & 0 & 0 & 0 \\ 0 & 1 & 0 & 0 \\ 0 & 0 & 1 & 0 \\ 0 & 0 & 0 & 0 \\ 0 & 0 & 0 & 1 \end{bmatrix} \eta_{3|v_2,s_0} + \begin{bmatrix} 0 \\ 0 \\ 0 \\ \Delta\hat{y}_{3x1} \end{bmatrix} \\ &= \begin{bmatrix} 0 \\ z_{v_2} \\ \tilde{\eta}_{v_1} \\ 0 \\ \eta_{s_0} - z_{r_1} \end{bmatrix} + \begin{bmatrix} 0 \\ 0 \\ 0 \\ 0 \\ z_{g_1} \\ 0 \end{bmatrix} \\ &= \begin{bmatrix} 0 \\ z_{v_2} \\ \tilde{\eta}_{v_1} \\ 0 \\ z_{g_1} \\ \eta_{s_0} - z_{r_1} \end{bmatrix}\end{aligned} \tag{D.170}$$

$$\Lambda_{3|v_2,s_2} = \begin{bmatrix} 1 & 0 & 0 & 0 \\ 0 & 1 & 0 & 0 \\ 0 & 0 & 1 & 0 \\ 0 & 0 & 0 & 0 \\ 0 & 0 & 0 & 0 \\ 0 & 0 & 0 & 1 \end{bmatrix} \Lambda_{3|v_2,s_0} \begin{bmatrix} 1 & 0 & 0 & 0 & 0 & 0 \\ 0 & 1 & 0 & 0 & 0 & 0 \\ 0 & 0 & 1 & 0 & 0 & 0 \\ 0 & 0 & 0 & 0 & 0 & 1 \end{bmatrix} + \begin{bmatrix} 0 & 0 & 0 & 0 & 0 & 0 \\ 0 & 0 & 0 & 0 & 0 & 0 \\ 0 & 0 & 0 & 0 & 0 & 0 \\ 0 & 0 & 0 & & & \\ 0 & 0 & 0 & & \Delta Y & \\ 0 & 0 & 0 & & & \end{bmatrix} \tag{D.171}$$

$$\begin{aligned}&= \begin{bmatrix} \boldsymbol{Q}_v^{-1} & -\boldsymbol{Q}_v^{-1}\boldsymbol{F}_v & 0 & 0 & 0 & 0 \\ -\boldsymbol{F}_v^\top\boldsymbol{Q}_v^{-1} & \boldsymbol{F}_v^\top\boldsymbol{Q}_v^{-1}\boldsymbol{F}_v + \boldsymbol{Q}_v^{-1} + \boldsymbol{R}_v & -\boldsymbol{Q}_v^{-1}\boldsymbol{F}_v & 0 & 0 & 0 \\ 0 & -\boldsymbol{F}_v^\top\boldsymbol{Q}_v^{-1} & \tilde{\Lambda}_{v_1v_1} & 0 & 0 & -\boldsymbol{R}_r \\ 0 & 0 & 0 & 0 & 0 & 0 \\ 0 & 0 & 0 & 0 & 0 & 0 \\ 0 & 0 & -\boldsymbol{R}_r & 0 & 0 & \Lambda_{s_0s_0} + \boldsymbol{R}_r \end{bmatrix} \\ &\quad + \begin{bmatrix} 0 & 0 & 0 & 0 & 0 & 0 \\ 0 & 0 & 0 & 0 & 0 & 0 \\ 0 & 0 & 0 & 0 & 0 & 0 \\ 0 & 0 & 0 & \boldsymbol{Q}_s^{-1} & -\boldsymbol{Q}_s^{-1}\boldsymbol{F}_s & 0 \\ 0 & 0 & 0 & -\boldsymbol{F}_s^\top\boldsymbol{Q}_s^{-1} & \boldsymbol{F}_s^\top\boldsymbol{Q}_s^{-1}\boldsymbol{F}_s + \boldsymbol{Q}_s^{-1} + \boldsymbol{R}_g & -\boldsymbol{Q}_s^{-1}\boldsymbol{F}_s \\ 0 & 0 & 0 & 0 & -\boldsymbol{F}_s^\top\boldsymbol{Q}_s^{-1} & \boldsymbol{F}_s^\top\boldsymbol{Q}_s^{-1}\boldsymbol{F}_s \end{bmatrix} \\ &= \begin{bmatrix} \boldsymbol{Q}_v^{-1} & -\boldsymbol{Q}_v^{-1}\boldsymbol{F}_v & 0 & & \\ -\boldsymbol{F}_v^\top\boldsymbol{Q}_v^{-1} & \boldsymbol{F}_v^\top\boldsymbol{Q}_v^{-1}\boldsymbol{F}_v + \boldsymbol{Q}_v^{-1} + \boldsymbol{R}_v & -\boldsymbol{Q}_v^{-1}\boldsymbol{F}_v & & \\ 0 & -\boldsymbol{F}_v^\top\boldsymbol{Q}_v^{-1} & \tilde{\Lambda}_{v_1v_1} & \cdots & \\ 0 & 0 & 0 & & \\ 0 & 0 & 0 & & \\ 0 & 0 & -\boldsymbol{R}_r & & \end{bmatrix} \\ &\qquad \begin{bmatrix} 0 & 0 & 0 \\ 0 & 0 & 0 \\ \cdots & 0 & 0 & -\boldsymbol{R}_r \\ \boldsymbol{Q}_s^{-1} & -\boldsymbol{Q}_s^{-1}\boldsymbol{F}_s & 0 \\ -\boldsymbol{F}_s^\top\boldsymbol{Q}_s^{-1} & \boldsymbol{F}_s^\top\boldsymbol{Q}_s^{-1}\boldsymbol{F}_s + \boldsymbol{Q}_s^{-1} + \boldsymbol{R}_g & -\boldsymbol{Q}_s^{-1}\boldsymbol{F}_s \\ 0 & -\boldsymbol{F}_s^\top\boldsymbol{Q}_s^{-1} & \boldsymbol{F}_s^\top\boldsymbol{Q}_s^{-1}\boldsymbol{F}_s + \Lambda_{s_0s_0} + \boldsymbol{R}_r \end{bmatrix}\end{aligned} \tag{D.172}$$

Again for ease of notation, after adding the ship states let

$$\eta_{3|2} = \eta_{3|v_2,s_2} \tag{D.173}$$
$$\Lambda_{3|2} = \Lambda_{3|v_2,s_2}. \tag{D.174}$$

Marginalize out Ship State at t_1

Now we are able to marginalize out the ship state at t_1 using equations (D.35) and (D.36),

$$\eta_{3|2}(\boldsymbol{x}_{v_3}, \boldsymbol{x}_{v_2}, \boldsymbol{x}_{v_1}, \boldsymbol{x}_{s_2}, \boldsymbol{x}_{s_0}) = \begin{bmatrix} 0 \\ z_{v_2} \\ \tilde{\eta}_{v_1} \\ 0 \\ \eta_{s_0} - z_{r_1} \end{bmatrix} - \begin{bmatrix} 0 \\ 0 \\ 0 \\ -\boldsymbol{Q}_s^{-1}\boldsymbol{F}_s \\ -\boldsymbol{F}_s^\top \boldsymbol{Q}_s^{-1} \end{bmatrix} (\boldsymbol{F}_s^\top \boldsymbol{Q}_s^{-1} \boldsymbol{F}_s + \boldsymbol{Q}_s^{-1} + \boldsymbol{R}_g)^{-1} z_{g_1} \tag{D.175}$$

$$= \begin{bmatrix} 0 \\ z_{v_2} \\ \tilde{\eta}_{v_1} \\ \tilde{\eta}_{s_2} \\ \tilde{\eta}_{s_0} \end{bmatrix} \tag{D.176}$$

where $\tilde{\eta}_{v_1}$ was defined in equation (D.149) and

$$\tilde{\eta}_{s_2} = \boldsymbol{Q}_s^{-1}\boldsymbol{F}_s(\boldsymbol{F}_s^\top \boldsymbol{Q}_s^{-1}\boldsymbol{F}_s + \boldsymbol{Q}_s^{-1} + \boldsymbol{R}_g)^{-1} z_{g_1} \tag{D.177}$$
$$\tilde{\eta}_{s_0} = \eta_{s_0} - z_{r_1} + \boldsymbol{F}_s^\top \boldsymbol{Q}_s^{-1}(\boldsymbol{F}_s^\top \boldsymbol{Q}_s^{-1}\boldsymbol{F}_s + \boldsymbol{Q}_s^{-1} + \boldsymbol{R}_g)^{-1} z_{g_1}. \tag{D.178}$$

Similarly for the information matrix,

$$\begin{aligned}
&\Lambda_{3|2}(\boldsymbol{x}_{v_3}, \boldsymbol{x}_{v_2}, \boldsymbol{x}_{v_1}, \boldsymbol{x}_{s_2}, \boldsymbol{x}_{s_0}) = \\
&\begin{bmatrix} \boldsymbol{Q}_v^{-1} & -\boldsymbol{Q}_v^{-1}\boldsymbol{F}_v & 0 & 0 & 0 \\ -\boldsymbol{F}_v^\top \boldsymbol{Q}_v^{-1} & \boldsymbol{F}_v^\top \boldsymbol{Q}_v^{-1}\boldsymbol{F}_v + \boldsymbol{Q}_v^{-1} + \boldsymbol{R}_v & -\boldsymbol{Q}_v^{-1}\boldsymbol{F}_v & 0 & 0 \\ 0 & -\boldsymbol{F}_v^\top \boldsymbol{Q}_v^{-1} & \tilde{\Lambda}_{v_1 v_1} & 0 & -\boldsymbol{R}_r \\ 0 & 0 & 0 & \boldsymbol{Q}_s^{-1} & 0 \\ 0 & 0 & -\boldsymbol{R}_r & 0 & \boldsymbol{F}_s^\top \boldsymbol{Q}_s^{-1}\boldsymbol{F}_s + \Lambda_{s_0 s_0} + \boldsymbol{R}_r \end{bmatrix} \\
&\quad - \begin{bmatrix} 0 \\ 0 \\ 0 \\ -\boldsymbol{Q}_s^{-1}\boldsymbol{F}_s \\ -\boldsymbol{F}_s^\top \boldsymbol{Q}_s^{-1} \end{bmatrix} (\boldsymbol{F}_s^\top \boldsymbol{Q}_s^{-1} \boldsymbol{F}_s + \boldsymbol{Q}_s^{-1} + \boldsymbol{R}_g)^{-1} \begin{bmatrix} 0 & 0 & 0 & -\boldsymbol{F}_s^\top \boldsymbol{Q}_s^{-1} & -\boldsymbol{Q}_s^{-1}\boldsymbol{F}_s \end{bmatrix} \\
&\qquad = \begin{bmatrix} \boldsymbol{Q}_v^{-1} & -\boldsymbol{Q}_v^{-1}\boldsymbol{F}_v & 0 & 0 & 0 \\ -\boldsymbol{F}_v^\top \boldsymbol{Q}_v^{-1} & \boldsymbol{F}_v^\top \boldsymbol{Q}_v^{-1}\boldsymbol{F}_v + \boldsymbol{Q}_v^{-1} + \boldsymbol{R}_v & -\boldsymbol{Q}_v^{-1}\boldsymbol{F}_v & 0 & 0 \\ 0 & -\boldsymbol{F}_v^\top \boldsymbol{Q}_v^{-1} & \tilde{\Lambda}_{v_1 v_1} & 0 & -\boldsymbol{R}_r \\ 0 & 0 & 0 & \tilde{\boldsymbol{\Lambda}}_{s_2 s_2} & \tilde{\boldsymbol{\Lambda}}_{s_2 s_0} \\ 0 & 0 & -\boldsymbol{R}_r & \tilde{\boldsymbol{\Lambda}}_{s_0 s_2} & \tilde{\boldsymbol{\Lambda}}_{s_0 s_0} \end{bmatrix}
\end{aligned} \tag{D.179}$$

where $\tilde{\boldsymbol{\Lambda}}_{v_1 v_1}$ was defined in equation (D.152) and

$$\tilde{\boldsymbol{\Lambda}}_{s_2 s_2} = \boldsymbol{Q}_s^{-1} - \boldsymbol{Q}_s^{-1}\boldsymbol{F}_s(\boldsymbol{F}_s^\top \boldsymbol{Q}_s^{-1}\boldsymbol{F}_s + \boldsymbol{Q}_s^{-1} + \boldsymbol{R}_g)^{-1}\boldsymbol{F}_s^\top \boldsymbol{Q}_s^{-1} \tag{D.180}$$

$$\tilde{\boldsymbol{\Lambda}}_{s_2 s_0} = -\boldsymbol{Q}_s^{-1}\boldsymbol{F}_s(\boldsymbol{F}_s^\top \boldsymbol{Q}_s^{-1}\boldsymbol{F}_s + \boldsymbol{Q}_s^{-1} + \boldsymbol{R}_g)^{-1}\boldsymbol{Q}_s^{-1}\boldsymbol{F}_s \tag{D.181}$$

$$\tilde{\boldsymbol{\Lambda}}_{s_0 s_2} = -\boldsymbol{F}_s^\top \boldsymbol{Q}_s^{-1}(\boldsymbol{F}_s^\top \boldsymbol{Q}_s^{-1}\boldsymbol{F}_s + \boldsymbol{Q}_s^{-1} + \boldsymbol{R}_g)^{-1}\boldsymbol{F}_s^\top \boldsymbol{Q}_s^{-1} \tag{D.182}$$

$$\tilde{\boldsymbol{\Lambda}}_{s_0 s_0} = \boldsymbol{F}_s^\top \boldsymbol{Q}_s^{-1}\boldsymbol{F}_s + \Lambda_{s_0 s_0} + \boldsymbol{R}_r - \boldsymbol{F}_s^\top \boldsymbol{Q}_s^{-1}(\boldsymbol{F}_s^\top \boldsymbol{Q}_s^{-1}\boldsymbol{F}_s + \boldsymbol{Q}_s^{-1} + \boldsymbol{R}_g)^{-1}\boldsymbol{Q}_s^{-1}\boldsymbol{F}_s \tag{D.183}$$

Range Measurement at t_3

$$\eta_{3|z_{rng_3}} = \eta_{3|2} + H_{rng}^\top r_{rng}^{-1} z_{rng}(t_3) \tag{D.184}$$

$$= \begin{bmatrix} 0 \\ z_{v_2} \\ \tilde{\eta}_{v_1} \\ \tilde{\eta}_{s_2} \\ \tilde{\eta}_{s_0} \end{bmatrix} + \begin{bmatrix} z_{r_3} \\ 0 \\ 0 \\ -z_{r_3} \\ 0 \end{bmatrix}$$

$$= \begin{bmatrix} z_{r_3} \\ z_{v_2} \\ \tilde{\eta}_{v_1} \\ \tilde{\eta}_{s_2} - z_{r_3} \\ \tilde{\eta}_{s_0} \end{bmatrix} \tag{D.185}$$

where we define $z_{r_3} = \begin{bmatrix} 1 \\ 0 \end{bmatrix} \frac{z_{rng}(t_3)}{r_{rng}}$. Similarly for the information matrix,

$$\Lambda_{3|z_{rng_3}} = \Lambda_{3|2} + H_{rng}^\top r_{rng}^{-1} H_{rng} \tag{D.186}$$

$$= \Lambda_{3|2} + \begin{bmatrix} R_r & 0 & 0 & -R_r & 0 \\ 0 & 0 & 0 & 0 & 0 \\ 0 & 0 & 0 & 0 & 0 \\ -R_r & 0 & 0 & R_r & 0 \\ 0 & 0 & 0 & 0 & 0 \end{bmatrix}$$

$$= \begin{bmatrix} \boldsymbol{Q}_v^{-1} + \boldsymbol{R}_r & -\boldsymbol{Q}_v^{-1}\boldsymbol{F}_v & 0 & -\boldsymbol{R}_r & 0 \\ -\boldsymbol{F}_v^\top \boldsymbol{Q}_v^{-1} & \boldsymbol{F}_v^\top \boldsymbol{Q}_v^{-1}\boldsymbol{F}_v + \boldsymbol{Q}_v^{-1} + \boldsymbol{R}_v & -\boldsymbol{Q}_v^{-1}\boldsymbol{F}_v & 0 & 0 \\ 0 & -\boldsymbol{F}_v^\top \boldsymbol{Q}_v^{-1} & \tilde{\boldsymbol{\Lambda}}_{v_1 v_1} & 0 & -\boldsymbol{R}_r \\ -\boldsymbol{R}_r & 0 & 0 & \tilde{\boldsymbol{\Lambda}}_{s_2 s_2} + \boldsymbol{R}_r & \tilde{\boldsymbol{\Lambda}}_{s_2 s_0} \\ 0 & 0 & -\boldsymbol{R}_r & \tilde{\boldsymbol{\Lambda}}_{s_0 s_2} & \tilde{\boldsymbol{\Lambda}}_{s_0 s_0} \end{bmatrix} \tag{D.187}$$

where we define $R_r = \begin{bmatrix} \frac{1}{r_{rng}} & 0 \\ 0 & 0 \end{bmatrix}$.

Once all of the measurements are incorporated for this time step, let

$$\eta_{3|3} = \eta_{3|z_{rng_3}} \tag{D.188}$$

$$\Lambda_{3|3} = \Lambda_{3|z_{rng_3}}. \tag{D.189}$$

Marginalize out $\boldsymbol{x}_s(t_0)$, Ship State at t_0

We will now marginalize out the ship state at t_0. This will illustrate what happens when a state associated with a range measurement is marginalized out.

Using equations (D.35) and (D.36),

$$\eta_{3|3}(\boldsymbol{x}_{v_3}, \boldsymbol{x}_{v_2}, \boldsymbol{x}_{v_1}, \boldsymbol{x}_{s_2}) = \begin{bmatrix} z_{r_3} \\ z_{v_2} \\ \tilde{\eta}_{v_1} \\ \tilde{\eta}_{s_2} - z_{r_3} \end{bmatrix} - \begin{bmatrix} 0 \\ 0 \\ -\boldsymbol{R}_r \\ \tilde{\boldsymbol{\Lambda}}_{s_2 s_0} \end{bmatrix} \tilde{\boldsymbol{\Lambda}}_{s_0 s_0}^{-1} \tilde{\eta}_{s_0} \tag{D.190}$$

$$= \begin{bmatrix} z_{r_3} \\ z_{v_2} \\ \hat{\eta}_{v_1} \\ \hat{\eta}_{s_2} \end{bmatrix} \tag{D.191}$$

where

$$\hat{\eta}_{v_1} = \tilde{\eta}_{v_1} + \boldsymbol{R}_r \tilde{\boldsymbol{\Lambda}}_{s_0 s_0}^{-1} \tilde{\eta}_{s_0} \tag{D.192}$$

$$\hat{\eta}_{s_2} = \tilde{\eta}_{s_2} - z_{r_3} - \tilde{\boldsymbol{\Lambda}}_{s_2 s_0} \tilde{\boldsymbol{\Lambda}}_{s_0 s_0}^{-1} \tilde{\eta}_{s_0}. \tag{D.193}$$

Similarly for the information matrix,

$$\Lambda_{3|3}(\boldsymbol{x}_{v_3}, \boldsymbol{x}_{v_2}, \boldsymbol{x}_{v_1}, \boldsymbol{x}_{s_2}) = \begin{bmatrix} \boldsymbol{Q}_v^{-1} + \boldsymbol{R}_r & -\boldsymbol{Q}_v^{-1}\boldsymbol{F}_v & 0 & -\boldsymbol{R}_r \\ -\boldsymbol{F}_v^\top \boldsymbol{Q}_v^{-1} & \boldsymbol{F}_v^\top \boldsymbol{Q}_v^{-1}\boldsymbol{F}_v + \boldsymbol{Q}_v^{-1} + \boldsymbol{R}_v & -\boldsymbol{Q}_v^{-1}\boldsymbol{F}_v & 0 \\ 0 & -\boldsymbol{F}_v^\top \boldsymbol{Q}_v^{-1} & \tilde{\boldsymbol{\Lambda}}_{v_1 v_1} & 0 \\ -\boldsymbol{R}_r & 0 & 0 & \tilde{\boldsymbol{\Lambda}}_{s_2 s_2} + \boldsymbol{R}_r \end{bmatrix}$$
$$- \begin{bmatrix} 0 \\ 0 \\ -\boldsymbol{R}_r \\ 0 \\ \tilde{\boldsymbol{\Lambda}}_{s_2 s_0} \end{bmatrix} \tilde{\boldsymbol{\Lambda}}_{s_0 s_0}^{-1} \begin{bmatrix} 0 & 0 & -\boldsymbol{R}_r & 0 & \tilde{\boldsymbol{\Lambda}}_{s_0 s_2} \end{bmatrix} \tag{D.194}$$

$$= \begin{bmatrix} \boldsymbol{Q}_v^{-1} + \boldsymbol{R}_r & -\boldsymbol{Q}_v^{-1}\boldsymbol{F}_v & 0 & -\boldsymbol{R}_r \\ -\boldsymbol{F}_v^\top \boldsymbol{Q}_v^{-1} & \boldsymbol{F}_v^\top \boldsymbol{Q}_v^{-1}\boldsymbol{F}_v + \boldsymbol{Q}_v^{-1} + \boldsymbol{R}_v & -\boldsymbol{Q}_v^{-1}\boldsymbol{F}_v & 0 \\ 0 & -\boldsymbol{F}_v^\top \boldsymbol{Q}_v^{-1} & \hat{\boldsymbol{\Lambda}}_{v_1 v_1} & \hat{\boldsymbol{R}}_{r_{v_1 s_0}} \\ -\boldsymbol{R}_r & 0 & \hat{\boldsymbol{R}}_{r_{s_0 v_1}} & \hat{\boldsymbol{\Lambda}}_{s_2 s_2} \end{bmatrix} \tag{D.195}$$

where

$$\hat{\boldsymbol{\Lambda}}_{v_1 v_1} = \tilde{\boldsymbol{\Lambda}}_{v_1 v_1} - \boldsymbol{R}_r \tilde{\boldsymbol{\Lambda}}_{s_0 s_0}^{-1} \boldsymbol{R}_r \tag{D.196}$$

$$\hat{\boldsymbol{\Lambda}}_{s_2 s_2} = \tilde{\boldsymbol{\Lambda}}_{s_2 s_2} + \boldsymbol{R}_r - \tilde{\boldsymbol{\Lambda}}_{s_2 s_0} \tilde{\boldsymbol{\Lambda}}_{s_2 s_2}^{-1} \tilde{\boldsymbol{\Lambda}}_{s_0 s_2} \tag{D.197}$$

$$\hat{\boldsymbol{R}}_{r_{v_1 s_0}} = \boldsymbol{R}_r \tilde{\boldsymbol{\Lambda}}_{s_0 s_0}^{-1} \tilde{\boldsymbol{\Lambda}}_{s_0 s_2} \tag{D.198}$$

$$\hat{\boldsymbol{R}}_{r_{s_0 v_1}} = \tilde{\boldsymbol{\Lambda}}_{s_2 s_0} \tilde{\boldsymbol{\Lambda}}_{s_0 s_0}^{-1} \boldsymbol{R}_r. \tag{D.199}$$

D.8 Comparison of Decentralized versus Centralized Results

Comparing the centralized results for η and Λ at t_3 after marginalizing out the ship state, (D.94) and (D.97), to the decentralized results, (D.191) and (D.195), we see that the vehicle estimates are identical. The ship estimates are not identical because the decentralized results do not have an estimate for the current ship state, i.e. the ship state at t_3, but instead only have an estimate of the ship state up to t_2, where t_2 is the time that the last range measurement was sent. However, if you compare the ship state estimate at t_3 in the decentralized results *before* the range measurement and *before* the ship state a t_0 is marginalized out, equations (D.176) and (D.179), to the ship state estimate at t_2 in the centralized results, equations (D.71) and (D.74), as expected the ship state estimates are identical. These results indicate that for a linear system with linear measurements we are able to locally recreate an exact replica of the centralized estimate of vehicle state at every time step. In addition, we are able to locally recreate an exact replica of the centralized estimate of ship state up to the time that the last range measurement was sent.

Bibliography

[1] J. C. Alleyne, "Position estimation from range only measurements," Master's thesis, Naval Postgraduate School, Monterey, California, 2000.

[2] *POS MV (Position and Orientation Systems for Marine Vessels)*, Applanix, Richmond Hill, ON, Canada, Nov. 2008, http://www.applanix.com/media/downloads/products/specs/ posmv_datasheet.pdf.

[3] P. Baccou and B. Jouvencel, "Homing and navigation using one transponder for AUV, postprocessing comparisons results with long base-line navigation," in *Proc. IEEE Int. Conf. Robot. Auto. (ICRA)*, vol. 4, 2002, pp. 4004–4009.

[4] ——, "Simulation results, post-processing experimentations and comparisons results for navigation, homing and multiple vehicles operations with a new positioning method using on transponder," in *Proc. IEEE/RSJ Intl. Conf. Intell. Robots Systems (IROS)*, vol. 1, Oct. 2003, pp. 811–817.

[5] A. Bahr, "Cooperative localization for autonomous underwater vehicles," Ph.D. dissertation, Massachusetts Institute of Technology, Cambridge, MA, USA, February 2009.

[6] A. Bahr and J. Leonard, "Cooperative localization for autonomous underwater vehicles," in *Proc. 10th International Symposium on Experimental Robotics (ISER)*, Rio de Janeiro, Brasil, July 2006, pp. 387–395.

[7] R. Ballard, W. Bryan, H. Dick, K. Emery, G. Thompson, E. Uchupi, K. Davis, J. De Boer, S. DeLong, P. Fox *et al.*, "Geological and geophysical investigation of the Midcayman Rise Spreading Center: initial results and observations," *Deep Drilling Results in the Atlantic Ocean: Ocean Crust: Washington (Am. Geophys. Union)*, pp. 66–93, 1979.

[8] Y. Bar-Shalom, X. Rong Li, and T. Kirubarajan, *Estimation with applications to tracking and navigation*. New York: John Wiley & Sons, Inc., 2001.

[9] J.-L. Blanco, J.-A. Fernandez-Madrigal, and J. Gonzalez, "Efficient probabilistic range-only slam," in *Proc. IEEE/RSJ Intl. Conf. Intell. Robots Systems (IROS)*, Sept. 2008, pp. 1017–1022.

[10] J.-L. Blanco, J. Gonzalez, and J.-A. Fernandez-Madrigal, "A pure probabilistic approach to range-only SLAM," in *Proc. IEEE Int. Conf. Robot. Auto. (ICRA)*, May 2008, pp. 1436–1441.

[11] N. Bowditch, *The new American practical navigator*, 1st ed. Newburyport, MA: Edward M. Blunt, 1802.

[12] A. D. Bowen, D. R. Yoerger, C. Taylor, R. McCabe, J. Howland, D. Gomez-Ibanez, J. C. Kinsey, M. Heintz, G. McDonald, D. Peters, J. Bailey, T. Shank, L. L. Whitcomb, S. C. Martin, S. E. Webster, M. V. Jakuba, C. Young, J. Buescher, B. Fletcher, P. Fryer, and S. Hulme, "Field trials of the *Nereus* hybrid underwater robotic vehicle in the Challenger Deep of the Mariana Trench," in *Proc. IEEE/MTS OCEANS Conf. Exhib.*, Biloxi, MS, Oct 2009, In Press.

[13] A. D. Bowen, D. R. Yoerger, C. Taylor, R. McCabe, J. Howland, D. Gomez-Ibanez, J. C. Kinsey, M. Heintz, G. McDonald, D. B. Peters, B. Fletcher, C. Young, J. Buescher, L. L. Whitcomb, S. C. Martin, S. E. Webster, and M. V. Jakuba, "The *Nereus* hybrid underwater robotic vehicle," *Underwater Technology: The International Journal of the Society for Underwater Technology*, vol. 28, no. 3, pp. 79–89, 2009.

[14] ——, "The *Nereus* hybrid underwater robotic vehicle for global ocean science operations to 11,000m depth," in *Proc. IEEE/MTS OCEANS Conf. Exhib.*, Quebec, Sept 2008.

[15] M. Bozorg, E. Nebot, and H. Durrant-Whyte, "A decentralised navigation architecture," in *Proc. IEEE Int. Conf. Robot. Auto. (ICRA)*, vol. 4, May 1998, pp. 3413–3418 vol.4.

[16] G. Calafiore, "Reliable localization using set-valued nonlinear filters," *IEEE Transactions on systems, man and cybernetics*, vol. 35, pp. 189–197, Mar. 2005.

[17] A. Carof, "Acoustic differential delay and Doppler tracking system for long range AUV positioning and guidance," in *Autonomous Underwater Vehicle Technology, 1994. AUV '94., Proceedings of the 1994 Symposium on*, 19-20 Jul 1994, pp. 370–375.

[18] T. Casey, B. Guimond, and J. Hu, "Underwater vehicle positioning based on time of arrival measurements from a single beacon," in *Proc. IEEE/MTS OCEANS Conf. Exhib.*, Vancouver, BC, Sep. 2007, pp. 1–8.

[19] *C-Nav2000*, C&C Technologies, Lafayette, LA, USA, http://www.cctechnol.com/printable.php?pageID=77.

[20] J. Curcio, J. Leonard, J. Vaganay, A. Patrikalakis, A. Bahr, D. Battle, H. Schmidt, and M. Grund, "Experiments in moving baseline navigation using autonomous surface craft," in *Proc. IEEE/MTS OCEANS Conf. Exhib.*, Washington, D.C., Sep. 2005, pp. 730–735 Vol. 1.

[21] S. Diop and M. Fliess, "Nonlinear observability, identifiability and persistent trajectories," in *IEEE International Conference on Decision and Control*, Brighton, UK, 1991, pp. 714–719.

[22] J. Diosdado and I. Ruiz, "Decentralised simultaneous localisation and mapping for AUVs," in *Proceedings of the IEEE OCEANS-Europe Conference and Exhibition*, June 2007, pp. 1–6.

[23] D. Djugash, S. Singh, and P. Corke, *Field and Service Robotics*, ser. Springer Tracts in Advanced Robotics. Berlin, Heidelberg: Springer Berlin / Heidelberg, 2006, vol. 25, ch. Further Results with Localization and Mapping Using Range from Radio, pp. 231–242.

[24] J. Djugash, S. Singh, G. Kantor, and W. Zhang, "Range-only slam for robots operating cooperatively with sensor networks," in *Proc. IEEE Int. Conf. Robot. Auto. (ICRA)*, May 2006, pp. 2078–2084.

[25] R. M. Eustice, "Large-area visually augmented navigation for autonomous underwater vehicles," Ph.D. dissertation, Massachusetts Institute of Technology / Woods Hole Oceanographic Institution Joint Program, Jun. 2005.

[26] R. M. Eustice, H. Singh, and J. J. Leonard, "Exactly sparse delayed-state filters for view-based SLAM," *IEEE Trans. Robot.*, vol. 22, no. 6, pp. 1100–1114, Dec. 2006.

[27] R. M. Eustice, L. L. Whitcomb, H. Singh, and M. Grund, "Recent advances in synchronous-clock one-way-travel-time acoustic navigation," in *Proc. IEEE/MTS OCEANS Conf. Exhib.*, Boston, MA, USA, Sep. 2006, pp. 1–6.

[28] ——, "Experimental results in synchronous-clock one-way-travel-time acoustic navigation for autonomous underwater vehicles," in *Proc. IEEE Int. Conf. Robot. Auto. (ICRA)*, Rome, Italy, Apr. 2007, pp. 4257–4264.

[29] M. F. Fallon, G. Papadopoulos, and J. J. Leonard, "Cooperative AUV navigation using a single surface craft," in *Proc. of Field and Service Robotics*, Cambridge, MA, Jul 2009.

[30] L. Freitag, M. Grund, J. Partan, K. Ball, S. Singh, and P. Koski, "Multi-band acoustic modem for the communications and navigation aid AUV," in *Proc. IEEE/MTS OCEANS Conf. Exhib.*, Washington, D.C., Sep. 2005, pp. 1080–1085.

[31] L. Freitag, M. Grund, S. Singh, J. Partan, P. Koski, and K. Ball, "The WHOI micro-modem: an acoustic communications and navigation system for multiple platforms," in *Proc. IEEE/MTS OCEANS Conf. Exhib.*, Washington, D.C., Sep. 2005, pp. 1086–1092.

[32] A. Gadre, "Observability analysis in navigation systems with an underwater vehicle application," Ph.D. dissertation, Virginia Polytechnic Institute and State University, Blacksburg, Virginia, Jan. 2007.

[33] A. S. Gadre and D. J. Stilwell, "Toward underwater navigation based on range measurements from a single location," in *Proc. IEEE Int. Conf. Robot. Auto. (ICRA)*, New Orleans, LA, Apr. 2004, pp. 4472–4477.

[34] A. Gadre and D. Stilwell, "A complete solution to underwater navigation in the presence of unknown currents based on range measurements from a single location," in *Proc. IEEE/RSJ Intl. Conf. Intell. Robots Systems (IROS)*, Edmonton AB, Canada, 2005, pp. 1420–1425.

[35] ——, "Underwater navigation in the presence of unknown currents based on range measurements from a single location," in *Proc. Am. Control Conf.*, vol. 1, Jun. 2005, pp. 656–661.

[36] A. Gelb, Ed., *Applied optimal estimation*. Cambridge, MA: MIT Press, 1982.

[37] C. R. German, A. Bowen, M. L. Coleman, J. A. Huber, J. Seewald, C. Van Dover, L. L. Whitcomb, D. Yoerger, D. Connelly, D. L. Honig, M. Jakuba, J. C. Kinsey, J. McDermott, K. Nakamura, C. Sands, J. Smith, and S. Sylva, "Hydrothermal Exploration of the Mid-Cayman Spreading Center: Isolated Evolution on Earth's Deepest Mid-Ocean Ridge?" *EOS, Transactions of the American Geophysical Union*, vol. 90, no. 52, Dec. 2009, Fall Meeting Supplement.

[38] C. German, S. Bennett, D. Connelly, A. Evans, B. Murton, L. Parson, R. Prien, E. Ramirez-Llodra, M. Jakuba, T. Shank, D. Yoerger, E. Baker, S. Walker, and K. Nakamura, "Hydrothermal activity on the southern mid-atlantic ridge: Tectonically- and volcanically-controlled venting at 4-5s," *Earth and Planetary Science Letters*, vol. 273, no. 3-4, pp. 332 – 344, 2008. [Online]. Available: http://www.sciencedirect.com/science/article/B6V61-4SXP6TF-1/2/976b220c0df55ef271a38c9c24f2c5a8

[39] M. Grund, J. Partan, P. Koski, and L. Freitag, "Synchronous navigation with the micro-modem," WHOI, Tech. Rep., 2005, document Revision: D.

[40] K. M. Haase, S. Petersen, A. Koschinsky, R. Seifert, C. W. Devey, R. Keir, K. S. Lackschewitz, B. Melchert, M. Perner, O. Schmale, J. Süling, N. Dubilier, F. Zielinski, S. Fretzdorff, D. Garbe-Schönberg, U. Westernströer, C. R. German, T. M. Shank, D. Yoerger, O. Giere, J. Kuever, H. Marbler, J. Mawick, C. Mertens, U. Stöber, M. Walter, C. Ostertag-Henning, H. Paulick, M. Peters, H. Strauss, S. Sander, J. Stecher, M. Warmuth, and S. Weber, "Young volcanism and related hydrothermal activity at 5degS on the slow-spreading southern Mid-Atlantic Ridge," *Geochemistry, Geophysics, Geosystems*, vol. 8, p. Q11002, Nov. 2007.

[41] R. Hartley and A. Zisserman, *Multiple View Geometry in Computer Vision*. Cambridge University Press, 2001.

[42] J. C. Hartsfield, "Single transponder range only navigation geometry (STRONG) applied to REMUS autonomous under water vehicles," Master's thesis, Massachusetts Institute of Technology and Woods Hole Oceanographic Institution, Aug. 2005.

[43] R. Hermann and A. Krener, "Nonlinear controllability and observability," *IEEE Transactions on Automated Control*, vol. 22, no. 5, pp. 728–740, 1977.

[44] M. Hunt, W. Marquet, D. Moller, K. Peal, W. Smith, and R. Spindel, "An acoustic navigation system," Woods Hole Oceanographic Institution, Tech. Rep. WHOI-74-6, Dec. 1974.

[45] *Model ITC-3013*, ITC International Transducer Corporation, Santa Barbara, CA, USA, http://www.itc-transducers.com/_storefiles/119.pdf.

[46] H. Jeffreys, *Operational methods in mathematical physics*, 2nd ed. New York: Hafner Publishing Company, 1972.

[47] H. Jeffreys and B. Jeffreys, *Methods of mathematical physics*, 3rd ed. Cambridge University Press, 1988.

[48] J. Jouffroy and J. Reger, "An algebraic perspective to single-transponder underwater navigation," in *Proceedings IEEE 2006 CCA/CACSD/ISIC*, Munich, Germany, 2006, pp. 1789–1794.

[49] F. S. K. Reif and R. Unbehauen, "An ekf-based nonlinear observer with a prescribed degree of stability," *Automatica*, vol. 34, no. 9, pp. 1119–1123, 1998.

[50] R. E. Kalman, "A new approach to linear filtering and prediction problems," *Transactions of the ASME–Journal of Basic Engineering*, vol. 82, no. Series D, pp. 35–45, 1960.

[51] G. Kantor and S. Singh, "Preliminary results in range-only localization and mapping," in *Proc. IEEE Int. Conf. Robot. Auto. (ICRA)*, 2002, pp. 1818–1823.

[52] A. Kehagias, J. Djugash, and S. Singh, "Range-only slam with interpolated range data," Robotics Institute, Pittsburgh, PA, Tech. Rep. CMU-RI-TR-06-26, May 2006.

[53] D. Kilfoyle and A. Baggeroer, "The state of the art in underwater acoustic telemetry," *Oceanic Engineering, IEEE Journal of*, vol. 25, no. 1, pp. 4–27, Jan 2000.

[54] J. C. Kinsey, R. M. Eustice, and L. L. Whitcomb, "A survey of underwater vehicle navigation: recent advances and new challenges," in *IFAC Conf. on Manoeuvring and Control of Marine Craft*, Lisbon, Portugal, Sep. 2006.

[55] D. Kurth, G. Kantor, and S. Singh, "Experimental results in range-only localization with radio," in *Proc. IEEE/RSJ Intl. Conf. Intell. Robots Systems (IROS)*, vol. 1, Oct. 2003, pp. 974–979.

[56] D. Kurth, "Range-only robot localization and slam with radio," Master's thesis, Carnegie Mellon University, Pittsburgh, PA, May 2004.

[57] C. E. LaPointe, "Virtual long baseline (vlbl) autonomous underwater vehicle navigation using a single transponder," Master's thesis, Massachusetts Institute of Technology and Woods Hole Oceanographic Institution, Jun. 2006.

[58] M. Larsen, "Synthetic long baseline navigation of underwater vehicles," in *Proc. IEEE/MTS OCEANS Conf. Exhib.*, vol. 3, 2000, pp. 2043–2050.

[59] M. B. Larsen, "Autonomous navigation of underwater vehicles," Ph.D. dissertation, Technical University of Denmark, Denmark, Feb. 2001.

[60] ——, "High performance autonomous underwater navigation," *Hydro International*, vol. 6, pp. 2043–2050, Jan. 2002.

[61] E. Larsson, "Cramer-rao bound analysis of distributed positioning in sensor networks," *Signal Processing Letters, IEEE*, vol. 11, no. 3, pp. 334–337, March 2004.

[62] P.-M. Lee, B.-H. Jun, and Y.-K. Lim, "Review on underwater navigation system based on range measurements from one reference," in *OCEANS 2008 - MTS/IEEE Kobe Techno-Ocean*, April 2008, pp. 1–5.

[63] J. Marçal, J. Jouffroy, and T. I. Fossen, "An extended set-valued observer for position estimation using single range measurements," in *Proc. Intl. Symp. Unmanned Untethered Subm. Tech. (UUST)*, Aug. 2005.

[64] E. Martinson and F. Dellaert, "Marco polo localization," in *Proc. IEEE Int. Conf. Robot. Auto. (ICRA)*, vol. 2, Sept. 2003, pp. 1960–1965 vol.2.

[65] S. McPhail and M. Pebody, "Range-only positioning of a deep-diving autonomous underwater vehicle from a surface ship," *Oceanic Engineering, IEEE Journal of*, vol. 34, no. 4, pp. 669–677, Oct. 2009.

[66] *Meinberg LANTIME/GPS Manual: EXT 1HE V4*, Meinberg Funkuhren GmbH & Co. KG, Bad Pyrmont, Germany, May 2004.

[67] E. Menegatti, A. Zanella, S. Zilli, F. Zorzi, and E. Pagello, "Range-only slam with a mobile robot and a wireless sensor networks," in *Proc. IEEE Int. Conf. Robot. Auto. (ICRA)*, Kobe, Japan, May 2009, pp. 8 –14.

[68] P. Milne, *Underwater acoustic positioning systems*. Houston: Gulf Publishing Company, 1983.

[69] D. Mirabello, A. C. Sanderson, and D. R. Blidberg, "Comparing Kalman and particle filter approaches to coordinated multi-vehicle navigation," in *Proc. Intl. Symp. Unmanned Untethered Subm. Tech. (UUST)*, Aug. 2007.

[70] A. G. O. Mutambara, *Decentralized Estimation and Control for Multisensor Systems*. Boca Raton, FL, USA: CRC Press, Inc., 1998.

[71] P. M. Newman and J. J. Leonard, "Pure range-only sub-sea slam," in *Proc. IEEE Int. Conf. Robot. Auto. (ICRA)*, 2003, pp. 1921–1926.

[72] E. Olson, J. Leonard, and S. Teller, "Robust range-only beacon localization," *IEEE J. Oceanic Eng.*, vol. 31, no. 4, pp. 949–958, Oct. 2006.

[73] E. Olson, M. Walter, S. Teller, and J. Leonard, "Single-cluster spectral graph partitioning for robotics applications," in *Proc. Robotics: Sci. & Sys. Conf.*, Cambridge, USA, June 2005.

[74] S. Reece and S. Roberts, "Robust, low-bandwidth, multi-vehicle mapping," in *Information Fusion, 2005 8th International Conference on*, vol. 2, July 2005, pp. 1319–1326.

[75] W. Respondek, "Geometry of static and dynamic feedback," 2001, lecture notes.

[76] B. Ristic, S. Arulampalam, and J. McCarthy, "Target motion analysis using range-only measurements: algorithms, performance and application to ISAR data," *Signal Processing*, vol. 82, no. 2, pp. 273–296, Feb. 2002.

[77] A. Ross and J. Jouffroy, "Remarks on the observability of single beacon underwater navigation," in *Proc. Intl. Symp. Unmanned Untethered Subm. Tech. (UUST)*, Aug. 2005.

[78] S. Russell and P. Norvig, *Artificial intelligence: a modern approach*. Upper Saddle River, NJ: Prentice Hall, 2003.

[79] E. F. S. Boyd, L. El Ghaoui and V. Balakrishnan, "Linear matrix inequalities in system and control theory," in *Proceedings Annual Allerton Conf. on Communication, Conotrol and Computing*. Monticello, Illinois: Allerton House, Oct. 1993.

[80] A. Scherbatyuk, "The AUV positioning using ranges from one transponder LBL," in *Proc. IEEE/MTS OCEANS Conf. Exhib.*, vol. 3, San Diego, California, 1995, pp. 1620–1623.

[81] H. Singh, J. Bellingham, F. Hover, S. Lerner, B. Moran, K. von der Heydt, and D. Yoerger, "Docking for an autonomous ocean sampling network," *IEEE J. Oceanic Eng.*, vol. 26, no. 4, pp. 498–514, Oct. 2001.

[82] H. Singh, A. Can, R. M. Eustice, S. Lerner, N. McPhee, O. Pizarro, and C. Roman, "SeaBED AUV offers new platform for high-resolution imaging," *EOS, Transactions of the American Geophysical Union*, vol. 85, no. 31, pp. 289,294–295, Aug. 2004.

[83] S. Singh, M. Grund, B. Bingham, R. M. Eustice, H. Singh, and L. Freitag, "Underwater acoustic navigation with the WHOI micro-modem," in *Proc. IEEE/MTS OCEANS Conf. Exhib.*, Boston, MA, Sep. 2006.

[84] S. Singh, S. E. Webster, L. Freitag, L. L. Whitcomb, K. Ball, J. Bailey, and C. Taylor, "Acoustic communication performance of the WHOI micro-modem in sea trials of the *Nereus* vehicle to 11,000 m depth," in *Proc. IEEE/MTS OCEANS Conf. Exhib.*, Biloxi, MS, Oct 2009, In Press.

[85] T. Song, "Observability of target tracking with range-only measurements," *IEEE J. Oceanic Eng.*, vol. 24, no. 24, pp. 383–387, Jul. 1999.

[86] J. R. Spletzer, "A new approach to range-only slam for wireless sensor networks," Lehigh University, Bethlehem, PA, Tech. Rep., 2003.

[87] S. Thrun, Y. Liu, D. Koller, A. Y. Ng, Z. Ghahramani, and H. Durrant-Whyte, "Simultaneous localization and mapping with sparse extended information filters," *International Journal of Robotics Research*, vol. 23, pp. 693–716, 2004.

[88] R. Urick, *Principles of underwater sound*. McGraw-Hill, Inc., 1983.

[89] J. Vaganay, P. Baccou, and B. Jouvencel, "Homing by acoustic ranging to a single beacon," in *Proc. IEEE/MTS OCEANS Conf. Exhib.*, vol. 2, 2000, pp. 1457–1462.

[90] J. Vaganay, J. Leonard, J. Curcio, and J. Willcox, "Experimental validation of the moving long base-line navigation concept," in *Autonomous Underwater Vehicles, 2004 IEEE/OES*, June 2004, pp. 59–65.

[91] D. Webb, P. Simonetti, and C. Jones, "Slocum: an underwater glider propelled by environmental energy," *Oceanic Engineering, IEEE Journal of*, vol. 26, no. 4, pp. 447 –452, Oct. 2001.

[92] S. E. Webster, R. M. Eustice, C. Murphy, H. Singh, and L. L. Whitcomb, "Toward a platform-independent acoustic communications and navigation system for underwater vehicles," in *Proc. IEEE/MTS OCEANS Conf. Exhib.*, Biloxi, MS, Oct 2009, pp. 1–7.

[93] S. E. Webster, R. M. Eustice, H. Singh, and L. L. Whitcomb, "Preliminary deep water results in single-beacon one-way-travel-time acoustic navigation for underwater vehicles," in *Proc. IEEE/RSJ Intl. Conf. Intell. Robots Systems (IROS)*, St. Louis, MO, Oct. 2009, pp. 2053–2060.

[94] S. E. Webster, L. L. Whitcomb, and R. M. Eustice, "Preliminary results in decentralized estimation for single-beacon acoustic underwater navigation," in *Proc. Robotics: Sci. & Sys. Conf.*, Zaragoza, Spain, June 2010, In Press.

[95] L. L. Whitcomb, M. V. Jakuba, J. C. Kinsey, S. C. Martin, S. E. Webster, J. C. Howland, C. L. Taylor, D. Gomez-Ibanez, and D. R. Yoerger, "Navigation and control of the *Nereus* hybrid underwater vehicle for global ocean science to 11,000m depth: Preliminary results," in *Proc. 14th Yale Workshop on Adaptive and Learning Systems*, Yale University, June 2008.

[96] ——, "Navigation and control of the Nereus hybrid underwater vehicle for global ocean science to 10,903 m depth: Preliminary results," in *Proc. IEEE Int. Conf. Robot. Auto. (ICRA)*, Anchorage, Alaska, May 2010, Accepted, To Appear.

[97] Woods Hole Oceanographic Institution, "R/V *Knorr*: Specifications," http://www.whoi.edu/page.do?pid=8496, Woods Hole, MA.

Vita

Sarah E. Webster was born in Winchester, Massachusetts, in 1977. After graduating from E. C. Glass High School and the Central Virginia Governor's School for Science and Technology in Lynchburg, Virginia, Sarah attended the Massachusetts Institute of Technology, where she studied Mechanical Engineering. She received a B. S. in Mechanical Engineering in February 2000 and worked as an engineer in the Deep Submergence Laboratory at Woods Hole Oceanographic Institution until March 2004. In August 2004 she enrolled in the Mechanical Engineering Ph.D. program at Johns Hopkins University and received her M. S. in June 2007.

While at Hopkins, Sarah was the recipient of several fellowships, including the JHU Mechanical Engineering Department Fellowship 2004-2005, the JHU Whiting School of Engineering Deans Fellowship 2004-2009, the NSF Graduate Research Fellowship 2005-2008, and the Link Foundation Doctoral Research Fellowship in Ocean Engineering and Instrumentation 2008-2009. She also received honorable mention for the IEEE Robotics and Automation Society Fellowship for Women in Robotics and Automation 2008-2009.

In addition to her studies Sarah was actively involved in the campus community. She was one of the founding members of *Ready, Set, Design!*, an engineering program for middle school girls, and the Mechanical Engineering Graduate Association (MEGA), created to foster community for graduate students within her department. She was also involved in Women of Whiting (WoW), which was created to foster a sense of community and an environment of support among the graduate women in the Whiting School of Engineering.

VITA